Durham E-Theses

Bright solitary waves and non-equilibrium dynamics in atomic Bose-Einstein condensates

BILLAM, THOMAS,PAUL

How to cite:

BILLAM, THOMAS,PAUL (2012) *Bright solitary waves and non-equilibrium dynamics in atomic Bose-Einstein condensates*, Durham theses, Durham University. Available at Durham E-Theses Online: http://etheses.dur.ac.uk/3561/

Bright solitary waves and non-equilibrium dynamics in atomic Bose-Einstein condensates

Thomas Paul Billam

Abstract

In this thesis we investigate the static properties and non-equilibrium dynamics of bright solitary waves in atomic Bose-Einstein condensates in the zero-temperature limit, and we investigate the non-equilibrium dynamics of a driven atomic Bose-Einstein condensate at finite temperature.

Bright solitary waves in atomic Bose-Einstein condensates are non-dispersive and soliton-like matter-waves which could be used in future atom-interferometry experiments. Using the mean-field, Gross-Pitaevskii description, we propose an experimental scheme to generate pairs of bright solitary waves with controlled velocity and relative phase; this scheme could form an important part of a future atom interferometer, and we demonstrate that it can also be used to test the validity of the mean-field model of bright solitary waves. We also develop a method to quantitatively assess how soliton-like static, three-dimensional bright solitary waves are; this assessment is particularly relevant for the design of future experiments.

In reality, the non-zero temperatures and highly non-equilibrium dynamics occurring in a bright solitary wave interferometer are likely to necessitate a theoretical description which explicitly accounts for the non-condensate fraction. We show that a second-order, number-conserving description offers a minimal self-consistent treatment of the relevant condensate – non-condensate interactions at low temperatures and for moderate non-condensate fractions. We develop a method to obtain a fully-dynamical numerical solution to the integro-differential equations of motion of this description, and solve these equations for a driven, quasi-one-dimensional test system. We show that rapid non-condensate growth predicted by lower-order descriptions, and associated with linear dynamical instabilities, can be damped by the self-consistent treatment of interactions included in the second-order description.

Bright solitary waves and non-equilibrium dynamics in atomic Bose-Einstein condensates

Thomas Paul Billam
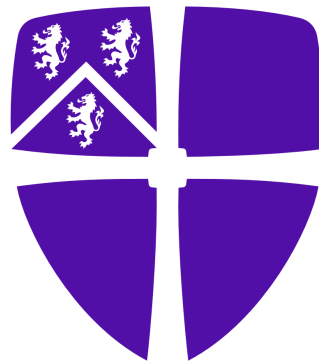
Thesis submitted in accordance with the
requirements for the degree of Doctor of Philosophy

Department of Physics
University of Durham
March 2012

Contents

List of Figures

8

Declaration

I confirm that no part of the material offered has previously been submitted by myself for a degree in this or any other University. Where material has been generated through joint work, the work of others has been indicated.

Thomas Paul Billam
March 2012

Acknowledgements

A great many people have contributed in a great many ways to the making of this thesis, and I wholeheartedly thank them all.

The rest of the AtMol group at Durham have conspired to make working a pleasure; my many office-mates at Durham — in particular Mark Bason, Paul Halkyard, Steven Wrathmall, David Holdaway, John Helm, and Christoph Weiss — contributed to countless enjoyable discussions, which always ended up demonstrating that the world would be a better place if only the occupants of Ph144D were in charge. I also very much enjoyed talking to Jon Pritchard about the more intricate details of atomic physics and computer programming, to Charles Adams about all things open source, to Ifan Hughes about science, sport, and the legendary "Planet Burgerland 3", and to Ulrich Krohn about the strange ways of the English.

Turning to academic issues, I thank my second supervisors, Simon Cornish and Robert Potvliege, for always taking an interest in my work and being eager to ask questions; Tania Monteiro, for a warm welcome on my visit to UCL; Hayder Salman, for advice on numerical methods used in Chapter 4; Nick Parker, Nick Proukakis and their students and postdocs from Newcastle, for being such a pleasant group to visit and to work with; and Ashton Bradley, for his assistance in finding something to spend my days on post-PhD. Most importantly, I thank my supervisor, Simon Gardiner, for taking me on as a PhD student and providing direction, inspiration, and encouragement that has shaped this thesis much for the better.

I thank my friends for their support during my PhD; in particular Alice and Aaron, who I now owe roughly my own body weight in cooked dinners, and Anna, without whose presence eight years in Durham would surely have driven me completely insane, and who can now bask in glory as the final surviving member of "team 2004". Finally, I'd like to thank my parents for the truly immeasurable amount of financial, logistical, and moral support that has brought me to where I am today.

To my parents, for their love and encouragement in everything I do.

Introduction

Bright solitary matter-waves

Mean-field description of an atomic Bose-Einstein condensate

The standard theoretical description of an ultracold atomic Bose-Einstein condensate (BEC) is the mean-field, Gross-Pitaevskii description [1]. In addition to the assumption that the temperature $T \to 0$ (and hence that $T \ll T_c$, where T_c is the condensation temperature) this description assumes that all atoms occupy a single, *condensate*, mode. In dimensionless form this *macroscopic wavefunction*, or *order parameter*, $\psi(\mathbf{r})$, then obeys the *Gross-Pitaevskii equation* (GPE):

$$i\frac{\partial \psi(\mathbf{r})}{\partial t} = \left[-\frac{\nabla^2}{2} + V(\mathbf{r}) + g_{3D}|\psi(\mathbf{r})|^2 \right] \psi(\mathbf{r}), \qquad (1)$$

where $V(\mathbf{r})$ is an external trapping potential, g_{3D} the effective interaction strength, which is dependent on the s-wave scattering length a_s, and $\psi(\mathbf{r})$ is normalized to the atom number N. Since the realization of the first atomic BECs [2, 3] this has been the description of choice for theorists and experimentalists in the field, and has proved very successful in predicting atomic BEC dynamics at low temperatures and close to equilibrium. Whilst the dynamics of the underlying quantum field can be thought of as fulfilling a linear, many-particle Schrödinger equation, the GPE effectively re-casts them in terms of a *nonlinear* equation for a *classical* field. This nonlinearity means the GPE supports a wide variety of topological excitations, and a great deal of work on atomic BECs has focused on identifying, understanding and observing these phenomena, which include vortices [4, 5], vortex lattices, [6, 7] and dark [8, 9] and bright [10–12] solitons.

Bright solitons and bright solitary waves

Solitons are non-dispersive, solitary waves that behave in a particle-like manner, emerging from mutual collisions intact except for shifts in their position and relative phase [13]. The GPE [Eq. (1)] only supports true solitons in the homogeneous, quasi-one-dimensional limit; here it reduces to the one-dimensional nonlin-

ear Schrödinger equation (NLSE)

$$i\frac{\partial \psi(x)}{\partial t} = \left[-\frac{1}{2}\frac{\partial^2}{\partial x^2} + g_{1D}|\psi(x)|^2 \right]\psi(x). \tag{2}$$

In addition to atomic BECs, the NLSE emerges in the description of a diverse range of physical phenomena, including deep-ocean waves [14] and optical fibres [15, 16], and its integrability leads to a spectrum of dark and bright soliton solutions [17–19]. Bright soliton solutions in particular have been extensively studied in the context of nonlinear optics [18, 19], where they occur in the case of a focusing nonlinearity; the atomic BEC analogue — a coherent, localized, non-dispersive matter-wave — occurs in the case of attractive inter-atomic interactions.

Outside the limit in which the system is described by a one-dimensional NLSE integrability is destroyed, precluding true solitons; however, solitary wave solutions with similar properties persist. In the inhomogeneous (trapped) quasi-one-dimensional limit these *bright solitary waves* remain particle-like for long times, and even display particle-like chaotic dynamics [20, 21]. Outside the quasi-one-dimensional regime bright solitary waves exist only for sufficiently low values of g_{3D} [22, 23], due to the instability against collapse of attractively-interacting Bose-Einstein condensates [24–26] but have nonetheless been observed in experiments [10–12]. Although the lack of integrability and the presence of the collapse instability significantly alters the collision dynamics of three-dimensional bright solitary waves [22, 27, 28], causing the degree to which they emerge from collisions unscathed to be strongly dependent on the trap geometry and their relative phase, there remain many stable parameter regimes where the soliton-like properties of bright solitary waves can be observed and potentially exploited.

Potential for precision measurement

Over the last two decades the advent of atom interferometry [29] has led to significant improvements in metrological precision for real-world measurements of, e.g., rotation [30] and the acceleration due to gravity [31]. The development of atomic BECs has enabled a new form of atom interferometry in which a *trapped* BEC is coherently split and recombined after a period of differential evolution. Following a pioneering early experiment [32], many BEC interferometers have been constructed based around the principle of a raised, and subsequently lowered, double-well potential [33–37]. This scheme allows long interaction times [38], and the small spatial scale potentially permits accurate measurements of, e.g., the Casimir-Polder

potential of a surface [37]. Provided the raising of the barrier is sufficiently fast, the GPE can provide a good description of the dynamics, in the sense that nearly all atoms remain in a single mode, which is coherent across the barrier [39]. The inter-acting nature of the BEC also provides the opportunity to exploit non-classical states to achieve quantum enhancement of the measurement precision [38, 40]. However, interactions also cause undesirable phase diffusion during the interaction time, and for this reason experiments have typically chosen to reduce or eliminate them where possible [36, 38, 40].

The properties of bright solitary waves offer a novel solution to the problem of inter-atomic interactions: one can envisage an analogue to the optical Mach-Zender interferometer in which a BEC is split into two coherent, non-dispersive, spatially-localized bright solitary waves, which are manipulated and eventually recombined using a time-dependent external potential. Proposals exist for the coherent beam-splitting of solitons in this fashion using potential barriers [41–43]. Interferometry devices based on bright solitary waves offer improved sensitivity in the measure-ment of atom-surface interactions [44], and possibly of rotation, using a Sagnac interferometer configuration in a toroidal trap [45–47].

Finite-temperature and non-equilibrium dynamics

Even at $T = 0$, atomic BECs contain a (typically small) non-condensate component due to inter-atomic interactions. The necessity of operating at finite temperatures, and the potential for further dynamical depletion [48, 49] of the condensate during collisions and manipulations of the bright solitary waves, makes it likely that any real bright solitary wave interferometer will involve far-from-equilibrium dynamics occurring in the presence of a non-negligible non-condensate fraction. An under-standing of such dynamics, and the prospect of creating future devices, thus requires a fully-dynamical, finite-temperature theoretical description going beyond the GPE. Due to the complexity of such descriptions, the far-from-equilibrium dynamics of atomic BECs in the presence of a significant non-condensate fraction (thermal or dynamically-depleted) remains a largely open problem [50, 51].

Bright solitary waves provide an excellent experimental test-bed for these complex, beyond-mean-field treatments: their size is experimentally controllable — their typ-ical size ($\lesssim 1000$ atoms) requires a theoretical description accounting for finite-size effects and not tied to the thermodynamic limit, but by gradually increasing the atom number one could probe the transition to mean field behaviour; their complex col-

lisional dynamics require a fully dynamical description capable of accounting for the effects of macroscopic quantum coherence — or lack thereof — between bright solitary waves; their direct relation to the integrable nonlinear Schrödinger equation in the quasi-one-dimensional limit provides an opportunity to explore the loss of integrability across the quasi-one-dimensional – three-dimensional transition; and, finally, the possibility of generating bright solitary waves at different temperatures offers a potential test of these theoretical descriptions across the $T = 0$ to $T = T_c$ temperature range.

In the context of a bright solitary wave interferometer, extremely cold initial states would help to increase sensitivity. Consequently, the regime most relevant for bright solitary wave interferometry is that in which a low temperature, highly condensed equilibrium state ($T \ll T_c$) is driven by the external potential, leading to dynamical depletion. Previous work in this regime has focused on atomic BEC analogues of quantum chaotic kicked systems; e.g., the kicked accelerator [52, 53], kicked harmonic oscillator [48, 54, 55], and kicked rotor [56–60]. While superficially appearing uncomplicated, these systems in fact offer an excellent test bed for exploring generic issues of quantum chaos [58, 61], quantum superposition [62], quantum resonances [54, 59, 60], dynamical instability and dynamical depletion [48, 56, 59, 60], and even entropy, thermalization and integrability [63–65].

In this low-temperature regime, correctly capturing the interplay between driving, condensate, and low-lying non-condensate excitations is vital, and using a theoretical description which self-consistently includes this interplay is of paramount importance. A particular example of this can be seen in the case of the δ-kicked-rotor-BEC [56–60]: for this system a first-order treatment of the non-condensate, as given by C. Gardiner [66] and Castin and Dum [67], predicts a general tendency for rapid, unbounded growth of the non-condensate due to the initial linear instability of the system. However, the equation describing the condensate in this first-order treatment is simply the GPE. Consequently, the condensate feels no-back action from the growing non-condensate, leaving open the question of whether the rapid growth of the non-condensate could be slowed or halted by the inclusion of a consistent back-action. A promising theoretical description, which includes a completely self-consistent back-action of this kind, is the second-order, number-conserving dynamical description of S. Gardiner and Morgan [68]. This description was used highly successfully by Morgan [69–71] within a linear response treatment to calculate the excitation frequencies of a BEC at finite temperature, as measured in experiments at JILA [72, 73] and MIT [74, 75]. However, due to the complexity of the

nonlocal terms appearing in the second order equations of motion, this description has not previously been implemented in a fully dynamical way.

Thesis outline

In this thesis, we take five principal steps toward a further understanding of the non-equilibrium dynamics of bright solitary waves in atomic BECs:

- Using the mean-field, Gross-Pitaevskii description, we identify a new method which could be used in experiment to create pairs of bright solitary waves with controlled velocity and relative phase. Such a method could form a key part of future bright solitary wave interferometry experiments.

- By analysing, using the GPE, the dynamics of bright solitary waves created using the above method and allowed to periodically re-collide at the centre of a harmonic trap, we demonstrate that the relation between the longevity of these waves and their relative phase can be used as a test of the accuracy of the mean-field description.

- We quantitatively assess the relationship between real bright solitary wave solutions at zero temperature and the bright soliton solutions of the one-dimensional NLSE, and show that the regime in which bright solitary waves are highly soliton-like is experimentally challenging.

- We develop the second-order number-conserving description of S. Gardiner and Morgan, and cast the integro-differential equations of motion in a form amenable to a fully dynamical numerical solution. We implement this numerically for a quasi-one-dimensional, periodic system — the δ-kicked-rotor-BEC — initially at zero-temperature equilibrium.

- Using this numerical implementation, we study the dynamics of the δ-kicked-rotor-BEC, and show that rapid non-condensate growth is indeed damped by the self-consistent back action included in the second-order description.

Thesis structure

Prelude: Atomic Bose-Einstein condensates

This thesis commences with a single-chapter prelude (Chapter 1) in which we discuss the background to Bose-Einstein condensation in weakly interacting, dilute

atomic gases. The material here — including a summary of the realization of atomic BEC, a review of experimental applications, a discussion of the basic theoretical concepts and the physical properties of atomic BECs, and an introduction to the mean-field and beyond mean-field descriptions — is common to both subsequent parts of this thesis.

Part I: bright solitary waves

In Part I of this thesis, we consider the phenomenon of bright solitary matter-waves in atomic BECs, working within the zero-temperature, mean-field description.

- In Chapter 2 we review the properties of, and the history of experimental and theoretical interest in, these intriguing non-dispersive, nonlinear wavepackets. In particular, we emphasise that in certain parameter regimes they can be directly theoretically connected to bright solitons of the focusing nonlinear Schrödinger equation, and can display soliton-like dynamics.

- In Chapter 3 we analyse the soliton-like dynamics of bright solitary waves further, and propose an experiment in which pairs of such waves could be created with controlled velocity and relative phase. If realized, this experiment would facilitate tests of mean-field theory for bright solitary waves, and possibly pave the way for future interferometry experiments using bright solitary waves.

- In Chapter 4, we use variational and numerical methods to address the issue of how soliton-like the ground state of an atomic BEC is, in various realistic experimental parameter regimes. Although we work in the mean-field description, our results in this Chapter are particularly important for future experiments seeking to exploit beyond-mean-field effects in bright solitary waves.

Part II: Instabilities and self-consistent non-equilibrium dynamics

In Part II of this thesis, we study the dynamics of driven BECs at finite temperature and far from equilibrium.

- In Chapter 5 we review existing theoretical descriptions of atomic BECs at finite temperature in some detail, and identify some of the major theoretical

and computational hurdles that exist in this field. In particular, we concentrate on the suitability of the various descriptions to describe the coupled, non-equilibrium dynamics of both the condensate and non-condensate in a driven atomic BEC in a self-consistent fashion; we argue that a second-order number-conserving description, if implemented in a fully dynamical fashion, would be the most suitable description for such a system.

- In Chapter 6 we introduce in detail the second-order description of S. Gardiner and Morgan. By recasting this theory in an unusual form we develop a feasible numerical method for computing a fully-time-dependent numerical solution.

- In Chapter 7, we implement this numerical method for a quasi-one-dimensional test system: the δ-kicked-rotor-BEC. Our implementation allows us to explicitly demonstrate a damping of condensate depletion due to the self-consistent back-action of the non-condensate in the second-order description. This is in contrast to the first-order description used previously, which predicts general, rapid, unbounded growth of the non-condensate. This Chapter is followed by our final conclusions.

Publications

Work relating to this thesis

[76] T. P. Billam, S. L. Cornish, and S. A. Gardiner, *Realizing bright-wave-soliton collisions with controlled relative phase*, Phys. Rev. A **83**, 041602(R) (2011) forms the basis of Chapter 3.

[77] T. P. Billam, S. A. Wrathmall, and S. A. Gardiner, *Variational determination of approximate bright wave soliton solutions in anisotropic traps*, Phys. Rev. A **85**, 013627 (2012) forms the basis of Chapter 4.

[78] T. P. Billam and S. A. Gardiner, *Coherence and instability in a driven Bose-Einstein condensate: a fully dynamical number-conserving approach*, New J. Phys. **14**, 013038 (2012) forms the basis of Chapter 7.

[79] S. A. Gardiner and T. P. Billam, *Number-conserving approaches for atomic Bose-Einstein condensates: an overview*, In N. P. Proukakis *et al.*, editors, *Quantum Gases: Finite temperature and non-equilibrium dynamics*, World Scientific, Singapore (to appear 2012) covers material common to Part II of this thesis.

Other work

[54] T. P. Billam and S. A. Gardiner, *Quantum resonances in an atom-optical δ-kicked harmonic oscillator*, Phys. Rev. A **80**, 023414 (2009).

[80] J. L. Helm, T. P. Billam, and S. A. Gardiner, *Bright matter-wave soliton collisions at narrow barriers*, arXiv:1203.3080.

[81] B. Gertjerenken, T. P. Billam, L. Khaykovich, and C. Weiss, *Scattering of bright quantum wave solitons*, In Preparation (2011).

Prelude: Atomic Bose-Einstein condensates

Chapter 1: Bose-Einstein condensation in weakly-interacting atomic gases

1.1 Introduction

The primary unifying theme in this thesis is the theoretical description of dilute gases of bosonic atoms in the ultracold, quantum-degenerate regime. Such gases, first realized in 1995 [2, 3], are now routinely created in atomic physics experiments. The behaviour of these gases is dominated by the presence of a Bose-Einstein condensate (BEC) — a single-particle eigenmode occupied by a macroscopic number of atoms. Due to the relatively weak interactions between the atoms, at experimentally feasible temperatures this condensate can easily comprise over 99% of the atoms. Consequently, such a gas is almost universally referred to as an *atomic Bose-Einstein condensate* [1, 82, 83]. The macroscopic quantum coherence associated with the condensate mode makes atomic BECs an intriguing system where quantum effects can be observed on a macroscopic scale [32, 41, 42, 81, 84, 85]. Among other potential impacts, this property opens the door to exciting possible applications for atomic BECs in the field of precision metrology [33–36], for example offering the potential to test developing theories of gravitation [86, 87], and to improve our understanding of atom-surface interactions [37, 44].

In this Chapter we briefly describe the physics of atomic BECs, and introduce the mean-field description of their dynamics. In Part I of this thesis we use this mean-field description to describe the dynamics of an atomic BEC at (and close to) $T = 0$. In Part II we use it as a starting point, from which we develop and numerically implement a consistent description of atomic BEC dynamics at finite-temperature.

We begin with a brief review of atomic BEC experiments in Section 1.2: in Section 1.2.1 we give a summary of the physical properties of a typical atomic BEC, and in Section 1.2.2 we review some of the investigations and applications of atomic BEC to date. In Section 1.3 we present the underlying theoretical model of an atomic BEC we use in this thesis. Central to this is the concept of an inhomogeneous and weakly-interacting Bose gas. This provides an excellent model of an alkali-atom BEC as generally realized in experiment. Having introduced the system Hamiltonian in Section 1.3.1, we introduce the condensate mode; this can be rigorously

defined in terms of the Penrose-Onsager criterion and the presence of off-diagonal long-range order (Section 1.3.2).

Unfortunately, the model of a weakly-interacting Bose gas is intractable in its full form, and approximations must be introduced in order to understand the behaviour of atomic BECs. In Section 1.4 we describe the most common such approximation; the concept of Bose symmetry-breaking. As we show in Section 1.4.1, this essentially consists of describing the condensate as a classical field, and introducing non-condensate creation and annihilation operators, which can be assumed to be small at low temperature. The symmetry-breaking technique leads to a description of an atomic BEC expressed in powers of these operators. Considering only the part of the Hamiltonian which is linear in the non-condensate creation and annihilation operators, in Section 1.4.2 we derive the mean-field, Gross-Pitaevskii equation. This equation describes the dynamics of the condensate at $T = 0$ and with total occupation of the condensate, and is the canonical description of an atomic BEC at low temperature; we use it extensively in Part I of this thesis. In Section 1.4.3 we introduce the minimal treatment of the non-condensate within a symmetry-breaking approach. This treatment consists of the static Bogoliubov-de Gennes equations, the solutions of which can be used to diagonalize the part of the Hamiltonian which is quadratic in the non-condensate creation and annihilation operators.

This diagonalization leads on to the final Section, 1.4.4, where we review superfluidity. This is the perhaps the most well-known phenomenon associated with the weakly interacting Bose gas, and hence atomic BECs, and can be understood in terms of the diagonalization of the quadratic part of the Hamiltonian. We highlight in particular the differences and similarities between an atomic BEC and liquid ^{4}He — in a historical sense the "canonical" superfluid.

1.2   Experimental realization

1.2.1   Formation of atomic BECs

Formation of the macroscopically-occupied single-particle state which constitutes a Bose-Einstein condensate is only possible in many-body systems obeying Bose-Einstein statistics. These statistics require that the many-body quantum state of such a system is completely symmetric under particle exchange. On a microscopic level, through the famous spin-statistics theorem [88] this means the particles themselves must be bosons and possess integer spin. This connection between statistics and

spin applies to both elementary and composite particles, provided we consider the latter in a situation where their interactions occur at an energy that is small compared to the energy of their internal structure [89]. Consequently atomic species with integer spin behave as composite bosons at low temperature, and macroscopic occupation of a single-particle state by such atoms is permitted. Thanks to advances in experimental atomic physics within the last quarter-century it has become possible to trap and dilute atomic gases of a bosonic species, and cool them until the onset of this quantum degeneracy [90]. In this Section we review the production and physical aspects of these atomic BECs.

Atomic BECs were first realized in 1995, using the alkali metals ^{87}Rb [2] and ^{23}Na [3]. Since these pioneering experiments, atomic BEC has been realized in the other stable bosonic alkali metal isotopes — ^{7}Li [91], ^{39}K [92], ^{41}K [93], ^{85}Rb [94], ^{133}Cs [95] — and in a variety of other atomic species suitable for laser cooling; ^{52}Cr [96], ^{40}Ca [97], ^{84}Sr [98, 99], ^{86}Sr [100], ^{88}Sr [101], ^{174}Yb [102], ^{170}Yb [103], ^{176}Yb [104], ^{164}Yb [105] , ^{164}Dy [106], ^{1}H [107], and metastable ^{4}He [108, 109]. Alongside the flourishing of atomic BECs, Bose-Einstein condensation (or close analogues of it) have also been observed in condensed matter systems such as exciton-polariton fluids in semiconductor microcavities [110], magnons in magnetic insulators [111, 112], and in photons in an optical cavity [113].

Several of these atomic species, and the non-atomic systems, lead to "exotic" condensates. For example ^{52}Cr [96] and ^{164}Dy [106] display long-range dipolar interactions, an exciton-polariton condensate is a strongly interacting and non-equilibrium [110] system, magnons interact strongly with the underlying lattice [112], and the photon condensate realized to date is extremely weakly interacting [113]. This "exotic" behaviour is in contrast to the "vanilla" atomic BEC which we will generally consider in this thesis; such an atomic BEC is characterized by short-range interactions which are well-described by an effective s-wave scattering length a_s, coupled with sufficient diluteness ($n^{1/3}a_s \ll 1$) that three-body collisions are negligible[1] and the model of a weakly-interacting Bose gas (discussed in the following Sections) is applicable. Alkali metal atom condensates are the most directly experimentally available system which meet these criteria, and the theoretical descriptions presented in this thesis can be taken to apply primarily to such systems. For the bosonic alkali metal species a typical atomic BEC consists of between 10^3 and 10^7 atoms, with a typical number density around 10^{11}–10^{15} cm^{-3}, and a critical temperature for

---

[1]Although, where three-body recombination leads to atom losses from a trap, this can to some extent be added in phenomenologically where appropriate.

Bose-Einstein condensation around 10–100 nK [90].

1.2.2   Experimental applications

Since 1995, the field of atomic BEC has burgeoned both experimentally and theoretically. A key feature of the field today is the substantial level of control afforded by coherent manipulation of atoms with lasers and magnetic fields, which has led to a diverse range of experimental applications for atomic BECs.

As will be shown in Section 1.4.4, an atomic BEC is a superfluid. This allows one to observe the same dynamical excitations observed in liquid ^{4}He [114–116], and more recently also observed in non-equilibrium exciton-polariton condensates [117, 118], such as quantized vortices [4, 5, 7] and vortex lattices [6, 119]. Recently, atomic BECs have become a system of interest in the study of classical and quantum turbulence [120–127].

Another interesting dynamic excitation exhibited by atomic BECs are solitons; non-dispersive nonlinear waves, stabilized by the inter-atomic interactions. These were first observed in the form of dark solitons [8, 9], which correspond to a mobile density "notch" within a condensate with repulsive inter-atomic interactions. Their counterparts in an attractively-interacting BEC are bright solitons, which correspond to self-stabilizing individual wavepackets. While BECs with attractive inter-atomic interactions were first created soon after the first atomic BECs [91, 128], these condensates are in general more difficult to work with. Indeed, a homogeneous BEC with attractive interactions is unstable to collapse, and an inhomogeneous atomic BEC is only stable in a particular regime of trap- and interaction strength. An important tool in their study is thus the use of Feshbach resonances to alter the s-wave scattering length of a BEC using external magnetic fields [129, 130], providing control over the magnitude and sign of the s-wave scattering length. This technique has allowed studies of the trap- and interaction strength-dependent instability threshold of attractively-interacting BECs [24, 91, 128, 131], and the creation of bright solitons [10–12], the theoretical investigation of which forms the subject of Part I of this thesis.

The realization of atomic BEC provides an intriguing way to extend the already well-developed field of atom interferometry [29], thanks to the macroscopic quantum coherence of BECs, as first demonstrated by the observation of interference between condensates [32]. Since then, BEC interferometers have been realized based on the raising and lowering of a double-well potential [33–37]. Such a BEC

interferometer offers the intriguing possibility of observing quantum effects on a macroscopic scale [41, 42, 81, 84, 85], and admits the possibility of using quantum effects to enhance measurement sensitivities [84, 132], thanks to the unique properties of BEC. Coherent beams of atoms emitted from a BEC — a so-called atom laser — have also been demonstrated [133–135]. We consider the possibility of atomic BEC interferometry using bright solitary waves in Chapter 7.

Another field which has seen significant development in the last decade is that of the trapping and manipulation of atomic BECs. A strong motivation for much research in this field is the quest to realize a "quantum simulator" of condensed matter systems using cold atoms [136, 137]. In particular, atomic BECs in optical lattices [138, 139] and magnetic microtraps and atom-chip traps [140] are heavily researched areas. Another growing area in the field of trapping and manipulation, which is relevant in particular to the δ-kicked-rotor BEC considered in Chapter 7 of this thesis, is that of toroidal atom traps [46, 47, 141–146]; such traps can be created by blocking the central region of a harmonic trap with a strong, blue-detuned laser [46], using radio-frequency dressing techniques [141], time-averaged "painted" optical traps [146], and most recently using Laguerre-Gaussian laser beams [47]. The periodic geometry of such traps makes them ideal for observing the ideal, inviscid flow of a superfluid [46, 47], and potentially for measuring the superfluid fraction of an atomic BEC [147].

While 20 years ago any kind of atomic BEC would have been regarded as extremely exotic, the rapid expansion of the field has also led to the realization of the new types of condensate lying outside the regime of validity of the weakly-interacting Bose gas model discussed in the previous Section. BECs of molecules of weakly bound fermions have been created [148, 149], leading to detailed exploration of the BEC-BCS crossover in such systems [150]. Two-component condensates, with atoms of different elements [151], or the same element but different spin states [152] have also been realized. As first proposed in Ref. [153], such a mixture presents one possible starting point for the creation of a molecular BEC of ground-state molecules, which has yet to be realized. Proposals also exist to introduce long-range interactions into BECs through excitation to Rydberg states [154], and even to engineer the interactions between Rydberg atoms to create a variation on the bright solitons discussed in Part I of this thesis [155].

1.3 Theoretical model

1.3.1 Many-body Hamiltonian

The theoretical model underlying the descriptions of alkali-metal atomic BECs developed and used in this thesis is that of the *weakly-interacting Bose gas*. This model was originally introduced by Bogoliubov [156] in the context of liquid ^{4}He. It has been the subject of a vast amount of study since, and reviews covering a much broader range of topics than this thesis can be found in, e.g., Refs. [50, 83, 157–160].

Provided a gas of interacting Bosonic atoms is sufficiently dilute[2] that three-body collisions can be safely neglected, it can be described by the many-body Hamiltonian

$$\hat{H} = \sum_{i=1}^{N}\left(-\frac{\hbar^2}{2m}\nabla_i^2 + V(\mathbf{r}_i, t)\right) + \frac{1}{2}\sum_{i\neq j=1}^{N} U(\mathbf{r}_i - \mathbf{r}_j), \tag{1.1}$$

where the N identical atoms are assumed to have mass m, $V(\mathbf{r}, t)$ is the external (typically trapping) potential, and $U(\mathbf{r} - \mathbf{r}')$ is the full two-body interaction potential. In this, first-quantized, formalism the Bose statistics of the particles are implicit in the choice of many-body wavefunction $\psi(\mathbf{r}_1, \mathbf{r}_2, \ldots, \mathbf{r}_N)$, which must be symmetric under the exchange of any atoms.

The first-quantized formalism of the many-body wavefunction quickly becomes unwieldy and uninsightful for increasing N. In contrast, the formalism of second quantization provides a convenient way to abstract away the Bose statistics and particle indices [161, 162]. In this formalism, the primary descriptor of the system is no longer the wavefunction, but the field operator

$$\hat{\Psi}(\mathbf{r}) = \sum_m \hat{a}_m \phi_m(\mathbf{r}), \tag{1.2}$$

and its hermitian conjugate $\hat{\Psi}^\dagger(\mathbf{r})$. In this expression the operators $\hat{a}_m$ and their hermitian conjugates $\hat{a}_m^\dagger$ are, respectively, annihilation and creation operators for the complete orthonormal basis of single-particle modes $\phi_m(\mathbf{r})$; their action on a Fock, or *number*, state [161, 162] is defined by

$$\hat{a}_m|n_0, n_1, \ldots, n_m, \ldots\rangle = \sqrt{n_m}|n_0, n_1, \ldots, n_m - 1, \ldots\rangle, \tag{1.3}$$

---

[2]The typical diluteness criterion can be stated as $n^{1/3}a_s \ll 1$, where n is the number density of atoms, and a_s the s-wave scattering length [83].

where n_m represents the number of particles occupying single-particle mode $\phi_m(\mathbf{r})$. Consequently, the field operators can be thought of as removing $[\hat{\Psi}(\mathbf{r})]$ or adding $[\hat{\Psi}^\dagger(\mathbf{r})]$ an atom to the system at position $\mathbf{r}$. The bosonic nature of the field is implicit in the commutation relations of the field operators;

$$\left[\hat{\Psi}(\mathbf{r}), \hat{\Psi}^\dagger(\mathbf{r}')\right] = \delta(\mathbf{r} - \mathbf{r}'), \tag{1.4}$$

$$\left[\hat{\Psi}(\mathbf{r}), \hat{\Psi}(\mathbf{r})\right] = \left[\hat{\Psi}^\dagger(\mathbf{r}), \hat{\Psi}^\dagger(\mathbf{r})\right] = 0. \tag{1.5}$$

Equivalent relations hold for $\hat{a}_m$ and $\hat{a}_m^\dagger$. In this second-quantized formalism, the Hamiltonian for the weakly-interacting Bose gas becomes

$$\hat{H} = \int d\mathbf{r}\, \hat{\Psi}^\dagger(\mathbf{r}) \left[-\frac{\hbar^2}{2m}\nabla^2 + V(\mathbf{r}, t)\right] \hat{\Psi}(\mathbf{r})$$
$$+ \frac{1}{2} \iint d\mathbf{r}\, d\mathbf{r}'\, U(\mathbf{r} - \mathbf{r}')\hat{\Psi}^\dagger(\mathbf{r})\hat{\Psi}^\dagger(\mathbf{r}')\hat{\Psi}(\mathbf{r}')\hat{\Psi}(\mathbf{r}). \tag{1.6}$$

As we have already hinted, a standard approximation to make for an ultracold, dilute gas is to replace the actual inter-atomic interaction $U(\mathbf{r}-\mathbf{r}')$ with a contact potential;

$$U(\mathbf{r} - \mathbf{r}') = U_0\, \delta(\mathbf{r} - \mathbf{r}'). \tag{1.7}$$

Firstly, this amounts to replacing the true inter-atomic potential, which diverges as $|\mathbf{r} - \mathbf{r}'| \rightarrow 0$, with a short-range, *smooth*, effective potential with *identical* low-momentum scattering properties [83]. Secondly, the Fourier transform of this effective potential is replaced with a constant, leading to the δ-function *pseudopotential* of Eq. (1.7) [161]. At long wavelengths, and in the first Born approximation, one finds [83, 161]

$$U_0 = \frac{4\pi\hbar^2 a_s}{m}, \tag{1.8}$$

where a_s is the s-wave scattering length. This replacement is entirely justified at the order of the mean-field, Gross-Pitaevskii description, which we derive in Section 1.4.2 and use extensively in Part I of this thesis. However, when going beyond mean-field theory — as is necessary in the finite-temperature theory developed in Part II of this thesis — replacing $U(\mathbf{r} - \mathbf{r}')$ with the contact pseudopotential is the source of many ultraviolet divergences[3]. While we encounter the first such divergence later in this Chapter (Section 1.4.3), we defer a detailed treatment of this issue and the introduction of procedures to renormalize these divergences (see, for

---

[3]Note that this ultraviolet divergence is suppressed in effectively one-dimensional descriptions, which we introduce in Chapter 2.

example, Ref. [163] or Ref. [68] and Refs. therein) until Chapter 5. For now, we simply introduce the contact potential into the Hamiltonian [Eq. (1.6)] "as-is". This produces the Hamiltonian

$$\hat{H} = \int d\mathbf{r}\, \hat{\Psi}^\dagger(\mathbf{r}) \left[-\frac{\hbar^2}{2m}\nabla^2 + V(\mathbf{r}, t) + \frac{U_0}{2}\hat{\Psi}^\dagger(\mathbf{r})\hat{\Psi}(\mathbf{r}) \right] \hat{\Psi}(\mathbf{r}), \qquad (1.9)$$

which suffices at the mean-field order of description considered in Part I of this thesis.

1.3.2   Condensate mode and off-diagonal long-range order

Condensation in trapped, weakly-interacting Bose gases

Deriving the statistical behaviour of a homogeneous ideal (non-interacting) Bose gas in the thermodynamic limit, using the grand canonical ensemble, is a perennial favourite of statistical physics texts; under these conditions, and in three dimensions, there is a true thermodynamic phase transition to Bose-Einstein condensation — macroscopic occupation of the ground state — at a critical temperature T_c [164]. However, it has also become a common text-book practice to explain Bose-Einstein condensation in a finite-sized, weakly-interacting atomic BEC in a harmonic trap by analogy to the former system. While such analogies undoubtedly can aid physical intuition, there are significant differences between the two cases. Indeed, a careful experiment can easily demonstrate that the condensation temperature of a trapped atomic BEC is different from the ideal gas prediction [165]. It is therefore worthwhile to guard against over-extension of analogies by carefully defining what is meant by the critical temperature, and indeed by Bose-Einstein condensation, in an atomic BEC.

In typical, homogeneous, condensed matter systems the number of particles is $> 10^{23}$, and edge effects can be safely neglected. Although any real such system is finite-sized, to experimental accuracy it exhibits infinitely sharp thermodynamic phase transitions, and the associated critical temperatures can be accurately predicted using the thermodynamic limit. In contrast, atomic BECs contain many orders of magnitude fewer particles, and the harmonic trap introduces "edge" effects in a global way [166]. While it is possible to define a thermodynamic limit, and hence obtain a critical temperature, in an atomic BEC, taking finite-size effects into account leads to a noticeably smoothed pseudo-phase transition [166, 167] even in the absence of interactions. As this pseudo-phase transition is no longer a true

thermodynamic one, the critical temperature T_c should be understood to be redefined in terms of some measure of the onset of condensation — typically taken to be the point at which the condensate fraction disappears [167, 168]. This critical temperature is not correctly predicted by the thermodynamic limit, even in the non-interacting case [165–167]. Inter-atomic interactions alter this picture still further, as was highlighted in a recent experiment [169]. For example, the shift in critical temperature due to interactions is a long-standing issue which has been addressed using some of the finite-temperature methods we discuss in Chapter 5 [170, 171], and in a recent experiment [168, 172].

Defining the condensate in trapped, weakly-interacting Bose gases

Having identified these discrepancies between the reality of an atomic BEC and the thermodynamic phase transition to Bose-Einstein condensation predicted in a homogeneous ideal gas, the question arises *is an atomic BEC really an example of Bose-Einstein condensation*? Naturally, one can choose the answer to this question by choosing how one defines a Bose-Einstein condensation [166]. In this thesis, we arrange an affirmative answer by taking macroscopic occupation of a single-particle mode to be the condition for Bose-Einstein condensation.

In more rigorous terms, we adopt the definition of Bose-Einstein condensation, applicable to finite-size and interacting Bose systems, introduced by Penrose and Onsager [173]; this definition makes use of the single-particle density matrix, defined in terms of the field operator as

$$\rho(\mathbf{r}, \mathbf{r}', t) = \left\langle \hat{\Psi}^\dagger(\mathbf{r}')\hat{\Psi}(\mathbf{r}) \right\rangle . \tag{1.10}$$

In Eq. (1.10) the brackets $\langle \cdots \rangle$ denote an expectation value with respect to the full many-particle density matrix; at finite-temperature this involves *thermal*, as well as quantum, averaging (see Part II of this thesis).

The single-particle density matrix $\rho(\mathbf{r}, \mathbf{r}', t)$ is hermitian. Thus, at any time t, it can be diagonalized to yield a complete orthonormal set of single-particle eigenstates $\phi_m(\mathbf{r}, t)$ with real eigenvalues $N_m(t)$ satisfying

$$\int d\mathbf{r} \, \rho(\mathbf{r}, \mathbf{r}', t)\phi_m(\mathbf{r}', t) = N_m(t)\phi_m(\mathbf{r}, t) . \tag{1.11}$$

The eigenvalue $N_m(t)$ expresses the average occupation of the single-particle eigenstate $\phi_m(\mathbf{r}, t)$, and one thus has $\sum_m N_m(t) = N$. Penrose and Onsager defined a Bose-

Einstein condensate as an eigenstate of the single-particle density matrix $\phi_c(\mathbf{r}, t)$ which is macroscopically occupied; that is, for which the average occupation is of order N, and consequently much greater all the others[4]. In this thesis, we refer to $\phi_c(\mathbf{r}, t)$ as the *condensate mode*.

The physical significance of such a macroscopically occupied condensate mode can be seen through the concept of off-diagonal long-range order, also introduced by Penrose and Onsager [173]. Separating out the contribution of $\phi_c(\mathbf{r}, t)$ to the single-particle density matrix yields

$$\rho(\mathbf{r}, \mathbf{r}', t) = N_c(t)\phi_c^*(\mathbf{r}', t)\phi_c(\mathbf{r}, t) + \sum_{m \neq c} N_m(t)\phi_m^*(\mathbf{r}', t)\phi_m(\mathbf{r}, t)\,. \tag{1.12}$$

In an infinite, homogeneous system, one can consider the limit $|\mathbf{r} - \mathbf{r}'| \to \infty$: in this limit the final term representing non-condensate is an incoherent summation which tends to zero. In contrast the first term representing the condensate remains finite and, in the case of a uniform, static condensate is equal to the condensate density, $n_c(t)$ for all $|\mathbf{r} - \mathbf{r}'|$:

$$\lim_{|\mathbf{r}-\mathbf{r}'|\to\infty} \rho(\mathbf{r}, \mathbf{r}', t) = N_c(t)\phi_c^*(\mathbf{r}', t)\phi_c(\mathbf{r}, t) = n_c(t)\,. \tag{1.13}$$

While the case of finite and inhomogeneous systems does not accommodate the limit $|\mathbf{r} - \mathbf{r}'| \to \infty$ in a rigorous way, similar behaviour does occur: the non-condensate summation decays rapidly with $|\mathbf{r} - \mathbf{r}'|$, while the term representing the condensate remains non-zero for $|\mathbf{r} - \mathbf{r}'|$ of the same order as the length of the condensate [159]. If one interprets the single-particle density matrix as representing the probability amplitude to add an atom to the system at $\mathbf{r}'$ and immediately remove it at $\mathbf{r}$, these non-zero values of the single-particle density matrix represent a non-zero amplitude for this process in the off-diagonal and long range limit (large $|\mathbf{r} - \mathbf{r}'|$). This off-diagonal long-range order presents a physical picture of the condensate as a macroscopic quantum body which mediates coherent interactions between atoms over a long distance, regardless of the range of the actual interaction potential between the atoms.

Considerations in low-dimensional systems

In this thesis, we will often consider (quasi-) one-dimensional (1D) systems, in which the constituent atoms are "frozen" into the lowest energy eigenstate of an ex-

---

[4]Using big-o notation one has $O(N_c) = O(N)$, while $O(N_m) = 1$ for $m \neq c$.

ternal trapping potential in two directions. Similar (quasi-) two-dimensional (2D) systems may be created by similarly "freezing" the motion in one direction only. The definition of Bose-Einstein condensation requires further care in these systems, because an infinite, homogeneous Bose gas in 1D or 2D does *not* undergo a condensation phase transition at finite temperature [83]. Consequently, these systems do not possess off-diagonal long-range order in the limit $|\mathbf{r} - \mathbf{r}'| \to 0$ as defined above. However, this does not constitute a major problem for the theoretical description applied in this thesis:

Firstly, in finite, trapped 1D and 2D systems, a condensation transition leading to macroscopic occupation of the ground state and long-range phase coherence can still be observed at finite temperature [174]. At temperatures slightly above this condensation temperature long-range phase coherence is destroyed, but density fluctuations remain suppressed, yielding a "quasi-condensate" [174] for temperatures up to a second critical temperature T_q. In the case of finite, trapped 1D systems, the theoretical description applied in this thesis applies below the "true" condensation temperature T_c.

Secondly, while we also consider infinite and homogeneous 1D systems in this thesis, we only do so for the case of attractive inter-atomic interactions. In this case, the eigenstates of the full many-body (Lieb-Liniger [175]) Hamiltonian are *localized* over a length scale determined by the interaction strength and atom number. This length scale can be associated with an effective condensation temperature, below which phase coherence is maintained over the solution length scale. Below this temperature the descriptions of atomic Bose-Einstein condensates we present in this thesis are applicable to such systems. Indeed, it can be explicitly shown that the ground states of the mean-field, Gross-Pitaevskii description we develop in Section 1.4.2 — which take the form of classical bright solitons — correspond to the exact ground states of the Lieb-Liniger Hamiltonian — which have been termed "quantum solitons" [41] — in the appropriate regimes of temperature, interaction strength, and atom number [176].

1.4 Theoretical description at low temperature

1.4.1 Spontaneous symmetry breaking

Working in the Heisenberg picture [161], the many-body Hamiltonian for the weakly-interacting Bose gas [Eq. (1.9)] can be directly inserted in to the Heisenberg equa-

tion

$$i\hbar\frac{\partial\hat{\Psi}(\mathbf{r})}{\partial t} = [\hat{\Psi}(\mathbf{r}), \hat{H}]\,, \tag{1.14}$$

to yield a full equation of motion [50]. Unfortunately the resulting equation of motion is intractable. This necessitates the development of approximate methods in order to describe and understand the dynamics of atomic BECs. The most common such approximate method is the *symmetry-breaking* technique: Today, the concept of spontaneous symmetry-breaking is commonly associated with the physics of elementary particles, where it is of crucial importance [177]. However, symmetry breaking actually has a longer history in the field of condensed matter physics [160]. In particular, it has a long and distinguished role in the history of the weakly-interacting Bose gas, having been first applied to this system by Bogoliubov [156].

As applied to the weakly-interacting Bose gas, the symmetry-breaking technique is reviewed in depth elsewhere, both in the formalism of equations of motion for field operators as used here [1, 50, 83, 158, 160, 178] and in the alternative formalism of many-body and finite-temperature Green's functions [179, 180]. It essentially consists of re-writing the field operator $\hat{\Psi}(\mathbf{r})$ as its own expectation value, plus an operator-valued fluctuation:

$$\hat{\Psi}(\mathbf{r}) = \left\langle\hat{\Psi}(\mathbf{r})\right\rangle + \left(\hat{\Psi}(\mathbf{r}) - \left\langle\hat{\Psi}(\mathbf{r})\right\rangle\right) \equiv \Psi(\mathbf{r}, t) + \hat{\delta}(\mathbf{r}, t)\,. \tag{1.15}$$

The notational simplicity of this manoeuvre belies the powerful concept underneath. The most obvious effect of introducing the macroscopic wavefunction $\Psi(\mathbf{r}, t)$, here chosen to be normalized to the number of condensate particles $N_c(t)$, is the breaking of the global $U(1)$ symmetry of the Hamiltonian (1.6). Bogoliubov's original motivation for doing so can be understood with reference to the Penrose-Onsager definition of Bose-Einstein condensation[5]; separating out the contribution of the condensate mode to the field operator [83] yields

$$\hat{\Psi}(\mathbf{r}) = \hat{a}_c\phi_c(\mathbf{r}, t) + \sum_{m\neq c}\hat{a}_m\phi_m(\mathbf{r}, t)\,. \tag{1.16}$$

The symmetry-breaking partition of the field operator follows from replacing the operator $\hat{a}_c$ with a complex number $\sqrt{N_c(t)}e^{i\Phi}$, where Φ is an arbitrary phase. This replacement [Eq. (1.15)], which results in the symmetry-breaking condensate wavefunction $\Psi(\mathbf{r}, t) = \sqrt{N_c(t)}e^{i\Phi}\phi_c(\mathbf{r}, t)$, can be justified in the limit $N_c(t) = \langle\hat{a}_c^\dagger\hat{a}_c\rangle \gg 1$; for large particle numbers the operators $\hat{a}_c$ and $\hat{a}_c^\dagger$ approximately commute [their

---

[5]Although, we note, this definition had yet to be formulated at the time.

commutator, equal to one, is much less than their magnitude $\sqrt{N_c(t)}$]. However, as we discuss in detail in Chapter 5, this symmetry-breaking partition breaks the original $U(1)$ gauge symmetry of the Hamiltonian, leading to non-conservation of the total atom number.

In terms of the off-diagonal long-range order considered in the previous Section, $\Psi(\mathbf{r}, t)$ can also be viewed as a macroscopic wavefunction introduced to give a non-zero value of the single-particle density matrix in the long range limit

$$\lim_{|\mathbf{r}-\mathbf{r}'|\to\infty} \rho(\mathbf{r}, \mathbf{r}', t) = \Psi^*(\mathbf{r}', t)\Psi(\mathbf{r}, t), \tag{1.17}$$

without any microscopic justification. Hence, the symmetry-breaking approach can be viewed as making a connection between the microscopic picture of the weakly-interacting Bose gas below the critical temperature T_c, and the macroscopic picture of a quantum fluid exhibiting off-diagonal long-range order described by a macroscopic order parameter.

At lowest order, as we present in the next Section, the symmetry-breaking approach leads to the Gross-Pitaevskii equation for $\Psi(\mathbf{r}, t)$. This equation describes the dynamics of the condensate, which at this (lowest) order comprises all the atoms. At higher orders it is possible to obtain descriptions of coupled condensate and non-condensate dynamics, in terms of coupled equations for $\psi(\mathbf{r}, t)$ and $\hat{\delta}(\mathbf{r}, t)$, using the same symmetry-breaking approach [50]; such descriptions are discussed in detail in Chapter 5, in Part II of this thesis. However, as we shall demonstrate in Chapter 5, such equations cannot be made to preserve orthogonality between $\psi(\mathbf{r}, t)$ and $\hat{\delta}(\mathbf{r}, t)$ in a self-consistent way. This blurring of the distinction between condensate and non-condensate during dynamical evolution can be undesirable, and avoiding such blurring motivates the introduction of alternative, number-conserving, approaches to coupled condensate – non-condensate dynamics [66–71, 163, 181] which we extend and apply in Part II of this thesis.

1.4.2   The Gross-Pitaevskii equation

Symmetry-breaking fluctuation expansion

Equations of motion for the weakly-interacting Bose gas based on Bogoliubov's original symmetry-breaking approach are obtained through a *fluctuation expansion* in terms of the operator $\hat{\delta}(\mathbf{r}, t)$. This operator is a well-defined fluctuation operator; its expectation value is equal to zero, giving $\hat{\Psi}(\mathbf{r})$ a mean value of $\Psi(\mathbf{r}, t)$, and the

expectation values of second-order products of $\hat{\delta}(\mathbf{r}, t)$ and $\hat{\delta}^\dagger(\mathbf{r}, t)$ are analogous to the variance of a distribution about the mean $\Psi(\mathbf{r}, t)$ [68]. Importantly, because $\hat{\delta}(\mathbf{r}, t)$ scales with the number of non-condensate atoms, we can justifiably neglect terms of high order in $\hat{\delta}(\mathbf{r}, t)$ or $\hat{\delta}^\dagger(\mathbf{r}, t)$ when dealing with a low-temperature atomic BEC with large condensate fraction.

After making the replacement (1.15) in the weakly-interacting Bose gas Hamiltonian (1.9), we can collect the terms in the resulting expansion together into powers of $\hat{\delta}(\mathbf{r}, t)$ and $\hat{\delta}^\dagger(\mathbf{r}, t)$. Because of the number non-conservation in the symmetry-breaking treatment, it is appropriate to work with a grand canonical Hamiltonian $\hat{H}' = \hat{H} - \mu\hat{N}$, where $\hat{N}$ is the number operator $\hat{\Psi}^\dagger(\mathbf{r})\hat{\Psi}(\mathbf{r})$ and μ is the chemical potential [50]. In the remainder of this Chapter, we drop the prime and write $\hat{H}$ directly in grand canonical form as

$$\hat{H} = H_0 + \hat{H}_1 + \hat{H}_2 + \hat{H}_3 + \hat{H}_4 \,, \tag{1.18}$$

where

$$H_0 = \int d\mathbf{r}\, \Psi^*(\mathbf{r}, t)\left(H_{\mathrm{sp}}(\mathbf{r}, t) - \mu + \frac{U_0}{2}|\Psi(\mathbf{r}, t)|^2\right)\Psi(\mathbf{r}, t)\,, \tag{1.19}$$

$$\hat{H}_1 = \int d\mathbf{r}\,\left[\hat{\delta}^\dagger(\mathbf{r}, t)\left(H_{\mathrm{sp}}(\mathbf{r}, t) - \mu + U_0|\Psi(\mathbf{r}, t)|^2\right)\Psi(\mathbf{r}, t) + \mathrm{h.c.}\right]\,, \tag{1.20}$$

$$\hat{H}_2 = \int d\mathbf{r}\,\left[\hat{\delta}^\dagger(\mathbf{r}, t)\left(H_{\mathrm{sp}}(\mathbf{r}, t) - \mu + 2U_0|\Psi(\mathbf{r}, t)|^2\right)\hat{\delta}(\mathbf{r}, t)\right.$$
$$\left. + \frac{U_0}{2}\left(\Psi^{*2}(\mathbf{r}, t)\hat{\delta}(\mathbf{r}, t)\hat{\delta}(\mathbf{r}, t) + \mathrm{h.c.}\right)\right]\,, \tag{1.21}$$

$$\hat{H}_3 = U_0 \int d\mathbf{r}\,\left[\Psi(\mathbf{r}, t)\hat{\delta}^\dagger(\mathbf{r}, t)\hat{\delta}^\dagger(\mathbf{r}, t)\hat{\delta}(\mathbf{r}, t) + \mathrm{h.c.}\right]\,, \tag{1.22}$$

$$\hat{H}_4 = \frac{U_0}{2} \int d\mathbf{r}\,\hat{\delta}^\dagger(\mathbf{r}, t)\hat{\delta}^\dagger(\mathbf{r}, t)\hat{\delta}(\mathbf{r}, t)\hat{\delta}(\mathbf{r}, t)\,. \tag{1.23}$$

Here, h.c. denotes the Hermitian conjugate, and we have defined the *single-particle Hamiltonian*

$$H_{\mathrm{sp}}(\mathbf{r}, t) = -\frac{\hbar^2}{2m}\nabla^2 + V(\mathbf{r}, t)\,. \tag{1.24}$$

Gross-Pitaevskii equation

Naturally, the lowest-order approach to the weakly-interacting Bose gas in this formulation is to discard all terms except H_0. This term has no operator character and is simply a complex-number quantity; consequently, this lowest-order approach is equivalent to treating the condensate as a *classical field*. The equation of motion for

$\Psi(\mathbf{r}, t)$ can be obtained simply by taking the functional derivative of H_0 with respect to $\Psi^*(\mathbf{r}, t)$,

$$i\hbar \frac{\partial \Psi(x, t)}{\partial t} = \frac{\delta H_0[\Psi(\mathbf{r}, t)]}{\delta \Psi^*(\mathbf{r}, t)} . \tag{1.25}$$

This yields the *Gross-Pitaevskii equation* (GPE)

$$i\hbar \frac{\partial \Psi(x, t)}{\partial t} = \left[H_{\mathrm{sp}} - \mu + U_0 |\Psi(\mathbf{r}, t)|^2 \right] \Psi(\mathbf{r}, t) , \tag{1.26}$$

where we have implicitly taken $N_c(t) = N$ because at this lowest order of description all atoms can be considered to be in the condensate. In Part I of this thesis we will also make frequent reference to the equation satisfied by stationary solutions of Eq. (1.26), the time-independent GPE

$$\left[H_{\mathrm{sp}} - \mu + U_0 |\Psi(\mathbf{r})|^2 \right] \Psi(\mathbf{r}) = 0 . \tag{1.27}$$

It is also possible to derive the GPE by attempting to construct a zeroth-order equation of motion for $\hat{\delta}(\mathbf{r}, t)$; this alternative is more insightful when one comes to extend the approach to higher orders in $\hat{\delta}(\mathbf{r}, t)$. In this case to obtain a zeroth-order equation of motion one substitutes Eq. (1.15) and a first-order Hamiltonian $\hat{H} = H_0 + \hat{H}_1$ into the Heisenberg equation of motion [Eq. (1.14)]. Subsequently taking an expectation value and using the identities

$$\left\langle \hat{\delta}(\mathbf{r}, t) \right\rangle = 0 , \tag{1.28}$$

and

$$\left[\hat{\delta}(\mathbf{r}, t), \hat{\delta}^\dagger(\mathbf{r}', t) \right] = \delta(\mathbf{r} - \mathbf{r}') , \tag{1.29}$$

both of which follow from Eq. (1.15), yields the GPE of Eq. (1.26).

Alternative interpretations

The derivation of the GPE presented above is valid for temperatures approaching $T = 0$ in the presence of a macroscopically-occupied mode. In particular, it involves the approximation that all atoms occupy this mode. Hence, in this regime, the GPE can be interpreted as describing a *single-particle wavefunction*, $\Psi(\mathbf{r}, t)$ which is shared by all particles through a *many-particle wavefunction* of the Hartree product form

$$\Psi(\mathbf{r}_1, \mathbf{r}_2, \ldots, \mathbf{r}_N) = \prod_{i=1}^{N} \Psi(\mathbf{r}_i, t) . \tag{1.30}$$

However, this *Hartree-product interpretation* is not the exclusive many-body interpretation of the GPE. The same GPE can also be considered as a classical field description of a multi-mode quantum field in the regime where *many* modes are highly occupied (typically taken as $n_i \gtrsim 5$ [182]). This interpretation is central to the description of finite-temperature BECs using *c-field methods* [171], and formally arises through a truncated Wigner expansion of the quantum field [171, 182]. In particular, the GPE is the leading-order description of the quantum field in the regime close to T_c, where many modes are highly occupied, and the temperature is sufficiently high for quantum fluctuations to be neglected; the truncated Wigner description appears at the next order [183]. In rigorous *c*-field approaches this GPE is slightly modified by the presence of an explicit projector into the *c*-field regime, yielding the so-called projected GPE (PGPE) [171, 184]: the application of *c*-field methods to finite temperature atomic BECs are briefly reviewed in Chapter 5.

This PGPE has been used successfully to treat problems around T_c, such as the interaction-shift of T_c [170]. The "pure" GPE (with no explicit projector) has also been used successfully in this regime, for example in studies of quantum turbulence [123–126]. This interpretation of the pure GPE has also been shown to be useful for driven systems at low temperature of the type considered in Chapter 7 [60]. Intriguingly, a recent study of quasi-1D scattering between a bright soliton and a δ-function has shown that even in a zero-temperature situation the GPE can evolve to a configuration where a simple Hartree-product interpretation of the many-body wavefunction is energetically forbidden [81]. Thus, whilst a Hartree-product interpretation of the GPE remains the most widely appropriate interpretation at low temperature, one must be wary of it when describing complex dynamics.

1.4.3   Quadratic Hamiltonian and static Bogoliubov-de Gennes equations

Since the realization of atomic BEC in 1995 the GPE has proved to be a remarkably good quantitative description of this new phenomenon. Indeed, the GPE provides quantitatively useful results at temperatures up to $T_c/2$ [1]. However, at low-temperature equilibrium, it can be safely interpreted as assuming all atoms to be in the condensate (the aforementioned Hartree-product interpretation). In an interacting atomic BEC this is never quite the case: even at $T = 0$ inter-atomic interactions lead to a *quantum depletion* of the condensate, and the introduction of quantum correlations into the system. Understanding the dynamics of atomic BEC at finite temperatures and far from equilibrium — where the non-condensate frac-

tion is significant, interacts strongly and exchanges population with the condensate, and introduces significant correlations into the system — requires a higher-order approach.

The development and implementation of higher-order dynamical approaches forms the basis of Part II of this thesis, and we defer a substantive introduction to Chapter 5. However, an explanation of one of the defining features of an atomic BEC — its superfluidity — is facilitated by a brief consideration of the simplest possible symmetry-breaking treatment beyond the GPE; this takes into account the quadratic part of the Hamiltonian, $\hat{H}_2$, for a static condensate. This quadratic Hamiltonian can be written as:

$$\hat{H}_2 = \iint d\mathbf{r}\, d\mathbf{r}' \left[\hat{\delta}^\dagger(\mathbf{r}) L(\mathbf{r}, \mathbf{r}') \hat{\delta}(\mathbf{r}') + \frac{1}{2} \hat{\delta}^\dagger(\mathbf{r}) M(\mathbf{r}, \mathbf{r}') \hat{\delta}^\dagger(\mathbf{r}') + \frac{1}{2} \hat{\delta}(\mathbf{r}) M^*(\mathbf{r}, \mathbf{r}') \hat{\delta}(\mathbf{r}') \right],$$

$$(1.31)$$

where

$$L(\mathbf{r}, \mathbf{r}') = \delta(\mathbf{r} - \mathbf{r}') \left[H_{\mathrm{sp}}(\mathbf{r}') - \mu + 2U_0 |\Psi(\mathbf{r}')|^2 \right], \qquad (1.32)$$

and

$$M(\mathbf{r}, \mathbf{r}') = \delta(\mathbf{r} - \mathbf{r}') U_0 \Psi^2(\mathbf{r}'). \qquad (1.33)$$

Provided $\Psi(\mathbf{r})$ satisfies the time-independent GPE [Eq. (1.27)], $\hat{H}_2$ is the only operator-valued part of the Hamiltonian up to second-order in $\hat{\delta}(\mathbf{r})$: satisfaction of the time-independent GPE causes $\hat{H}_1$ to vanish identically, and H_0 is not operator valued. Using the commutation relation $[\hat{\delta}(\mathbf{r}), \hat{\delta}^\dagger(\mathbf{r}')] = \delta(\mathbf{r} - \mathbf{r}')$, Eq. (1.31) can be rewritten in the form

$$\hat{H}_2 = \frac{1}{2} \iint d\mathbf{r}\, d\mathbf{r}' \left(\hat{\delta}^\dagger(\mathbf{r}), -\hat{\delta}(\mathbf{r}) \right) \begin{pmatrix} L(\mathbf{r}, \mathbf{r}') & M(\mathbf{r}, \mathbf{r}') \\ -M^*(\mathbf{r}, \mathbf{r}') & -L^*(\mathbf{r}, \mathbf{r}') \end{pmatrix} \begin{pmatrix} \hat{\delta}(\mathbf{r}') \\ \hat{\delta}^\dagger(\mathbf{r}') \end{pmatrix}$$
$$- \frac{1}{2} \iint d\mathbf{r}\, d\mathbf{r}' \, \delta(\mathbf{r} - \mathbf{r}') L(\mathbf{r}, \mathbf{r}'). \quad (1.34)$$

While non-standard, the representation we use in Eq. (1.34) is chosen to closely match that used in Part II of this thesis. Unfortunately this has the side-effect of leaving the divergence in the final term of Eq. (1.34) somewhat opaque. This term contains an ultraviolet divergence which arises from use of the first-order Born approximation for U_0 beyond its regime of validity; however, this divergence can be

renormalized by appropriate application of the second-order Born approximation [83, 161]. In order to reduce the non-divergent, operator part of $\hat{H}_2$ to diagonal form, one can make the *Bogoliubov transformation*

$$\begin{pmatrix} \hat{\delta}(\mathbf{r}) \\ \hat{\delta}^\dagger(\mathbf{r}) \end{pmatrix} = \sum_k \hat{b}_k \begin{pmatrix} u_k(\mathbf{r}) \\ v_k(\mathbf{r}) \end{pmatrix} + \hat{b}_k^\dagger \begin{pmatrix} v_k^*(\mathbf{r}) \\ u_k^*(\mathbf{r}) \end{pmatrix} ,$$ (1.35)

where the mode functions $u_k(\mathbf{r})$ and $v_k(\mathbf{r})$ diagonalize the matrix operator of Eq. (1.34)

$$\int d\mathbf{r} \begin{pmatrix} L(\mathbf{r}, \mathbf{r}') & M(\mathbf{r}, \mathbf{r}') \\ -M^*(\mathbf{r}, \mathbf{r}') & -L^*(\mathbf{r}, \mathbf{r}') \end{pmatrix} \begin{pmatrix} u_k(\mathbf{r}') \\ v_k(\mathbf{r}') \end{pmatrix} = \epsilon_k \begin{pmatrix} u_k(\mathbf{r}) \\ v_k(\mathbf{r}) \end{pmatrix} .$$ (1.36)

Eq. (1.36) are commonly known as the *Bogoliubov-de Gennes equations* (BdGE).

The operators $\hat{b}_k^\dagger$ and $\hat{b}_k$ are *quasiparticle* creation and annihilation operators. If one additionally imposes the normalization condition

$$\int d\mathbf{r} \left[|u_k(\mathbf{r})|^2 - |v_k(\mathbf{r})|^2 \right] = 1 ,$$ (1.37)

on the quasiparticle mode functions $u_k(\mathbf{r})$ and $v_k(\mathbf{r})$, then these operators obey the canonical commutation relations $[\hat{b}_k, \hat{b}_l^\dagger] = \delta_{k,l}$ and $[\hat{b}_k, \hat{b}_l] = [\hat{b}_k^\dagger, \hat{b}_l^\dagger] = 0$ and diagonalize the quadratic Hamiltonian $\hat{H}_2$ to give

$$\hat{H}_2 = \sum_k \left[\epsilon_k \hat{b}_k^\dagger \hat{b}_k - \epsilon_k \int d\mathbf{r} \, |v_k(\mathbf{r})|^2 \right] ,$$ (1.38)

where we have correctly renormalized the divergent constant term (see above). In Eq. (1.38), we have a description of a weakly-interacting Bose gas, up to second-order in $\hat{\delta}(\mathbf{r})$, which consists of *non-interacting* Bogoliubov quasiparticles. These quasiparticles are thus the elementary excitations of the system, and their dispersion relation is given by ϵ_k. While only valid up to second-order in $\hat{\delta}(\mathbf{r})$, this already provides an extremely useful physical insight into the weakly-interacting Bose gas.

1.4.4   Superfluidity

Perhaps the most interesting property of the weakly-interacting Bose gas is its superfluidity. The first experimental realization of superfluidity was in liquid ^{4}He, observed jointly by Kapitza [114] and Allen and Misener [115] in 1938. It was suggested almost immediately by London [185] and Tisza [186] that the phenomenon of superfluidity was due to the presence of a Bose-Einstein condensed fraction in
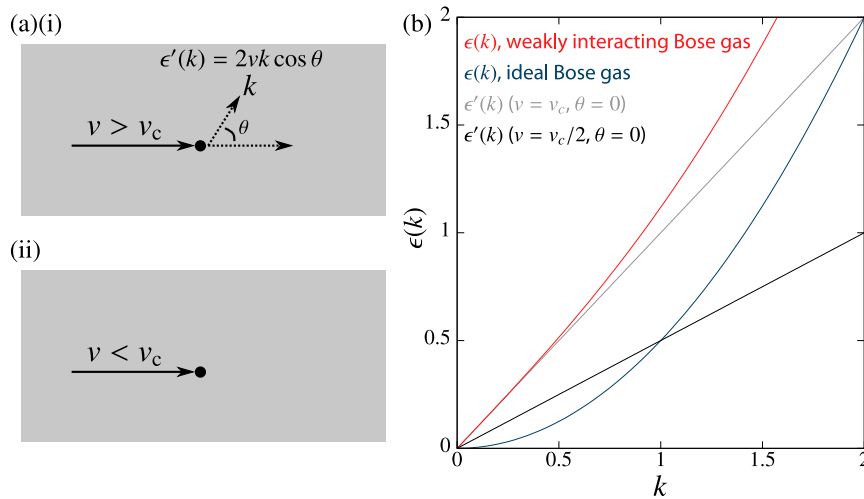
Figure 1.1: Origin of superfluidity in a homogeneous weakly-interacting Bose gas [for convenience, we set $\hbar = m = U_0 n_c = 1$, where n_c is the (uniform) condensate density]: (a) illustrates an external impurity moving with velocity v in a static fluid, which can elastically scatter elementary excitations in the fluid with wavevector k, if the condition $\epsilon'(k) = \epsilon(k)$ is satisfied. Here $\epsilon(k)$ is the energy of an elementary excitation with wavevector k, and $\epsilon'(k)$ is the energy change associated with the elastic scattering event. (a)(i) shows the situation in a superfluid where v exceeds the critical velocity v_c [or, equivalently, the case of a normal fluid with dispersion relation $\epsilon(k) = k^2/2$]. In this case it is always possible to satisfy $\epsilon(k) = \epsilon'(k)$ for some θ, as shown in (b), leading to creation of quasiparticle excitations. The resulting transfer of momentum gives rise to viscosity. (a)(ii) Shows the case of a weakly-interacting Bose gas with $v < v_c$. In this case, as shown in (b), the Bogoliubov dispersion relation [Eq. (1.39)] makes it impossible to satisfy $\epsilon(k) = \epsilon'(k)$, and hence the impurity cannot create quasiparticle excitations, giving rise to superfluidity.

the gas. However, this interpretation remained controversial for some time, especially when the first quantitatively successful description of superfluidity in ^{4}He, given by Landau in 1941 [187], made no reference to Bose-Einstein condensation [157, 160]. Instead, Landau considered the role of the excitation spectrum of elementary excitations in a fluid. Using this approach he showed, through a simple physical argument, that the observed excitation spectrum of liquid ^{4}He suppressed the creation of elementary excitations below a certain threshold velocity [Fig. 1.1.] However, this phenomenological explanation made no attempt to explain how an excitation spectrum leading to superfluidity arises in liquid ^{4}He on a microscopic

level.

In the case of a weakly-interacting Bose gas, the pioneering work of Bogoliubov [156] on the static quadratic Hamiltonian — which we have outlined in the previous Section — provides exactly such an explanation. In the infinite, homogeneous case, with uniform condensate, the quasiparticle modes are simply plane waves: $u_k(\mathbf{r}) = U_k e^{i\mathbf{k}\cdot\mathbf{r}}$, $v_k(\mathbf{r}) = V_k e^{-i\mathbf{k}\cdot\mathbf{r}}$. The dispersion relation is given by

$$\epsilon(\mathbf{k}) = \sqrt{\frac{\hbar^2 k^2}{2m}\left(\frac{\hbar^2 k^2}{2m} + 2U_0 n_c\right)}, \qquad (1.39)$$

where n is the number density of the condensate. This celebrated *Bogolibov dispersion relation* is free-particle like at large momentum $\mathbf{k}$, but phonon-like at small momentum. This feature immediately gives rise to superfluidity via the mechanism introduced by Landau, as illustrated in Fig. 1.1, with critical velocity $v_c = \sqrt{U_0 n_c / \hbar m}$.

However, while Bogoliubov demonstrated that a weakly-interacting Bose gas gives rise to superfluidity, the interactions in liquid ^{4}He are in reality quite strong, and lead to an elementary excitation spectrum which is significantly different from the Bogoliubov spectrum [Eq. (1.39)]. Consequently the GPE, and higher-order descriptions of the weakly-interacting Bose gas, fail to give a general quantitative description of liquid ^{4}He. The presence of a condensate at $T = 0$ in equilibrium liquid ^{4}He has been demonstrated using quantum Monte-Carlo methods [189], but the condensate fraction is estimated to only be around 10% due to the considerable strength of the interactions[6]. Despite this low condensate fraction, the superfluid fraction of liquid ^{4}He remains significant (>90%) for $T \ll T_c$ because there are few thermally excited quasiparticles, and below the critical velocity it is impossible to excite more. Indeed, the fact that the large quantum-depleted fraction participates in superflow is what makes a description of superfluid ^{4}He in terms of a macroscopic order parameter possible.

The distinction between non-condensate fraction and superfluid fraction is often ignored in the field of atomic BECs, where the quantum depletion is typically less than 1% [see Fig. 1.2]. Here the condensate and superfluid fractions can be considered to be equivalent for many purposes. Nonetheless, proposals to experimentally determine the superfluid fraction independently of the condensate fraction exist [147], and offer an interesting challenge for future experiments.

---

[6]It is interesting to note that Penrose and Onsager achieved a very accurate prediction of the non-condensate fraction, 8%, using an approximate many-body wavefunction, in Ref. [173].
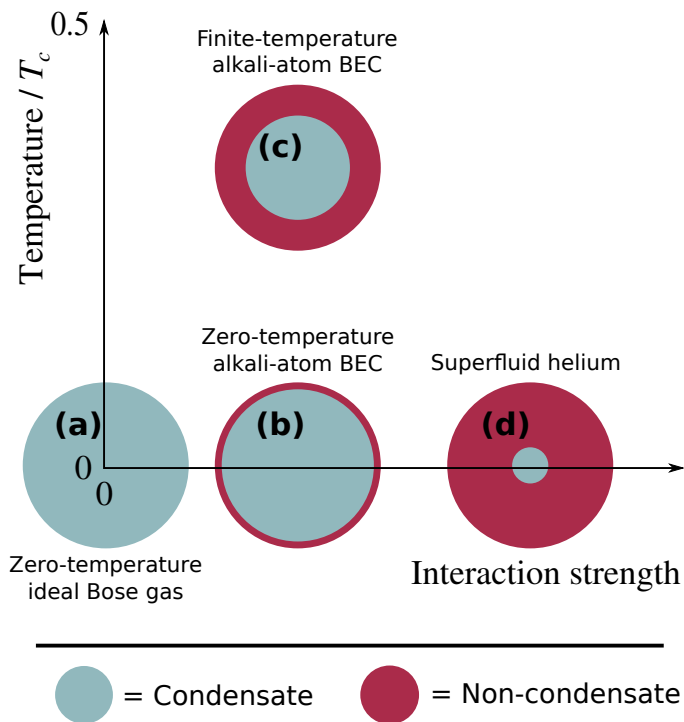
Figure 1.2: Illustrated condensate-to-non-condensate ratios for Bose gases at various interaction strengths and temperatures. Whilst the ideal (non-interacting) Bose gas, (a), has no non-condensate fraction at $T = 0$, the weak interactions present in atomic Bose gases create a small [less than 1% for typical experimental atom numbers [188]] non-condensate fraction even at $T = 0$, (b). The non-condensate fraction in atomic Bose gases grows with temperature, (c), but sufficiently slowly that condensate-only equations of motion yield useful results at temperatures as high as $T_c/2$. Because of strong inter-particle interactions, the non-condensate fraction of liquid ^{4}He, (d), at $T = 0$ is estimated to be around 90% [173, 189].

Part I

Bright solitary waves

Chapter 2: Solitons and solitary waves in atomic Bose-Einstein condensates

2.1 Introduction

Bright solitary waves [10–12] are nonlinear, self-focusing wavepackets occurring in atomic BECs with attractive inter-atomic interactions (with negative s-wave scattering length $a_s < 0$). In the quasi-one-dimensional (quasi-1D), homogeneous limit, bright solitary waves become completely analogous — within the mean-field (GPE) description — to classical bright solitons of the 1D, focusing nonlinear Schödinger equation (NLSE) [190–192]. The classical bright soliton solutions of this equation have been extensively studied in the context of optical solitons [16–19, 193, 194]. The same equation, and its bright soliton solutions, appear in many other fields, including biophysics, astrophysics and particle physics [195], and in the study of deep ocean waves [14]. Within the context of this thesis, bright solitary waves in atomic BECs have the potential to form a rich and fertile testing ground for theoretical descriptions going beyond the mean-field model, which we discuss in Part II of this thesis. Several of the properties of bright solitary waves are relevant in this regard: they typically contain $\lesssim 1000$ atoms, placing them well-outside the thermodynamic limit and potentially outside the reach of the mean-field description; they constitute macroscopic quantum objects, and hence the coherence between bright solitary waves plays a key role in their collisions, and must be correctly accounted for in any theoretical model; and, finally, their dynamics can provide a sensitive experimental test of the various theoretical descriptions discussed in Chapter 5, potentially over a large portion of the $T = 0$ to $T = T_c$ temperature range.

In this Chapter we give an overview of the properties of bright solitary waves, in various regimes of trap and interaction strength, in the mean-field description. We emphasise two properties in particular: Firstly, the analogy of bright solitary waves to the bright soliton solutions of the NLSE; it is this analogy which underlies their soliton-like properties of non-dispersion, robustness against mutual collisions, and propagation along particle-like trajectories. Secondly, we emphasise the importance of the collapse instability of attractive condensates in three dimensions (3D); this instability means that bright solitary waves can only be realized in a restricted pa-

rameter regime, and that they only ever represent a metastable state of the system.

We begin by defining the quasi-1D limit of the GPE, obtained in the limit of strong radial trapping (Section 2.2.1). In the case of an axially homogeneous external potential this quasi-1D reduces to the 1D focusing NLSE. We then review the bright soliton solutions of this equation — which are solitons in the exact mathematical sense of the inverse scattering transform; in Section 2.2.2 we describe the single-bright soliton solution, and in Section 2.2.3 the multiple-bright soliton solution. In Section 2.2.4 we review the dynamics of NLSE bright solitons, which can be described by a phase-independent particle model with short-range interactions between solitons. In Section 2.3 we consider the bright solitary waves which exist in the quasi-1D GPE with a harmonic external axial potential. While these no longer satisfy the mathematical requirements to be true solitons (Section 2.3.1), their dynamics are nonetheless highly soliton-like, and can be described by an adapted particle model (Section 2.3.2).

In Section 2.4 we discuss bright solitary waves in 3D. The properties of such waves are fundamentally linked to the collapse instability of attractive condensates in 3D, which we introduce in Section 2.4.1. The collapse instability restricts the realization of bright solitary wave solutions to certain parameter regimes, which we explore in Section 2.4.2 and Section 2.4.3, using variational and numerical methods. Finally, in Section 2.4.4, we discuss the dynamics of 3D bright solitary waves in waveguide-like (axially homogeneous) trap potentials.

Having introduced this relevant background, in the remainder of Part I of this thesis (Chapters 3 and 4) we explore the experimental production of bright solitary waves, and the dynamics and soliton-likeness of 3D bright solitary waves in prolate harmonic traps. We also discuss the role of beyond mean-field effects on solitary wave dynamics and propose an experimental test of the applicability of the mean-field description, examine the possibility of constructing a bright solitary wave interferometry device, and quantitatively assess the feasibility of conducting future experiments which realize the effective quasi-1D limit we introduce in this Chapter.

2.2 Bright solitons in the NLSE

2.2.1 Quasi-one-dimensional limit

Quasi-one-dimensional GPE

As outlined in Chapter 1, the mean-field description of an attractively-interacting, 3D atomic BEC in a general potential $V(\mathbf{r})$ is given by the Gross-Pitaevskii equation [83]

$$i\hbar\frac{\partial\psi(\mathbf{r})}{\partial t} = \left[-\frac{\hbar^2}{2m}\nabla^2 + V(\mathbf{r}) - \frac{4\pi\hbar^2 N|a_s|}{m}|\psi(\mathbf{r})|^2\right]\psi(\mathbf{r}),\qquad(2.1)$$

where N is the number of atoms, and the macroscopic wavefunction, or order parameter, $\psi(\mathbf{r})$, is normalized to unity. In typical experiments the external potential $V(\mathbf{r})$ is approximately harmonic and of the form $V(\mathbf{r}) = m(\omega_x^2 x^2 + \omega_y^2 y^2 + \omega_z^2 z^2)/2$; within Part I of this thesis we will generally assume such a potential. Attractive interactions imply that the s-wave scattering length $a_s < 0$.

The time-independent eigenstate solutions of Eq. (2.1) obey the stationary GPE

$$\left[-\frac{\hbar^2}{2m}\nabla^2 + V(\mathbf{r}) - \frac{4\pi\hbar^2 N|a_s|}{m}|\psi(\mathbf{r})|^2 - \mu\right]\psi(\mathbf{r}) = 0,\qquad(2.2)$$

where μ is a (real) eigenvalue, equivalent to the chemical potential at mean-field level (Chapter 1). The lowest-energy solution to Eq. (2.2) represents the static mean-field ground state of the BEC.

The quasi-1D limit is associated with cylindrically symmetric ($\omega_y = \omega_z = \omega_r$) and highly anisotropic, prolate ($\omega_r \gg \omega_x$) traps. For sufficiently strong radial confinement, one can assume that the radial modes of the condensate will remain "frozen" into the relevant harmonic oscillator ground state, allowing the factorization

$$\psi(\mathbf{r}) = \sqrt{\frac{m\omega_r}{\pi\hbar}}\exp\left[\frac{-m\omega_r(y^2 + z^2)}{2\hbar}\right]\psi(x).\qquad(2.3)$$

Integrating over the y- and z-directions (and dropping constant terms) then yields the quasi-1D GPE for $\psi(x)$ [20, 45];

$$i\hbar\frac{\partial\psi(x)}{\partial t} = \left[-\frac{\hbar^2}{2m}\frac{\partial^2}{\partial x^2} + \frac{m\omega_x^2 x^2}{2} - 2\hbar\omega_r N|a_s||\psi(x)|^2\right]\psi(x).\qquad(2.4)$$

This reduces to the standard focusing 1D NLSE in the axially untrapped limit ($\omega_x \rightarrow$

0). In the static case, one obtains the stationary quasi-1D GPE

$$\left[-\frac{\hbar^2}{2m}\frac{\partial^2}{\partial x^2} + \frac{m\omega_x^2 x^2}{2} - 2\hbar\omega_r N|a_s||\psi(x)|^2 - \mu\right]\psi(x) = 0\,, \tag{2.5}$$

which describes the bright solitary wave stationary states of the system.

This factorization has often been applied in the study of attractively-interacting condensates (in both dynamic and static situations) [20, 21, 196–199]. However, the regime in which this factorization is valid can be significantly restricted for attractively-interacting condensates; we will revisit this issue in detail in Chapter 4.

One-dimensional equations with 3D effects

Alternatives to the factorization presented above exist; these yield quasi-1D equations retaining more 3D character than the quasi-1D GPE of Eq. (2.4) by choosing to incorporate the coupling between axial and radial modes, and time-dependent dynamics of the radial modes [200–203]. These effects are manifested in the resulting quasi-1D equation through the appearance of higher-order terms. Consequently, the resulting equations have a wider range of validity than the quasi-1D GPE [Eq. (2.4)], but are no longer isomorphous to the NLSE in the axially untrapped limit $\omega_x \to 0$.

For example, Salasnich *et al.* [200, 201] chose to factorize the 3D GPE wavefunction into a slowly-varying axial function, multiplied by a rapidly varying radial function. The radial function was also given a dependence on the axial function itself; this incorporates the effect unique to attractive interactions in a cigar-shaped trap, where an increase in axial density leads to an associated increase in radial density. A variational calculation then yields [200] the non-polynomial Schrödinger equation

$$i\hbar\frac{\partial\psi(x)}{\partial t} = -\frac{\hbar^2}{2m}\frac{\partial^2\psi(x)}{\partial x^2} + \frac{m\omega_x^2 x^2}{2}\psi(x) + \frac{2\hbar^2|a_s|N|\psi(x)|^2\psi(x)}{ma_r\sqrt{1-2|a_s|N|\psi(x)|^2}}$$
$$+ \frac{\hbar\omega_x}{2}\left(\frac{1}{\sqrt{1-2|a_s|N|\psi(x)|^2}} + \sqrt{1-2|a_s|N|\psi(x)|^2}\right)\psi(x)\,. \tag{2.6}$$

When $|a_s|N|\psi(x)|^2 \ll 1$ for all x, this reduces first to an effective 1D equation with both cubic and quintic nonlinearities [203], and then to the quasi-1D GPE itself. An even more general approach can be taken, incorporating even fewer assumptions about the form of the ground state, but leading to a coupled system of effective 1D equations [202]. Similar reductions also exist for the case of axially rotating

BECs [204] and for effectively 2D situations [205]. However, aside from discussing results obtained by other authors, we do not make use of reductions with extra 3D effects such as Eq. (2.6) in this thesis.

2.2.2   Single-bright-soliton solution

In the homogeneous limit $\omega_x \to 0$, the quasi-1D GPE [Eq. (2.4)] becomes

$$i\hbar \frac{\partial \psi(x)}{\partial t} = \left[-\frac{\hbar^2}{2m} \frac{\partial^2}{\partial x^2} - 2\hbar\omega_r N |a_s| |\psi(x)|^2 \right] \psi(x), \qquad (2.7)$$

which is exactly the standard form of the focusing 1D NLSE [195]. The 1D NLSE is a classical field equation which is integrable, in the sense that its solutions possess an infinite and complete set of conserved quantities [13, 206]. This is analogous to a discrete system which possesses as many conserved quantities as it does degrees of freedom [13, 207]. The integrability of the focusing NLSE leads to a spectrum of true bright soliton solutions [13, 208], first analytically described by Zakharov and Shabat in Ref. [17] using the inverse scattering technique. This technique is a general and powerful framework for identifying analytic solutions to several nonlinear PDEs arising in mathematical physics, including the NLSE [208]. A detailed review of the mathematical details exceeds the scope of this thesis; however, it is informative to understand in principle how *soliton* solutions arise within the inverse scattering framework. The interested reader would be advised to consult Refs. [208, 209] for a deeper overview, and Refs. [13, 17, 18, 206] for advanced technical details.

Put briefly, the inverse scattering technique for the NLSE consists of drawing an analogy between Eq. (2.7) and a so-called Zakharov-Shabat (ZS) system of the form

$$i\zeta \begin{pmatrix} u(x,t) \\ v(x,t) \end{pmatrix} = \begin{pmatrix} -\dfrac{\partial}{\partial x} & \psi(x,t) \\ -\psi^*(x,t) & \dfrac{\partial}{\partial x} \end{pmatrix} \begin{pmatrix} u(x,t) \\ v(x,t) \end{pmatrix}, \qquad (2.8)$$

where $\psi(x,t)$ is a solution of Eq. (2.7). It can be divided into three stages:

Scattering transform Find the eigenvalues of the scattering problem Eq. (2.8) at an initial time t_i, with $\psi(x, t_i)$ as an initial condition. The spectrum of the problem consists of discrete eigenvalues — corresponding to solitons — and a continuous component — corresponding to the radiation (non-soliton) component.

Time evolution of scattering spectrum With some mathematical insight, one can

choose a time evolution equation for $[u(x, t), v(x, t)]^T$ such that the compatibility condition $\partial_{xt}[u(x, t), v(x, t)]^T = \partial_{tx}[u(x, t), v(x, t)]^T$ guarantees that $\psi(x, t)$ solves the NLSE [Eq. (2.7)]. Constructing such an equation allows one to determine the time-evolution of the scattering problem spectrum: while the evolution of the continuous (radiation) component is generally complicated, the discrete (soliton) eigenvalues are time-independent.

Inverse scattering transform The scattering transform can be inverted through an integral equation at a final time t_f to yield $\psi(x, t_f)$.

One can carry out the above procedure analytically for an M-soliton solution, obtaining an expression in terms of $4M$ real parameters. In the case of a single soliton ($M = 1$) one obtains

$$\psi(x, t) = \frac{a}{2\sqrt{b_x}}\text{sech}\left(\frac{a(x - x_0 - vt)}{2b_x}\right)$$
$$\times \exp\left(i\left[\frac{m}{\hbar}\left\{v(x - x_0) + \frac{v^2 t}{2} + \frac{\omega_r^2|a_s|^2 N^2 a^2 t}{2}\right\} + \Phi\right]\right). \quad (2.9)$$

which can be easily verified to solve [Eq. (2.7)]. This solution describes a single bright soliton with norm[1] a, velocity v, displacement x_0, and phase Φ. It propagates at velocity v without dispersing. The parameter $b_x \equiv \hbar/2m\omega_r|a_s|N$ is a length scale characterizing the soliton's spatial extent.

The static case in the homogeneous limit $\omega_x \to 0$ is described by the static NLSE

$$\left[-\frac{\hbar^2}{2m}\frac{\partial^2}{\partial x^2} - 2\hbar\omega_r N|a_s||\psi(x)|^2 - \mu\right]\psi(x) = 0. \quad (2.10)$$

The single-soliton ground state of Eq. (2.10) is given exactly by Eq. (2.9) with $a = 1$, $v = 0$, and arbitrary Φ and x_0. The quantity Φ can be chosen arbitrarily because it corresponds to a global phase of the wavefunction, and Eq. (2.10) possesses a $U(1)$ global phase symmetry. Similarly, the displacement x_0 may be chosen arbitrarily because the static 1D NLSE [Eq. (2.10)] possesses a translational symmetry. However, the choice of displacement x_0 in Eq. (2.9) for the ground state breaks this symmetry; in the context of atomic BECs, this symmetry-breaking is a feature of the mean-field description. This feature is at odds with a fully quantum-mechanical treatment; in the latter, the ground state of the system retains the translational sym-

---

[1] In contrast to our definition here, a common convention in the literature is to define an amplitude A such that the norm is $2A$ [19]

metry of the equation, leading to a delocalized ground state [176].

2.2.3 Multiple-bright-soliton solutions

In multiple-bright-soliton solutions each soliton has a similar form to Eq. (2.9) when well-separated from the others. In such multiple-soliton solutions, the total norm of all solitons is given by $\sum_j a_j$, where a_j is the norm of the jth soliton. If the solution is entirely composed of solitons, then $\sum_j a_j = 1$ is necessary to satisfy our convention that the norm of ψ is 1. These multiple-soliton solutions contain additional, dynamic phase and position shifts to account for the nonlinear interactions between solitons.

The most general M-soliton solution to Eq. (2.7), containing no radiation, can be written as [19]

$$\psi(x,t) = \sum_{j=1}^{M} \psi_j(x,t), \qquad (2.11)$$

where the functions $\psi_j(x,t)$ satisfy the simultaneous equations

$$\sum_{j=1}^{M} \frac{\gamma_k^{-1} + \gamma_j^*}{\lambda_k + \lambda_j^*} \psi_j(x,t) = \frac{1}{\sqrt{b_x}}, \qquad (2.12)$$

for $k = 1 \ldots M$. Here we have defined the quantities

$$\lambda_j = \frac{a_j}{2} + \frac{iv_j}{2\omega_r|a_s|N}, \qquad (2.13)$$

and

$$\gamma_j = \exp\left(\lambda_j\left[\frac{x - x_j}{b_x}\right] + i\lambda_j^2 \frac{2m\omega_r^2 a_s^2 N^2}{\hbar} t + i\Phi_j\right), \qquad (2.14)$$

in addition to the characteristic soliton length b_x. Each soliton is described by a real amplitude a_j, velocity v_j, position offset x_j, and phase Φ_j. In the case that the jth soliton is well-separated from the other $M-1$ solitons, the linear system defined by Eq. (2.12) can be approximately solved to give [19]

$$\psi(x,t) = \frac{a_j}{2\sqrt{b_x}}\mathrm{sech}\left(\frac{a_j(x - x_j - v_jt)}{2b_x} + q_j\right)$$

$$\times \exp\left(i\left[\frac{m}{\hbar}\left\{v_j(x - x_j) + \frac{v_j^2 t}{2} + \frac{\omega_r^2 a_s^2 N^2 a_j^2 t}{2}\right\} + \Phi_j + \Psi_j\right]\right). \quad (2.15)$$

Here, q_j and Ψ_j are time-dependent position- and phase-shifts which appear as a

result of collisions with the other $N - 1$ solitons. They are given by

$$q_j + i\Psi_j = \sum_{k \neq j} \pm \log\left(\frac{a_j + a_k + i(v_j - v_k)/2\omega_r|a_s|N}{a_j - a_k + i(v_j - v_k)/2\omega_r|a_s|N}\right), \qquad (2.16)$$

where the sign is positive when the jth soliton is to the left of the kth, and vice versa [19]. While the jth soliton is well-separated these shifts remain approximately constant, and only change significantly during collisions.

2.2.4 Bright soliton dynamics and collisions

Particle model for multiple solitary waves

With zero (or constant) background potential, the dynamics of a single bright soliton in the NLSE are determined entirely by their nonlinear interactions with the remainder of the solution. We shall focus primarily on dynamics due to soliton-soliton interactions (i.e., on the dynamics of soliton-only solutions) in this thesis. The interaction of solitons with radiation is generally complicated [18, 194, 210–214], and we will deal with it only when the need arises in Chapter 3.

In the absence of radiation, the dynamics of multiple bright solitons are dominated by the interactions and collisions between solitons. One of the defining characteristics of true solitons, associated with the integrability of the system, is that they survive mutual collisions entirely unchanged in form. The only observable effects of the collision are the asymptotic position and phase shifts introduced in Section 2.2.3. The main characteristics of soliton dynamics are illustrated in a solution where two equal-amplitude solitons collide at the origin; this is shown, for various relative phases $\Delta\Phi = \Phi_1 - \Phi_2$, in Fig. 2.1. As expected, the solitons survive such a collision completely unchanged in form, and the position shifts q_j are visible as the deviation of both solitons from their initial linear trajectories. Although the wave dynamics of the collision itself differ with the relative phase $\Delta\Phi$, the position shift q_j is unchanged.

This independence of the position shifts q_j from the solitons' relative phase $\Delta\Phi$ allows one, in principle, to predict their asymptotic trajectories independently of their phase. Disregarding the phase information in this way leaves each soliton described by a position, velocity, and amplitude. One can then treat the solitons as classical particles with an effective mass proportional to their norm and some appropriate inter-particle potential. This approach was developed for optical NLSE
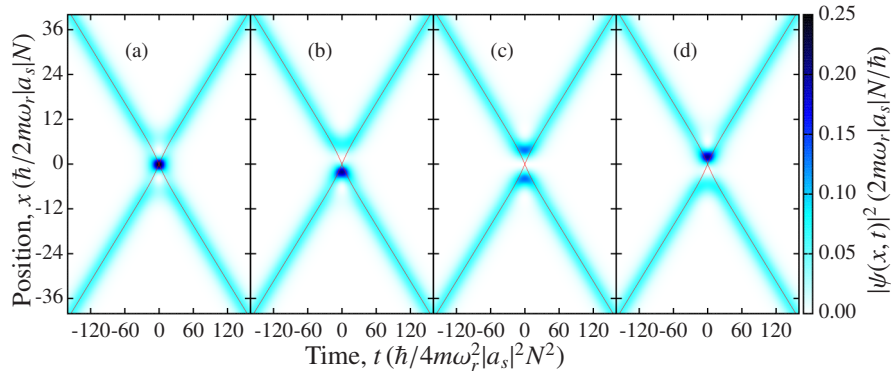
Figure 2.1: Bright soliton collisions in the nonlinear Schrödinger equation, for solitons with equal amplitude and relative phase $\Delta\Phi = 0$ (a), $\pi/2$ (b), π (c), and $3\pi/2$ (d). In each case the density profile of the solution is superimposed with the soliton trajectories predicted by a particle model [20, 21]. This phase-independent model fails to describe the dynamics of the collision in detail, but correctly incorporates the asymptotic position shift of the solitons.

solitons [215–218], using the inter-particle potential

$$V(x_j - x_k) = -2\eta_j\eta_k(\eta_j + \eta_k)\text{sech}^2\left(\frac{2\eta_j\eta_k(x_j - x_k)}{b_x(\eta_j + \eta_k)}\right), \qquad (2.17)$$

where the solitons are treated as classical particles of effective mass $\eta_j = a_j/4$. This potential reproduces the correct asymptotic position shifts provided the velocities and effective masses satisfy the condition $|\eta_j - \eta_k| \ll |v_j - v_k|/4\omega_r|a_s|N$ [20]. The particle model therefore reproduces the asymptotic shift exactly for the equal-effective-mass collisions in Fig. 2.1. For non-equal-effective-mass collisions the particle model becomes correct in the limit of a high collision velocity.

2.3 Bright solitary wave dynamics in quasi-1D

2.3.1 Destruction of integrability: bright solitary waves

In the presence of axial harmonic trapping, and assuming a quasi-1D description is appropriate, the mean-field description of atomic BEC dynamics is given by the quasi-1D GPE [Eq. (2.4)] with $\omega_x > 0$. Unlike the 1D NLSE [Eq. (2.7)], this equation is non-integrable. Consequently, it contains no true soliton solutions, in the sense of discrete eigenvalues of a well-defined scattering transform. Nonetheless, as we illustrate in this Section, the quasi-1D GPE with $\omega_x > 0$ continues to support

bright solitary wave solutions, which take the same form as the static eigenstate solutions of the quasi-1D GPE. While they do not satisfy the strict mathematical requirements to be solitons [13, 208], these solutions are soliton-like in so far as: (a) they are non-dispersive due to the attractive inter-atomic interaction; (b) they are extremely robust to mutual collisions; (c) their dynamics can be described by a particle-like model [20, 21].

The possibility to observe solitary waves of this type was examined in considerable generality by Morgan *et al.* in Ref. [219]. In this work, 1D, 2D, and 3D nonlinear Schrödinger equations were considered, with a generalized nonlinear term and both an arbitrary static external potential and an arbitrary time-dependent external potential. Two conditions were found to be necessary for the static eigenstates (i.e., those obtained with the arbitrary time-dependent potential set to zero) to behave as solitary waves: firstly, the nonlinearity must be decoupled from the absolute position — a requirement immediately satisfied by the conventional cubic form of the nonlinearity appearing in the GPE. Secondly, the potential experienced by the eigenstate in a moving frame (including the time-dependent external potential) should differ no more than linearly in the spatial coordinates from the static potential. In the case of the quasi-1D GPE we consider, this second condition is satisfied for any time-dependent potential which is at most linear in x. In this Section we consider only the "non-driven" case with zero time-dependent potential. However, the retention of solitary-wave characteristics under an external linear potential provides an excellent means for experimental control of bright solitary waves; indeed, this concept underpins our work on soliton-splitting in Chapter 3.

We shall also restrict our attention to solitary waves whose form is that of the bright solitary wave ground state; that is, the lowest-energy static eigenstate solution of the quasi-1D GPE. Like NLSE bright solitons, these solitary waves have a single-peak density profile[2]. In this case, and with no time-dependent external potential, the solitary wave has the same spatial profile as the ground state, but its centre of mass moves as a classical particle in the static harmonic potential. If free from the influence of other solitary waves or other components of the solution, its centre of mass undergoes simple harmonic motion [20, 21, 219]. This oscillation of the mean-field GPE ground state is analogous to the Kohn mode of the many-body ground state [176][3].

---

[2]It is also possible to consider multiple-peak solitary waves formed from higher-energy nonlinear stationary states of the quasi-1D GPE, as examined in Ref. [220].

[3]The Kohn mode arises from the Kohn theorem, which guarantees that the true quantum mechanical ground state of N bosons in a harmonic trap can be expressed as a separable tensor product of a

2.3.2   Particle model for multiple solitary waves

Isolated bright solitary waves in the quasi-1D GPE behave as classical particles in a harmonic potential provided they are well-separated from other components of the solution. However, if they are not well-separated their dynamics are influenced by the nonlinear interaction with the other solitary waves[4]. For true bright solitons in the NLSE, the asymptotic effects of such interactions are entirely described by phase and position shifts (Section 2.2.4). For bright solitary waves this is no longer strictly true, but can be considered a satisfactory approximation assuming: (a) that the external potential is approximately constant over the region of the collision, and (b) that the solitary waves are approximately bright-soliton-shaped. Making these approximations, one can combine the particle model of soliton collisions (Section 2.2.4) with the behaviour of a particle in a harmonic trap. This leads to a combined particle model for multiple bright solitary waves in a harmonic trap, which is most accurate for: (a) weaker harmonic traps; (b) faster solitary wave collisions, and; (c) in-phase solitary wave collisions [20, 21].

The dynamics of binary bright solitary wave collisions in the quasi-1D GPE are illustrated in Fig. 2.2. This shows the resulting dynamics when two copies of the bright solitary wave ground state of the trap are displaced by equal and opposite distances from the trap centre. Each ground state contains $N/2$ atoms, such that the total atom number remains fixed at N. As anticipated by the particle model (shown with red lines in Fig. 2.2), the dynamics are dominated by harmonic particle-like motion when the waves are well-separated; however, when the waves collide, periodically, at the trap centre, a soliton-like collision results in a position shift. There is no overall phase shift between collisions [20]. The complex dynamics of three or more solitary waves oscillating and colliding in a harmonic trap can be effectively predicted using the particle model; interestingly, the model is itself non-integrable for three or more solitary waves, leading to chaotic particle-like dynamics [20, 21].

---

single-body wavefunction in the centre of mass coordinate with a general $N - 1$-body wavefunction in the remaining inter-particle coordinates.

[4]Potentially, solitary waves can also interact with non-solitary-wave excitations such as sound waves [221], although we will not consider such interactions in detail in this thesis.
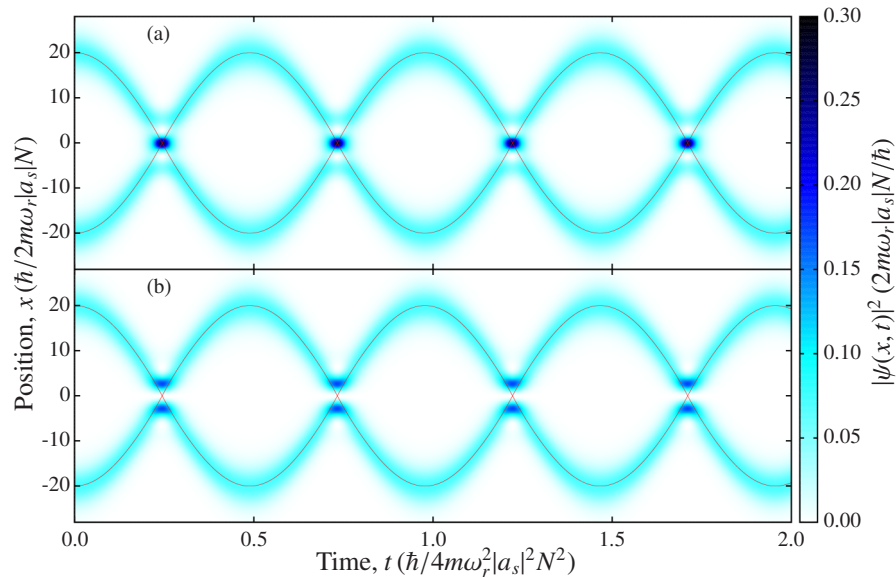
Figure 2.2: Bright solitary wave collisions in the quasi-1D Gross-Pitaevskii equation, with a harmonic axial trap potential. The initial solitary waves are ground states of the trap potential displaced by $\pm \approx 10.35$ in x and with zero initial velocity and relative phase $\Delta\Phi = 0$ (a), and π (b). In each case the density profile of the solution is superimposed with the soliton trajectories predicted by a particle model [20, 21]. This phase-independent model predicts the trajectories well over short times, as shown here. However, over longer times deviations from the model do build up; these deviations are due to the variation of the harmonic axial potential over the characteristic length scale of the collision, and appear first in the case $\Delta\Phi = \pi$ [20, 21].

2.4   Bright solitary waves in three dimensions

2.4.1   The collapse phenomenon and the critical parameter

While a 3D, attractively-interacting BEC is, in general, unstable to collapse, by introducing harmonic trapping in two or three dimensions one can ensure the existence of metastable bright solitary wave ground states in a restricted parameter regime [24–26, 128, 131, 222–225]. The collapse instability in trapped, attractively-interacting atomic BECs has been the subject of much theoretical investigation [23, 26, 200, 222, 226–235], and a series of experiments have investigated collapse dynamics by tuning the s-wave scattering length a_s, using a Feshbach resonance [130], to a negative (attractive) value outside of the range of condensate stability [24, 25, 128, 131]. The resulting dynamics are the subject of continuing theoretical study [28, 236–239].

In addition to the study of collapse *dynamics*, much research has focused on the identification of the parameter regimes where a metastable bright solitary wave ground state either does, or does not, exist. To answer this question in the mean-field description is to identify the parameter regimes where the 3D GPE has a metastable ground-state solution. Numerous studies have focused on identifying the parameters associated with the onset of collapse in various geometries, using variational [23, 200, 231, 232], perturbative [233], and numerical [23, 26, 222, 231, 234, 235] methods.

We illustrate the phenomenology of 3D attractive BECs associated with the collapse instability for the case of a cylindrically symmetric trap potential. Not only is this specific case the easiest to compare with the quasi-1D limit (which corresponds to tight radial and weak axial trapping), it has also been shown that the results for completely asymmetric trap potentials are not qualitatively different [234, 235]. For a cylindrically symmetric trap, we write the stationary 3D GPE as

$$\left[-\frac{\hbar^2}{2m}\nabla^2 + \frac{m\omega_r^2}{2}(\lambda^2 x^2 + r^2) - \frac{4\pi\hbar^2|a_s|N}{m}|\psi(\mathbf{r})|^2 \right]\psi(\mathbf{r}) = 0, \qquad (2.18)$$

where $r^2 = y^2 + z^2$, and we have set $\omega_y = \omega_z = \omega_r = \omega_x/\lambda$. Hence, λ represents the anisotropy of the trap potential, with $\lambda < 1$ (> 1) corresponding to a prolate (oblate) trap. The existence of a bright solitary wave ground state is dependent on the relative strength of the trap and the inter-atomic interactions, and also on the trap geometry. In the cylindrically symmetric traps we consider, this dependence is best illustrated by considering the interaction strength parameter [23]

$$k \equiv \frac{|a_s|N}{a_r}, \qquad (2.19)$$

where $a_r = \sqrt{\hbar/m\omega_r}$ is the harmonic oscillator length in the radial direction. The choice to use the radial harmonic oscillator length here is advantageous as it allows us to consider the case of zero axial trapping ($\lambda = 0$) with relative ease. Note, however, that in many other works k has been defined in terms of a geometric average of trap frequencies (e.g. Refs. [12, 25, 26, 226–230, 233–235]).

The collapse phenomenon results in the disappearance of metastable bright solitary wave ground states when the interaction strength parameter k exceeds a critical value k_c. The critical parameter k_c is dependent on the exact trap geometry. Within the subset of cylindrically symmetric trap geometries we consider four cases in particular, distinguished by different values of the anisotropy λ:

$\lambda^2 = 0$ Zero axial trapping ($\omega_x = 0$), resulting in a waveguide-like trap. Realizing a quasi-1D limit in such a trap would result in a system exactly described by the 1D NLSE with a constant potential, exhibiting true bright soliton solutions.

$0 < \lambda^2 \leq 1$ A prolate, or isotropic, trapping potential ($\omega_x \leq \omega_r$). While the quasi-1D limit for such a trap, reached at low λ, is the non-integrable quasi-1D GPE rather than 1D NLSE, this is nonetheless a more readily accessible regime for experiments to realize bright solitary waves [10, 12]. The case $\lambda = 1$ corresponds to an isotropic trap.

$1 < \lambda^2$ An oblate trapping potential ($\omega_x > \omega_r$). The existence of bright solitary wave ground states in such traps has been investigated theoretically [235]. However, experimental and theoretical studies of bright solitary waves have not focused on this geometry, primarily because the lack of a direct analogy to bright solitons in the 1D NLSE.

$\lambda^2 < 0$ The self-trapping nature of a bright solitary wave means it can exist in weakly *expulsive* axial potential ($|\omega_x| < \omega_r$, $\omega_x^2 < 0$). Such a potential, with an expulsive harmonic trap ($\lambda^2 < 0$), was realized in the bright solitary wave experiment of Ref. [11].

The parameter regime where metastable solutions of the 3D GPE with $a_s < 0$ exist can be determined numerically, by solving the 3D GPE. While this is the most accurate method, analytic variational methods give a more generally insightful view of the problem. In the next Section (Section 2.4.2) we introduce two variational ansatzes to treat this problem — a *Gaussian* ansatz with Gaussian radial and axial profiles, and a *soliton* ansatz with a Gaussian radial profile and a sech axial profile — and discuss the numerical methods that can be used to provide a more quantitatively accurate solution. In the subsequent Section (Section 2.4.3) we discuss the results obtained using these methods, for the four aspect ratio categories enumerated above. For the variational ansatzes these results are summarized in Figs. 2.3 and 2.4. Details of the analytic and numerical techniques needed to solve the ansatz-energy-minimization equations appearing in the following Sections can be found in Chapter 4, alongside details of an accurate pseudospectral numerical solution of the stationary GPE. In Section 2.4.4 we briefly review previous work on the dynamics of bright solitary waves in 3D; these dynamics form a key part of Chapter 3.

2.4.2 Variational and numerical analysis

Variational analysis: Gaussian ansatz

The solution of the 3D GPE for a cylindrically symmetric trap [Eq. (2.18)] can be approximated by a normalized Gaussian ansatz of the form

$$\left(\frac{1}{\pi^{3/2} a_r^3 \ell_{r,\mathrm{G}}^2 \ell_{x,\mathrm{G}}} \right)^{1/2} \exp\left(-\frac{1}{2a_r^2} \left[\frac{x^2}{\ell_{x,\mathrm{G}}^2} + \frac{r^2}{\ell_{r,\mathrm{G}}^2} \right] \right), \tag{2.20}$$

where $\ell_{x,\mathrm{G}}$ and $\ell_{r,\mathrm{G}}$ are, respectively, axial and radial variational length parameters associated with the Gaussian ansatz. Such an ansatz has been considered in Refs. [23] and [232], is used in Chapter 4, and is most appropriate in parameter regimes where the strength of the trap potential dominates over the strength of interactions in all directions (axial and radial). Substituting this Gaussian ansatz [Eq. (2.20)] into the classical field Hamiltonian for Eq. (2.18),

$$H_{3\mathrm{D}}[\psi] = \int d\mathbf{r} \left[\frac{\hbar^2}{2m} |\nabla\psi(\mathbf{r})|^2 + V(\mathbf{r})|\psi(\mathbf{r})|^2 - \frac{2\pi N |a_s| \hbar^2}{m} |\psi(\mathbf{r})|^4 \right], \tag{2.21}$$

where $V(\mathbf{r}) = m\omega_r^2(\lambda^2 x^2 + r^2)/2$, yields

$$H_{3\mathrm{D}}[\psi] = \hbar\omega_r \left(\frac{1}{4\ell_{x,\mathrm{G}}^2} + \frac{1}{2\ell_{r,\mathrm{G}}^2} + \frac{\lambda^2 \ell_{x,\mathrm{G}}^2}{4} + \frac{\ell_{r,\mathrm{G}}^2}{2} - \frac{k}{\sqrt{2\pi} \ell_{r,\mathrm{G}}^2 \ell_{x,\mathrm{G}}} \right). \tag{2.22}$$

Differentiating this variational energy functional with respect to the axial and radial lengths $\ell_{x,\mathrm{G}}$ and $\ell_{r,\mathrm{G}}$ produces, respectively, the conditions

$$\lambda^2 \ell_{x,\mathrm{G}}^4 + \frac{2k\ell_{x,\mathrm{G}}}{\sqrt{2\pi} \ell_{r,\mathrm{G}}^2} - 1 = 0, \tag{2.23}$$

and

$$\ell_{r,\mathrm{G}}^4 + \frac{2k}{\sqrt{2\pi} \ell_{x,\mathrm{G}}} - 1 = 0, \tag{2.24}$$

which must be satisfied by the variational energy-minimizing lengths. Simultaneously solving Eqs. (2.23) and (2.24) to obtain a consistent physical solution, where one exists, must generally be done numerically. In the case of prolate and oblate trap potentials this can be implemented as a straightforward iterative procedure, and for the axially free case an analytic solution can be found (see Chapter 4 for details). The energy of this Gaussian variational ansatz is shown for various system parameters in Fig. 2.3.
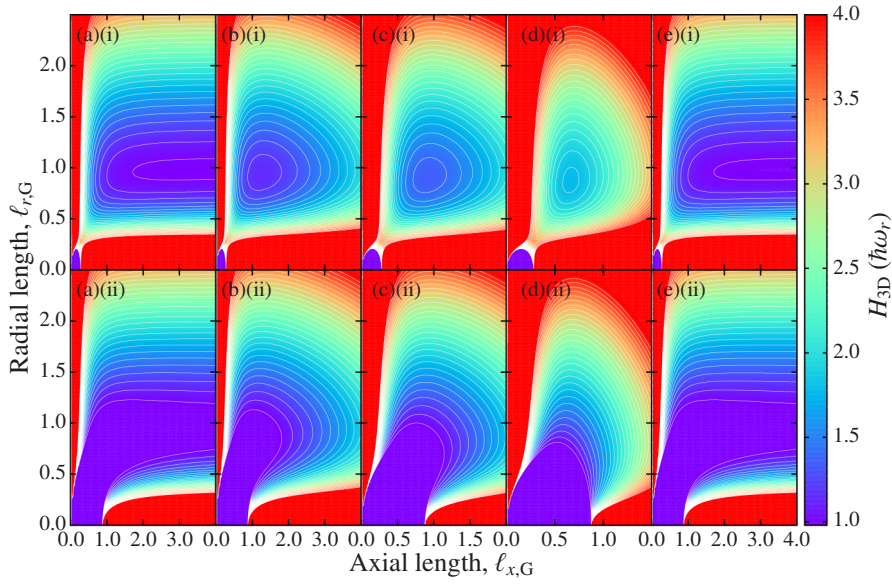
Figure 2.3: Per-particle energy functional, H_{3D}, determined using a Gaussian ansatz [Eq. (2.20)] for a BEC in a cylindrically symmetric, harmonic trap potential. Trap anisotropies shown are; (a) $\lambda = 0$, (b) $\lambda = 1/2$, (c) $\lambda = 1$, (d) $\lambda = 2$, (e) $\lambda^2 = -4 \times 10^{-4}$ (expulsive axial potential). The top row [sub-label (i)] shows the case $k = 0.35$, for which all the trap geometries are stable to collapse. In this case there is a stable local minimum in the Gaussian ansatz variational energy, which corresponds to the (metastable) bright solitary wave ground state. The bottom row [sub-label (ii)] shows the case $k = 1.1$, for which all the trap geometries are unstable to collapse.

Variational analysis: soliton ansatz

Similarly to the case for the Gaussian ansatz, the 3D GPE for a cylindrically symmetric trap [Eq. (2.18)] can be solved using a normalized soliton ansatz of the form

$$\left(\frac{1}{4\pi a_r^3 \ell_{r,S}^2 \ell_{x,S}}\right)^{1/2} \operatorname{sech}\left(\frac{x}{2a_r \ell_{x,S}}\right) \exp\left(-\frac{r^2}{2a_r^2 \ell_{r,S}^2}\right), \qquad (2.25)$$

where $\ell_{x,S}$ and $\ell_{r,S}$ are, respectively, axial and radial variational length parameters. Such an ansatz has been considered in Refs. [23] and [231], and is most appropriate in parameter regimes where the strength of the *radial* trap potential dominates over the strength of interactions, but the strength of interactions dominates over the strength of the *axial* trap potential. Substituting this soliton ansatz [Eq. (2.25)] into
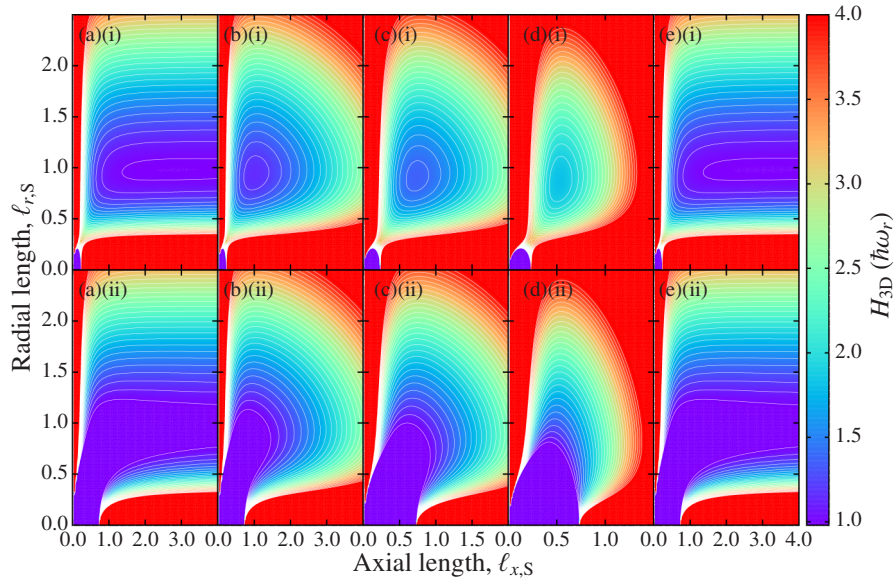
Figure 2.4: Per-particle energy functional, H_{3D}, determined using a soliton ansatz [Eq. (2.25)] for a BEC in a cylindrically symmetric, harmonic trap potential. Trap anisotropies shown are; (a) $\lambda = 0$, (b) $\lambda = 1/2$, (c) $\lambda = 1$, (d) $\lambda = 2$, (e) $\lambda^2 = -4\times10^{-4}$ (expulsive axial potential). The top row [sub-label (i)] shows the case $k = 0.35$, for which all the trap geometries are stable to collapse. In this case there is a stable local minimum in the soliton ansatz variational energy, which corresponds to the (metastable) bright solitary wave ground state. The bottom row [sub-label (ii)] shows the case $k = 1.1$, for which all the trap geometries are unstable to collapse.

the classical field Hamiltonian Eq. (2.21) yields

$$H_{3D}[\psi] = \hbar\omega_r \left(+\frac{1}{6\ell_{x,S}^2} + \frac{1}{2\ell_{r,S}^2} + \frac{\pi^2\lambda^2\ell_{x,S}^2}{24} + \frac{\ell_{r,S}^2}{2} - \frac{k}{3\ell_{r,S}^2\ell_{x,S}} \right). \qquad (2.26)$$

Differentiating this variational energy functional with respect to the axial and radial lengths $\ell_{x,S}$ and $\ell_{r,S}$ produces the conditions

$$\lambda^2\ell_{x,S}^4 + \frac{4k\ell_{x,S}}{\pi^2\ell_{r,S}^2} - \frac{4}{\pi^2} = 0, \qquad (2.27)$$

and

$$\ell_{r,S}^4 + \frac{2k}{3\ell_{x,S}} - 1 = 0, \qquad (2.28)$$

which must be satisfied by the variational energy-minimizing lengths. As for the Gaussian ansatz, numerically solving Eqs. (2.27) and (2.28) simultaneously to ob-

tain a consistent physical solution, where one exists, can be implemented as a straightforward iterative procedure (again, see Chapter 4). The soliton ansatz yields a variational energy surface, shown in Fig. 2.4, which is quantitatively very similar in structure to that yielded by the Gaussian ansatz [23, 231]. Again, we analyse this structure in detail in Section 2.4.3.

Numerical analysis

A variational approach to the stability of bright solitary waves in 3D yields considerable qualitative insight, particularly with regard to the collapse phenomenon. However, the approach is not particularly accurate in its prediction of the critical parameter k_c; the imposition of a certain shape on the wavefunction via the variational anstatz causes variational methods to consistently over-estimate k_c. Consequently, a great deal of work in the field of attractively-interacting BECs has focused on accurately identifying k_c, for various trap configurations, using numerical methods [240]. The numerical and variational results can also be compared in order to investigate how bright-soliton-like the bright solitary wave metastable ground-states become in cases which approach the quasi-1D limit: such an analysis forms the subject of Chapter 4.

Studies have investigated traps with spherical [26, 222] and cylindrical [234] symmetry, cylindrically symmetric waveguides without axial trapping [23], and the case of a generally asymmetric trap [235]. Several works also investigated the configurations of specific experiments in detail [27, 231]. A wide variety of numerical methods have been deployed, including imaginary-time propagation on both finite-difference [234] and pseudospectral [231] grids, an adiabatic ramping method within a Crank-Nicolson scheme [23, 222], and a modified Newton method in a pseudospectral scheme as we use in Chapter 4 (see also Appendix B). All the methods above are standard techniques for the GPE [240], and the resulting values of k_c are in reasonable agreement with each other.

2.4.3   Bright solitary wave metastable ground state properties

Constant axial potential

The case of a constant axial potential, resulting in a waveguide-like trap, effectively removes one of the two free parameters of the cylindrically symmetric 3D GPE [Eq. (2.18)], since $\lambda = 0$. This leads to some algebraic simplification and, in the case of the soliton ansatz, the variational energy-minimizing lengths ℓ_x and ℓ_r

and the critical parameter $k_c = 3^{-1/4}$ can be found analytically (see Ref. [231] and Chapter 4).

More insight into the physical situation can be gleaned from the energy surfaces shown in Figs. 2.3(a) and 2.4(a): these show the variational per-particle energy H_{3D}, for Gaussian and soliton ansatzes respectively, as a function of the variational lengths ℓ_x and ℓ_r in parameter regimes where a metastable solitary wave ground state either; (i) exists, or (ii) does not exist. For both ansatzes the energy surface forms a relatively flat "plain" for larger ℓ_x and ℓ_r, with sharply rising "ridges" occurring when either length becomes small. However, the (negative) interaction term in the energy functional leads to a distinct "chute" [231] at the meeting point of these two ridges (when both ℓ_x and ℓ_r are small). For low k a raised saddle point separates the chute from the plain; as k increases this saddle lowers, until at $k = k_c$ it disappears and the entire parameter regime of the plain becomes unstable. For the soliton ansatz, this occurs at exactly $k_c = 1/3^{1/4} \approx 0.76$ [231]. For the Gaussian ansatz the critical value is $k_c \approx 0.778$ [232]. For comparison, the non-polynomial Schrödinger equation (an extended quasi-1D approach) predicts $k_c = 2/3$, through a simpler calculation [201].

In regimes where a metastable bright solitary wave ground state does exist, the energy of the saddle point relative to that of the local energy minimum on the plain sets an energy scale at which the bright solitary wave will be unstable to collapse when excited. Excitations with sufficient energy could allow the condensate to overcome the barrier formed by the saddle point and lead to a dynamical collapse in which ℓ_x decreases to zero [23, 223, 231]. A second channel of instability also arises; because the lack of an axial trap results in a finite-valued energy as $\ell_x \to \infty$; thus, there exists a "dispersive channel" in which excitations of the metastable ground state above a certain energy threshold can lead to dynamics where ℓ_x increases without bound [23, 231].

Prolate and isotropic trap potentials

The addition of a harmonic axial trapping potential to the previous case results in a 3D GPE with two free parameters (expressed here as the interaction strength parameter k, and the trap anisotropy $\lambda = \omega_x/\omega_r$). For anisotropies $0 < \lambda < 1$ the trap has a prolate geometry, and for $\lambda = 1$ it is spherically symmetric. In such cases it is not possible to find entirely analytic variational solutions for either Gaussian or soliton ansatz; however, only a simple numerical procedure is required (see Chapter 4).

The energy landscape for prolate trap potentials is similar to that for the waveguide trap $\lambda = 0$ in and around the region of the collapse instability (low ℓ_x and ℓ_r), and is shown in Figs. 2.3(b) and 2.4(b) [Figs. 2.3(c) and 2.4(c) show the isotropic case $\lambda = 1$]. Again there is the same structure of chute and plain, separated by a saddle point in the metastable case (i), and connected without a saddle point in the unstable case (ii). The exact structure is dependent on the trap geometry, however, and therefore the critical parameter for collapse, k_c, varies with λ. Although the energy landscape around the collapse instability remains similar, in the high-ℓ_x limit the potential energy of the trap leads to an infinite total energy in the limit $\ell_x \to \infty$, eliminating the dispersive channel altogether.

Oblate trap potential

If the axial trap frequency is increased to the extent that it exceeds the radial trap frequency, one obtains an oblate trap potential ($\lambda > 1$). Such a geometry is not typical for the study of bright solitary waves, as in this geometry no clear analogy can be drawn with an integrable NLSE supporting bright soliton solutions.

Nonetheless, when an oblate trap possesses a metastable ground state it is a solitary wave [219], and such ground states have been previously studied using the 3D GPE [23], and 2D reductions with 3D effects [205]. The appearance of such a ground state is directly determined by the collapse instability in a similar way to the prolate and isotropic traps, as can be seen from the variational energy surface for the oblate case shown in Fig. 2.3(d) for the Gaussian ansatz and Fig. 2.4(d) for the soliton ansatz. Interestingly, the soliton ansatz gives a similar picture to the Gaussian ansatz in this case despite its apparently inappropriate shape in this geometry. Both ansatzes give a similar picture to the prolate and isotropic traps, although the critical parameter k is lower in the oblate case.

Expulsive axial potential

The self-trapped nature of bright solitary waves means they can withstand being placed in a trap with a weakly expulsive harmonic axial potential ($\lambda^2 < 0$) without dispersing. This was the case in the experiment of Ref. [11], and the stability and form of such potentials have been the subject of subsequent theoretical investigation using the 3D GPE [23, 231].

The variational energy surfaces for the Gaussian and soliton ansatzes are shown, respectively, in Figs. 2.3(e) and 2.4(e); again in each case the parameters in (i) ad-

mit the existence of a metastable ground state, while (ii) shows a parameter regime unstable against collapse. However, in addition to the collapse channel, an expulsive potential leads to a second instability, which has been termed the "expansive channel" [23]. This is similar to the "dispersive channel" in the waveguide-like trap ($\lambda = 0$), and corresponds to axial spreading of the solutions $\ell_x \to \infty$. In contrast to the dispersive channel — which never completely prevents the existence of a metastable ground state, but renders it unstable to (potentially very small) excitations — the expansive channel can destabilize the solitary wave. Like the collapse channel's "chute", the expansive channel is separated from the ground state by a saddle point, which disappears for sufficiently low k, or high $|\lambda|$. In addition to the critical parameter due to collapse, k_c, this introduces a critical parameter due to expansion k_e, such that one must have $k_e < k < k_c$ in order to observe a metastable ground state. In particular, $|\lambda|$ must be relatively close to zero to avoid the cusp point where $k_c = k_e$, and metastable solutions are no longer found.

2.4.4 Bright solitary waves dynamics in 3D

Overview

In 3D situations, it is not only the addition of trapping which leads to a loss of integrability, but but also three-dimensional effects. While the metastable 3D ground state is still a solitary wave [219], 3D effects can lead to much more significant deviations from soliton-like behaviour than are observed in the quasi-1D GPE with $\omega_x > 0$. Nonetheless, there are regimes where highly soliton-like dynamics can still be observed. We will consider the dynamics of 3D bright solitary waves in prolate traps in detail in Chapter 3. However, we introduce here some of the previously known results relating to bright solitary waves in waveguide-like traps ($\omega_x = 0$).

Bright solitary wave dynamics in a waveguide

In the absence of analytic solutions for binary solitary wave collisions in a waveguide-like trap, such collisions must be simulated numerically. This can be done from an initial condition composed of two copies of the (numerically obtained) ground state for $N/2$ particles, displaced from each other by some distance and given some velocity toward each other[5]. This is similar to the procedure used in Fig. 2.2 in the quasi-1D case. For equal-sized solitary waves the resulting collisions can be studied

---

[5]Such a velocity is imparted numerically by applying a spatially varying phase of $e^{\pm ivx}$. Experimentally, this could be achieved by applying a linear external potential to each solitary wave for a short time; a related scheme is explored in detail in Chapter 3

within the parameter space of collision velocity v, interaction strength parameter k, and relative phase $\Delta\Phi$ [27].

As in the case of the metastable ground state itself, the key parameter determining the stability of collisions of this type is the interaction strength parameter k; this must remain below some threshold k_{col} in order to avoid a dynamically-induced collapse when the waves meet. However, k_{col} itself is dependent on the other collision parameters. In particular, k_{col} is larger for faster collisions, and for collisions with a relative phase closer to π. The latter effect is most noticeable for low velocities, with the phase-dependence of k_{col} disappearing in the high-velocity limit. At low velocity, this phase-dependence can be understood from the collision profiles illustrated for the NLSE in Fig. 2.1; in the case $\Delta\Phi = \pi$ the density profile of the collision itself resembles two solitons interacting *repulsively* [19] and never overlapping, whereas in the case $\Delta\Phi = 0$ the solitons overlap, leading to a strong density peak. While this peak is of no consequence in the NLSE or the quasi-1D GPE, in the 3D GPE this peak in the atomic density can trigger the collapse instability. This phase dependence of the collisional stability is also predicted by effective 1D equations retaining more 3D character than the quasi-1D GPE [203].

The dependence of k_{col} on the collision velocity v can be understood in terms of the relationship between the characteristic time for collapse of the condensate, $t_{collapse}$, and the characteristic time for the collision-interaction to take place, t_{int}. In Ref. [27] it was illustrated, for the parameters of the JILA solitary wave experiment [12], that the critical collision velocity, below which collapse occurred in numerical simulations of collisions, corresponds to a collision-interaction time t_{int} approximately equal to the experimentally measured collapse time, $t_{collapse}$. Theoretical investigation of the role of the two timescales has not proceeded further to date, in part because the GPE has not been generally considered an accurate predictor of $t_{collapse}$. However, recent results suggesting that the GPE can accurately predict $t_{collapse}$ when a three-body loss term with the correct coefficients is included [239] offer the possibility of further progress in this area.

Population transfer in solitary wave collisions

Another effect occurring as a result of the 3D nature of the system is that of population transfer between bright solitary waves. In both the 1D NLSE, and in the 3D GPE for a waveguide trap, collisions between solitons or solitary waves with relative phases $\Delta\Phi = 0$ and π have a density profile which remains completely symmetric in x after the collision; in this respect the 1D NLSE and 3D GPE are

analogous. The two descriptions lead to very different dynamics for intermediate phases $0 < \Delta\Phi < \pi$ and $\pi < \Delta\Phi < 2\pi$, however. In the 1D NLSE the density profile, which is initially symmetric in x, loses its symmetry during the collision and regains it afterwards. In the 3D GPE for a waveguide trap, the initially-symmetric density profile loses its symmetry during the collision, and this loss of symmetry leads to population transfer between the two waves: the first solitary wave grows in amplitude and slows down, while the second wave loses amplitude and speeds up. In addition to the 3D GPE, this effect can also be seen in effective-1D approaches retaining extra 3D character [203].

This transfer can be approximated using a simple two-mode model [27], which bears considerable analogy to the model of a Josephson junction between superconductors and displays similar behaviour [241]. The amount of population transferred shows interesting dependences on the relative phase and velocity of the solitary waves: for fast collisions the amount of population transfer depends sinusoidally on the relative phase; the maximum transfer occurs at $\Delta\Phi = \pi/2$ and $\Delta\Phi = 3\pi/2$, and the magnitude of this transfer decreases with velocity. At lower velocities, however, this dependence becomes skewed, with the maximum transfer occurring closer to $\Delta\Phi = 0$: this seems to be a consequence of nonlinear effects, and in certain parameter regimes almost certainly involves the collapse instability [27].

Chapter 3: Bright solitary wave production, splitting, and interferometry

3.1 Introduction

The unique properties of bright solitary waves makes them promising candidates for a variety of future applications. Areas of current research towards future applications include the development of soliton atom-lasers [242–244], the stabilization and manipulation of bright solitary waves using spatially and temporally varying traps and inter-atomic *s*-wave scattering lengths [245, 246], manipulation of bright solitary waves in periodic potentials [247, 248], with the potential for applications in quantum information [249], and for use in the study of atom-surface interactions [44]. Other current research areas include dipolar [250–252], Rydberg-induced [155], and Bose-Fermi [253, 254] bright solitary waves. One particularly interesting possibility is the development of interferometry devices based on bright solitary waves [10, 41–44, 80]; we focus on this possibility in this Chapter.

We begin, in Section 3.2, with a brief review of experimental and beyond-mean-field aspects of bright solitary waves, both of which represent vital considerations in the construction of a viable interferometric device. We briefly review the production of bright solitary waves in atomic BEC experiments, and discuss the mean-field interpretation of their observed dynamics (Section 3.2.1). In the case of multiple bright solitary waves the mean-field analysis of previous experiments suggests an preference for the formation of out-of-phase solitons. Studies of bright solitary waves beyond the mean-field treatment have attempted to elucidate the cause of this preference (Section 3.2.2); while these studies agree with each other that many-body effects will lead to the breakdown of the mean-field picture of the dynamics over relatively fast timescales, there remains some underlying discrepancy with previous experimental observations which, we propose, can be best be resolved by further experiments.

In Section 3.3 we propose a new experimental technique which would allow one to answer the question *are experimentally observed atomic bright solitary waves well-described by an effective single-particle wavefunction, propagated by the GPE?* Specifically, we propose a method to split the ground state of an attractively in-

teracting atomic BEC into two bright solitary waves with controlled relative phase and velocity (Section 3.3.1 and 3.3.2). Using the GPE, we analyse the stability of these waves against their subsequent re-collisions at the centre of a cylindrically symmetric, prolate harmonic trap as a function of relative phase, velocity, and trap anisotropy; we do this both in quasi-1D (Section 3.3.3) and in 3D (Section 3.3.4). We show that the collisional stability is strongly dependent on relative phase at low velocity, and we identify previously unobserved oscillations in the collisional stability as a function of the trap anisotropy. This analysis constitutes a testable prediction of the mean-field description. An experimental implementation of our method, which we demonstrate the feasibility of in Section 3.3.5, could be used to explore the regime of validity of the mean field description of bright solitary waves.

Finally, our phase-controlled splitting method could also form an important step towards atom interferometry experiments involving bright solitary waves. In Section 3.4.1 we review the possibility of, and current proposals for, bright solitary wave interferometers. In contrast to our phase controlled technique, current proposals favour the use of potential barriers for the splitting and recombination of bright solitary waves. We review this technique, and discuss the relevance of beyond-mean-field effects — including the possibility to exploit macroscopic quantum superpositions of bright solitary waves to enhance measurement precision, in Section 3.4.2.

3.2 Experimental aspects of bright solitary waves

3.2.1 Experimental production and solitary wave dynamics

As discussed in Chapter 2, bright solitary waves require attractive interatomic interactions in order to form. However, due to the collapse instability, atomic BECs with attractive interactions (negative s-wave scattering length a_s) are difficult to produce experimentally. Much of the inherent difficulty can be overcome by selecting an atomic species and hyperfine state where a Feshbach resonance can be used to *tune* the interactions simply by applying an external magnetic field. In the case of an optically-trapped BEC and a Feshbach resonance between two hyperfine levels of the atomic species, one can adjust the magnetic field to obtain a very wide range of different s-wave scattering lengths without affecting the harmonic confinement [130].

Control of interactions using Feshbach resonances has been central to the experi-

ments to date which have observed both individual [11] and multiple [10, 12] bright solitary waves. In each case, these solitary waves were realized as *collapse remnants* from a larger atomic BEC which was rendered unstable by rapidly tuning the scattering length from a positive value to a negative one outside the regime of stability. During this collapse the majority of the atoms in the original condensate are lost to the thermal cloud, while those that remain group into one or several bright solitons, each containing less than the critical number of atoms. The species used in these experiments have been ^{7}Li [10, 11] and ^{85}Rb [12].

As we have already seen (Chapter 2) bright solitary waves retain, in the mean-field description, many soliton-like characteristics, including an absence of dispersion and the existence of a well-defined relative phase between bright solitary waves. The bright solitary waves observed in experiment were capable, in the case of multiple bright solitary waves, of surviving many mutual re-collisions at the trap centre [10, 12]. The experiment of Ref. [10] operated close to the quasi-1D regime; here the observed bright solitary wave motion has been shown to match the GPE description of bright solitary waves with relative phase $\Phi = \pi$ between neighbouring solitary waves [10, 197, 255]. In contrast, the experiment of Ref. [12] operated in a 3D regime. Here bright solitary waves are not universally stable against multiple re-collisions (see Chapter 2). However, numerical simulations of the 3D GPE have indicated that slow 3D bright solitary waves retain their form for fewer collisions when their relative phase, Φ, is equal to 0 than when $\Phi = \pi$ [22, 27]. The long lifetimes of 3D bright solitary waves seen in the experiment of Ref. [12] thus seem to also imply that the relative phase of neighbouring solitary waves is $\Phi = \pi$ [22, 27].

3.2.2   Relative phase and the role of beyond-mean-field effects

Working largely within a mean-field model, the mechanism of modulational instability, and the shorter lifetime of colliding 3D bright solitary waves when $\Phi = 0$, have been identified as contributory causes to these apparent anti-phase relations in both experiments [22, 27, 197, 198, 255]. In Ref. [198] in particular it was proposed that modulational instability in the mean field model could be seeded by initial beyond-mean-field fluctuations imparted by the collapse process. While this mechanism would not guarantee $\Phi = \pi$ phase relations of itself, it has been proposed that the fragility of in-phase bright solitary waves against collisions could lead to such phase relations [198].

While they are considerably more complex than simulations of the mean-field GPE,

studies of bright solitary waves beyond the mean-field description have now been conducted for a range of specific configurations [28, 41–43, 238, 256, 257]. These studies can be divided into two broad categories: Refs. [28, 43, 238, 256] added in the effects of quantum noise using the truncated Wigner method (see Chapter 5), while Refs. [41, 42, 257] used approximate analytic and numerical methods to simulate the full quantum many-body problem. Within these works, those of Refs. [41–43] focused on the case of bright solitary waves colliding with fixed potential barriers, to which we return in Section 3.4.

Of the remaining studies, those of Davis and co-workers [28, 238, 256] focused on simulating bright solitary wave collisions using the truncated Wigner method. Their results suggest that the effects of quantum noise on such collisions is to make them resemble mean-field bright solitary wave collisions with relative phase $\Phi = \pi$ (see Fig. 2.2(b)) for *all initial phases*. Potentially, this provides an alternative explanation for the fact that observed dynamics of multiple bright solitary waves are well-described by the mean-field GPE with $\Phi = \pi$; however, only single collisions were simulated in Ref. [28] — the full long-time dynamics of multiple 3D bright solitons repeatedly re-colliding at the centre of a harmonic trap has not yet been fully explored.

A similar study was undertaken by Streltsov and co-workers in Ref. [257], using the MCTDHB computational method [258, 259]. They also found that many-body effects rapidly give rise to an effective repulsive interaction between bright solitary waves, which they also predict to rapidly become incoherent, fragmented objects [257]. However, they also find: (a) that this fragmentation occurs on a much faster timescale than the bright solitary wave dynamics observed in experiment (particularly in Ref. [10], to which they explicitly make a comparison), and (b) that the effective repulsive interactions between the fragmented remnants are much weaker than the mean-field interactions with $\Phi = \pi$. In light of these two predictions, and those of Davis and co-workers, the full answer to the question of how the mean-field description with $\Phi = \pi$ succeeds so well at predicting the observed dynamics remains somewhat murky. Answering this question incontrovertibly will prove extremely difficult without recourse to further bright solitary wave experiments, and the ability to generate bright solitary waves with *controlled initial relative phase* would be a significant advantage to future experiments investigating this question. In the next Section we propose exactly such a method to, in a velocity- and phase-controlled way, split a single bright solitary wave in an axisymmetric harmonic trap into two outgoing bright solitary waves which repeatedly re-collide at the trap cen-

tre. By investigating the subsequent mean-field dynamics of these solitary waves in detail, we provide a benchmark prediction of the mean-field description which can be experimentally tested.

3.3 Controlled, phase-coherent splitting of bright solitary waves

3.3.1 Physical system and soliton units

In order to realize velocity- and phase-controlled splitting of bright solitary waves, we consider an atomic BEC of N atoms of mass m and (attractive) s-wave scattering length $a_s < 0$, held within a cylindrically symmetric, prolate harmonic trap $V(\mathbf{r}) = m[\omega_x^2 x^2 + \omega_r^2(y^2 + z^2)]/2$. As described in Chapter 2, with strong radial confinement the system can be described by the quasi-1D GPE

$$i\hbar \frac{\partial \Psi(x,t)}{\partial t} = \left[-\frac{\hbar^2}{2m}\frac{\partial^2}{\partial x^2} + \frac{m\omega_x^2 x^2}{2} - 2\hbar\omega_r N|a_s||\Psi(x,t)|^2 \right]\Psi(x,t). \tag{3.1}$$

This problem features two key length scales; the harmonic length $a_x = \sqrt{\hbar/m\omega_x}$, and the soliton length $b_x = \hbar/2m\omega_r N|a_s|$. A mathematically convenient way to express the single free parameter of Eq. (3.1) is as the square of the ratio of these two length scales;

$$\omega \equiv \left(\frac{b_x}{a_x}\right)^2 \equiv \frac{\hbar\omega_x}{4m\omega_r^2|a_s|^2 N^2}. \tag{3.2}$$

To do so, we work in a system of "soliton units" [260] by moving to the dimensionless variables

$$x' = \frac{x}{b_x} = \frac{2m\omega_r N|a_s|}{\hbar}x, \tag{3.3}$$

$$t' = \frac{4m\omega_r^2 N^2|a_s|^2}{\hbar}t, \tag{3.4}$$

$$\psi(x,t) = \sqrt{b_x}\Psi(x,t) = \sqrt{\frac{\hbar}{2m\omega_r N|a_s|}}\Psi(x,t), \tag{3.5}$$

and rescaling to energy units of $4m\omega_r^2 N^2|a_s|^2$. This system of units can be codified as $\hbar = m = g_{1D}N = 1$. Dropping primes from herein, this produces the dimensionless 1D GPE

$$i\frac{\partial \psi(x,t)}{\partial t} = \left[-\frac{1}{2}\frac{\partial^2}{\partial x^2} + \frac{\omega^2 x^2}{2} - |\psi(x,t)|^2 \right]\psi(x,t). \tag{3.6}$$

Here, the parameter $\omega = (b_0/a_0)^2$ can be interpreted as a dimensionless effective trap strength.

3.3.2 Splitting protocol

To develop our desired splitting mechanism, we consider the effect of abruptly increasing the magnitude of the (negative) s-wave scattering length in an attractively-interacting atomic BEC. Specifically, we consider changing the scattering length from an initial value of a_s^0 to a final value of $a_s = \alpha^2 a_s^0$, where $\alpha > 1$ (and hence $a_s, a_s^0 < 0$). We assume that this change can be performed quasi-instantaneously (hence giving an interaction-strength "quench") for the modulated initial condition

$$\psi(x, t = 0) = \psi_0(x) = \psi_\alpha(x) \cos\left(\frac{kx}{2\alpha^2} + \frac{\Phi}{2}\right), \tag{3.7}$$

where $\psi_\alpha(x)$ is the bright solitary wave ground state of the BEC at the *initial* scattering length a_s^0. In the quasi-1D limit, which we consider first, a stable ground state $\psi_\alpha(x)$ always exists. However, when we subsequently consider the same problem in 3D, we restrict our attention to regimes of $|a_s^0|$ below the critical value for the onset of collapse, $|a_s^c|$, in which a metastable ground state $\psi_\alpha(\mathbf{r})$ exists.

The ground state $\psi_\alpha(x)$ may be made by using a magnetic Feshbach resonance to adiabatically change the scattering length from an initially repulsive to a weakly negative value, a_s^0, with $|a_s^0| < |a_s^c|$. While this mechanism for "smoothly" creating a single bright solitary wave has not been experimentally realized to date, such a technique is expected to be feasible in the Durham ^{85}Rb BEC experiment currently being developed [261]. The subsequent rapid change from a_s^0 to $a_s = \alpha^2 a_s^0$ could then exploit the same Feshbach resonance.

The density modulation that transforms $\psi_\alpha(x)$ into $\psi_0(x)$ may be achieved by using a second internal atomic state in an interference protocol: denoting two relevant atomic states by $|+\rangle$ and $|-\rangle$, we write the total state of the condensed atoms as

$$|\psi\rangle = \psi_+(x)|+\rangle + \psi_-(x)|-\rangle, \tag{3.8}$$

we begin with all atoms in internal state $|+\rangle$, such that

$$\psi_+(x) = \psi_\alpha(x), \tag{3.9}$$

$$\psi_-(x) = 0. \tag{3.10}$$

Applying a resonant $\pi/2$ pulse to the internal state transition transforms this [45] to

$$\psi_+(x) = \psi_-(x) = \frac{\psi_\alpha(x)}{\sqrt{2}}. \tag{3.11}$$

The heart of our interferometric protocol now follows, which consists of imprinting equal and opposite momenta on the two internal states, giving

$$\psi_\pm(x) = \frac{e^{\pm i(Kx+\Phi)/2}}{\sqrt{2}} \psi_\alpha(x). \tag{3.12}$$

This is then transformed into

$$\psi_+(x) = \cos\left[(Kx+\Phi)/2\right]\psi_\alpha(x), \tag{3.13}$$

and

$$\psi_-(x) = i\sin\left[(Kx+\Phi)/2\right]\psi_\alpha(x), \tag{3.14}$$

by a second resonant $\pi/2$ pulse. By rapidly expelling atoms in state $|-\rangle$ from the trap — using, for example, a resonant light pulse — we leave the remaining atoms in the state

$$\psi_+(x) = \psi_0(x), \tag{3.15}$$

$$\psi_-(x) = 0, \tag{3.16}$$

where $\psi_0(x)$ is exactly the desired initial condition [Eq. (3.7)], with $k = \alpha^2 K$, and with Φ determined by the phase accumulated at the centre of the bright solitary wave. Note that the loss of atoms between $\psi_\alpha(x)$ and $\psi_0(x)$ [an apparently inevitable consequence of the nonunitarity of multiplying $\psi_\alpha(x)$ (in isolation) by a sinusoid] is balanced by the change in normalization; N explicitly denotes the *initial* atom number, and $\psi_0(x)$ is normalized to $1/2$. There are many potential implementations of this protocol; we explicitly consider one based on ^{85}Rb atoms in Section 3.3.5.

3.3.3 Quasi-1D dynamics

Neglecting the axial trapping (setting $\omega = 0$) the 1D GPE [Eq. (3.6)] reduces to the dimensionless NLSE

$$i\frac{\partial\psi(x,t)}{\partial t} = \left[-\frac{1}{2}\frac{\partial^2}{\partial x^2} - |\psi(x,t)|^2\right]\psi(x,t). \tag{3.17}$$
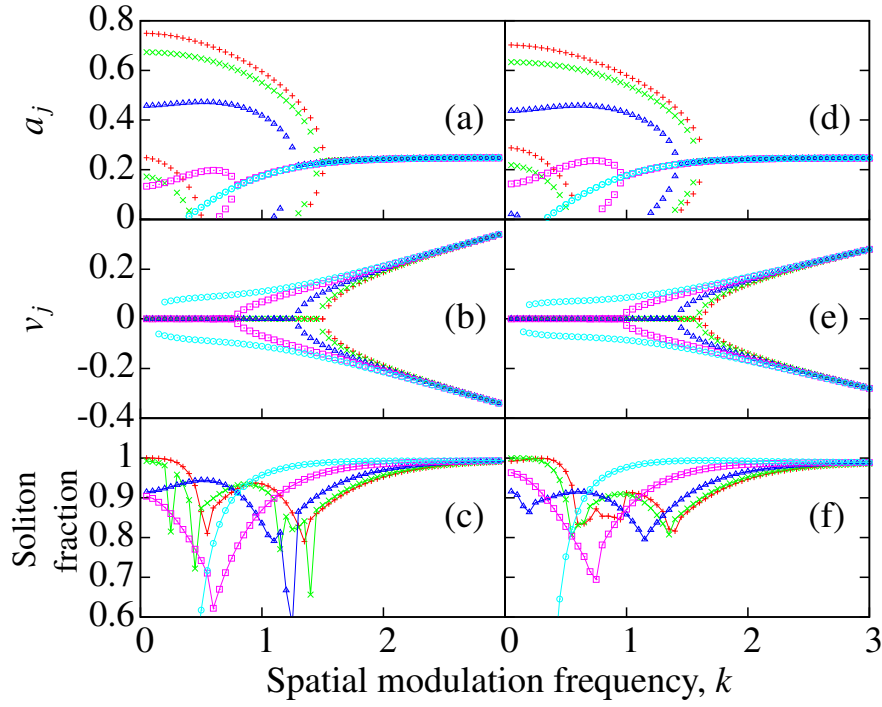
Figure 3.1: The structure of a multi-soliton pulse. The panels show the soliton amplitudes a_j, velocities v_j, and fractions associated with the initial condition $\psi_0(x)$ [Eq. (3.18)] in the NLSE [Eq. (3.17)], computed using a numerical scattering transform [210], as a function of spatial modulation frequency k. Panels (a–c) correspond to $\alpha = 2$ and (d–f) to $\alpha = 2.2$. Relative phases are $\Phi = 0$ (+), $\pi/4$ (×), $\pi/2$ (△), $3\pi/4$ (□), π (○). Soliton fraction is the ratio of the combined norm of the constituent solitons, $\sum_j a_j$, to the total norm $\int_{-\infty}^{\infty} |\psi_0(x)|^2 dx$. In the limit $k \to \infty$, when $\alpha = 2$, $a_j \to 1/4$ $[\sum_j a_j \to \int_{-\infty}^{\infty} |\psi_0(x)|^2 dx \to 1/2]$, and $v_j \to \pm k/8$ [193, 194].

In this limit, the ground state of the BEC before the change in scattering length, $\psi_\alpha(x)$, is a single, stationary bright soliton. After density modulation this has the form

$$\psi_0(x) = \frac{1}{2\alpha}\mathrm{sech}\left(\frac{x}{2\alpha^2}\right)\cos\left(\frac{kx}{2\alpha^2} + \frac{\Phi}{2}\right), \tag{3.18}$$

which is no longer simply a bright soliton solution.

While they were not explored in Chapter 2, solutions of the NLSE for the initial condition Eq. (3.18) are well-known in the context of nonlinear optics [18, 193, 194]. The case $k = 0$ was studied analytically by Satsuma and Yajima [18] using the inverse scattering transform: for integer $\alpha = J$, Eq. (3.18) is exactly a bound state, or multi-soliton pulse, of J solitons with unequal amplitudes a_j and zero velocity

($v_j = 0$). For non-integer $\alpha = J + \beta$ (with $0 < \beta < 1$), Eq. (3.18) consists of J solitons plus radiation, with the norm of the soliton component given by $\sum_j a_j$ [18] (see Chapter 2), and does not admit an exact analytic solution. The modulated case (general k) has been considered both analytically and numerically by Kodama and Hasegawa [193] and Afanasjev and Vysloukh [194]. Fig. 3.1 shows how the modulation alters the character of a two soliton pulse ($\alpha \gtrsim 2$): beyond a certain threshold value of k the pulse "splits" into two solitons with equal amplitudes, opposite velocities, and relative phase Φ, plus a negligible radiation component. Crucially, control of the modulation corresponds to control over the relative velocity and phase of a pair of generated bright solitons.

While the soliton parameters shown in Fig. 3.1 can be obtained by analytic methods of approximation, this is a lengthy and involved process [193, 194]. In practice, a much simpler method is to generate them numerically from the initial condition $\psi_0(x)$ by solving the Zakharov-Shabat scattering problem associated with the NLSE [Eq. (2.8)] numerically. Details of how to perform such a *discrete scattering transform* using a propagator method can be found in [210].

In the presence of axial trapping ($\omega > 0$) the quasi-1D GPE no longer supports bright solitons (see Chapter 2); in this case we study the dynamics of initial condition $\psi_0(x)$ numerically. For simplicity, we concentrate on the case $\alpha = 2$. Other cases $\alpha \gtrsim 2$ are similar except for a slightly altered relationship between k and the resulting soliton speed; consequently an experiment would need to achieve only the latter condition ($\alpha \gtrsim 2$) in order to observe qualitatively similar dynamics. In this axially trapped case, a pair of equal amplitude bright solitary waves are generated with relative phase Φ and velocities controlled by k [Fig. 3.2]. The axial trap confines the outgoing bright solitary waves and causes subsequent re-collisions at the trap centre, for which the relative phase upon re-collision is always identical to the original imposed relative phase [20]. The bright solitary waves remain highly soliton-like: the density profile during bright solitary wave collisions is similar to that for bright solitons [19] [Fig. 3.2(d,f)], the bright solitary wave trajectories are well described by the particle model introduced in Chapter 2 [20, 21, 247] [Fig. 3.2(c–f)], and the bright solitary waves are stable against their mutual collisions. Indeed, they retain their form for a sufficiently large number of collisions that atom losses, unaccounted for in the GPE, would be the lifetime-limiting factor in an experiment.
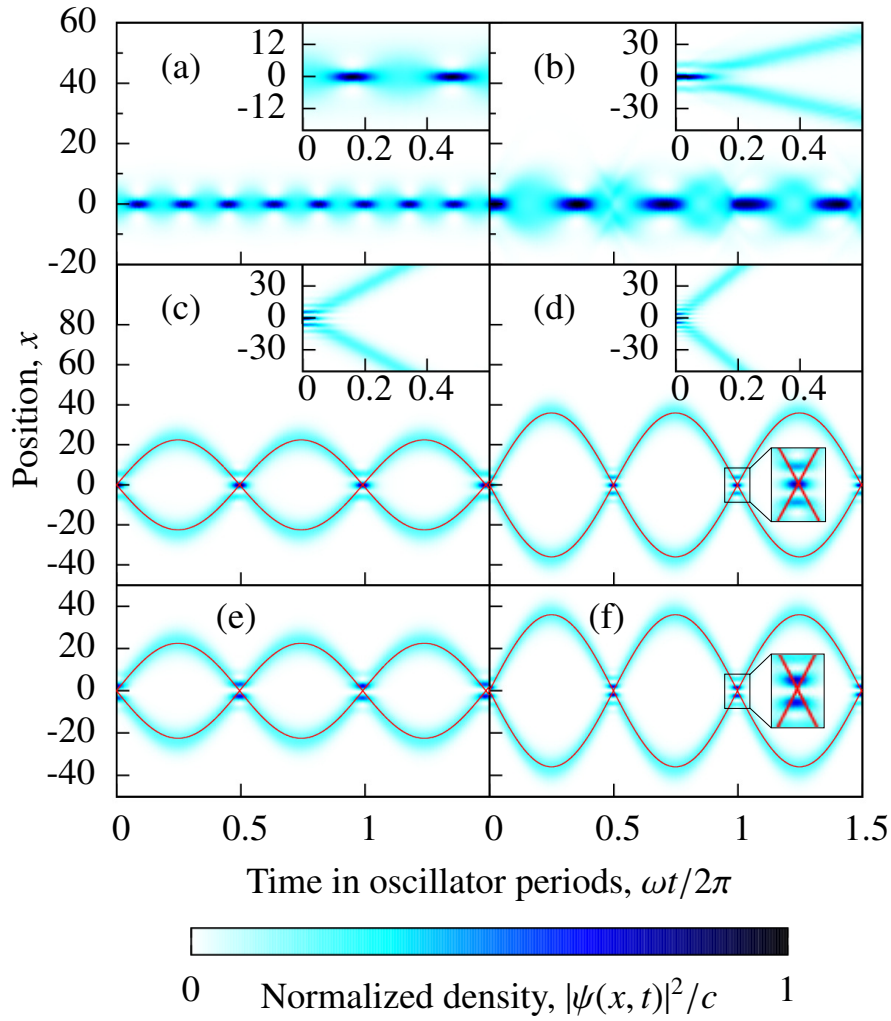
Figure 3.2: Generation of bright solitary waves with controlled relative phase via the interference protocol, in the quasi-1D limit. Panels (a–f) show the evolution of 1D GPE with trap frequency $\omega = 0.02$ [$\omega = 0$ inset in (a–d)] and initial condition $\psi_0(x)$ for $\alpha = 2$, $\Phi = 0$ and $k = 0$ (a), $k = 2$ (b), $k = 4$ (c), $k = 6$ (d), and $\Phi = \pi$ and $k = 4$ (e), $k = 6$ (f), computed using a pseudospectral split-step method (see Appendix B). Particle model [20, 21] bright solitary wave trajectories, for effective masses and velocities obtained from the numerical scattering transform of $\psi_0(x)$, are overlaid as lines in (c–f). Panels (e) and (f) reproduce (c) and (d) for the case $\Phi = \pi$ to show the difference in collision profile. The density (colour) axes are normalized by $c = 0.35$ (inset $c = 0.25$) in (a) and $c = 0.12$ (inset $c = 0.07$) in (b–f).

3.3.4   3D dynamics

Moving beyond the quasi-1D regime, we can generate pairs of 3D bright solitary waves with controlled velocity and relative phase using the same method. However, dynamics in the radial directions can affect the stability of the bright solitary waves; in certain cases this drastically reduces the number of collisions for which they retain their form.

With respect to the quasi-1D GPE, the 3D GPE has a second free parameter, which we choose to express as the (dimensionless) trap anisotropy

$$\kappa = \frac{\omega_r}{\omega_x}. \tag{3.19}$$

Note that this is the **inverse** of the anisotropy λ defined in the previous Chapter; however, κ proves more appropriate for our purposes in this Chapter, and those in Chapter 4. Hence, we write the 3D GPE as

$$i\frac{\partial \psi(\mathbf{r}, t)}{\partial t} = \left[-\frac{\nabla^2}{2} + V(\mathbf{r}) - \frac{2\pi}{\kappa\omega}|\psi(\mathbf{r}, t)|^2 \right]\psi(\mathbf{r}, t), \tag{3.20}$$

where $V(\mathbf{r}) = \omega^2[x^2 + \kappa^2(y^2 + z^2)]/2$, and ensuring unit norm for $\psi(\mathbf{r}, t)$ requires $\psi(\mathbf{r}, t) = b_0^{3/2}\Psi(\mathbf{r}, t)$. We use the same soliton variables as in Eq. (3.6); one advantage of this choice is that the integrated axial density

$$\rho_{\text{axial}}(x, t) = \iint_{-\infty}^{\infty} |\psi(\mathbf{r}, t)|^2 dy\, dz, \tag{3.21}$$

is equivalent to the quasi-1D density $|\psi(x, t)|^2$. We again study the dynamics of the bright solitary waves numerically, quantifying their stability against collisions in terms of their positions and maximum integrated axial densities at the point of maximum separation — this being much easier to measure, on typical experimental scales, than the exact density profile during the collision. Fig. 3.3(a) shows how the number of 1D-like collisions C_{1D} (taken to be those where the positions and maximum integrated densities of the BSWs subsequently return to within 75% of their original values) depends on velocity, relative phase, and trap anisotropy. We term these collisions 1D-like because all collisions of quasi-1D bright solitary waves satisfy these criteria ($C_{1D} \to \infty$).

As expected, Fig. 3.3(a) shows that C_{1D} is strongly dependent on the relative phase at low velocity, with the bright solitary waves being most stable around $\Phi = \pi$ when

outside the quasi-1D regime[1]. At higher velocity this phase-dependence weakens and the quasi-1D regime is reached at lower anisotropy. Fig. 3.3(a) also reveals a previously unobserved feature: C_{1D} shows a strong, oscillatory dependence on the anisotropy at all velocities. This dependence arises from the bright solitary waves being broken up by the transfer of energy to radial oscillations [Fig. 3.3(b–d)]. These oscillations are started by the abrupt change in scattering length, and subsequently amplified by collisions if the bright solitary waves collide when their radial width is close to its oscillatory maximum. Consequently, one observes enhanced stability of the solitary waves if the axial trap period is a whole multiple of the period of the solitary waves' radial oscillations, and reduced stability if the axial trap period is an *odd* multiple of *half* the period of the solitary waves' radial oscillations. Since the frequency of the radial oscillations is primarily determined by ω_r; this leads to the observed oscillations of C_{1D} as a function of κ. The amplifying effect of collisions decreases with the bright solitary wave velocity, and at low velocity a phase-dependent amplification of the radial oscillations emerges [Fig. 3.3(e–g)], which we attribute to the higher densities at the point of collision when $\Phi = 0$ delivering a larger "kick" than when $\Phi = \pi$. However, for intermediate phases symmetry-breaking population transfer [27, 203] during collisions also contributes to the reduction in C_{1D} [Fig. 3.3(f)]. Within the GPE description, Fig. 3.3 represents a comprehensive prediction of the bright solitary wave dynamics resulting from our splitting protocol. Experimental observation of the dynamics we predict would support the validity of the GPE description of bright solitary waves and, in the case of the oscillatory dependence of C_{1D} on κ, open the possibility of controlling the bright solitary wave lifetime directly.

3.3.5   Summary and experimental implementation

In the preceding Sections we have proposed an experiment that produces a pair of bright solitary waves with controlled relative phase and velocity in a harmonically trapped atomic BEC, and we have analysed the subsequent collisions of these bright solitary waves using the GPE. In the quasi-1D regime the bright solitary waves are highly soliton-like and stable against their re-collisions. In the fully 3D regime, we confirm that the collisional stability of the bright solitary waves depends on their relative phase and velocity, and demonstrate for the first time a strong oscillatory dependence on the trap anisotropy. The presence, or absence, of these effects in experiments provides a direct test of whether experimentally observed atomic BSWs

---

[1]In the case $k = 3$ quasi-1D behaviour is reached (the phase dependence of C_{1D} ends) at $\kappa \approx 20$, but this has been omitted from the plotted range for clarity.
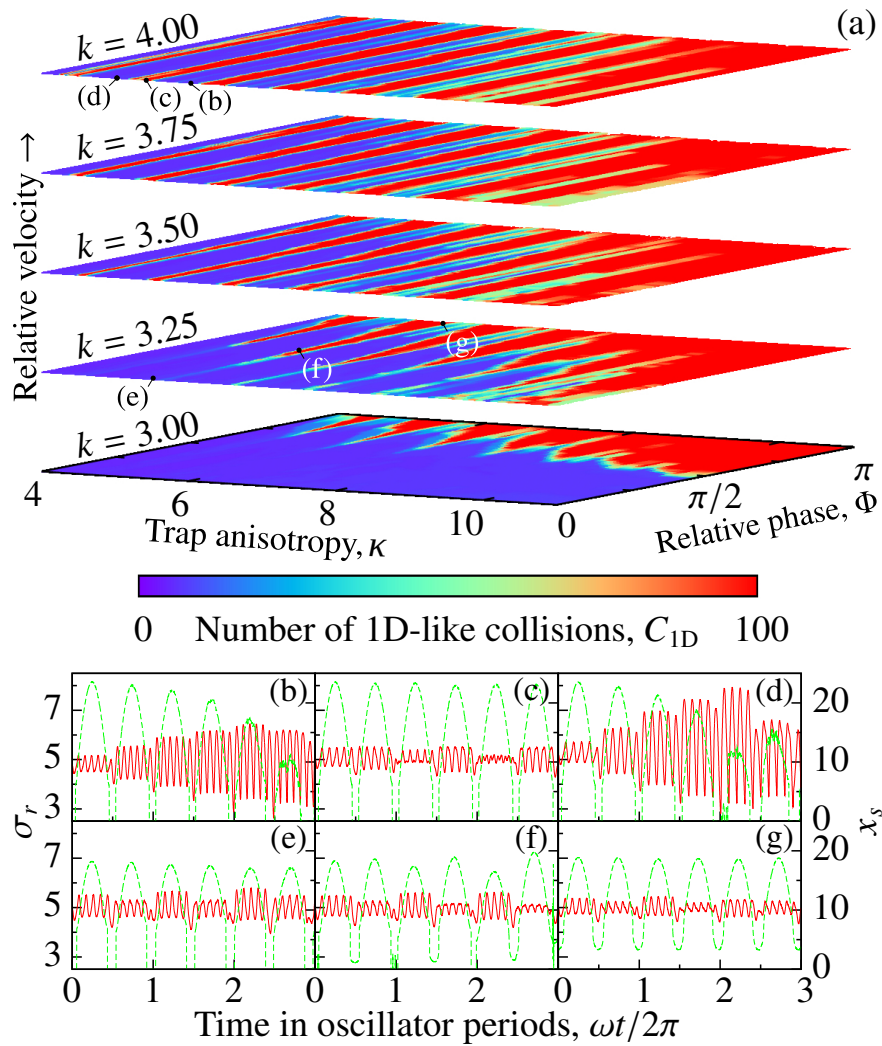
Figure 3.3: Stability of bright solitary wave collisions in 3D. Panel (a) shows the number of 1D-like bright solitary wave collisions, C_{1D}, as a function of k, Φ, and κ. In the case $k = 3$ quasi-1D behaviour is reached (the phase dependence of C_{1D} ends) at $\kappa \approx 20$, but this has been omitted from the plotted range for clarity. Effective trap frequency $\omega = 0.02$ and $\alpha = 2$. Also shown is the evolution of the positively displaced bright solitary wave position, x_s (dashed green line, right vertical axis), and the full width at half maximum of the integrated radial density distribution, σ_r (solid red line, left vertical axis), at the indicated points on the $k = 4$ (b–d) and $k = 3.25$ planes in (a). These quantities demonstrate the enhanced stability which arises when the radial breathing period of the waves is commensurate with the axial trap period.

can be described in terms of a coherent effective single-particle wavefunction, propagated by the GPE.

We now consider the question of the experimental feasibility of our interferometric splitting protocol. Using a two-component GPE, we have simulated an implementation that uses ^{85}Rb atoms in the quasi-1D regime with an applied magnetic field gradient to transfer momentum: we find this simple prototype to be capable of generating initial conditions close to Eq. (3.7) using current experimental technology. We consider an experiment using the hyperfine ground states $|F = 2, m_f = -2\rangle$ and $|3, -2\rangle$ of ^{85}Rb. We assume an instantaneous $\pi/2$ pulse on the two-photon rf/microwave transition coupling $|2, -2\rangle$ and $|3, -2\rangle$, and evolve the resulting state for time τ under a linear applied magnetic field $\mathbf{B}$ given by

$$\mathbf{B} = [B_0 + C(x - x_0)]\hat{\mathbf{B}}, \tag{3.22}$$

where B_0 is a background constant value, and C the field gradient. We assume the scattering length of the $|3, -2\rangle$ state and the inter-state scattering length is $a_\infty = -443a_0$; this choice for the interspecies scattering length represents a "worst-case" scenario. The $|2, -2\rangle$ state has a prominent Feshbach resonance centred on $B_F = 155.0$ Gauss [262]. We account for the consequent spatial variation in scattering length for this state using the model

$$a_s = a_\infty \left[1 - \frac{\Delta}{|\mathbf{B}| - B_F} \right], \tag{3.23}$$

where $\Delta = 10.7$ Gauss is the measured width of the resonance [262]. In soliton units, the components experience potentials (in additional to the harmonic trap potential $V(\mathbf{r})$, which we assume to be generated by all-optical means) $U(x) = \Gamma \pm \gamma(x - x_0)$, where

$$\Gamma = \frac{|g_F||m_f|\mu_B(B_0 - B_F)}{4m\omega_r^2|a_s|^2N^2}, \tag{3.24}$$

and

$$\gamma = \frac{|g_F||m_f|\mu_B C\hbar}{8m^2\omega_r^3|a_s|^3N^3}. \tag{3.25}$$

After time τ we assume another instantaneous $\pi/2$ pulse, and subsequent instantaneous expulsion of the $|3, -2\rangle$ component with resonant light. A good approximation to the initial condition $\psi_0(x)$ [Eq. (3.7)] is obtained when, for example $\omega_x \approx 2\pi(10\,\text{Hz})$, $\omega_r \approx 2\pi(150\,\text{Hz})$, $N \approx 800$, $a_s \approx -20a_0$ ($B_0 \approx 166$ Gauss), $C \approx 75$ Gauss cm^{-1} and $\tau \approx 10\mu$s. The resulting bright solitary wave evolution is shown in Fig. 3.4.
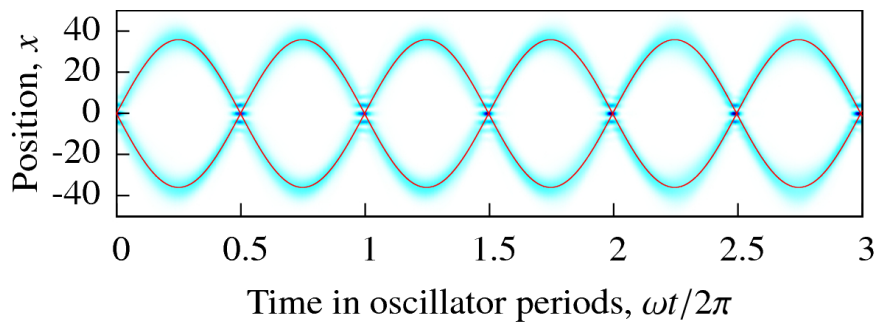
Figure 3.4: Two-component quasi-1D GPE simulation of the interferometric soliton splitting protocol. Following simulation of the splitting with a two-component quasi-1D GPE, as described in Section 3.3.5, we show the evolution of the resulting split bright solitary waves in a harmonic trap. Parameters are as described in Section 3.3.5, and the red line indicates the particle model trajectories for the bright solitary waves.

3.4   Bright solitary wave interferometry

3.4.1   Proposals for a bright solitary wave interferometer

As we have already discussed in the introduction to this thesis, the non-dispersive nature of bright solitary waves in atomic BECs potentially offers a novel solution to the interaction-problem in atomic BEC interferometers [36, 38, 40]. In contrast to a BEC interferometer based on a double-well [33–37], a Mach-Zender interferometer using bright solitary waves could exploit their non-dispersive nature to suppress the problems commonly associated with repulsive interactions. Furthermore, their small size has led to them being proposed as an ideal tool to study atom-surface interactions [44], as well as for general interferometry [10, 43, 263] and in a Sagnac-interferometer configuration in a toroidal trap [80]. In such a bright solitary wave analogue of the optical Mach-Zender interferometer, a BEC would be split into two coherent, non-dispersive, spatially-localized bright solitary waves, which are subsequently manipulated so as to take separate paths and then eventually recombined using a time-dependent external potential. Despite the apparently rapidly decohering nature of many-body effects [28, 257], such an interferometer could potentially be feasible for sufficiently short interrogation times.

The method for phase-controlled coherent splitting of bright solitary waves developed in the previous Section represents one potential realization of the splitting part of a bright solitary wave interferometer. However, contemporary proposals for such

interferometers [43, 80] instead focus on the use of a narrow potential barrier to realize both splitting and recombination of solitary waves. In the next Section we review the operation of these interferometers in the mean-field picture, and consider carefully the potential role of beyond-mean-field effects.

3.4.2   Realizing a solitary wave interferometer

Splitting bright solitary waves at a potential barrier

A simple method to split bright solitary waves is afforded by collisions with a potential barrier. In return for experimental simplicity, however, this method lacks the same fine-grained control over the relative phase. Within the mean field description, the dynamics of NLSE bright soliton collisions with potential barriers and wells has been widely explored (see, e.g., [212, 264–267] and Refs. therein). The behaviour of bright solitary waves is similar in soliton-like regimes; in particular, fast bright solitary wave collisions with a narrow barrier lead to smooth splitting of an incoming solitary wave into transmitted and reflected solitary waves [43, 80, 81, 263, 267]. This behaviour is analogous to bright solitons in the NLSE scattering from a δ-function potential: it can be analytically demonstrated in such a situation that the incoming bright soliton is split into transmitted and reflected components, each of which consist mainly of a bright soliton, plus a small amount of radiation [267]. Bright solitary waves interacting with barriers much narrower than their width largely follow this prediction [43, 80, 263].

In addition to providing a bright solitary wave beamsplitter, a narrow potential barrier can also be used for phase-sensitive recombination of bright solitary waves [43, 80]. When two roughly equal-sized bright solitary waves collide at a narrow barrier the number of atoms emerging to the left (right) of this barrier following recombination, N_L (N_R), is sensitive to the relative phase difference $\delta\Phi$. In particular, nonlinear effects make the relative number difference $(N_L - N_R)/N$ a rapidly changing function of $\delta\Phi$ for small phase differences. A wide-ranging quasi-analytical treatment of this recombination process (and the splitting process) within the mean-field description has been presented by Helm and co-workers (including the present author) in Ref. [80].

Potential barrier collisions of this nature have been proposed as another means to realize bright solitary wave interferometers, potentially based on solitary wave molecules [263], oscillating bright solitary waves in a harmonic trap [43] and bright solitary waves in a toroidal trap [80]. In Ref. [43], Martin and Ruostekoski consider

a bright solitary wave interferometer in which a bright solitary wave consisting of N atoms, oscillating in a quasi-1D harmonic trap, is split into two equal-sized waves by a narrow Gaussian potential raised at the trap centre. Exactly half an oscillator period after this beamsplitter stage the bright solitary waves are recombined again when they return to the potential at the trap centre. In Ref. [80] a related set-up using two narrow barriers in a quasi-1D toroidal trap is proposed. In both cases the enhancement of the relative number difference $(N_L - N_R)/N$ due to nonlinear effects offers the potential to construct a very sensitive interferometric device. In the set-up of Ref. [80] this device would be able to measure rotation.

Beyond-mean-field effects

To fully understand the operation of such an interferometer, however, one must quantitatively account for number fluctuations. This is especially important with regard to achieving sub-shot-noise measurement precision [38, 40, 43, 84, 132, 268, 269]. The mean-field GPE yields no definitive information on number statistics. Although the GPE is often interpreted as describing a system with a wavefunction of Hartree product form (that is, a single macroscopically occupied single particle mode) and hence free of many-body correlations [42], this is not the sole interpretation: it can also give an appropriate a classical-field description of a multi-mode system with multiple macroscopically occupied modes, as in the widely-used c-field methods [171] (see also Chapter 1 and Chapter 5). Indeed, a recent work (involving the present author) work explicitly demonstrates that, for the exact case of a bright soliton split by a δ-function potential, the GPE can evolve itself into a state where a Hartree-product interpretation is energetically forbidden [81]. Hence, one should at least be wary of *universally* using the Hartree product assumption to state that the GPE implies zero number fluctuations, as in Refs. [42] and [257].

In Ref. [43] a truncated Wigner method [171] (see Chapter 5) is used to study number fluctuations. This study reveals that the enhanced sensitivity due to nonlinear effects is generally destroyed by enhanced number fluctuations, although the authors suggest that a change of experimental scheme could alleviate this difficulty. However, the truncated Wigner method only allows for a limited degree of macroscopic superposition between the split solitons [43]; for any state approaching a maximally entangled "NOON" state [268] of solitons a full many-body approach is required [41, 42]. Such an approach for scattering a BEC bright soliton on a potential is challenging; even in 1D, with a potential barrier the many-body Hamiltonian can no longer be solved using the Bethe ansatz [41]. Nonetheless it was demonstrated

in Ref. [41], using an effective potential approximation, that a condensate bright soliton of 100 atoms could be placed in a coherent macroscopic superposition between reflected and transmitted solitons via a slow collision with a wide Gaussian barrier — a state entirely dominated by many-body correlations rather than free of them. Similar collisions were investigated in Ref. [42] using the MCTDHB many-body computational method [258, 259]. In this work, the condensate was found to fragment, leaving two macroscopically occupied orbitals. One of these orbitals corresponded to a transmitted, and the other to a reflected, bright soliton, implying creation of a macroscopic coherent superposition between spatially distinct states.

This potential to realize macroscopic quantum effects using bright solitary waves offers exciting potential for future interferometric devices, as states with macroscopic quantum superposition could be exploited to achieve quantum enhancement of the measurement precision [38, 40, 84, 85]. Typically, when discussing the precision of interferometric schemes, one considers precision relative to: (a) the *shot-noise limit*, which is defined by a measurement precision scaling as $N^{-1/2}$ — where N is the number of particles — and corresponds to the limit imposed by classical, poissonian statistics; and (b) the *Heisenberg limit*, which is defined by a measurement precision scaling as N^{-1} and corresponds to the absolute quantum limit of precision achievable with *non-interacting* [132]. While interferometric schemes exploiting quantum effects using non-interacting particles can be used to surpass the shot-noise limit [84], a more spectacular improvement in precision can, in principle, be obtained in interacting systems; in a system where all possible k-body interactions appear a measurement precision scaling up to N^{-k}, and hence surpassing the Heisenberg limit, can in principle be achieved [270]. While without the use of entangled initial states this precision scaling is reduced to $N^{-(k-1/2)}$ [270], a bright solitary wave interferometer operating with a non-entangled, mean-field input such as we describe above has the potential to achieve a measurement precision scaling as $N^{-3/2}$, surpassing the Heisenberg limit.

Chapter 4: Realizing a soliton-like regime with bright solitary waves

4.1 Introduction

In the preceding two Chapters we have explored in some detail the dynamics and collisions of bright solitary waves, in both quasi-1D and 3D regimes. In particular we have demonstrated that bright solitary waves can display highly soliton-like *dynamics* in three-dimensional (3D) parameter regimes (Chapter 3). However, we have not directly addressed the question of exactly how soliton-like the (metastable) ground state of the system is. In this regard, the experimental feasibility of reaching the quasi-1D limit of an attractively-interacting BEC, and hence obtaining a highly soliton-like ground state, remains an area lacking a thorough quantitative exploration. Obtaining such a ground state, in addition to being interesting in its own right, would be highly advantageous in experiments seeking to probe quantum effects beyond the mean-field description [41, 42, 258], and possibly to exploit the effects of macroscopic quantum superposition to enhance metrological precision as discussed in the previous Chapter [84, 132]. Similar concerns regarding adverse residual 3D effects in interferometric protocols prompted a recent perturbative study of residual 3D effects in highly anisotropic, repulsively-interacting BECs [271].

The potential instability to collapse of attractively-interacting BECs [23–25, 131, 222, 223, 234–236, 239] is the key obstacle to realizing soliton-like behaviour in a 3D BEC. This instability was explored at length using variational methods in Chapter 2. To recap, previous studies of bright solitary wave dynamics, using variational and numerical solutions of partially-quasi-1D GPEs [200–203] [reductions of the GPE to a 1D equation which retain some 3D character, in contrast to the full quasi-1D limit] and the 3D GPE [22, 23, 27], have shown the collapse instability to be associated with non-soliton-like behaviour. However, previous studies of metastable bright solitary wave ground states — including the analysis in Chapter 2 — have focused on identifying the critical parameters at which collapse occurs [23, 196, 201, 222, 231, 233–235, 272].

In this Chapter we use analytic variational and highly accurate numerical solutions of the stationary GPE to systematically and quantitatively assess how soliton-like

the ground state of an attractively-interacting BEC in a prolate, cylindrically symmetric harmonic trap is, over a wide regime of trap and interaction strengths. Beginning with previously-considered variational ansatzes based on Gaussian [23, 196, 272] and soliton [23, 231] profiles (which we also introduced in Chapter 2) we obtain new, analytic variational solutions for the GPE ground state. Comparing the soliton-ansatz variational solution to highly accurate numerical solutions of the stationary GPE, which we calculate over an extensive parameter space, gives a quantitative measure of how soliton-like the ground state is. In the regime where the axial and radial trap strengths dominate over the interactions, we show that the Gaussian ansatz variational solution gives an excellent approximation to the true ground state for all anisotropies; in this regime the ground state is not soliton-like. In the regime in which the interactions dominate over the axial, but *not* the radial, trap strength we demonstrate that the soliton-ansatz variational solution does approximate the true, highly soliton-like ground state. However, we show that the goodness of the approximation and the extent of this regime, where it exists at all, is highly restricted by the collapse instability; even at large anisotropies it occupies a narrow window adjacent to the regime where interactions begin to dominate over *all* trap strengths, leading to non-quasi-1D, non-soliton-like solutions and, ultimately, collapse.

Our results have substantial practical value for future experiments using attractively-interacting BECs; primarily they define the challenging experimental regime required to realize a highly soliton-like ground state, which would be extremely useful to observe quantum effects beyond the mean-field description such as macroscopic superposition of solitons [41, 42, 258]. We note that bright solitary wave experiments to date have not reached this regime [10–12]. Secondly, our quantitative analysis of a wide parameter space provides a picture of the ground state in a wide range of possible attractively-interacting BEC experiments. In particular, it indicates the regimes in which a full numerical solution of the 3D GPE is well-approximated by one of our analytic variational solutions, which are significantly easier and less time-consuming to determine.

We begin by introducing the most general classical field Hamiltonian and stationary GPE we consider in Section 4.2, and we discuss the quasi-1D limit and our choice of soliton units in Section 4.3. Our variational ansatzes are motivated by the limiting behaviours of the solution in the quasi-1D case; in this case we define them as Gaussian and soliton profiles, parametrized by their axial lengths. In Sections 4.3.2 and 4.3.3 we find, analytically, the energy-minimizing axial lengths for each ansatz as a function of the dimensionless effective trap strength ω. Comparison of the

resulting ansatz solutions to highly accurate numerical solutions of the stationary quasi-1D GPE allows us to determine, in the quasi-1D limit, the regimes of low ω in which highly soliton-like ground states can be realized (Section 4.3.4). We then consider the 3D GPE in Section 4.4, which has a second free parameter in κ, the (dimensionless) trap anisotropy. In Sections 4.4.2 to 4.4.5 we define 3D Gaussian and soliton ansatzes, adapted from their quasi-1D analogues and each parametrized by an axial and a radial length, and find the energy-minimizing lengths for each ansatz. In general this requires only a very simple numerical procedure, and in the limit of a waveguide-like trap can be expressed analytically (Section 4.4.6). In Section 4.4.7 we compare the ansatz solutions to highly accurate numerical solutions of the stationary 3D GPE and, in Section 4.5, assess the potential for realizing truly soliton-like ground states. We provide a final summary of the results of this Chapter in Section 4.6.

4.2 System overview

As in previous Chapters, we consider a BEC of N atoms of mass m and (attractive) s-wave scattering length $a_s < 0$, held within a cylindrically symmetric, prolate (the radial frequency ω_r is greater than the axial frequency ω_x) harmonic trap. The ground state is described by the stationary Gross-Pitaevskii equation

$$\left[-\frac{\hbar^2}{2m}\nabla^2 + V(\mathbf{r}) - \frac{4\pi N|a_s|\hbar^2}{m}|\psi(\mathbf{r})|^2 - \mu \right]\psi(\mathbf{r}) = 0, \tag{4.1}$$

where the trapping potential $V(\mathbf{r}) = m[\omega_x^2 x^2/2 + \omega_r^2(y^2 + z^2)/2]$, μ is the chemical potential, and the Gross-Pitaevskii wavefunction $\psi(\mathbf{r})$ is again normalized to one. This equation is generated by the classical field Hamiltonian (through the functional derivative $\delta H[\psi]/\delta\psi^* = \mu\psi$)

$$H[\psi] = \int d\mathbf{r} \left[\frac{\hbar^2}{2m}|\nabla\psi(\mathbf{r})|^2 + V(\mathbf{r})|\psi(\mathbf{r})|^2 - \frac{2\pi N|a_s|\hbar^2}{m}|\psi(\mathbf{r})|^4 \right]. \tag{4.2}$$

This functional of the classical field ψ describes the total energy per particle, and the ground state solution minimizes the value of this functional.

When dealing with variational ansatzes for the ground state solution, we proceed by analytically minimizing an energy functional in the same form as [Eq. (4.2)] for a given ansatz. In contrast, highly accurate numerical ground states are more conveniently obtained by solving a stationary GPE of the same form as [Eq. (4.1)].

4.3   Quasi-1D limit

4.3.1   Soliton units

As in Chapter 2, for sufficiently tight radial confinement ($\omega_r \gg \omega_x$), such that the atom-atom interactions are nonetheless essentially 3D [$a_s \ll (\hbar/m\omega_r)^{1/2}$], it is conventional [20, 21, 196, 200, 201, 272] to assume a reduction to an quasi-1D stationary GPE

$$\left[-\frac{\hbar^2}{2m}\frac{\partial^2}{\partial x^2} + \frac{m\omega_x^2 x^2}{2} - 2\hbar\omega_r |a_s| N |\psi(x)|^2 - \mu \right] \psi(x) = 0. \qquad (4.3)$$

Here, we remind the reader that this equation [identical to Eq. (2.5)] arises from the assumption that $\psi(\mathbf{r})$ can be factorized into $\psi(x)$ and the radial harmonic ground state. In the absence of the axial harmonic confining potential ($\omega_x \to 0$) the exact bright soliton solutions to this equation have the general form [Eq. (2.9)]

$$\psi(x, t) = \frac{a}{2\sqrt{b_x}}\mathrm{sech}\left(\frac{a(x - x_0 - vt)}{2b_x}\right)$$

$$\times \exp\left(i\left[\frac{m}{\hbar}\left\{v(x - x_0) + \frac{v^2 t}{2} + \frac{\omega_r^2 |a_s|^2 N^2 a^2 t}{2}\right\} + \Phi\right]\right), \quad (4.4)$$

where we recall that $b_x = \hbar/2m\omega_r |a_s| N$ is a length scale characterizing the soliton's spatial extent, v is the soliton velocity, x_0 is an arbitrary displacement, and Φ is an arbitrary phase.

As in Chapter 3, we use a system of soliton units (Section 3.3.1) in order that the dimensionless effective trap strength $\omega = (b_x/a_x)^2$ is the single free parameter. This yields the dimensionless, stationary, quasi-1D GPE

$$\left[-\frac{1}{2}\frac{\partial^2}{\partial x^2} + \frac{\omega^2 x^2}{2} - |\psi(x)|^2 - \mu \right] \psi(x) = 0. \qquad (4.5)$$

The corresponding classical field Hamiltonian is

$$H_{1D}[\psi] = \int dx \left[\frac{1}{2}\left|\frac{\partial}{\partial x}\psi(x)\right|^2 + \frac{\omega^2 x^2}{2}|\psi(x)|^2 + \frac{1}{2}|\psi(x)|^4 \right]. \qquad (4.6)$$

The choice of ω for the single free parameter in the 1D GPE [Eq. (4.5)] and the classical field Hamiltonian [Eq. (4.6)] can be most directly pictured as choosing to hold interaction strength constant while varying the axial trap strength, parametrized by

ω. Experimentally, however, any of ω_x, ω_r, a_s, and N may be varied in order to vary ω. In the case $\omega = 0$ the exact ground state solution is a single, stationary bright soliton: $\psi(x) = \mathrm{sech}(x/2)/2$. In the following Sections we develop analytic variational solutions $\psi(x)$ for general ω. Comparing these solutions to highly accurate numerical solutions of the quasi-1D GPE then gives a picture of the behaviour of the ground state with ω. Furthermore, these quasi-1D variational solutions motivate the later 3D variational solutions and yield several mathematical expressions which reappear in the more complex 3D calculations.

4.3.2   Variational solution: Gaussian ansatz

We first consider the Gaussian variational ansatz

$$\psi(x) = \left(\frac{\omega}{\pi \ell_G^2}\right)^{1/4} e^{-\omega x^2 / 2\ell_G^2}, \tag{4.7}$$

where the variational parameter, ℓ_G, quantifies the axial length. In the trap-dominated limit ($\omega \to \infty$), the true solution tends to a Gaussian with $\ell_G = 1$. Substituting Eq. (4.7) into Eq. (4.6) yields (using identities from Appendix A.2)

$$H_{1D}(\ell_G) = \frac{\omega}{4}\left(\ell_G^2 + \frac{1}{\ell_G^2} - \frac{2}{(2\pi\omega)^{1/2}\ell_G}\right), \tag{4.8}$$

where H_{1D} is now expressed as a function of the axial length ℓ_G. Setting $\partial H_{1D}/\partial \ell_G = 0$ reveals that the variational energy described by Eq. (4.8) is minimized when ℓ_G is a positive, real solution to the quartic equation

$$\ell_G^4 + \frac{\ell_G}{(2\pi\omega)^{1/2}} - 1 = 0. \tag{4.9}$$

The positive, real solution to this quartic is (see solution in Appendix A.3)

$$\ell_G = \frac{[\chi(\omega)]^{1/2}}{2^{4/3}(\pi\omega)^{1/6}}\left\{\left[\left(\frac{2}{\chi(\omega)}\right)^{3/2} - 1\right]^{1/2} - 1\right\}, \tag{4.10}$$

where we have, for notational convenience, defined χ to have ω-dependence such that

$$\chi(\omega) = \left[1 + \left(1 + \frac{1024\pi^2\omega^2}{27}\right)^{1/2}\right]^{1/3} + \left[1 - \left(1 + \frac{1024\pi^2\omega^2}{27}\right)^{1/2}\right]^{1/3}. \tag{4.11}$$

4.3.3   Variational solution: soliton ansatz

Secondly, we consider a soliton ansatz

$$\psi(x) = \frac{1}{2\ell_S^{1/2}} \text{sech}\left(\frac{x}{2\ell_S}\right), \qquad (4.12)$$

where the variational parameter, ℓ_S, again quantifies the axial length. In the axially un-trapped limit ($\omega \to 0$), the true solution tends to a classical bright soliton, as described by the above ansatz with $\ell_S = 1$. The variational energy per particle is given by (using identities from Appendix A.2)

$$H_{1D}(\ell_S) = \frac{\pi^2\omega^2}{6}\left(\ell_S^2 + \frac{1}{4\pi^2\omega^2\ell_S^2} - \frac{1}{2\pi^2\omega^2\ell_S}\right), \qquad (4.13)$$

which is minimized when

$$\ell_S^4 + \frac{\ell_S}{4\pi^2\omega^2} - \frac{1}{4\pi^2\omega^2} = 0. \qquad (4.14)$$

Again, this quartic can be solved analytically (see solution in Appendix A.3) to give the positive, real minimizing value of ℓ_S;

$$\ell_S = \frac{[\chi(\omega)]^{1/2}}{2^{11/6}(\pi\omega)^{2/3}}\left\{\left[\left(\frac{2}{\chi(\omega)}\right)^{3/2} - 1\right]^{1/2} - 1\right\}, \qquad (4.15)$$

with χ defined as in Eq. (4.11).

4.3.4   Analysis and comparison to 1D numerical solutions

The energy-minimizing axial lengths ℓ_G and ℓ_S, defined by Eq. (4.10) and Eq. (4.15) respectively, are shown as a function of ω in Fig. 4.1(a). There is no collapse instability in the quasi-1D GPE, and solutions are obtained for all (positive, real) ω. As intended by the chosen forms of the ansatzes, the limiting cases are $\ell_G \to 1$ as $\omega \to \infty$ and $\ell_S \to 1$ as $\omega \to 0$. To evaluate the accuracy of the ansatzes for general ω, we compare each ansatz with the numerically determined ground state of the quasi-1D GPE. The computation of a numerically exact ground state $\psi_0(x)$, and the corresponding ground state energy E_{1D}, uses a pseudospectral method in a basis of symmetric Gauss-Hermite functions; this is a simplified version of the pseudospectral method used for 3D calculations, which is explained in more detail in the next Section, and in Appendix B. Several quantities are compared in Fig. 4.1(b–d): the variational minimum energies H_{1D} for each ansatz and the numerical ground state
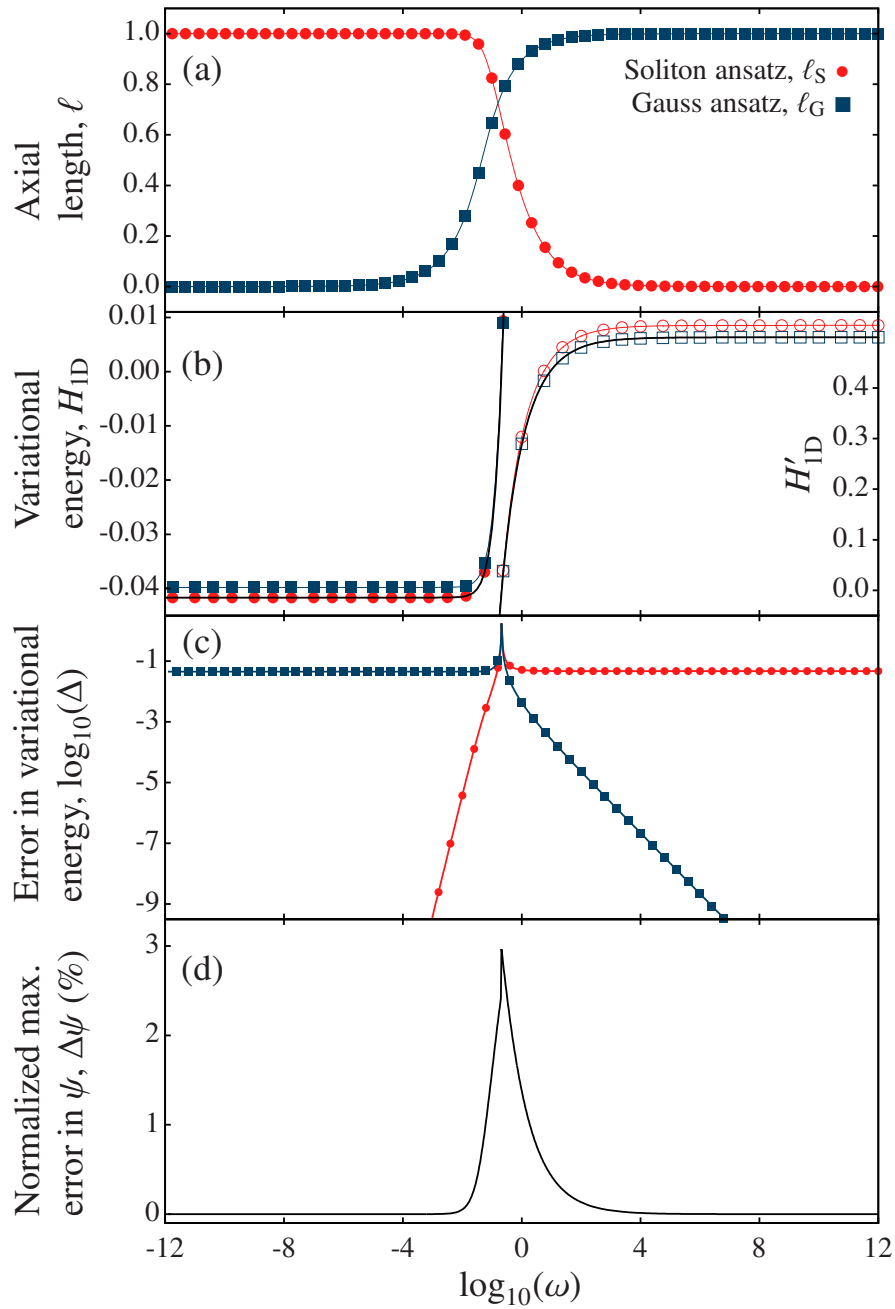
Figure 4.1: Comparison of quasi-1D variational and numerical solutions as a function of the ratio between trap strength and interaction strength, ω: (a) Energy-minimizing axial lengths ℓ_G (Gaussian ansatz, squares) and ℓ_S (soliton ansatz, circles) for the quasi-1D GPE. (b) Minimum variational energy compared with the numerically calculated ground state energy E_{1D} (black line) for each ansatz: for low ω we show H_{1D} (solid symbols), which tends to $-1/24$ as $\omega \to 0$; for high ω we show $H'_{1D} = H_{1D}/\omega$ (hollow symbols), which tends to $1/2$ as $\omega \to \infty$ (H'_{1D} is equal to the energy expressed in the "harmonic units," $\hbar = m = \omega_x = 1$). (c) Relative error in the variational energy, $\Delta = (H_{1D} - E_{1D})/E_{1D}$. (d) Normalized maximum deformation of the best-fitting ansatz wavefunction ψ_{Ansatz} with respect to the numerical ground state ψ_0, $\Delta\psi = \max(|\psi_{Ansatz} - \psi_0|)/\max(\psi_0)$, expressed as a percentage. For clarity in (a,b) [(c)], every 16th [20th] datum is marked by a symbol.

energy E_{1D} are shown in Fig. 4.1(b); the relative error between H_{1D} and E_{1D}, defined as $\Delta = (H_{1D} - E_{1D})/|E_{1D}|$, is shown for each ansatz in Fig. 4.1(c); and the maximum difference between the most appropriate ansatz wavefunction (that with lowest Δ) and the numerical ground state wavefunction, expressed as a percentage of the maximum value of the numerically exact ground state, $\Delta\psi = \max(|\psi_{\text{Ansatz}} - \psi_0|)/\max(\psi_0)$ [Fig. 4.1(d)]. All the shown computed quantities are insensitive to a doubling of the numerical basis size from 500 to 1000 states.

Both the Gaussian and soliton ansatzes provide an excellent approximation to the exact solutions over a large range of ω. In the regimes where the relative error in the energy Δ becomes significantly lower than 10^{-9} in particular, the difference between the ansatz solutions and numerical solutions becomes generally indistinguishable from numerical round-off error. For the Gaussian ansatz the convergence to this regime is noticeably slower than for the soliton ansatz [Fig. 4.1(c)]. This effect is a consequence of the parametrization in terms of ω and the corresponding "soliton units": increasing ω leads not only to to higher trap strength, but also to higher peak densities $|\psi(x)|^2$, and hence a stronger nonlinear effect.

For later comparison to the 3D case, it is useful to define a benchmark value of the relative error Δ that indicates excellent agreement between the ansatz and the numerically exact solution. Such a definition, however, will vary according to purpose. As our objectives in this Chapter relate significantly to the *shape* of the ground state, this forms the basis of our benchmark; a maximum deformation of the wavefunction below 0.1% of the peak value [as measured by $\Delta\psi$ in Fig. 4.1(d)] corresponds very closely to $\Delta < 10^{-5}$. Because the relative error Δ saturates to a background value of $\approx 10^{-1}$ in regimes where the chosen ansatz is inapplicable, a value of Δ four orders of magnitude below this background value thus corresponds to an excellent match in shape between the ansatz and the numerically exact solution. With respect to this benchmark, the Gaussian ansatz represents an excellent fit for $\log_{10}(\omega) > 1.15$, while the ground state is highly soliton-like (the soliton ansatz represents an excellent fit) for $\log_{10}(\omega) < -0.95$.

4.4 Bright solitary wave ground states in 3D

4.4.1 Rescaling to effective 1D soliton units

We now consider the cylindrically symmetric 3D Gross-Pitaevskii equation given by Eq. (4.1). Compared to the quasi-1D effective Gross-Pitaevskii equation of

Eq. (4.5), three-dimensionality introduces an additional relevant length scale, the radial harmonic length $a_r = (\hbar/m\omega_r)^{1/2}$. As in Chapter 3 we incorporate this into the dimensionless trap anisotropy $\kappa \equiv \omega_r/\omega_x$, which forms an additional free parameter. Expressed in the same "soliton units" as Eq. (4.5), Eq. (4.1) becomes

$$\left[-\frac{1}{2}\nabla^2 + V(\mathbf{r}) - \frac{2\pi}{\kappa\omega}|\psi(\mathbf{r})|^2 - \mu \right]\psi(\mathbf{r}) = 0, \tag{4.16}$$

with corresponding energy functional

$$H_{3D}[\psi] = \int d\mathbf{r} \left[\frac{1}{2}\nabla\psi(\mathbf{r})\cdot\nabla\psi^*(\mathbf{r}) + V(\mathbf{r})|\psi(\mathbf{r})|^2 - \frac{\pi}{\kappa\omega}|\psi(\mathbf{r})|^4 \right], \tag{4.17}$$

where $V(\mathbf{r}) = \omega^2[x^2 + \kappa^2(y^2 + z^2)]/2$.

In the following Sections we obtain variational solutions for general κ and ω using ansatzes similar to the Gaussian and soliton ansatzes employed in the previous Section, with an additional variable-width Gaussian radial profile. Contrary to the case in the quasi-1D limit, a self-consistent energy-minimizing solution for both the axial and radial length parameters cannot be expressed entirely analytically. However, we reduce the numerical work required to the simultaneous solution of two equations, and introduce a straightforward iterative technique to achieve this. We also consider the case of a waveguide-like trap ($\omega_x = 0$) separately, where an entirely analytic variational solution exists (Section 4.4.6). Subsequently, in Section 4.4.7, we again compare the ansatz solutions to high-accuracy numerics.

4.4.2   Variational solution: Gaussian ansatz

We first consider an ansatz composed of Gaussian axial and radial profiles. We phrase this as

$$\psi(\mathbf{r}) = \frac{\kappa^{1/2}\omega^{3/4}k_{\mathrm{G}}}{\pi^{3/4}\ell_{\mathrm{G}}^{1/2}} e^{-\kappa\omega k_{\mathrm{G}}^2(y^2+z^2)/2} e^{-\omega x^2/2\ell_{\mathrm{G}}^2}. \tag{4.18}$$

Here, the first variational parameter, ℓ_{G}, quantifies the axial length of the ansatz in analogy to the quasi-1D case. The *reciprocal* of the second variational parameter, k_{G}^{-1}, quantifies the radial length of the ansatz. In the trap-dominated limit ($\omega \to \infty$) both these lengths approach unity ($\{\ell_{\mathrm{G}}, k_{\mathrm{G}}\} \to 1$). Substitution of this ansatz into Eq. (4.17) yields (using identities from Appendix A.2)

$$H_{3D}(\ell_{\mathrm{G}}, k_{\mathrm{G}}) = \frac{\omega}{4}\left(\ell_{\mathrm{G}}^2 + \frac{1}{\ell_{\mathrm{G}}^2} - \frac{2k_{\mathrm{G}}^2}{(2\pi\omega)^{1/2}\ell_{\mathrm{G}}} + 2\kappa k_{\mathrm{G}}^2 + \frac{2\kappa}{k_{\mathrm{G}}^2} \right). \tag{4.19}$$

Setting the partial derivatives with respect to both ℓ_G and k_G equal to zero, we deduce that ℓ_G must solve the quartic equation

$$\ell_G^4 + \frac{k_G^2 \ell_G}{(2\pi\omega)^{1/2}} - 1 = 0, \tag{4.20}$$

and that k_G must solve

$$k_G = \left(\frac{(2\pi\omega)^{1/2} \kappa \ell_G}{(2\pi\omega)^{1/2} \kappa \ell_G - 1} \right)^{1/4}. \tag{4.21}$$

From Eq. (4.21) it follows that we must have $\ell_G > 1/(2\pi\omega)^{1/2}\kappa$ to obtain a physically reasonable solution, i.e., a real, positive value of k_G, consistent with our initial ansatz. For a given such value of k_G, Eq. (4.20) is solved (see solution in Appendix A.3) by

$$\ell_G = \frac{\left[\chi\left(\omega k_G^{-4} \right) \right]^{1/2} k_G^{2/3}}{2^{4/3}(\pi\omega)^{1/6}} \left\{ \left[\left(\frac{2}{\chi\left(\omega k_G^{-4} \right)} \right)^{3/2} - 1 \right]^{1/2} - 1 \right\}, \tag{4.22}$$

with χ defined as in Eq. (4.11).

4.4.3 Analysis of Gaussian ansatz solution

Contrary to the quasi-1D limit, minimization of the variational energy in 3D requires simultaneous solution of two equations for the radial length, k_G^{-1}, and the axial length, ℓ_G. These equations are, respectively, Eq. (4.21) and [rearranged from Eq. (4.20)]

$$k_G = \left[\frac{(2\pi\omega)^{1/2}}{\ell_G} \left(1 - \ell_G^4 \right) \right]^{1/2}. \tag{4.23}$$

These equations dictate that physical solutions must have

$$\frac{1}{(2\pi\omega)^{1/2}\kappa} < \ell_G < 1, \tag{4.24}$$

and hence that $\omega > 1/2\pi\kappa^2$ must be satisfied in order for physical solutions to exist.

Where solutions exist, they must be found numerically. However, a very practical method of numerical solution follows from the shape of the ℓ_G surface defined by Eq. (4.22), and shown in Fig. 4.2(a), which is a decreasing function of k_G for all (real, positive) ω. The method can be considered graphically, in terms of locating the intersection(s) of Eq. (4.21) and Eq. (4.23). These curves are shown, for various κ, in Fig. 4.2(b–d), along with the lower bound from inequality Eq. (4.24). Below a
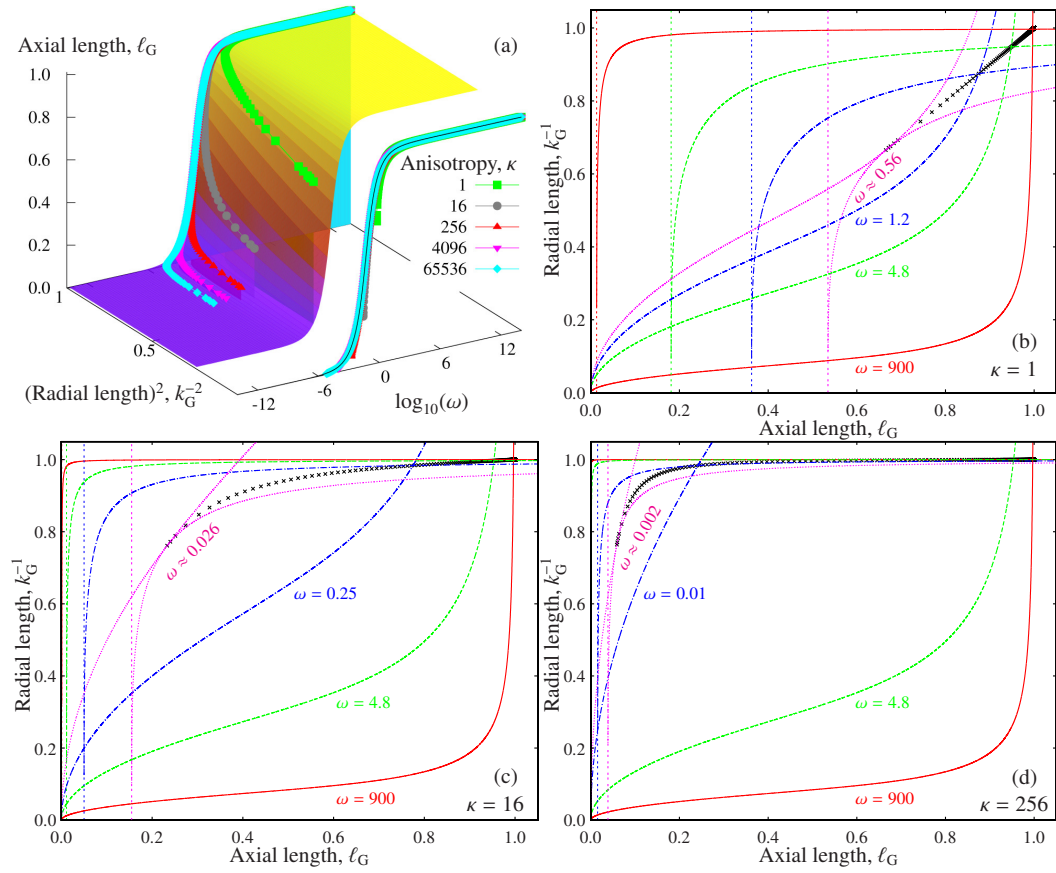
Figure 4.2: Energy-minimizing variational parameters for the 3D GPE using a Gaussian ansatz: (a) axial length ℓ_G as a function of the radial length k_G^{-1} and the parameter ω [Eq. (4.22)]. Lines show the simultaneous solutions of Eqs. (4.21) and (4.23) for the axial length ℓ_G and radial length k_G^{-1}, for different anisotropies κ and values of ω. Projections of these solutions on the ω–ℓ_G plane are also shown; here the black line indicates the quasi-1D result [from Fig. 4.1(a)]. (b–d) Illustration of the intersections of Eq. (4.21) [lines with vertical asymptote $\ell_G = 1/(2\pi\omega)^{1/2}\kappa$ shown with fine dashes] and Eq. (4.23) for various κ: the higher-ℓ_G intersection, which corresponds to a physical solution for the axial length ℓ_G and radial length k_G^{-1}, can be found using a "staircase" method starting from $k_G = 1$. The numerical solutions obtained this way, and shown by points in (a), are shown by crosses in (b–d). The lowest values of ω plotted in (b–d) are the lowest for which a self-consistent Gaussian ansatz solution is found.

κ-dependent threshold value of ω the curves fail to intersect, indicating instability of the BEC to collapse. At the threshold value [dotted curves in Fig. 4.2(b–d)] there is exactly one intersection, and above the threshold value [other curves in Fig. 4.2(b–d)] there are two intersections. In the latter case the higher-ℓ_G intersection, which smoothly deforms to the limiting case $\{\ell_G, k_G\} \rightarrow 1$ as $\omega \rightarrow \infty$, represents the physical, minimal-energy variational solution. This solution can be located using a simple "staircase" method: substituting a trial value $\bar{k}_G$, satisfying $1 \leq \bar{k}_G < k_G$, into Eq. (4.22) produces a trial value, $\bar{\ell}_G$, satisfying $\ell_G < \bar{\ell}_G \leq 1$, and subsequently substituting this trial value into Eq. (4.21) produces an iterated trial value, $\bar{k}'_G$, satisfying $\bar{k}_G < \bar{k}'_G < k_G$. Thus, beginning with $\bar{k}_G = 1$, iteration of this process converges the trial values to the true k_G and ℓ_G.

The physical solutions to Eqs. (4.20) and (4.21) for different anisotropies κ are shown on the ℓ_G surface, and projected into the ℓ_G–ω plane, in Fig. 4.2(a). These solutions are also shown as black crosses in the ℓ_G–k_G plane in Figs. 4.2(b–d), where they form a line connecting the physical-solution intersections of Eqs. (4.21) and (4.23) for the various ω shown. In Fig. 4.2(a) the collapse instability is manifest as a rapid rise in k_G — corresponding to a decrease in radial extent — and fall in ℓ_G — corresponding to a decrease in axial extent — just above a κ-dependent threshold value of ω. There are no self-consistent solutions for these quantities below this collapse threshold. For increasing anisotropies κ, this collapse threshold occurs at lower values of ω. For the highest two values of κ considered the collapse threshold lies in the regime where ℓ_G is already approaching 0; our analysis of the Gaussian ansatz in the quasi-1D limit indicates that the 3D Gaussian ansatz will be a poor approximation to the true solution in this regime. Importantly, for ω above the collapse threshold the projected curves for each anisotropy agree well with the Gaussian ansatz in the quasi-1D GPE, suggesting that the Gaussian ansatz gives a good approximation to the true solution here.

4.4.4   Variational solution: soliton ansatz

Secondly, we consider a soliton ansatz composed of a axial sech profile and a radial Gaussian profile. We phrase this as

$$\psi(\mathbf{r}) = \frac{\omega^{1/2} \kappa^{1/2} k_S}{(2\pi\ell_S)^{1/2}} e^{-\kappa\omega k_S^2 (y^2 + z^2)/2} \text{sech}(x/2\ell_S). \tag{4.25}$$

As with the 3D Gaussian ansatz, the first variational parameter, ℓ_G, quantifies the axial length of the ansatz and the *reciprocal* of the second variational parameter,
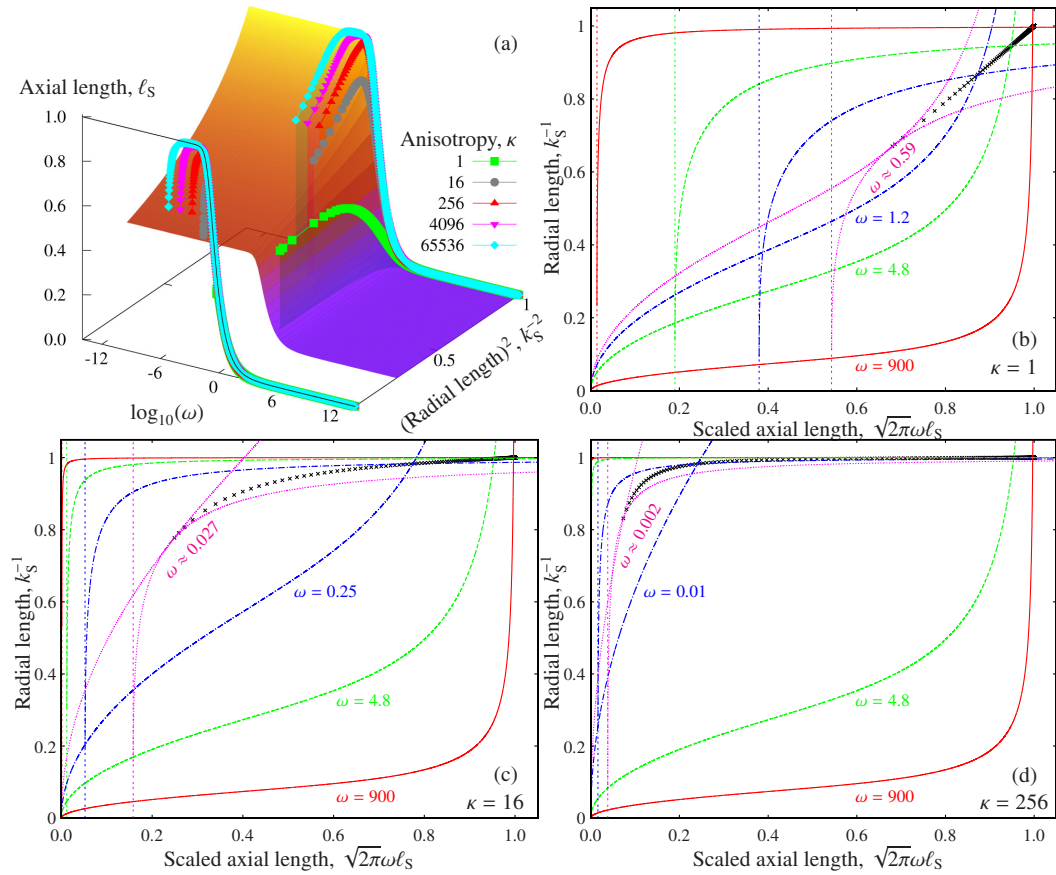
Figure 4.3: Energy-minimizing variational parameters for the 3D GPE using a soliton ansatz: (a) axial length ℓ_S as a function of the radial length k_S^{-1} and the parameter ω [Eq. (4.29)]. Lines show the simultaneous solutions of Eqs. (4.32) and (4.33) for the axial length ℓ_S and radial length k_S^{-1}, for different anisotropies κ and values of ω. Projections of these solutions on the ω–ℓ_S plane are also shown; here the black line indicates the quasi-1D result [from Fig. 4.1(a)]. (b–d) Illustration of the intersections of Eq. (4.32) [lines with vertical asymptote $\ell_S = (\pi/3)/(2\pi\omega)^{1/2}\kappa$ shown with fine dashes] and Eq. (4.33) for various κ: the higher-ℓ_S intersection, which corresponds to a physical solution for the axial length ℓ_S and radial length k_S^{-1}, can be found using a "staircase" method starting from $k_S = 1$. The numerical solutions obtained this way, and shown by points in (a), are shown by crosses in (b–d). The lowest values of ω plotted in (b–d) are the lowest for which a self-consistent soliton ansatz solution is found.

k_G^{-1}, quantifies its radial length. In the quasi-1D limit both lengths consequently approach unity ($\{\ell_G, k_G\} \to 1$). Substituting this ansatz into Eq. (4.17) yields (using identities from Appendix A.2)

$$H_{3D}(\ell_S, k_S) = \frac{\pi^2 \omega^2}{6} \left(\ell_S^2 + \frac{1}{4\pi^2 \omega^2 \ell_S^2} - \frac{k_S^2}{2\pi^2 \omega^2 \ell_S} + \frac{3\kappa k_S^2}{\pi^2 \omega} + \frac{3\kappa}{\pi^2 \omega k_S^2} \right). \qquad (4.26)$$

Once again, setting partial derivatives with respect to both ℓ_S and k_S equal to zero allows us to deduce that:

$$\ell_S^4 + \frac{k_S^2 \ell_S}{4\pi^2 \omega^2} - \frac{1}{4\pi^2 \omega^2} = 0, \qquad (4.27)$$

and that k_S must solve

$$k_S = \left(\frac{6\kappa \omega \ell_S}{6\kappa \omega \ell_S - 1} \right)^{1/4}. \qquad (4.28)$$

From Eq. (4.28) it follows that we must have $\ell_S > 1/6\kappa\omega$ to obtain a physically reasonable solution, i.e., a real, positive value of k_S, consistent with our initial ansatz. For a given such value of k_S, Eq. (4.27) is solved (see solution in Appendix A.3) by

$$\ell_S = \frac{\left[\chi \left(\omega k_S^{-4} \right) \right]^{1/2} k_S^{2/3}}{2^{11/6} (\pi \omega)^{2/3}} \left\{ \left[\left(\frac{2}{\chi \left(\omega k_S^{-4} \right)} \right)^{3/2} - 1 \right]^{1/2} - 1 \right\}, \qquad (4.29)$$

with χ defined as in Eq. (4.11).

4.4.5 Analysis of soliton ansatz solution

As in the case of the Gaussian ansatz, minimization of the variational energy in 3D requires the simultaneous solution of equations for the radial length k_S^{-1} and the axial length ℓ_S. These equations are, respectively, Eq. (4.28) and [rearranged from Eq. (4.27)]

$$k_S = \left[\frac{1}{\ell_S} \left(1 - 4\pi^2 \omega^2 \ell_S^4 \right) \right]^{1/2}. \qquad (4.30)$$

These equations dictate that physical solutions must have

$$\frac{1}{6\kappa\omega} < \ell_S < \frac{1}{(2\pi\omega)^{1/2}}, \qquad (4.31)$$

and hence that $\omega > (\pi/3)^2/2\pi\kappa^2$ must be satisfied in order for physical solutions to exist. These equations and constraints can be further simplified by casting them in

terms of $\ell_S' = (2\pi\omega)^{1/2}\ell_S$; this yields two equations,

$$k_S = \left(\frac{(2\pi\omega)^{1/2}\kappa\ell_S'}{(2\pi\omega)^{1/2}\kappa\ell_S' - \pi/3}\right)^{1/4}, \tag{4.32}$$

and

$$k_S = \left[\frac{(2\pi\omega)^{1/2}}{\ell_S'}\left(1 - \ell_S'^4\right)\right]^{1/2}, \tag{4.33}$$

and an inequality,

$$\frac{\pi/3}{(2\pi\omega)^{1/2}\kappa} < \ell_S' < 1, \tag{4.34}$$

which are extremely similar to those encountered in the case of the Gaussian ansatz. The numerical solution of these equations for the physical solution, which can only exist when $\omega > (\pi/3)^2/2\pi\kappa^2$, follows the same procedure as used for the Gaussian ansatz.

Variational-energy-minimizing solutions to the soliton ansatz equations for different anisotropies κ are shown in Fig. 4.3; these are shown superimposed on the ℓ_S surface and projected into the ℓ_S–ω plane in Fig. 4.3(a), and alongside Eqs. (4.27) and (4.28) and Eq. (4.34) in Fig. 4.3(b–d). The collapse instability is even more evident in the soliton ansatz than in the Gaussian ansatz, since it occurs in a region with a larger background value of ℓ_S. Once again, the collapse is manifest as a rapid rise in k_S and drop in ℓ_S — corresponding to both axial and radial contraction of the solution— immediately prior to a κ-dependent threshold value of ω. Below the threshold, no self-consistent solutions exist. For increasing anisotropies κ, this collapse threshold again occurs at lower values of ω. In contrast to the case of the Gaussian ansatz, however, the collapse instability precludes solutions in exactly the limit where one expects the soliton ansatz to be accurate ($\omega \to 0$). This property of the collapse instability severely restricts the possibility of observing highly bright-soliton-like ground states in 3D. The solution curves in Fig. 4.3(a) illustrate that this effect is worst for low trap anisotropies κ, but is to some extent mitigated for higher κ. However, a full comparison with numerically exact solutions is necessary to quantify these effects; we undertake such a comparison in Section 4.4.7.

4.4.6   Variational solution: waveguide configuration

In broad experimental terms, the collapse instability sets a maximum value for the ratio of interaction strength to trap strength (equivalent to a minimum value of ω) which increases (and hence the minimum value of ω decreases) with the trap

anisotropy κ. In the context of atomic BEC experiments one would typically think of controlling the interaction–trap strength ratio by varying either $|a_s|$ or N while holding ω_r and ω_x constant; in this situation the collapse instability places a trap-anisotropy-dependent upper limit on the product $|a_s|N$. However, the minimum value of ω does not increase without limit in the trap anisotropy κ: In an experiment one can, in principle, remove all axial trapping to create a waveguide-like configuration; in this case $\omega_x = 0$ and the trap anisotropy $\kappa \to \infty$, while the parameter $\omega \to 0$. In this limit a reparametrization is necessary, and only needs to be performed for the soliton ansatz, which is clearly more appropriate in this context.

Elimination of the axial trap eliminates one of the two free parameters of the 3D GPE [Eq. (4.16)]. The remaining free parameter is $\Omega = \omega\kappa = (a_r/2|a_s|N)^2$, where $a_{\rm r} = (\hbar/m\omega_r)^{1/2}$ is the radial harmonic oscillator length scale. The soliton ansatz may be re-written in terms of Ω as

$$\psi(\mathbf{r}) = \frac{\Omega^{1/2}k_{\rm S}}{(2\pi\ell_{\rm S})^{1/2}}e^{-\Omega k_{\rm S}^2(y^2+z^2)/2}\operatorname{sech}(x/2\ell_{\rm S}).\tag{4.35}$$

Substituting this into Eq. (4.17) with $\omega_x = 0$ yields (using identities from Appendix A.2),

$$H_{\rm 3D}(\ell_{\rm S}, k_{\rm S}) = \left(\frac{1}{24\ell_{\rm S}^2} - \frac{k_{\rm S}^2}{12\ell_{\rm S}} + \frac{\Omega k_{\rm S}^2}{2} + \frac{\Omega}{2k_{\rm S}^2}\right),\tag{4.36}$$

from which we deduce that the energy-minimizing variational parameters satisfy

$$\ell_{\rm S} = \frac{1}{k_{\rm S}^2},\tag{4.37}$$

and

$$k_{\rm S} = \left(\frac{6\Omega\ell_{\rm S}}{6\Omega\ell_{\rm S} - 1}\right)^{1/4}.\tag{4.38}$$

Contrary to the more general 3D case, an analytic simultaneous solution of Eqs. (4.37) and (4.38) exists when $\ell_{\rm S}$ satisfies the depressed cubic equation

$$\ell_{\rm S}^3 - \ell_{\rm S} + \frac{1}{6\Omega} = 0.\tag{4.39}$$

Using the general solution for a depressed cubic equation from Appendix A.3, one finds that the physical root (with real, positive $\ell_{\rm S}$ satisfying the limit $\ell_{\rm S} \to 1$ as $\Omega \to \infty$) is given by

$$\ell_{\rm S} = \left[-\frac{1}{12\Omega} + \frac{1}{3^{3/2}\Omega}\left(\frac{3}{16} - \Omega^2\right)^{1/2}\right]^{1/3} + \left[-\frac{1}{12\Omega} - \frac{1}{3^{3/2}\Omega}\left(\frac{3}{16} - \Omega^2\right)^{1/2}\right]^{1/3}.\tag{4.40}$$
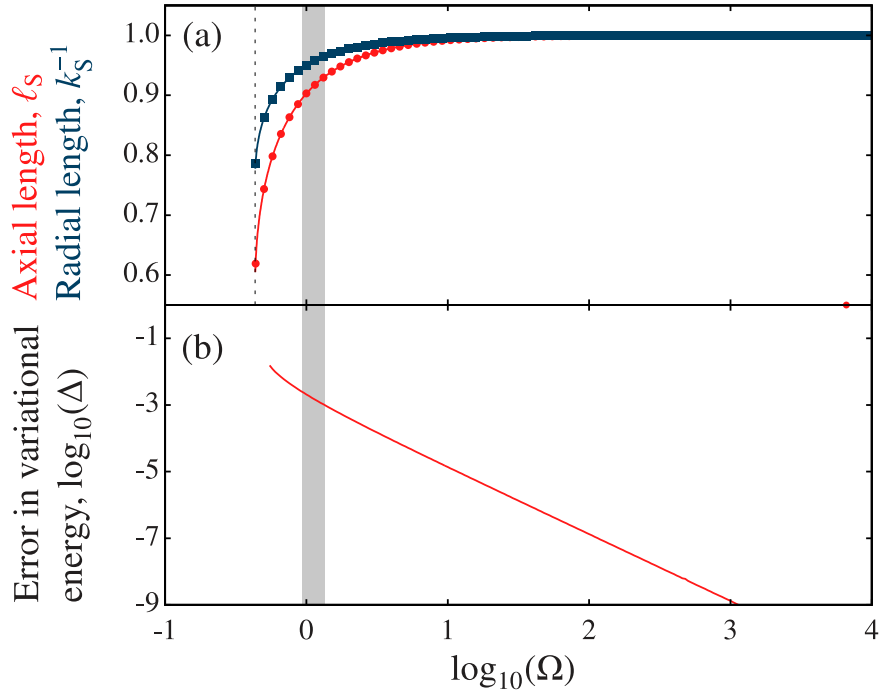
Figure 4.4: Comparison of 3D variational and numerical solutions in a waveguide configuration ($\omega_x = 0$: (a) Energy-minimizing axial length ℓ_S and radial length k_S^{-1} for the soliton ansatz. Solutions, given by Eq. (4.40), exist for all $\Omega = \kappa\omega > 3^{1/2}/4$. (b) Relative error in the minimum variational energy of the soliton ansatz, $\Delta = (H_{3D} - E_{3D})/E_{3D}$, where E_{3D} is the numerically determined ground state energy. The shaded area represents the parameter regime of previous bright solitary wave experiments (see Table 4.1).

Consequently, solutions only exist for $\Omega > 3^{1/2}/4$, as shown in Fig. 4.4(a).

4.4.7   Comparison to 3D numerical solutions

The variational energy-minimizing axial lengths ℓ_G and ℓ_S are shown as functions of ω in Fig. 4.5(a) for the general 3D case; for the waveguide limit both axial and radial lengths ℓ_S and k_S^{-1} are shown as functions of Ω in Fig. 4.4(a). As in the quasi-1D case, we quantitatively evaluate the accuracy of the ansatz solutions for general ω (Ω) by comparing the variational minimum energy H_{3D} with the numerically determined ground state energy E_{3D}. We calculate E_{3D} using a pseudospectral method in a basis of optimally-scaled harmonic oscillator eigenstates; this is formed from a tensor product of symmetric Gauss-Hermite functions (axial direction) and generalized Laguerre functions (radial direction). The ansatz with the lowest variational energy is used both to optimize the scaling of the basis functions and as an initial
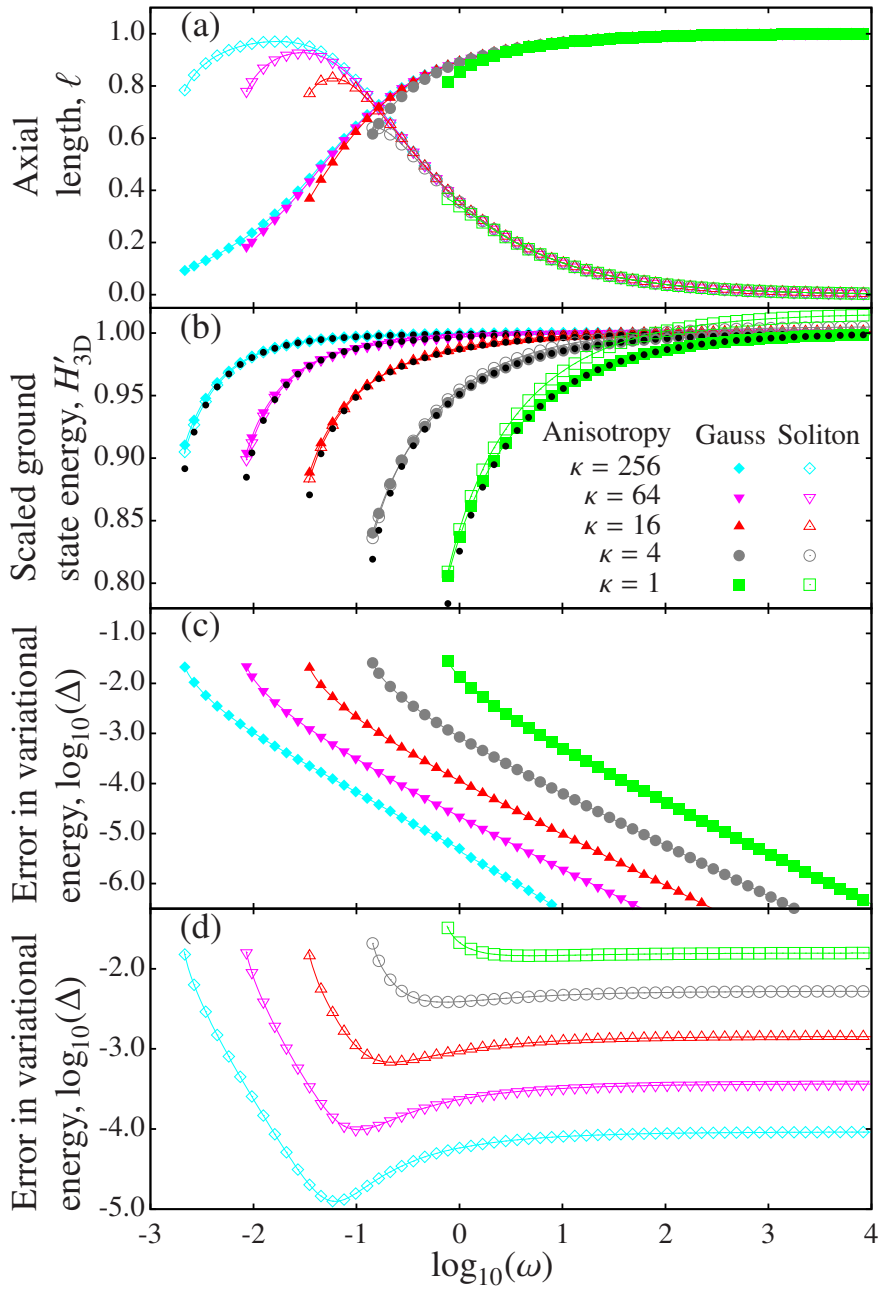
Figure 4.5: Comparison of 3D variational and numerical solutions: (a) Energy-minimizing axial lengths ℓ_G (Gaussian ansatz, solid symbols) and ℓ_S (soliton ansatz, hollow symbols). (b) Scaled variational energies $H'_{3D} = \kappa H_{3D}/\omega(\kappa + 1/2)$ [a similarly scaled ground state energy $E'_{3D} = \kappa E_{3D}/\omega(\kappa + 1/2)$ tends to 1 in the limit $\omega \to \infty$ for all anisotropies κ] compared with the numerically calculated ground state energies E_{3D} (black dots). (c,d) Normalized relative error in the variational energy $\Delta = (H_{3D} - E_{3D})/E_{3D}$ for the Gaussian (c) and soliton (d) ansatzes. For clarity every 4th datum is marked by a symbol in (a–d).

Experiment	κ	$\log_{10}(\omega)$	$\log_{10}(\Omega)$
Rice [10]	11.4	-1.04	0.014
ENS [11]	?	?	0.11
JILA [12]	2.5	-0.41	-0.0074

Table 4.1: Typical parameters associated with previous bright solitary wave experiments. No ω or κ values are given for the ENS experiment [11] as it featured an *expulsive* axial potential, incompatible with the variational analysis presented in this chapter. In each case an approximate value of Ω is estimated by assuming a waveguide-like trap could be produced by complete removal of the axial potential in each experiment, regardless of the actual feasibility of this procedure.

estimate for the solution. Expanding the stationary 3D GPE in such a basis produces a system of nonlinear equations which are solved iteratively using a modified Newton method; a detailed explanation is given in Appendix B. A similar method was used to solve a similar cylindrically symmetric, stationary 3D GPE, with repulsive interactions, in Ref. [71].

As in the quasi-1D case, we compare several quantities between the ansatz and numerical solutions. Fig. 4.5(b) shows the *scaled* energy $H'_{3D} = (H_{3D}/\omega)/(1 + 1/2\kappa)$ in the general 3D case. This scaling is such that E'_{3D} — which is defined analogously to H'_{3D} with respect to E_{3D} — tends to 1 as $\omega \to \infty$. Figs. 4.5(c) and (d) show the relative error in the variational minimum energy $\Delta = (H_{3D} - E_{3D})/E_{3D}$ for the Gaussian and soliton ansatzes, respectively. The same quantity Δ is shown for the waveguide limit in Fig. 4.4(b). All quantities shown in Figs. 4.5 and 4.4 are computed using between 2000 and 12000 basis states (κ-dependent) and are insensitive to a doubling of the number of basis states.

In the general 3D case, a close inspection of Fig. 4.5(b–d) is necessary to reveal the overall relation between the ansatz solutions and the numerically obtained ground state. In the high-ω limit Fig. 4.5(b) shows that both the Gaussian variational energies (solid symbols) and the ground state energy E_{3D} (black dots) approach 1 as $\omega \to \infty$, whereas the soliton ansatz energies (hollow symbols) tend to higher energies. This corresponds to the actual ground state most closely matching the Gaussian ansatz in this limit, as one would expect. Indeed, the relative error in variational energy, Δ, for the Gaussian ansatz [Fig. 4.5(c)] continues to drop exponentially with ω for all anisotropies κ, making it possible to find regimes of ω where

the Gaussian ansatz gives an excellent approximation to the true ground state.

In the opposite, low-ω limit, collapse occurs at a κ-dependent value of ω; this corresponds to the points in Fig. 4.5(a–d) where solution curves abruptly cease. Prior to collapse (at higher values of ω) the relation between the Gaussian ansatz, the soliton ansatz, and the actual ground state is highly dependent on the trap anisotropy κ [Fig. 4.5(b)]. In the case of a spherically symmetric trap, where the anisotropy $\kappa = 1$, the soliton ansatz variational energy is *never* closer to the true ground state energy E_{3D} than the Gaussian ansatz variational energy. A regime of soliton-like ground states consequently cannot exist at this low anisotropy; as the soliton ansatz is intrinsically asymmetric, this is to be expected. For higher anisotropies, the soliton ansatz energy is closer to E_{3D} than the Gaussian ansatz energy in a small regime prior to collapse. Exactly how soliton-like the ground state is in this regime can be quantitatively assessed using the relative error Δ. This is shown for the soliton ansatz in [Fig. 4.5(d)]. For each κ the "background" value of Δ in the limit $\omega \to \infty$ is different; this effect is due to the decreasing size of the axial part of the energy with respect to the radial part for increasing ω. In the opposite, low-ω, limit Δ increases sharply close to the collapse point as the ground state wavefunction rapidly contracts. The maximum extent to which Δ decreases from its high-ω limit, *before* this increase due to collapse-related contraction at low ω, quantifies how soliton-like the ground state becomes in this regime. Even for the highest anisotropy shown, $\kappa = 256$, the regime of ω over which Δ drops below its background value is rather narrow, and the actual drop in Δ is only one order of magnitude. Compared to benchmark of Section 4.3.4, this indicates that the true ground state remains considerably deformed with respect to the soliton ansatz. The minimum error in the soliton ansatz energy does, however, improve with increasing anisotropy κ. Excellent agreement can be achieved in the waveguide limit ($\kappa \to \infty$): Fig. 4.4 shows that excellent agreement, with respect to the benchmark figure of Section 4.3.4, can be obtained for $\Omega > 10^{3/2}$.

4.5   Physical interpretation of results

A physical interpretation of the above results follows from considering two conditions that must be satisfied in order to realize a soliton-like ground state; (1) the radial profile should be "frozen" to a Gaussian, thus realizing a quasi-1D limit; and (2) interactions should dominate over the axial trapping. On first inspection these conditions seem mutually compatible, and satisfiable simply by increasing the radial trap frequency ω_r with other parameters held constant. However, condition (1)

can only be satisfied if the maximum density remains low enough to avoid any deformation of the radial profile due to the collapse instability. Increasing ω_r leads to exactly such deformation, and ultimately to collapse, as it has the secondary effect of strongly increasing the density. This strong increase in density with ω_r is particular to the case of attractive interactions. Increasing ω_r in a repulsively-interacting BEC likewise acts to increase the density, but this increase is counteracted by the interactions; these act to reduce the density, and cause the BEC to expand axially. In the attractively-interacting case the response of the interactions is the opposite: increasing ω_r leads to axial *contraction* of the BEC. Consequently condition (1) is far harder to satisfy for an attractively-interacting BEC than a repulsively-interacting one. Responding to this problem simply by reducing the interaction strength (either through $|a_s|$ or N) leads to violation of condition (2). The nature of the problem is made particularly clear by considering the waveguide limit: here condition (2) is automatically satisfied ($\omega_x = 0$). This makes it possible to achieve a highly soliton-like ground state by satisfying condition (1) alone. However, such a ground state is achieved by *lowering* the product $\omega_r^{1/2}|a_s|N$, and thus by progressing towards the limit of extreme diluteness.

This physical behaviour of the system presents considerable challenges for experiments aiming to realize a highly soliton-like ground state. In essence, the most desirable configuration is to have extremely high anisotropies κ, while keeping ω_r as low as possible. Realizing such a configuration through extremely low, or zero, axial trap frequencies ω_x is problematic: such frequencies are hard to set precisely experimentally as they require a very smooth potential to be generated, potentially over a considerable length. Furthermore, in the case $\omega_x = 0$ the mean-field approximation ceases to be valid for an attractively-interacting BEC; the true wavefunction should be translationally invariant in this case, but the mean-field solution breaks this symmetry [273]. Even for very low but non-zero ω_x the mean-field approximation can lose validity due to the extreme diluteness of the BEC, and the energy gap from the ground state to states with excited axial modes can become low enough to cause significant population of the excited states at experimentally feasible temperatures.

It is informative to consider the parameters used in bright solitary wave experiments to date [10–12], listed in Table 4.1. None of these aimed to realize highly soliton-like ground states in the sense considered here. However, they nonetheless indicate regimes which have proved to be experimentally accessible and offer a guide to future possibilities. All have operated outside the regime of highly soliton-like ground

states; direct comparison of the experiments of Refs. [10] and [12] with our results reveals that κ is too small in these experiments ($\kappa \approx 11$ and $\kappa \approx 3$ respectively) to achieve a highly soliton-like ground state. The experiment of Ref. [11] featured an expulsive axial potential, which does not yield a value of κ suitable for direct comparison with our results. However, it is possible to assume the waveguide limit $\omega_x = 0$ in each experiment and compare the values of Ω with our results, as given in Table 4.1 and indicated on Fig. 4.4: in each case Ω lies outside the regime of highly soliton-like ground states. Thus, experiments with weaker traps and lower densities than previously realized with attractive condensates appear to be necessary in order to achieve a highly soliton-like ground state.

4.6 Summary

In this Chapter we considered attractively-interacting atomic BECs in cylindrically symmetric, prolate harmonic traps, and introduced variational ansatzes, based on Gaussian and bright-soliton profiles, for the GPE ground state. We compared new, analytic variational solutions based on these ansatzes with highly accurate numerical solutions of the GPE over an extensive parameter space, and hence determined how soliton-like the ground state is. Initially assuming the quasi-1D limit to be valid, we showed that the true solution to the GPE is (not) soliton like when interactions do (not) dominate over the trap strength. In 3D, this picture is complicated by the collapse instability; in the regime where all trap strengths dominate over the interactions a Gaussian variational ansatz gives an excellent approximation to the true, and non-soliton-like ground state. In contrast to the quasi-1D limit, however, we have shown that the regime in which the ground state is truly soliton-like (well approximated by a soliton variational ansatz) is either non-existent, or highly restricted, depending on the trap anisotropy. For low anisotropies, as one raises the strength of the interactions such that they approach and exceed the strength of the axial trap the true ground state ceases to be well-described by a Gaussian variational ansatz, but does not become well-described by a soliton variational ansatz before the interaction strength also exceeds the radial trapping strength, leading to collapse. Only by raising the anisotropy significantly can one open a parameter window in which the true ground-state becomes soliton-like before the interaction strength is sufficient to cause collapse.

Our results describe the nature of the ground state over a wide parameter regime, and offer a straightforward, accurate approximation to the full 3D GPE solution in many cases. Our results are particularly relevant for experiments using attractively-

interacting condensates, as they identify the potentially challenging parameter regime required to observe a truly soliton-like ground state. In particular, we have shown that for previous experimental configurations even complete elimination of the axial trap is not sufficient to reach a soliton-like regime: one must also adjust other parameters so as to achieve roughly an order-of-magnitude increase in the parameter Ω (see Fig. 4.4). Experimentally, this would require lowering of any combination of the radial trap frequency ω_r, scattering length magnitude $|a_s|$, and atom number N so as to achieve an order-of-magnitude decrease in the product $\omega_r|a_s|^2N^2$. Based on the difficulties associated with producing and imaging small and dilute condensates, we suggest that lowering $|a_s|$ may be the most viable option, although this would require extremely good magnetic field stability and control.

Nonetheless, reaching a regime with a highly soliton-like ground state will be advantageous for experiments seeking to explore and exploit beyond-mean field effects such as a macroscopic superposition of bright solitons. Also, given that previous studies have shown that the dynamics and collisions of bright solitary waves can be soliton-like over a much wider parameter regime than our approach reveals the ground state to be, extending the variational approach used here to dynamical situations is an interesting direction for future work.

Part II

Instabilities and self-consistent non-equilibrium dynamics

Chapter 5: Atomic Bose-Einstein condensates at finite temperature

5.1 Introduction

In Part I of this thesis we have applied the zero-temperature, mean-field, Gross-Pitaevskii description of an atomic BEC to the study of bright matter solitary waves. In Part II, we now turn our attention to the description of atomic BECs at finite temperature, with an emphasis on describing non-equilibrium dynamics at low temperatures, where the quantum nature of the interaction between the condensate and non-condensate plays a crucial role. In particular, we seek a theory which describes both the condensate and non-condensate fractions of an atomic BEC, and the interactions between the two, in regimes where the relative size of the non-condensate is small but non-negligible. The size of the non-condensate is determined by three primary factors:

1. **Interaction strength:** The strength of inter-atomic interactions determines the magnitude of the non-condensate fraction — the *quantum depletion* — at zero temperature.

2. **Finite-temperature:** Temperatures greater than $T = 0$ lead initially to a thermal population of the elementary quasiparticle excitations of the system, and ultimately to the loss of a condensate altogether above T_c.

3. **Dynamical depletion:** Non-equilibrium dynamics provide a *dynamical* mechanism, even when beginning at $T = 0$ equilibrium, for atoms to leave or enter the condensate. Such dynamics can be caused by, for example, external driving or an interaction strength quench.

These factors should not be viewed as entirely independent: in particular finite-temperature and dynamical depletion are fundamentally related in the sense that a system that is temporarily driven, and hence dynamically depleted, would, if allowed to rethermalize, then have a higher temperature. However these factors form a useful motivating check-list for the capabilities of beyond-mean-field theories we consider in Part II of this thesis; specifically, we seek a theory capable of describing

an atomic BEC with: (a) sufficiently weak interactions that the quantum depletion is around 1%; (b) temperature $T > 0$ such that the total non-condensate fraction considerably exceeds the quantum depletion; and (c) *doing so in a completely dynamical way*. In view of the intimate link between non-equilibrium dynamics and finite temperatures, a theoretical description satisfying (c) without satisfying (b) is impossible.

A theoretical description which correctly captures non-equilibrium dynamics of condensate and non-condensate in a consistent fashion is our central goal in Part II of this thesis. Such a description represents an important extension to the GPE for describing driven, or otherwise excited, atomic BECs, potentially useful for exploring phenomena such as dynamical chaos, thermalization, and integrability in non-equilibrium atomic BECs. In particular, this description would provide a logical pathway to extend the analysis of bright solitary waves in Part I of this thesis to account for the role of the non-condensate; such an extension will likely be necessary to further understand the operation of bright solitary wave interferometry devices in the future. Importantly, in developing a theoretical description we will place greater emphasis on successfully describing non-equilibrium *dynamics* at low temperatures, even if this comes at the expense of being able to describe behaviour (either equilibrium or non-equilibrium) at higher temperatures.

With this central goal in place, in this Chapter we review in some detail the theoretical finite-temperature descriptions of atomic BECs currently available. We begin with the symmetry-breaking descriptions encountered in Chapter 1, which we review in Section 5.2. After summarizing the previously introduced symmetry-breaking approach (Section 5.2.1), we introduce the Hartree-Fock-Bogoliubov description, which represents the highest possible order symmetry-breaking mean-field treatment of condensate and non-condensate in the static case (Section 5.2.2). This description extends the zero-temperature quadratic Hamiltonian which we diagonalized in the static case in Chapter 1, and gives an ideal introduction to several issues which arise when developing beyond-quadratic-Hamiltonian treatments — particularly the issues of ultraviolet divergences and energy gaps in the excitation spectrum, which we discuss in Section 5.2.3. Having introduced these issues, and their potential cures, we discuss symmetry-breaking descriptions of coupled condensate and non-condensate dynamics in Section 5.2.4. However, while these descriptions have proved highly successful at higher temperatures, they fail to provide the consistent treatment of condensate and non-condensate interactions at low temperature which we desire (Section 5.2.5).

The problems with the symmetry-breaking description, for our purposes, can be avoided by instead adopting a *number-conserving* description. We give an overview of number-conserving descriptions in Section 5.3; in such descriptions the necessary partition of the field operator (Section 5.3.1) and fluctuation expansion (Section 5.3.2) is similar to the symmetry-breaking approach. However, enforcing explicit number-conservation leads to non-local terms which guarantee orthogonality between the condensate and non-condensate, and lead to a correct description of the phonon-like character of non-condensate excitations at low temperature in both static (Section 5.3.3) and dynamic (Section 5.3.4) formulations. In particular, the dynamical, second-order, number-conserving description of S. Gardiner and Morgan, introduced in Section 5.3.4, fulfils our central goal: it is this description which we proceed to develop in Chapter 6 and implement in a fully dynamical calculation in Chapter 7.

Finally, we briefly review alternative, "*c*-field", descriptions of finite temperature atomic BECs (Section 5.4). These methods are developed along different theoretical lines to the symmetry-breaking and number-conserving descriptions, and have proved very successful at temperatures around T_c. However, they do not represent as good a description of low-temperature non-equilibrium dynamics as the number-conserving description, and consequently we do not use *c*-field methods further in this thesis.

5.2 Symmetry-breaking descriptions

5.2.1 Partition of field operator and fluctuation expansion

The symmetry-breaking approach, as introduced in Chapter 1, offers perhaps the least mathematically complicated route to a finite-temperature description of atomic BECs. To recap, the symmetry-breaking approach involves replacing the annihilation operator for the condensate mode with a complex number: $\hat{a}_c \rightarrow \sqrt{N_c(t)}e^{i\Phi}$ (where Φ is an arbitrary phase). This replacement leads to the following partition of the field operator

$$\hat{\Psi}(\mathbf{r}) = \Psi(\mathbf{r},t) + \hat{\delta}(\mathbf{r},t), \tag{5.1}$$

where the non-condensate field operator $\hat{\delta}(\mathbf{r},t)$ is a well-defined *fluctuation operator*, since its expectation value is equal to zero; $\left\langle \hat{\delta}(\mathbf{r},t) \right\rangle = 0$. This gives $\hat{\Psi}(\mathbf{r})$ a mean value of $\psi(\mathbf{r},t)$, and the expectation values of second-order products of $\hat{\delta}(\mathbf{r},t)$ and $\hat{\delta}^\dagger(\mathbf{r},t)$ are analogous to the variance of a distribution about the mean

$\psi(\mathbf{r}, t)$ [68]. Importantly, $\hat{\delta}(\mathbf{r}, t)$ scales with the number of non-condensate atoms, allowing one to justifiably neglect terms of high order in $\hat{\delta}(\mathbf{r}, t)$ or $\hat{\delta}^\dagger(\mathbf{r}, t)$ when the non-condensate is small compared to the condensate, as is the case in atomic BECs sufficiently below T_c.

In the case of the weakly-interacting Bose gas considered here, this *fluctuation expansion* procedure [68] corresponds to substituting Eq. (5.1) into the Hamiltonian Eq. (1.9), and subsequently collecting powers of $\hat{\delta}(\mathbf{r}, t)$ and $\hat{\delta}^\dagger(\mathbf{r}, t)$ to give

$$H_0 = \int d\mathbf{r}\, \Psi^*(\mathbf{r}, t)\left(H_{\mathrm{sp}}(\mathbf{r}, t) - \mu + \frac{U_0}{2}|\Psi(\mathbf{r}, t)|^2\right)\Psi(\mathbf{r}, t), \tag{5.2}$$

$$\hat{H}_1 = \int d\mathbf{r}\,\left[\hat{\delta}^\dagger(\mathbf{r}, t)\left(H_{\mathrm{sp}}(\mathbf{r}, t) - \mu + U_0|\Psi(\mathbf{r}, t)|^2\right)\Psi(\mathbf{r}, t) + \mathrm{h.c.}\right], \tag{5.3}$$

$$\hat{H}_2 = \int d\mathbf{r}\,\left[\hat{\delta}^\dagger(\mathbf{r}, t)\left(H_{\mathrm{sp}}(\mathbf{r}, t) - \mu + 2U_0|\Psi(\mathbf{r}, t)|^2\right)\hat{\delta}(\mathbf{r}, t)\right.$$
$$\left. + \frac{U_0}{2}\left(\Psi^{*2}(\mathbf{r}, t)\hat{\delta}(\mathbf{r}, t)\hat{\delta}(\mathbf{r}, t) + \mathrm{h.c.}\right)\right], \tag{5.4}$$

$$\hat{H}_3 = U_0 \int d\mathbf{r}\,\left[\Psi(\mathbf{r}, t)\hat{\delta}^\dagger(\mathbf{r}, t)\hat{\delta}^\dagger(\mathbf{r}, t)\hat{\delta}(\mathbf{r}, t) + \mathrm{h.c.}\right], \tag{5.5}$$

$$\hat{H}_4 = \frac{U_0}{2} \int d\mathbf{r}\, \hat{\delta}^\dagger(\mathbf{r}, t)\hat{\delta}^\dagger(\mathbf{r}, t)\hat{\delta}(\mathbf{r}, t)\hat{\delta}(\mathbf{r}, t); \tag{5.6}$$

this expression has already been given in Eq. (1.19), but is repeated here for convenience. With $\hat{\delta}(\mathbf{r}, t)$ scaling with the size of the non-condensate, truncating the Hamiltonian at some finite order provides perturbative descriptions of the systems, as was done for the example of the quadratic Hamiltonian $(H_0 + \hat{H}_1 + \hat{H}_2)$ in Chapter 1.

5.2.2 Static description: Hartree-Fock-Bogoliubov (HFB)

We have already discussed the symmetry-breaking Bogoliubov quasiparticle description in the static case in Chapter 1, which arises from considering the quadratic Hamiltonian $(H_0 + \hat{H}_1 + \hat{H}_2)$. In the context of static, finite-temperature descriptions using the symmetry-breaking formalism, a key role is played by the Hartree-Fock-Bogoliubov (HFB) Hamiltonian: this extends the simple quadratic Hamiltonian $H_0 + \hat{H}_1 + \hat{H}_2$ by including some effects of $\hat{H}_3$ and $\hat{H}_4$ perturbatively. This is achieved by applying the cubic and quartic Hartree-Fock factorizations (we suppress position- and time-dependence for clarity in the following two expressions)

$$\hat{\delta}^\dagger\hat{\delta}\hat{\delta} \approx 2\left\langle\hat{\delta}^\dagger\hat{\delta}\right\rangle\hat{\delta} + \hat{\delta}^\dagger\left\langle\hat{\delta}\hat{\delta}\right\rangle, \tag{5.7}$$

and

$$\hat{\delta}^\dagger \hat{\delta}^\dagger \hat{\delta} \hat{\delta} \approx 4 \left\langle \hat{\delta}^\dagger \hat{\delta} \right\rangle \hat{\delta}^\dagger \hat{\delta} + \left\langle \hat{\delta}^\dagger \hat{\delta}^\dagger \right\rangle \hat{\delta} \hat{\delta} + \left\langle \hat{\delta} \hat{\delta} \right\rangle \hat{\delta}^\dagger \hat{\delta}^\dagger - 2 \left\langle \hat{\delta}^\dagger \hat{\delta} \right\rangle^2 - 2 \left\langle \hat{\delta} \hat{\delta} \right\rangle \left\langle \hat{\delta}^\dagger \hat{\delta}^\dagger \right\rangle, \quad (5.8)$$

to $\hat{H}_3$ and $\hat{H}_4$ respectively. These factorizations are motivated by Wick's theorem [50, 161], which in this context implies that all higher-order correlation functions of a *non-interacting* gas at equilibrium can be exactly expressed in terms of first- and second-order correlation functions. Applied to an interacting gas, as here, these factorizations constitute a fairly rough approximation. In terms of inter-atomic collisions, the cubic factorization approximation [Eq. (5.7)] is equivalent to ignoring collisions in which; (a) two non-condensate atoms collide, with one atom being scattered into the condensate; (b) a condensate and a non-condensate atom collide, with the former atom being scattered out of the condensate. In similar terms, the quartic factorization approximation [Eq. (5.8)] is equivalent to ignoring collisions between two non-condensate atoms in which neither is scattered into the condensate. The cubic factorization approximation has thus been identified as ignoring effects leading to growth and decay of the condensate which can be important at finite temperatures [50, 274, 275]. However, we note that at low temperatures these effects are small; the dominant growth and decay effects at low temperature are due to Bogoliubov pair excitations, which lead to transfer of population into, or out of, the condensate in non-equilibrium situations.

Two distinct pair averages of fluctuation operators appear above (allowing for the possibility of off-diagonal pair averages, which do not appear in Eqs. (5.7) and (5.8) but will appear in later expressions):

$$\tilde{n}(\mathbf{r}, \mathbf{r}', t) = \left\langle \hat{\delta}^\dagger(\mathbf{r}', t) \hat{\delta}(\mathbf{r}, t) \right\rangle, \quad (5.9)$$

$$\tilde{m}(\mathbf{r}, \mathbf{r}', t) = \left\langle \hat{\delta}(\mathbf{r}', t) \hat{\delta}(\mathbf{r}, t) \right\rangle. \quad (5.10)$$

We refer to these as the *normal* and *anomalous* pair averages. The diagonal part of the normal average, $\tilde{n}(\mathbf{r}, \mathbf{r}, t)$ gives the non-condensate density. As suggested by the name, neither the diagonal nor the off-diagonal parts of the anomalous average $\tilde{m}(\mathbf{r}, \mathbf{r}, t)$ have a similarly simple interpretation. They are loosely analogous, however, to anomalous correlations appearing in the BCS theory of superconductivity [50, 159, 161].

The above procedure leads to the HFB Hamiltonian

$$\hat{H}_{\mathrm{HFB}} = H_0 + \delta H_0 + \hat{H}_1 + \delta\hat{H}_1 + \hat{H}_2 + \delta\hat{H}_2. \quad (5.11)$$

Here δH_0 and $\delta\hat{H}_2$ represent terms which are, respectively, scalar and quadratic in the fluctuation operators and which appear as a result of the quartic factorization approximation [Eq. (5.8)] on $\hat{H}_4$. Similarly, $\delta\hat{H}_1$ represents terms which are linear in the fluctuation operators and appear as a result of the cubic factorization approximation [Eq. (5.7)] on $\hat{H}_3$ (see, e.g., Ref. [50] for exact expressions).

In this description, Ψ, $\tilde{n}$, and $\tilde{m}$ play the role of *generalized* mean-fields[1]. The static condensate wavefunction resulting from $\hat{H}_{\text{HFB}}$ obeys a *generalized* GPE (which we term the HFB-GGPE)

$$\left[H_{\text{sp}}(\mathbf{r}) - \mu + U_0|\Psi(\mathbf{r})|^2 + 2U_0\tilde{n}(\mathbf{r}, \mathbf{r})\right]\Psi(\mathbf{r}) + U_0\tilde{m}(\mathbf{r}, \mathbf{r})\Psi^*(\mathbf{r}) = 0\,, \qquad (5.12)$$

containing diagonal normal and anomalous pair averages. As was shown for the simple quadratic part of the Hamiltonian, $\hat{H}_2$, in Chapter 1, the quadratic part of the HFB Hamiltonian can be diagonalized by the Bogoliubov transformation Eq. (1.35), where the mode functions satisfy the new Bogoliubov-de Gennes equations

$$\int d\mathbf{r}'\left(\begin{array}{cc} L_{\text{HFB}}(\mathbf{r}, \mathbf{r}') & M_{\text{HFB}}(\mathbf{r}, \mathbf{r}') \\ -M^*_{\text{HFB}}(\mathbf{r}, \mathbf{r}') & -L^*_{\text{HFB}}(\mathbf{r}, \mathbf{r}') \end{array}\right)\left(\begin{array}{c} u_k(\mathbf{r}') \\ v_k(\mathbf{r}') \end{array}\right) = \epsilon_k\left(\begin{array}{c} u_k(\mathbf{r}) \\ v_k(\mathbf{r}) \end{array}\right). \qquad (5.13)$$

The operators appearing in these modified Bogoliubov-de Gennes equations (which we term the HFB-MBdGE) differ from those in Chapter 1 through the inclusion of the diagonal parts of the normal and anomalous pair averages, and can be written as

$$L_{\text{HFB}}(\mathbf{r}, \mathbf{r}') = \delta(\mathbf{r} - \mathbf{r}')\left[H_{\text{sp}}(\mathbf{r}') - \mu + 2U_0|\Psi(\mathbf{r}')|^2 + 2U_0\tilde{n}(\mathbf{r}', \mathbf{r}')\right], \qquad (5.14)$$

and

$$M_{\text{HFB}}(\mathbf{r}, \mathbf{r}') = \delta(\mathbf{r} - \mathbf{r}')\left[U_0\Psi^2(\mathbf{r}') + U_0\tilde{m}(\mathbf{r}', \mathbf{r}')\right]. \qquad (5.15)$$

Within this description, the effects of finite-temperature can be taken into account by thermally populating the (modified) Bogoliubov quasiparticle modes according to

$$\left\langle \hat{b}_k^\dagger \hat{b}_l \right\rangle = \delta_{kl}N_k = \delta_{kl}\left(e^{(\epsilon_k - \mu)/k_{\text{B}}T} - 1\right)^{-1}, \qquad (5.16)$$

$$\left\langle \hat{b}_k\hat{b}_l \right\rangle = \left\langle \hat{b}_k^\dagger\hat{b}_l^\dagger \right\rangle = 0. \qquad (5.17)$$

Here, ϵ_k are the energies of the quasiparticle modes, and the thermal distribution N_k of the non-interacting, bosonic quasiparticles is assumed to be of the Bose-Einstein

---

[1]This terminology should not be confused with our prior use of 'mean-field' to refer to the GPE-only description!

form [276]. Through the Bogoliubov transformation [Eq. (1.35)] this implies the following relations for the pair averages

$$\tilde{n}(\mathbf{r}, \mathbf{r}') = \sum_k N_k u_k(\mathbf{r}, t) u_k^*(\mathbf{r}', t) + \sum_k (N_k + 1) v_k^*(\mathbf{r}, t) v_k(\mathbf{r}', t), \qquad (5.18)$$

$$\tilde{m}(\mathbf{r}, \mathbf{r}') = \sum_k N_k u_k(\mathbf{r}, t) v_k^*(\mathbf{r}', t) + \sum_k (N_k + 1) v_k^*(\mathbf{r}, t) u_k(\mathbf{r}', t). \qquad (5.19)$$

In principle, this system of equations can be solved self-consistently to yield the equilibrium values of Ψ, $\tilde{n}$, $\tilde{m}$, and the quasiparticle energies ϵ_k at finite temperature T [50, 276–278]. However, the HFB approach presented here suffers from two particular issues which affect its usefulness.

5.2.3   Problems with HFB: Divergences and energy gap

The two issues occurring with the symmetry-breaking HFB description are not specific to HFB, but plague the description of weakly-interacting Bose gases at finite temperature. They also appear in other descriptions, in modified form, whenever one seeks to include effects forming part of $\hat{H}_3$ and $\hat{H}_4$ in the symmetry-breaking description.

The first such issue is that of ultra-violet divergences due to the use of the contact potential approximation [Eq. (1.7)]. Specifically, the sum over quasiparticle modes in the diagonal part of the anomalous average $\tilde{m}(\mathbf{r}, \mathbf{r})$ diverges as $k \to \infty$. Due to the complicated nature of the true inter-atomic interactions in an atomic BEC, however, the contact potential approximation is vital to obtaining a computationally tractable finite-temperature theory: for example, treating two-body collisions perturbatively in terms of the true inter-atomic interaction would be impossible [68] . Fortunately, the ultra-violet divergences do not arise through a fundamental problem with the contact approximation; this constitutes a small and well-controlled approximation for low-energy scattering in dilute gases. Rather, the divergences arise through a crude application of the contact potential to describe high-energy collisions.

Rather than approximating the two-body interaction potential, the contact interaction is the zero-momentum limit of the two-body T-matrix [50, 68, 83, 160, 163, 279–281]. However, the T-matrix is defined by a (convergent) sum over an infinite series of virtual two-body collisions, each described by a "ladder diagram" [282], and hence implicitly includes two-body effects to all orders [68]. A close inspection of the quasiparticle summation defining the diagonal part of the anomalous average [Eq. (5.19)] reveals that these two-body effects are inadvertently double-counted.

This can be demonstrated explicitly in the homogeneous case, where the quasiparticle mode functions u_k and v_k approach an analytic free-particle limit as $k \to \infty$; substituting this analytic limit into Eq. (5.19) and carefully comparing terms reveals that the same summation already included by the contact approximation reappears [281]. It is therefore generally valid, and necessary, to eliminate this double counting through the ultraviolet renormalization of the anomalous average [50]:

$$\tilde{m}(\mathbf{r}, \mathbf{r}) \to \tilde{m}^{\mathrm{R}}(\mathbf{r}, \mathbf{r}) = \tilde{m}(\mathbf{r}, \mathbf{r}) - \lim_{k \to \infty} u_k(\mathbf{r}) v_k^*(\mathbf{r}) . \tag{5.20}$$

One particular occasion where this is *not* necessary is when describing systems in the quasi-1D limit, as defined in Chapter 2 [282][2]. We will consider such systems extensively in the following Chapters.

The second issue arising in the HFB description, and other finite-temperature descriptions, is the appearance of a spurious energy gap in the quasiparticle spectrum. In the case of a homogeneous weakly-interacting Bose gas, the Hugenholtz-Pines theorem requires that the energy of an elementary excitation relative to the condensate should vanish as $k \to 0$ [163, 281, 283][3]; within a symmetry-breaking treatment this can also be viewed a consequence of the Goldstone theorem [50]. However, while the Bogoliubov dispersion relation [Eq. (1.39)] associated with the simple quadratic Hamiltonian is correctly *gapless*, self-consistently solving the static HFB-GGPE and HFB-MBdGE leads to an excitation spectrum with a gap at $k \to 0$ [50].

Within the symmetry-breaking description this is generally dealt with in one of two ways. In the first method, one simply discards all terms in the HFB-GGPE and HFB-MBdGE involving the (renormalized) anomalous average $\tilde{m}^{\mathrm{R}}$, resulting in what has commonly been referred to as the HFB-Popov approximation [160, 188, 284, 285]. Interestingly, this approximation has been found to be highly accurate at *higher* temperatures $T \lesssim T_c$ where $|m(\tilde{\mathbf{r}}, \mathbf{r})| \ll n(\tilde{\mathbf{r}}, \mathbf{r})$, but inaccurate for $T \ll T_c$ where $|m(\tilde{\mathbf{r}}, \mathbf{r})| \approx n(\tilde{\mathbf{r}}, \mathbf{r})$ [286][4].

In the second method, one seeks to eliminate the gap by adding, rather than removing, terms; there are several approaches to doing this, leading to so-called

---

[2]Note that our quasi-1D case is distinct from the true 1D case, in which the atomic scattering occurs strictly in 1D. This latter case is the main subject in Ref. [282], hence our quasi-1D case is (potentially confusingly) referred to as "quasi-3D" in that work.

[3]Note that the theorem as stated here only applies to repulsive interactions, as an attractively interacting BEC is unstable in 3D (see Chapter 2).

[4]The authors of Ref. [286] also argue against the use of Popov's name in relation to this method.

generalized HFB descriptions. For example, the off-diagonal terms appearing in the HFB-MBdGE (M_{HFB}) can be interpreted as introducing a many-body T-matrix description of atomic interactions, explicitly accounting for the fact that the interactions take place in the presence of the background medium of the condensate [281, 282]. However, the diagonal terms (L_{HFB}) only describe interactions at the level of the two-body T-matrix. One can thus argue that "upgrading" the description of interactions in L_{HFB} is provides a consistent way to eliminate the gap; such generalized descriptions have been considered in Refs. [163, 277, 287–289]. An alternative example is provided by Ref. [286], where the gap is eliminated by introducing separate chemical potentials for the condensate and non-condensate, based on a thermodynamic argument.

5.2.4   Dynamical descriptions

Obtaining a dynamical description of condensate and non-condensate in the HFB approximation is mathematically straightforward. The full Heisenberg equation of motion for the field operator $\hat{\Psi}(\mathbf{r})$ is given by

$$i\frac{d\hat{\Psi}(\mathbf{r})}{dt} = \left[H_{\text{sp}}(\mathbf{r}, t) - \mu\right]\hat{\Psi}(\mathbf{r}) + U_0\hat{\Psi}^\dagger(\mathbf{r})\hat{\Psi}(\mathbf{r})\hat{\Psi}(\mathbf{r})\,. \tag{5.21}$$

Treating the the final "triplet" of field operators using the cubic mean-field factorization Eq. (5.7), and taking the expectation value of the resulting equation (see, for example, Ref. [276]) yields the time-dependent HFB-GGPE

$$i\frac{\partial\psi(\mathbf{r}, t)}{\partial t} = \left[H_{\text{sp}}(\mathbf{r}, t) - \mu + U_0|\Psi(\mathbf{r}, t)|^2 + 2U_0\tilde{n}(\mathbf{r}, \mathbf{r}, t)\right]\Psi(\mathbf{r}, t) + U_0\tilde{m}(\mathbf{r}, \mathbf{r}, t)\Psi^*(\mathbf{r}, t)\,. \tag{5.22}$$

Carefully combining Eq. (5.22) and Eq. (5.21), using the symmetry-breaking partition of the field operator, reveals the accompanying equations of motion for the non-condensate quasiparticle modes to be the time-dependent HFB-MBdGE

$$i\frac{\partial}{\partial t}\begin{pmatrix} u_k(\mathbf{r}, t) \\ v_k(\mathbf{r}, t) \end{pmatrix} = \int d\mathbf{r}' \begin{pmatrix} L_{\text{HFB}}(\mathbf{r}, \mathbf{r}', t) & M_{\text{HFB}}(\mathbf{r}, \mathbf{r}', t) \\ -M_{\text{HFB}}^*(\mathbf{r}, \mathbf{r}', t) & -L_{\text{HFB}}^*(\mathbf{r}, \mathbf{r}', t) \end{pmatrix}\begin{pmatrix} u_k(\mathbf{r}', t) \\ v_k(\mathbf{r}', t) \end{pmatrix}, \tag{5.23}$$

where L_{HFB} and M_{HFB} are defined as in Eqs. (5.14) and (5.15) (although now with explicit time-dependence).

This dynamical version of the HFB description suffers from the same problems of gaplessness and inconsistent treatment of interactions as the static version considered in the previous Section, and has not been employed in a fully time-dependent

implementation without adjustments. It was, however, employed by Giorgini [290] within a linear response framework to describe condensate excitations at finite temperature [290]: within this perturbative framework the energy gap justifiably ceases to be a problem, and only the ultra-violet renormalization discussed in the previous Section is necessary to ensure the consistent treatment of interactions.

Aside from the work of Giorgini, the dynamical HFB description is typically altered either by making the "Popov approximation" $\tilde{m} = 0$, or by adding a self-consistent perturbative treatment of the remaining parts of $\hat{H}_3$ and $\hat{H}_4$, or by some combination of the above. Implementations of the HFB-Popov description, with varying levels of dynamical freedom, have been applied to the study of finite-temperature excitations [188, 285, 291, 292]. A range of kinetic descriptions, which perturbatively include the remaining parts of $\hat{H}_3$ and $\hat{H}_4$, have been developed by Walser *et al.* [293, 294] and Proukakis *et al.* [274, 275]. These descriptions have been proven to be equivalent to each other, and to an alternative cumulant formalism [295]. The beyond-mean-field treatment of $\tilde{n}$ and $\tilde{m}$ in these descriptions is equivalent to accounting more fully for collisions between condensate and non-condensate atoms, and introducing the effect of collisions between non-condensate atoms. These considerations enter the dynamical description in the form of collision integrals which, although they result in a more complete description of the dynamics at higher temperatures, can be particularly cumbersome to deal with [50].

A compromise between the (relatively) simple HFB-Popov and the aforementioned kinetic descriptions is offered by the method of Zaremba, Nikuni and Griffin (ZNG) developed in Ref. [296], and reviewed at length in the monograph by the same authors [160]. In the ZNG method a form of Popov approximation is made[5], *and* perturbative treatment of non-condensate collisions is introduced through a quantum Boltzmann equation. This coupling is made self consistent through enforced local conservation of energy and momentum. The ZNG description has been used to model a variety of dynamics at finite temperatures, including elementary excitations [297, 298], vortices and vortex nucleation [299, 300], and dark solitons in trapped condensates [301]. As such, it has proved to be the most successful numerically implemented symmetry-breaking description of finite-temperature dynamics in atomic BECs.

However, while these descriptions are all highly successful in some aspects, there

---

[5]As this approximation is made in the context of a reformulation of the Hamiltonian it can be considered to have a wider range of validity than the simple $\tilde{m} = 0$ approximation [160].

remain distinct weaknesses in each description. HFB-Popov suffers at low temperature from an inconsistent treatment of the anomalous average, and at high temperature from approximate treatment of non-condensate collisions. The ZNG description provides a tractable treatment of non-condensate collisions, making it very useful at higher temperatures. However, its enforcement of *local* energy and momentum conservation and neglect of the anomalous average implicitly ignores any non-local quantum effects; thus the description poorly models the phonon-like excitations which dominate the weakly-interacting Bose gas at low temperature. The alternative kinetic descriptions can potentially bridge these two regimes, but their complexity has precluded any fully time-dependent implementations to date.

5.2.5 Issues with symmetry-breaking

Lack of explicit number-conservation

As discussed in Chapter 1, the symmetry breaking partition of the field operator [Eq. (5.1)] breaks the global $U(1)$ symmetry of the Hamiltonian (1.9) and is equivalent to assuming a coherent state for the field[6] [see Fig. 5.1]. While such an assumption can be justified in the limit $N \to \infty$, as previously discussed in Section 1.3.2 an atomic BEC is a distinctly finite-sized system which is not necessarily correctly described by a thermodynamic limit. Indeed, the applicability of the thermodynamic limit and the grand canonical ensemble to atomic BECs can both be questioned [166, 303].

With regard to the atom number in particular, there is a very strong argument that the state of an atomic BEC system ought to be an eigenstate of the total atom number operator $\hat{N}$; while all atomic BEC experiments to date undoubtedly involve some experimental uncertainty in the atom number in any given "shot", in the absence of any mechanism for quantum coherence between shots, this uncertainty must be regarded as *statistical* in nature. Within the (presumably appropriate) framework of non-relativistic quantum mechanics, this implies a fixed atom number[7]. However,

---

[6]At finite temperatures $\langle \cdots \rangle$ should be interpreted as including a thermal as well as a quantum average; consequently a finite value for this average does not imply a coherent state of the field. Nonetheless, the symmetry-breaking procedure as outlined here can be rigorously developed in terms of thermal averages by introducing an infinitesimal symmetry-breaking term into the Hamiltonian [160, 178, 302]. Crucially, the issue of atom-number non-conservation we discuss in this Section continues to apply at finite temperature [158, 160].

[7]This argument is justified in the absence of atom-losses due to, e.g., three-body recombination or imperfections in the vacuum. It is thus restricted to timescales where these processes are negligible and the weakly-interacting Bose gas Hamiltonian applies; in this thesis we make no attempt to go beyond these timescales. If one attempted to take consistent account of these experimental atom losses further complications to this argument would probably be introduced. However, it is not at all
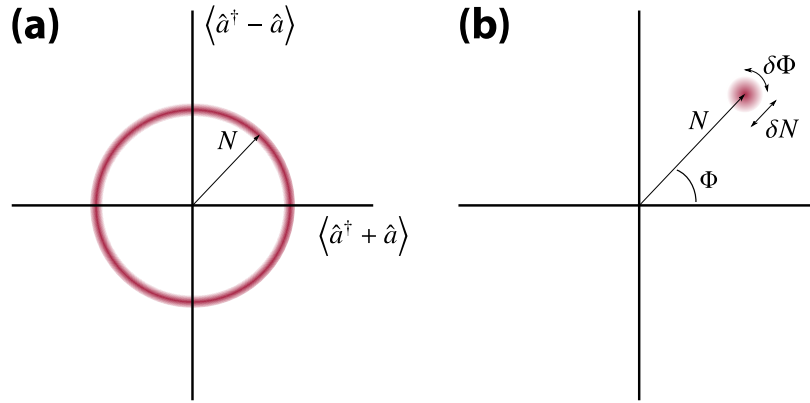
Figure 5.1: Q-function $[Q(\phi) = |\langle \alpha | \phi \rangle|^2 / \pi$, where $|\alpha\rangle$ is a general coherent state] representations of a number state (a) and a coherent state (b), for a single particle mode with creation and annihilation operators $\hat{a}^\dagger$ and $\hat{a}$. The $U(1)$-symmetric number state (a) has a well-defined number of particles and an undefined phase Φ, whereas the coherent state (b) has an uncertainty in both phase and number. However, as $N \to \infty$, the relative number uncertainty of the coherent state $\delta N / N \to 0$; hence the symmetry-breaking formalism is justified in this limit.

taking the expectation value of $\hat{\Psi}(\mathbf{r})$ for an eigenstate of total particle number yields (in illustrative schematic form):

$$\langle N | \hat{\Psi}(\mathbf{r}) | N \rangle = \sqrt{N} \langle N | N - 1 \rangle = 0 \,, \tag{5.24}$$

and hence that $\hat{\delta}(\mathbf{r}, t) = \hat{\Psi}(\mathbf{r})$. This potential issue with the symmetry-breaking description in an atomic BEC system can, however, be overcome by adopting one of a variety of *number-conserving* descriptions described in the following Section; these methods explicitly conserve the total atom number N. The lack of explicit atom-number-conservation in symmetry-breaking descriptions is potentially a strong argument in favour of these number-conserving alternatives. However, the above criticism of the symmetry-breaking methodology remains controversial; indeed, in the literature one can find spontaneous symmetry-breaking viewed as anything from a genuine physical reality [178] through to a convenient mathematical construction only having validity in the high-N limit [158].

---

clear that such considerations would favour a symmetry-breaking approach.

Lack of orthogonality between condensate and non-condensate

The lack of explicit atom-number-conservation is not the only issue with dynamical symmetry-breaking descriptions of atomic BECs, however. A second issue arises in that the symmetry-breaking non-condensate operator, $\hat{\delta}(\mathbf{r}, t)$, is not strictly orthogonal to the condensate $\Psi(\mathbf{r}, t)$ in an inhomogeneous system. That this is the case can be seen by applying the symmetry-breaking partition of the field operator [Eq. (5.1)] *following* a partition using the Penrose-Onsager definition of the condensate [see Eq. (1.16)]

$$\hat{\Psi}(\mathbf{r}) = \hat{a}_c(t)\phi_c(\mathbf{r}, t) + \sum_{m \neq c} \hat{a}_m \phi_m(\mathbf{r}, t), \qquad (5.25)$$

$$= \hat{a}_c(t)\phi_c(\mathbf{r}, t) + \delta\hat{\Psi}(\mathbf{r}, t), \qquad (5.26)$$

where, by the Hermiticity of the single-particle density matrix [see Section 1.4.1] $\delta\hat{\Psi}(\mathbf{r}, t)$ is explicitly orthogonal to $\phi_c(\mathbf{r}, t)$. This yields

$$\Psi(\mathbf{r}, t) = \langle \hat{a}_c(t) \rangle \phi_c(\mathbf{r}, t) + \left\langle \delta\hat{\Psi}(\mathbf{r}, t) \right\rangle, \qquad (5.27)$$

$$\hat{\delta}(\mathbf{r}, t) = [\hat{a}_c(t) - \langle \hat{a}_c(t) \rangle] \phi_c(\mathbf{r}, t) + \left[\delta\hat{\Psi}(\mathbf{r}, t) - \left\langle \delta\hat{\Psi}(\mathbf{r}, t) \right\rangle \right]. \qquad (5.28)$$

In a general inhomogeneous case $\left\langle \delta\hat{\Psi}(\mathbf{r}, t) \right\rangle \neq 0$, and consequently the symmetry-breaking macroscopic wavefunction $\Psi(\mathbf{r}, t)$ will contain a contribution from non-condensate modes. In such a case, $\Psi(\mathbf{r}, t)$ and $\hat{\delta}(\mathbf{r}, t)$ are no longer strictly orthogonal.

While we stress that this argument does not demonstrate in any way that symmetry-breaking is *incorrect*, it does highlight a problem which arises if one wishes to self-consistently determine *coupled condensate and non-condensate dynamics* in a symmetry-breaking description; namely, that the ambiguous distinction between condensate and non-condensate makes it difficult to formulate, and to interpret the results of, such a description. In a number-conserving description, on the other hand, the condensate and non-condensate are *always explicitly orthogonal*; this makes the formulation and interpretation of a theory of coupled condensate and non-condensate dynamics considerably easier [68]. This issue takes on an enhanced relevance with reference to the dynamical HFB-Popov and ZNG methods when working at low temperatures: here the phonon nature of the elementary excitations is more important than collisions within the non-condensate, and a theory which consistently treats the dynamical coupling between condensate and non-condensate through the anomalous average is preferable [70]. The number-conserving descrip-

tions we review in the next Section allow one to construct exactly such a theory, an example of which we will develop and implement in the following Chapters.

5.3 Number-conserving descriptions

5.3.1 Number-conserving partition of field operator

The second direction from which a theoretical description of atomic BECs at finite temperature can be approached is a *number-conserving* approach. In contrast to the grand-canonical symmetry-breaking approach, number-conserving approaches yield a canonical description of the system in which the total atom number N is a *fixed* parameter. The development of such number-conserving descriptions of atomic BECs have been pioneered by C. Gardiner [66], Castin and Dum [67, 181], Morgan [68–71, 163], and S. Gardiner [68]. However, these number-conserving descriptions also represent something of a "re-discovery" and extension of techniques which had already been introduced for weakly interacting Bose gases in the homogeneous case [304–307] long before the advent of atomic BEC (see, e.g., Ref. [281] for a more comprehensive overview of these previous treatments).

Like symmetry-breaking descriptions, a partition of the field operator lies at the core of number-conserving descriptions. However, in number-conserving descriptions this partition is based exactly on the Penrose-Onsager definition of the condensate mode $\phi_c(\mathbf{r}, t)$:

$$\hat{\Psi}(\mathbf{r}) = \hat{a}_c(t)\phi_c(\mathbf{r}, t) + \delta\hat{\Psi}(\mathbf{r}, t) \,. \tag{5.29}$$

Here

$$\delta\hat{\Psi}(\mathbf{r}, t) = \sum_{m \neq c} \hat{a}_m(t)\phi_m(\mathbf{r}, t) \,; \tag{5.30}$$

the components $\phi_c(\mathbf{r}, t)$ and $\delta\hat{\Psi}(\mathbf{r}, t)$ represent the condensate and non-condensate respectively, and the operator $\hat{a}_c(t)$ annihilates a particle from the condensate mode $\phi_c(\mathbf{r}, t)$. The condensate mode $\phi_c(\mathbf{r}, t)$ is the eigenmode of the single-particle density matrix $\rho(\mathbf{r}, \mathbf{r}', t)$ having a macroscopically large eigenvalue (occupation) N_c, in accordance with the Penrose-Onsager definition [173] [Fig. 5.2] (see Chapter 1).

This partition [Eq. (5.29)] is identical to that introduced to illustrate that $\Psi(\mathbf{r}, t)$ and $\hat{\delta}(\mathbf{r}, t)$ are not orthogonal in a symmetry-breaking treatment [Eq. (5.25)]. The condensate mode $\phi_c(\mathbf{r}, t)$ is *explicitly orthogonal* to the non-condensate operator $\delta\hat{\Psi}(\mathbf{r}, t)$. Using this orthogonality, one can use Eq. (5.29) to derive projections from
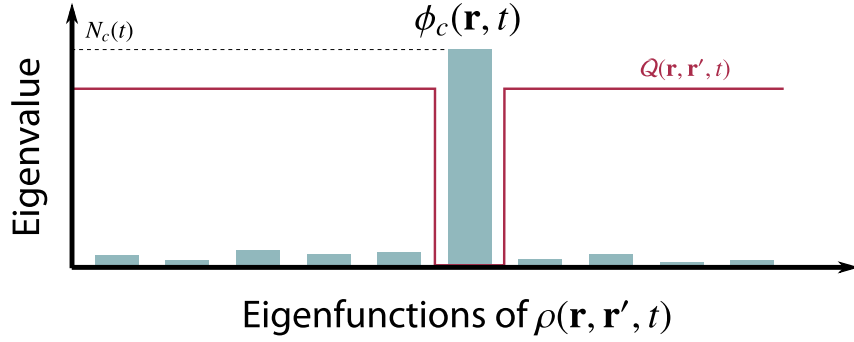
Figure 5.2: The Penrose-Onsager definition of Bose-Einstein condensation, presented pictorially. The condensate mode, $\phi_c(\mathbf{r}, t)$, is defined as the instantaneous eigenfunction of the single-body density matrix $\rho(\mathbf{r}, \mathbf{r}', t) = \left\langle \hat{\Psi}^\dagger(\mathbf{r}')\hat{\Psi}(\mathbf{r}) \right\rangle$ with a macroscopically large eigenvalue N_c — which is equal to the occupation of the condensate mode. The action of the projector $Q(\mathbf{r}, \mathbf{r}', t)$ [defined in equation (5.33)], which projects onto the subspace of non-condensate particles, is illustrated in red.

the full field operator $\hat{\Psi}(\mathbf{r})$ to the operators $\hat{a}_c(t)$ and $\delta\hat{\Psi}(\mathbf{r}, t)$:

$$\hat{a}_c(t) = \int d\mathbf{r}\, \phi_c^*(\mathbf{r}, t)\hat{\Psi}(\mathbf{r}), \tag{5.31}$$

$$\delta\hat{\Psi}(\mathbf{r}, t) = \int d\mathbf{r}'\, Q(\mathbf{r}, \mathbf{r}', t)\hat{\Psi}(\mathbf{r}'), \tag{5.32}$$

where we have introduced the projector $Q(\mathbf{r}, \mathbf{r}', t)$, defined by

$$Q(\mathbf{r}, \mathbf{r}', t) = \delta(\mathbf{r} - \mathbf{r}') - \phi_c(\mathbf{r}, t)\phi_c^*(\mathbf{r}', t); \tag{5.33}$$

the action of $Q(\mathbf{r}, \mathbf{r}', t)$ is also shown pictorially in Fig. 5.2.

The projection equations [Eqs. (5.31) and (5.32)] allow one to obtain commutation relations for $\hat{a}_c(t)$, $\delta\hat{\Psi}(\mathbf{r}, t)$, and their Hermitian conjugates in terms of the commutation relations of $\hat{\Psi}(\mathbf{r})$ and $\hat{\Psi}^\dagger(\mathbf{r})$. The only non-zero commutators that can be obtained this way are [68]

$$\left[\hat{a}_c(t), \hat{a}_c^\dagger(t) \right] = 1, \tag{5.34}$$

$$\left[\delta\hat{\Psi}(\mathbf{r}, t), \delta\hat{\Psi}^\dagger(\mathbf{r}', t) \right] = Q(\mathbf{r}, \mathbf{r}', t). \tag{5.35}$$

5.3.2 Number-conserving fluctuation operator

Requirements for a suitable operator

Having made a number-conserving partition of the field operator [Eq. (5.29)], the approach of number-conserving descriptions is similar to that of the symmetry-breaking descriptions, in that it consists of identifying a suitable fluctuation operator in terms of which the equations of motion can be perturbatively expanded. We wish such a fluctuation operator to retain as many of the favourable properties of the symmetry-breaking operator $\hat{\delta}(\mathbf{r}, t)$ as possible. In particular, $\hat{\delta}(\mathbf{r}, t)$ has the following key properties:

$\left\langle \hat{\delta}(\mathbf{r}, t) \right\rangle = 0$**:** The fluctuation operator is indeed a true fluctuation operator (provided this is true in a non-trivial sense [68]).

$\left[\hat{\delta}(\mathbf{r}, t), \hat{\delta}^{\dagger}(\mathbf{r}, t) \right] = \delta(\mathbf{r} - \mathbf{r}')$**:** The fluctuation operator describes *bosonic* quasiparticles.

$\hat{\delta}(\mathbf{r}, t) \propto \sqrt{N_t(t)}$**:** The fluctuation operator scales with the number of non-condensate atoms.

In trying to find a number-conserving operator with such properties, the first hurdle which arises is that the expectation values of all creation and annihilation operators are trivially equal to zero when working in a number-conserving formalism. In consequence, the non-condensate field operator $\delta\hat{\Psi}(\mathbf{r}, t)$ cannot be used as a fluctuation operator because its expectation value is *trivially* zero. However, one can instead find a suitable basis for a fluctuation operator by recourse, once again, to the Penrose-Onsager definition of Bose-Einstein condensation. Recalling that $\phi_c(\mathbf{r}, t)$ is an instantaneous eigenstate of the single-body density matrix, with eigenvalue $N_c(t)$, we can write

$$\int d\mathbf{r}' \, \rho(\mathbf{r}, \mathbf{r}', t) \phi_c(\mathbf{r}', t) = N_c(t) \phi_c(\mathbf{r}, t) \,. \tag{5.36}$$

Making the replacement $\rho(\mathbf{r}, \mathbf{r}', t) = \left\langle \hat{\Psi}^{\dagger}(\mathbf{r}') \hat{\Psi}(\mathbf{r}) \right\rangle$, and then substituting for the field operators using Eq. (5.29), one can obtain the relations

$$\left\langle \hat{a}_c^{\dagger}(t) \hat{a}_c(t) \right\rangle = N_c(t) \,, \tag{5.37}$$

$$\left\langle \hat{a}_c^{\dagger}(t) \delta\hat{\Psi}(\mathbf{r}, t) \right\rangle = 0 \,. \tag{5.38}$$

The product of operators $\hat{a}_c^\dagger(t)\delta\hat{\Psi}(\mathbf{r}, t)$ appearing in Eq. (5.38) is a good candidate for the basis of a number-conserving fluctuation operator as it has a non-trivial, zero expectation value.

However, the scaling of $\hat{a}_c^\dagger(t)\delta\hat{\Psi}(\mathbf{r}, t)$ is not correct, and it does not have bosonic commutation relations: while the latter are not essential, they can be a considerable convenience when considering quasiparticles and elementary excitations at a later stage in the treatment. Unfortunately, it appears to be an unavoidable consequence of the number-conserving description that one cannot find a fluctuation operator which exactly fulfils the expectation, commutation and scaling requirements. We now briefly review three fluctuation operators which have been introduced in the literature; each of these represents a different compromise with respect to fulfilling these requirements.

Candidate fluctuation operators

The first fluctuation operator we consider is

$$\hat{\Lambda}_c(\mathbf{r}, t) = \frac{1}{\sqrt{\hat{N}_c(t)}}\hat{a}_c^\dagger(t)\delta\hat{\Psi}(\mathbf{r}, t)\,. \tag{5.39}$$

Here $\hat{N}_c(t)$ is the condensate number operator, $\hat{a}_c^\dagger(t)\hat{a}_c(t)$, the square root of which scales with N_c like $\hat{a}_c^\dagger(t)$. The fluctuation operator $\hat{\Lambda}_c(\mathbf{r}, t)$ has two main advantages; firstly, the commutator of $\hat{\Lambda}_c(\mathbf{r}, t)$ with its Hermitian conjugate is exactly equal to $Q(\mathbf{r}, \mathbf{r}', t)$;

$$\left[\hat{\Lambda}_c(\mathbf{r}, t), \hat{\Lambda}_c^\dagger(\mathbf{r}', t)\right] = \left[\delta\hat{\Psi}(\mathbf{r}, t), \hat{\Psi}^\dagger(\mathbf{r}', t)\right] = Q(\mathbf{r}, \mathbf{r}', t)\,. \tag{5.40}$$

This leads to bosonic quasiparticles[8]. Secondly, $\hat{\Lambda}_c(\mathbf{r}, t)$ scales exactly with the number of non-condensate particles;

$$\int d\mathbf{r}\,\hat{\Lambda}_c^\dagger(\mathbf{r}, t)\hat{\Lambda}_c(\mathbf{r}, t) = \int d\mathbf{r}\,\delta\hat{\Psi}^\dagger(\mathbf{r}, t)\delta\hat{\Psi}(\mathbf{r}, t) = \hat{N}_t(t)\,. \tag{5.41}$$

Unfortunately, despite its useful properties, $\hat{\Lambda}_c(\mathbf{r}, t)$ has a fundamental flaw as a fluctuation operator; due to the introduction of the renormalizing factor $1/\sqrt{\hat{N}_c(t)}$, the expectation value $\left\langle\hat{\Lambda}_c(\mathbf{r}, t)\right\rangle$ is not exactly equal to zero. Hence $\hat{\Lambda}_c(\mathbf{r}, t)$ is *not* a well-defined fluctuation operator.

A second approach to rescaling the fluctuation operator is that introduced by C. Gar-

---

[8]Technically, they are only bosonic in the space orthogonal to the condensate, but within a number-conserving description this technicality is unimportant.

diner and Castin and Dum [66, 67]. In this approach $\hat{a}_c^\dagger(t)\delta\hat{\Psi}(\mathbf{r},t)$ is rescaled using the *total* number operator $\hat{N}$ to give the fluctuation operator

$$\hat{\Lambda}(\mathbf{r},t) = \frac{1}{\sqrt{\hat{N}}}\hat{a}_c^\dagger(t)\delta\hat{\Psi}(\mathbf{r},t)\,. \tag{5.42}$$

Since we assume the total number of atoms to be fixed and constant, the expectation value $\left\langle\hat{\Lambda}(\mathbf{r},t)\right\rangle$ is indeed zero at all times. Thus $\hat{\Lambda}(\mathbf{r},t)$ represents a well defined fluctuation operator. However, $\hat{\Lambda}(\mathbf{r},t)$ scales like

$$\sqrt{\frac{N_c(t)N_t(t)}{N}} = \sqrt{N_t(t)\frac{N-N_t(t)}{N}}\,; \tag{5.43}$$

consequently the scaling of $\hat{\Lambda}(\mathbf{r},t)$ is only correct — that is, equal to $\sqrt{N_t(t)}$ — in the limit $N_t(t) \ll N$. In general, the norm of $\hat{\Lambda}(\mathbf{r},t)$ is only approximately equal to the number of non-condensate atoms. Secondly,

$$\left[\hat{\Lambda}_c(\mathbf{r},t),\hat{\Lambda}_c^\dagger(\mathbf{r}',t)\right] \approx \left[\delta\hat{\Psi}(\mathbf{r},t),\hat{\Psi}^\dagger(\mathbf{r}',t)\right] = Q(\mathbf{r},\mathbf{r}',t)\,, \tag{5.44}$$

leading to commutation relations for quasiparticles which are only approximately bosonic.

A third and final fluctuation operator was definied by S. Gardiner and Morgan [68];

$$\tilde{\Lambda}(\mathbf{r},t) = \frac{1}{\sqrt{N_c(t)}}\hat{a}_c^\dagger(t)\delta\hat{\Psi}(\mathbf{r},t)\,, \tag{5.45}$$

where $N_c(t) = \left\langle\hat{N}_c(t)\right\rangle$. Since this definition only rescales $\hat{a}_c^\dagger(t)\delta\hat{\Psi}(\mathbf{r},t)$ by a *scalar* factor, the expectation value $\left\langle\tilde{\Lambda}(\mathbf{r},t)\right\rangle$ is exactly equal to zero at all times and $\tilde{\Lambda}(\mathbf{r},t)$ is a good fluctuation operator. It also scales correctly as $\sqrt{N_t(t)}$. Unfortunately, as in the case of $\hat{\Lambda}(\mathbf{r},t)$, the operator $\tilde{\Lambda}(\mathbf{r},t)$ leads to only approximately bosonic quasiparticles;

$$\left[\tilde{\Lambda}(\mathbf{r},t),\tilde{\Lambda}^\dagger(\mathbf{r}',t)\right] = \frac{\hat{N}_c(t)}{N_c(t)}Q(\mathbf{r},\mathbf{r}',t) - \frac{1}{N_c(t)}\hat{\Psi}^\dagger(\mathbf{r}',t)\delta\hat{\Psi}(\mathbf{r},t)\,. \tag{5.46}$$

Summary

Of the three candidates for a number-conserving fluctuation operator, none is completely ideal. The "obvious" choice, $\hat{\Lambda}_c(\mathbf{r},t)$, scales correctly and gives bosonic quasiparticles, but turns out not to be a well-defined fluctuation operator at all. The

first alternative, $\hat{\Lambda}(\mathbf{r}, t)$, is a well-defined fluctuation operator, but it gives only approximately bosonic quasiparticles and scales only approximately correctly. The final alternative, $\tilde{\Lambda}(\mathbf{r}, t)$, is also a well-defined fluctuation operator; it too gives only approximately bosonic quasiparticles, but unlike $\hat{\Lambda}(\mathbf{r}, t)$ it does scale correctly.

As none of these candidate fluctuation operators can be said to be superior to the others in general, the choice of which fluctuation operator to use is strongly influenced by exactly what type of calculation one wishes to conduct. For example, in an extensive calculation of static properties at finite temperature (described in the next Section) Morgan chose to use the first candidate fluctuation operator $\hat{\Lambda}_c(\mathbf{r}, t)$ [163]: in the context of this calculation bosonic quasiparticles are a considerable convenience, while the fact that $\left\langle \hat{\Lambda}_c(\mathbf{r}, t) \right\rangle \neq 0$ results (indirectly) in needing to expand inverse-square-root number-operators in Taylor series to a consistent order [68, 281].

In the development of a dynamical description to first-order in the fluctuation operator, C. Gardiner [66] and Castin and Dum [67, 181] chose to use the operator $\hat{\Lambda}(\mathbf{r}, t)$, largely because the difference between $\hat{N}$ and $\hat{N_c}(t)$ is unimportant at this order. In developing the second-order dynamical description we consider in detail in the following Chapters, S. Gardiner and Morgan [68] chose to use $\tilde{\Lambda}(\mathbf{r}, t)$, since the property $\left\langle \tilde{\Lambda}(\mathbf{r}, t) \right\rangle = 0$ is of particular use when obtaining coupled equations of motion for condensate and non-condensate (although, to the order of the calculation, the same results can also be obtained using $\hat{\Lambda}_c(\mathbf{r}, t)$ [69–71]).

5.3.3 Static descriptions

While our intended purpose for number-conserving descriptions is a self-consistent description of coupled condensate and non-condensate dynamics, in this Section we briefly review the static number-conserving description of Morgan [163, 281]. In relation to the static symmetry-breaking descriptions discussed in Sections 5.2.2 and 5.2.3, this description constitutes a beyond-HFB treatment which remains self-consistent and gapless. However, the perturbative treatment of high-order terms leads to a complex series of integrals for quasiparticle energy-shifts which have not yet been numerically implemented [281].

For comparison to the symmetry-breaking description, Morgan's approach is effectively[9] to expand the Hamiltonian in terms of the fluctuation operator $\hat{\Lambda}_c(\mathbf{r}, t)$,

---

[9]Note that in Refs. [163] and [281] a formalism of second quantized creation and annihilation operators and single-particle matrix elements is adopted, rather than the field operator formalism we

yielding an expansion analogous to Eq. (5.2) with

$$\hat{H}_0 = \int d\mathbf{r}\, \phi_c^* \hat{N}_c \left(H_{\mathrm{sp}} + \frac{\tilde{U}}{2} \frac{\hat{N}_c - 1}{N_c} |\phi_c|^2 \right) \phi_c \,, \tag{5.47}$$

$$\hat{H}_1 = \int d\mathbf{r} \left[\hat{\Lambda}_c^\dagger \sqrt{\hat{N}_c} \left(H_{\mathrm{sp}} + \tilde{U} \frac{\hat{N}_c - 1}{N_c} |\phi_c|^2 \right) \phi_c + \mathrm{h.c.} \right] \,, \tag{5.48}$$

$$\hat{H}_2 = \int d\mathbf{r} \left[\hat{\Lambda}_c^\dagger \left(H_{\mathrm{sp}}(\mathbf{r}, t) + 2\tilde{U} \frac{\hat{N}_c - 1}{N_c} |\phi_c|^2 \right) \hat{\Lambda}_c \right.$$
$$\left. + \frac{\tilde{U}}{2} \left(\phi_c^{*2} \frac{\hat{N}_c}{N_c} \hat{\Lambda}_c \hat{\Lambda}_c + \hat{\Lambda}_c^\dagger \hat{\Lambda}_c^\dagger \frac{\hat{N}_c}{N_c} \phi_c^{\,2} \right) \right] \,, \tag{5.49}$$

$$\hat{H}_3 = \int d\mathbf{r} \left[\hat{\Lambda}_c^\dagger \tilde{U} \frac{\sqrt{\hat{N}_c}}{N_c} \hat{\Lambda}_c^\dagger \hat{\Lambda}_c \phi_c + \mathrm{h.c.} \right] \,, \tag{5.50}$$

$$\hat{H}_4 = \int d\mathbf{r}\, \hat{\Lambda}_c^\dagger \frac{\sqrt{\hat{N}_c}}{N_c} \hat{\Lambda}_c^\dagger \frac{\tilde{U}}{2(\hat{N}_c - 1)} \hat{\Lambda}_c \sqrt{\hat{N}_c} \hat{\Lambda}_c \,, \tag{5.51}$$

where we have grouped products of the effective coupling constant $\tilde{U} = N_c U_0$, and we have omitted position and time arguments $(\mathbf{r}, t)$ for clarity. Following this expansion, which remains exact, the condensate number operators appearing above should be expanded to an order consistent with the calculation being undertaken. Note that this Hamiltonian, unlike its symmetry-breaking equivalent [Eq. (5.2)], is *not* written in the grand canonical ensemble; hence there is no equivalent of the chemical potential μ appearing in the Hamiltonian itself.

At lowest order one obtains, from functional differentiation of $\hat{H}_0$ (after correct expansion of $\hat{N}_c$ and ordering of terms [163])

$$\left[H_{\mathrm{sp}}(\mathbf{r}) + N_c U_0 |\phi_c(\mathbf{r})|^2 - \lambda_0 \right] \phi_c(\mathbf{r}) = 0 \,, \tag{5.52}$$

where λ_0 is the nonlinear eigenvalue defined by

$$\lambda_0 = \int d\mathbf{r}\, \phi_c^*(\mathbf{r}) \left[H_{\mathrm{sp}}(\mathbf{r}) + N_c U_0 |\phi_c(\mathbf{r})|^2 \right] \phi_c(\mathbf{r}) \,. \tag{5.53}$$

Note that at this level of approximation $N_c = N$ and Eq. (5.52) is the *same* static GPE as obtained using symmetry-breaking treatments. At this level of approximation, therefore, λ_0 can be identified with the chemical potential.

The first difference from a symmetry-breaking treatment is encountered at the level

---

adopt here, and some quantities are defined slightly differently. However, the Hamiltonian presented here captures the essence of the approach within the formalism and definitions we have made, and avoids the need to introduce further notation.

of the simple quadratic Hamiltonian $\hat{H}_2$ (again, subject to consistent expansion of $\hat{N}_c$ and ordering of terms). In a similar manner to symmetry-breaking treatments, this can be diagonalized by the Bogoliubov transformation

$$\left(\begin{array}{c} \hat{\Lambda}_c(\mathbf{r}) \\ \hat{\Lambda}_c^\dagger(\mathbf{r}) \end{array} \right) = \sum_k \hat{b}_k \left(\begin{array}{c} u_k(\mathbf{r}) \\ v_k(\mathbf{r}) \end{array} \right) + \hat{b}_k^\dagger \left(\begin{array}{c} v_k^*(\mathbf{r}) \\ u_k^*(\mathbf{r}) \end{array} \right), \tag{5.54}$$

to yield static number-conserving modified Bogoliubov-de Gennes equations (MB-dGE)

$$\int d\mathbf{r}' \left(\begin{array}{cc} \mathcal{L}(\mathbf{r}, \mathbf{r}') & \mathcal{M}(\mathbf{r}, \mathbf{r}') \\ -\mathcal{M}^*(\mathbf{r}, \mathbf{r}') & -\mathcal{L}^*(\mathbf{r}, \mathbf{r}') \end{array} \right) \left(\begin{array}{c} u_k(\mathbf{r}') \\ v_k(\mathbf{r}') \end{array} \right) = \epsilon_k \left(\begin{array}{c} u_k(\mathbf{r}) \\ v_k(\mathbf{r}) \end{array} \right), \tag{5.55}$$

where

$$\begin{aligned} \mathcal{L}(\mathbf{r}, \mathbf{r}') =& \delta(\mathbf{r} - \mathbf{r}') \left[H_{\text{sp}}(\mathbf{r}') + U_0 N_c |\phi_c(\mathbf{r}')|^2 - \lambda_0 \right] \\ &+ U_0 N_c \int d\mathbf{r}'' \, Q(\mathbf{r}, \mathbf{r}'') \, |\phi_c(\mathbf{r}'')|^2 Q(\mathbf{r}'', \mathbf{r}') , \end{aligned} \tag{5.56}$$

and

$$\mathcal{M}(\mathbf{r}, \mathbf{r}') = U_0 N_c \int d\mathbf{r}'' \, Q(\mathbf{r}, \mathbf{r}'') \, \phi_c^2(\mathbf{r}'') Q^*(\mathbf{r}'', \mathbf{r}') . \tag{5.57}$$

The appearance of the projector Q in the static MBdGE acts to explicitly orthogonalize the quasiparticle modes with the condensate.

The beyond-quadratic-Hamiltonian theory developed by Morgan proceeds further by, firstly, including the quadratic averages associated with $\hat{H}_3$ and $\hat{H}_4$ in a modified quadratic Hamiltonian as in the symmetry-breaking HFB theory; this results in an "upgrade" of the GPE to a number-conserving GGPE containing terms including the projector Q which are not found in the HFB-GGPE, and an "upgrade" of the terms $\mathcal{L}$ and $\mathcal{M}$ in the number-conserving MBdGE to include the non-condensate normal and anomalous averages (now defined by $\tilde{n}(\mathbf{r}, \mathbf{r}') = \left\langle \hat{\Lambda}_c^\dagger(\mathbf{r}') \hat{\Lambda}_c(\mathbf{r}) \right\rangle$ and $\tilde{m}(\mathbf{r}, \mathbf{r}') = \left\langle \hat{\Lambda}_c(\mathbf{r}') \hat{\Lambda}_c(\mathbf{r}) \right\rangle$). Secondly, further effects of $\hat{H}_3$ and $\hat{H}_4$ are included perturbatively in order to make the resulting theory gapless. The resulting theory is, however, complex for even static calculations, and we refer the reader to Refs. [163] and [281] for details.

5.3.4 Dynamical descriptions

Overview

Having introduced the number-conserving description to quadratic order in a static treatment, we now briefly review the development, and applications, of fully dynamical treatments within the number-conserving description. We shall, for now, omit the mathematical details, as these are dealt with extensively for the second-order case in Chapter 6.

As with dynamical symmetry-breaking treatments, dynamical number-conserving treatments consist of a consistent expansion of the equation of motion for the field operator $\hat{\Psi}(\mathbf{r})$ up to some order in the chosen fluctuation operator. To date, essentially equivalent treatments including terms up to first (linear) order in the fluctuation operators have been given by C. Gardiner [66] and Castin and Dum [67], while treatments including terms up to second (quadratic) order in the fluctuation operators have been Morgan [69–71], and S. Gardiner and Morgan [68]. As discussed in Section 5.3.2, there are three particular fluctuation operators which these previous authors have employed: $\hat{\Lambda}$ [66, 67], $\hat{\Lambda}_c$ [69–71], and $\tilde{\Lambda}$ [68]. However, in consistent expansions up to linear order these fluctuation operators are all equivalent. At quadratic order $\hat{\Lambda}_c$ and $\tilde{\Lambda}$ remain essentially equivalent [68].

First-order description

The first-order description of C. Gardiner and Castin and Dum, which we derive as a limiting case of a second-order description in Chapter 6, consists of a time-dependent version of the GPE and number-conserving MBdGE presented in the previous Section:

$$i\frac{\partial \phi_c(\mathbf{r}, t)}{\partial t} = \left[H_{\text{sp}}(\mathbf{r}, t) + N_c U_0 |\phi_c(\mathbf{r}, t)|^2 - \lambda_0 \right] \phi_c(\mathbf{r}, t), \quad (5.58)$$

and

$$i\frac{\partial}{\partial t} \begin{pmatrix} u_k(\mathbf{r}, t) \\ v_k(\mathbf{r}, t) \end{pmatrix} = \int d\mathbf{r}' \begin{pmatrix} \mathcal{L}(\mathbf{r}, \mathbf{r}', t) & \mathcal{M}(\mathbf{r}, \mathbf{r}', t) \\ -\mathcal{M}^*(\mathbf{r}, \mathbf{r}', t) & -\mathcal{L}^*(\mathbf{r}, \mathbf{r}', t) \end{pmatrix} \begin{pmatrix} u_k(\mathbf{r}', t) \\ v_k(\mathbf{r}', t) \end{pmatrix}, \quad (5.59)$$

where

$$\begin{aligned} \mathcal{L}(\mathbf{r}, \mathbf{r}', t) =& \delta(\mathbf{r} - \mathbf{r}') \left[H_{\text{sp}}(\mathbf{r}', t) + U_0 N_c |\phi_c(\mathbf{r}', t)|^2 - \lambda_0 \right] \\ &+ U_0 N_c \int d\mathbf{r}'' \, Q(\mathbf{r}, \mathbf{r}'', t) \, |\phi_c(\mathbf{r}'', t)|^2 Q(\mathbf{r}'', \mathbf{r}', t), \end{aligned} \quad (5.60)$$

and

$$\mathcal{M}(\mathbf{r}, \mathbf{r}', t) = U_0 N_c \int d\mathbf{r}'' \, Q(\mathbf{r}, \mathbf{r}'', t) \, \phi_c^2(\mathbf{r}'', t) Q^*(\mathbf{r}'', \mathbf{r}', t) \,. \tag{5.61}$$

The nonlinear eigenvalue λ_0 retains its previous definition [Eq. (5.53)] for an equilibrium initial condition. This first-order description has been widely used to explore non-condensate growth, starting from low-temperature equilibrium, in driven atomic BECs [48, 56, 57, 59, 181, 308]. This is exactly the scenario where a number-conserving description's consistent treatment of the anomalous average between condensate and non-condensate and exclusion of collisions between non-condensate atoms constitute an advantage over a symmetry-breaking treatment; we discuss exactly such a system (using a second-order approach) extensively in Chapter 7.

To actually evolve Eqs. (5.58) and (5.59) in this way requires an initial equilibrium initial condition. This can be obtained in a self-consistent fashion by initially setting $N_c = N$ and then repeating the following steps until convergence: (a) solve the static GPE Eq. (5.52) for the condensate mode $\phi_c(\mathbf{r}, 0)$ and eigenvalue $\lambda_)$; (b) use the obtained condensate mode and eigenvalue to solve the static number-conserving MBdGE [Eq. (5.55)]; (c) compute the expected non-condensate population $N_t = \langle \hat{N}_t \rangle = \int d\mathbf{r} \, \tilde{n}(\mathbf{r}, \mathbf{r})$ though Eq. (5.18), using a Bose distribution to find the quasiparticle populations, and set $N_c = N - N_t$. It should be noted, however, that this procedure first-order description will only yield valid results at low temperatures $\ll T_c$ where $N_t \ll N_c$.

As in the static case the projector Q acts to keep the condensate and non-condensate orthogonal, in this case in a dynamical sense. In principle, the presence of the projector Q makes the numerical evolution of these equations a highly non-trivial problem. However, one can in fact prove that the evolution generated by Eq. (5.59) is exactly equivalent to an "un-projected" evolution with $Q = 1$, followed by a separate action of Q on the non-condensate, equivalent to projection of the quasiparticle modes orthogonal to the condensate mode [48, 309]. The fundamental reason such a simplification of the dynamical evolution can be achieved is that the GPE [Eq. (5.58)] evolves in *isolation* from the non-condensate: the only non-condensate-dependent term appearing in the GPE is N_c, but at the order of this calculation this is formally *time-independent*.

This separation between GPE and MBdGE also constitutes the primary drawback of the first-order description, as the non-condensate population N_t is time-dependent and the non-condensate can grow, but this has no back-action on the condensate.

The description thus exhibits rapid and unbounded growth of the non-condensate in regimes where the condensate dynamics have a linear instability [48, 49]. Attempting to fix this instability using the ad-hoc procedure of adjusting N_c to be time-dependent according to $N_c(t) = N - N_t(t)$ does not eliminate this rapid growth, and leads to unphysical negative condensate populations very quickly in linearly unstable regimes. To consistently incorporate the back-action of the non-condensate on the condensate, and hence determine whether such a back-action has a restraining effect on condensate depletion, a second-order approach is required [49].

Second-order description

The second-order description of S. Gardiner and Morgan [68–71], which we derive in detail in Chapter 6, yields a number-conserving generalized GPE (GGPE) for the condensate

$$
\begin{aligned}
i\hbar \frac{\partial \phi(\mathbf{r}, t)}{\partial t} = {} & \left\{ H_{\mathrm{sp}}(\mathbf{r}, t) + \tilde{U} \left[\left(1 - \frac{1}{N_c} \right) |\phi(\mathbf{r}, t)|^2 + 2 \frac{\tilde{n}(\mathbf{r}, \mathbf{r}, t)}{N_c} \right] - \lambda_2 \right\} \phi(\mathbf{r}, t) \\
& + \tilde{U} \frac{\tilde{m}(\mathbf{r}, \mathbf{r}, t)}{N_c} \phi^*(\mathbf{r}, t) \\
& - \tilde{U} \int d\mathbf{r}' \, |\phi(\mathbf{r}', t)|^2 \left(\frac{\tilde{n}(\mathbf{r}, \mathbf{r}', t)}{N_c} \phi(\mathbf{r}', t) + \frac{\tilde{m}(\mathbf{r}, \mathbf{r}', t)}{N_c} \phi^*(\mathbf{r}', t) \right),
\end{aligned}
\tag{5.62}
$$

coupled to the *same* MBdGE for the non-condensate quasiparticles as in the first-order description [Eq. (5.59)]. Note that, in general, the anomalous average $\tilde{m}$ appearing in Eq. (5.62) must be renormalized to prevent ultraviolet divergence (see Section 5.2.3). The GGPE eigenvalue λ_2 is given by

$$
\begin{aligned}
\lambda_2 = {} & \int d\mathbf{r} \, \phi_c^*(\mathbf{r}, t) \left\{ H_{\mathrm{sp}}(\mathbf{r}, t) + \tilde{U} \left[\left(1 - \frac{1}{N_c} \right) |\phi(\mathbf{r}, t)|^2 + 2 \frac{\tilde{n}(\mathbf{r}, \mathbf{r}, t)}{N_c} \right] \right\} \phi(\mathbf{r}, t) \\
& + \tilde{U} \int d\mathbf{r} \, \frac{\tilde{m}(\mathbf{r}, \mathbf{r}, t)}{N_c} \phi^{*2}(\mathbf{r}, t).
\end{aligned}
\tag{5.63}
$$

Importantly, this eigenvalue is in general complex, allowing a transfer of population between condensate and non-condensate; $N_c(t)$ and $N_t(t)$ are now *both* time-dependent and satisfy $N_c(t) + N_t(t) = N$. The final term can be interpreted as a dynamic projection which ensures that the condensate and non-condensate remain orthogonal despite the presence of population transfer (see Chapter 6).

This self-consistency of number-dynamics is a key feature of this second-order description; indeed, second-order is the minimal order at which such self-consistency

can be non-trivially realized[10]. This number-self-consistency arises directly from *not* "upgrading" the MBdGE for the non-condensate to include the normal and anomalous averages $\tilde{n}$ and $\tilde{m}$, as in the symmetry-breaking HFB description (Section 5.2.2), or the static number-conserving description of Morgan (Section 5.3.3). This is an important, and somewhat counter-intuitive result [68].

An implementation of this second-order description in the linear response regime was used by Morgan to model the shift of excitation frequencies at finite-temperature in an atomic BEC — as measured at JILA [72, 73] and MIT [74, 133]; this involved calculation is described in Refs. [69–71]. In particular, the second-order number-conserving description was shown to successfully capture the upward shift, at finite temperature, of the frequency of the $m = 0$ quadrupolar oscillation in a cylindrically symmetric and slightly prolate harmonic trap, as observed at JILA [73]. In this context, the number-conserving treatment yields results quantitatively closer to experiment than symmetry-breaking descriptions such as the ZNG description [50], and also demonstrates the origin of the shift to be a transition from direct driving of the condensate by the time-dependent perturbing potential to indirect driving via the non-condensate [69].

In Part II of this thesis, our aim is to extend the reach of this theory beyond the perturbative, linear response regime used successfully by Morgan by realizing a fully dynamical implementation. This is a computationally involved problem, and we therefore restrict our initial implementation to quasi-1D systems. Nonetheless, even with the restriction to quasi-1D, the fully time-dependent second-order description we implement in this thesis allows one to explore the issues of, and the links between, condensate depletion, instability and dynamical chaos, quantum coherence, and thermalization and integrability in driven BECs.

5.4 *c*-field descriptions

Overview

Common to both the symmetry-breaking and number-conserving descriptions we have discussed in this Chapter so far is the notion of a perturbative fluctuation expansion of the Hamiltonian and/or the equations of motion of the field. We conclude this Chapter by briefly discussing an alternative approach which avoids such an expansion and builds on a different premise: the classical field or *c-field* approach. A

---

[10]Technically, the zero-order (GPE-only) description is self-consistent, but this is trivially guaranteed, since in this description $N_t \equiv 0$.

variety of successful recent applications of this approach strongly justifies its brief inclusion in this overview of finite-temperature and beyond-mean-field methods. A thorough and relatively recent overview of *c*-field methods was given by Blakie *et al.* [171].

Using the GPE at finite temperature

In the symmetry-breaking and perturbative descriptions already discussed in this Chapter, and in Chapter 1, the GPE has consistently appeared as the zeroth-order description of the quantum field in the case of a single macroscopically occupied mode. In this role it constitutes an entirely zero-temperature description; it contains no treatment of the non-condensate. However, as hinted at in Section 1.4.2, the GPE is fundamentally a *classical field* equation; consequently it can be used to describe the classical aspects of a general quantum field [183]. As well as for a zero temperature condensate with one highly occupied mode, this classical field approximation can be accurate for a field with multiple occupied modes, provided all the modes are highly occupied ($N_k \gg 1$). Exactly such a situation in fact arises in atomic BECs at temperatures $T_c/2 \lesssim T \lesssim T_c$ [302, 310–313]. The GPE therefore provides an approximate description of such a finite-temperature system, essentially because classical thermal effects dominate over quantum effects.

The classical field described by the GPE can be expanded in terms of the appropriate single-particle modes as

$$\Psi(\mathbf{r}, t) = \sum_m a_m(t)\phi_m(\mathbf{r}) \,. \tag{5.64}$$

The use of the GPE in such a finite-temperature situation typically proceeds as follows: (a) populate the modes of the system with essentially arbitrarily chosen a_k [314]. However, these a_k should be chosen to be consistent with the desired atom number and total energy, as this description constitutes a microcanonical approach [171]; (b) evolve this randomized initial condition in the GPE. This evolution conserves the total energy, but the nonlinearity of the equation rapidly acts to thermalize the system, distributing energy amongst the modes according to a classical thermal distribution; (c) although the exact details of the dynamics predicted by the GPE may be dependent on the intial condition, the evolution can reasonably be assumed to be ergodic [171]. Hence, with all microstates being equally likely to be visited by the evolution over long times, the time-averaged value of an observable over a sufficiently long evolution corresponds to the microcanonical ensemble-average in the steady-state [314, 315]. It is also possible to extract a "dynamical temeperature" from such an evolution [316, 317]. This use of the GPE as a leading order descrip-

tion of a finite temperature quantum field has been adopted in, for example, studies of quantum turbulence [123–126].

The projected GPE

The technique of using the GPE at finite temperature can potentially suffer from the problem of the nonlinear evolution leading to sparsely populated modes, and the equation consequently evolving itself outside of its own regime of validity. Fortunately this problem is typically restricted implicitly by the finite size of a numerical grid in any simulation. However, one can carefully control the evolution to remain within a defined *classical field region* using a projection term; the resulting *projected* GPE (PGPE) then represents the lowest rung of the hierarchy of *c*-field methods, which are based upon a division of the system into a classical field region with high mode occupation, and an *incoherent region* with sparse mode occupation. This incoherent region is itself restricted by a high-energy cut-off, yielding an effective field theory free of the problems of ultraviolet divergences due to the use of the contact potential discussed in Section 5.2.3 (although this raises the new non-trivial problem of where to position this cut-off) [171].

Despite its relatively recent introduction by Davis, Morgan and Burnett [184, 314, 318] the PGPE has been widely applied to atomic BECs (see Ref. [171] for a comprehensive review). In particular it has been used for the study of the shift of T_c due to interactions [170] and vortex formation [319].

The truncated Wigner PGPE

As has been shown by Polkovnikov, the first correction to the GPE description of a highly-occupied multi-mode quantum system is given by the truncated Wigner method [183]. This method can be thought of as extending the PGPE treatment to a regime where quantum fluctuations are no longer dominated by thermal ones. It can be developed by writing the equation of motion for the Wigner function of the full quantum field, and subsequently truncating this equation by removing higher-order derivatives. Rather than solving for the evolution of the entire Wigner function, one can interpret the Wigner function as a quasi-probability distribution and estimate its evolution by evolving an appropriate ensemble of single trajectories [50]. Adopting such an approach, the evolution equation for each trajectory is simply the PGPE [171]. The most commonly adopted sampling technique is based on the static number-conserving MBdGE of Eq. (5.55) [320–322]. The truncated Wigner PGPE has been applied to diverse problems in atomic BECs, such as vortex lattice

formation [323], colliding [324], reflecting [325] and collapsing [238, 256] condensates, collisions of bright solitary waves [28], and atom interferometers [43, 326]. However, as the truncated Wigner method can be viewed as introducing a one-half quantum of noise per mode, the evolution of trajectories in the PGPE can give rise to spurious thermalization; consequently, the dynamics predicted by the truncated Wigner method are limited to short times and close-to-equilibrium dynamics [322].

The stochastic PGPE

The final c-field method we discuss here is the stochastic projected GPE (SPGPE) [182, 327–329]. Although different in formulation, the SPGPE is similar in overall outlook to the symmetry-breaking ZNG method [160, 296] in which the GPE description of the condensate is consistently coupled to a quantum Boltzmann equation for the non-condensate by enforcing local momentum and energy conservation (see Section 5.2.4). In the SPGPE case it is the truncated Wigner PGPE description of the low-lying c-field region which is coupled to an incoherent reservoir which is assumed to be in local equilibrium. Indeed, the space between the c-field SPGPE approach and the ZNG theory is home to an alternative stochastic GPE description (SGPE) formulated by Stoof [330, 331], which has been extensively reviewed and implemented by Proukakis and Cockburn [50, 332–334].

The first key feature of the inherently grand-canonical SPGPE approach is a consistent treatment of interactions predicated on the upper energy cut-off for the incoherent region: this eliminates the problems of ultraviolet divergence and the need to introduce the many-body T-matrix into non-condensate collisions. Secondly, the use of a c-field (truncated Wigner PGPE) treatment of the low-lying modes leads to inclusion of non-local quantum effects up to $T = T_c$: in the ZNG theory these are ignored, and in the SGPE these are not treated consistently as $T \to T_c$. These features, combined with the (as yet unrealized) possibility to consistently model the dynamics of the incoherent reservoir, make the SPGPE ideal for simulating the formation of atomic BECs. Indeed, the SPGPE has proved remarkably successful both in this role [329, 335], and in the study of quantized vortex dynamics and superfluid turbulence [122, 329, 336]. However at low temperatures, where the incoherent region is unimportant, the SPGPE reduces to the truncated Wigner PGPE. As such, it too fails to give the completely consistent account of coupled condensate and non-condensate dynamics, particularly those occurring over long times and in highly non-equilibrium situations, offered by a fully dynamical number-conserving treatment.

Chapter 6: Self-consistent, number-conserving dynamical description

6.1 Introduction

In the preceding Chapter we discussed a wide range of theoretical descriptions which have been successfully applied to atomic BECs at finite temperatures. Among these descriptions, we identified the second-order number-conserving description of S. Gardiner and Morgan [68] as the most promising description of non-equilibrium dynamics involving both condensate and non-condensate at low temperature. This description's conservation of total atom number, preservation of orthogonality between condensate and non-condensate, and its full and consistent treatment of the anomalous average — which ensures that it successfully captures the phonon-like nature of excitations at low temperature — constitute its particular strengths in this area.

However, the only previous treatment of atomic BEC dynamics using this theory has been the calculation of finite-temperature excitation frequencies performed by Morgan [69–71]. While highly successful (see, for example, the comparison of theoretical descriptions in Ref. [50]) this calculation was restricted to the linear response regime. In this Chapter we outline the first fully-dynamical implementation of the second-order number-conserving equations of motion, which we subsequently apply, in the following Chapter, to the case of an initially-zero-temperature, quasi-1D atomic BEC driven by δ-kicks from an external potential.

We begin by introducing in detail the second-order, number-conserving description of the dynamics, which was briefly summarized in the previous Chapter (Section 5.3.4): In Section 6.2 we construct, via a number-conserving fluctuation expansion (Section 6.2.1) and consistent Gaussian fluctuation approximation (Section 6.2.2), the approximate cubic Hamiltonian upon which the second-order description is based. This Gaussian fluctuation approximation necessitates a Hartree-Fock factorization of third order terms; this is, however, consistent with the order of the description. In Section 6.3 we derive the second-order equations of motion (Sections 6.3.1 and 6.3.2), although we omit some details which can be found in Ref. [68] (the notation of which we largely adhere to). We then present a thorough

discussion of the validity of the necessary approximations and the resulting description at higher temperatures (Section 6.3.3). In particular, we discuss potential problems finding equilibrium initial conditions at higher temperatures. However, these problems are not critical for our purposes in this thesis, as we restrict our consideration to zero-temperature initial conditions and low depletion.

In Section 6.4 we develop a pseudospectral, split-step numerical method to compute the time evolution of the second-order equations of motion. This method is developed via a re-normalizing re-definition of the condensate mode (Section 6.4.1), expansion of the non-condensate equations of motion in terms of initially-equilibrium Bogoliubov quasiparticles (Section 6.4.2), and a recasting of the coupled equations for the condensate and quasiparticle modes into a matrix equation in a spinor superspace (Section 6.4.3). This re-casting of the equations exploits underlying symmetries between the condensate and non-condensate equations of motion, explicitly includes the projection terms which maintain orthogonality between the condensate and non-condensate, and is amenable to numerical treatment using a split-step method (Section 6.4.4).

6.2 Cubic Hamiltonian

6.2.1 Fluctuation expansion

As discussed in Section 5.3, we develop a number-conserving description by expanding the total Hamiltonian in terms of a suitable number-conserving fluctuation operator. To recap, the total Hamiltonian (in the contact potential approximation) is given by

$$\hat{H} = \int d\mathbf{r}\, \hat{\Psi}^{\dagger}(\mathbf{r}) \left[H_{\mathrm{sp}}(\mathbf{r}, t) + \frac{U_0}{2} \hat{\Psi}^{\dagger}(\mathbf{r}) \hat{\Psi}(\mathbf{r}) \right] \hat{\Psi}(\mathbf{r}) , \qquad (6.1)$$

[Eq. (1.9)]. We partition the field operator into a condensate mode $\phi_c(\mathbf{r}, t)$, as defined by Penrose and Onsager [173], and a non-condensate part $\delta\hat{\Psi}(\mathbf{r}, t)$ which is explicitly orthogonal to the condensate

$$\hat{\Psi}(\mathbf{r}) = \hat{a}_c(t)\phi_c(\mathbf{r}, t) + \delta\hat{\Psi}(\mathbf{r}, t) , \qquad (6.2)$$

(see Section 5.3.1). We then collect products of the number-conserving fluctuation operator $\tilde{\Lambda}(\mathbf{r}, t)$, defined by

$$\tilde{\Lambda}(\mathbf{r}, t) = \frac{1}{\sqrt{N_c(t)}} \hat{a}_c^{\dagger}(t)\delta\hat{\Psi}(\mathbf{r}, t) . \qquad (6.3)$$

In this choice of fluctuation operator we follow S. Gardiner and Morgan [68], as $\tilde{\Lambda}(\mathbf{r}, t)$ in particular avoids the need to consistently expand inverse-square-root number-operators when expanding the Hamiltonian (see Section 5.3.2).

We proceed by substituting Eq. (6.2) into the Hamiltonian Eq. (6.1) and collecting powers of $\tilde{\Lambda}$. For this purpose the identity

$$\hat{a}_c \frac{1}{\hat{a}_c} \frac{1}{\hat{a}_c^\dagger} \hat{a}_c^\dagger \equiv \hat{a}_c \frac{1}{\hat{N}_c} \hat{a}_c^\dagger \equiv 1 \,, \tag{6.4}$$

is particularly useful. Note that, in Eq. (6.4), we work with the inverse creation and annihilation operators of the form

$$\frac{1}{\hat{a}^\dagger} |n\rangle = \frac{1}{\sqrt{n}} |n-1\rangle \,, \tag{6.5}$$

$$\frac{1}{\hat{a}} |n\rangle = \frac{1}{\sqrt{n+1}} |n+1\rangle \,, \tag{6.6}$$

and an inverse number-operator of the form

$$\frac{1}{\hat{N}} |n\rangle = \frac{1}{n} |n\rangle = \frac{1}{\hat{a}} \frac{1}{\hat{a}^\dagger} |n\rangle \,. \tag{6.7}$$

This number-conserving expansion of the Hamiltonian yields $\hat{H} = \hat{H}_0 + \hat{H}_1 + \hat{H}_2 + \hat{H}_3 + \hat{H}_4$, where

$$\hat{H}_0 = N_c \int d\mathbf{r} \, \phi_c^*(\mathbf{r}) \frac{\hat{N}_c}{N_c} \left(H_{\text{sp}}(\mathbf{r}) + \frac{\tilde{U}}{2} \frac{\hat{N}_c - 1}{N_c} |\phi_c(\mathbf{r})|^2 \right) \phi_c(\mathbf{r}) \,, \tag{6.8}$$

$$\hat{H}_1 = \sqrt{N_c} \int d\mathbf{r} \left[\phi_c^*(\mathbf{r}) \left(H_{\text{sp}}(\mathbf{r}) + \tilde{U} \frac{\hat{N}_c - 1}{N_c} |\phi_c(\mathbf{r})|^2 \right) \tilde{\Lambda}(\mathbf{r}) + \text{h.c.} \right] \,, \tag{6.9}$$

$$\begin{aligned} \hat{H}_2 = \int d\mathbf{r} & \left[\tilde{\Lambda}^\dagger(\mathbf{r}) \left(H_{\text{sp}}(\mathbf{r}) + 2\tilde{U} \frac{\hat{N}_c - 1}{N_c} |\phi_c(\mathbf{r})|^2 \right) \frac{N_c}{\hat{N}_c} \tilde{\Lambda}(\mathbf{r}) \right. \\ & \left. + \frac{\tilde{U}}{2} \left(\phi_c^*(\mathbf{r})^2 \tilde{\Lambda}(\mathbf{r})^2 + \text{h.c.} \right) \right] \,, \end{aligned} \tag{6.10}$$

$$\hat{H}_3 = \frac{\tilde{U}}{\sqrt{N_c}} \int d\mathbf{r} \left[\tilde{\Lambda}^\dagger(\mathbf{r}) \frac{N_c}{\hat{N}_c} \tilde{\Lambda}(\mathbf{r})^2 \phi_c^*(\mathbf{r}) + \text{h.c.} \right] \,, \tag{6.11}$$

$$\hat{H}_4 = \frac{\tilde{U}}{2N_c} \int d\mathbf{r} \, \tilde{\Lambda}^\dagger(\mathbf{r})^2 \frac{N_c^2}{\hat{N}_c(\hat{N}_c - 1)} \tilde{\Lambda}(\mathbf{r})^2 \,. \tag{6.12}$$

Note that we have omitted temporal arguments (t) in Eqs. 6.8–6.12 for clarity. While we will in general retain spatial arguments in subsequent expressions, we will generally continue to omit temporal arguments for the same reason.

6.2.2 Reduction to cubic form and Gaussian approximation

While Eqs. 6.8–6.12 are grouped into powers of the fluctuation operators in a similar way to symmetry-breaking treatments, number-operator terms remain which must be consistently expanded in order to develop equations of motion. In order to obtain obtain final equations of motion to second-order in the non-condensate fluctuation operators it is necessary to consistently expand the Hamiltonian to cubic order in the same operators [68].

A consistent expansion of $\hat{N}_c$ in terms of $\tilde{\Lambda}(\mathbf{r})$ can be deduced from explicit number-conservation: formally, the number fluctuations of condensate and non-condensate must be equal and opposite. This requires that

$$\hat{N}_c = N_c + \int d\mathbf{r} \left[\left\langle \delta\hat{\Psi}^\dagger(\mathbf{r})\delta\hat{\Psi}(\mathbf{r}) \right\rangle - \delta\hat{\Psi}^\dagger(\mathbf{r})\delta\hat{\Psi}(\mathbf{r}) \right]. \tag{6.13}$$

Replacing $\delta\hat{\Psi}(\mathbf{r})$ with $\tilde{\Lambda}(\mathbf{r})$ yields

$$\hat{N}_c = N_c + \int d\mathbf{r} \left[\left\langle \tilde{\Lambda}^\dagger(\mathbf{r})\frac{N_c}{\hat{N}_c}\tilde{\Lambda}(\mathbf{r}) \right\rangle - \tilde{\Lambda}^\dagger(\mathbf{r})\frac{N_c}{\hat{N}_c}\tilde{\Lambda}(\mathbf{r}) \right]. \tag{6.14}$$

To obtain high-order expressions for $\hat{N}_c$ it would generally be necessary to expand $N_c/\hat{N}_c$ in powers of $\hat{N}_c/N_c - 1$ as

$$\frac{N_c}{\hat{N}_c} = \frac{1}{1 + (\hat{N}_c/N_c - 1)} = 1 - \left(\frac{\hat{N}_c}{N_c} - 1\right) + \left(\frac{\hat{N}_c}{N_c} - 1\right)^2 - \cdots . \tag{6.15}$$

However, noting that the first correction beyond $N_c/\hat{N}_c = 1$ would appear at quartic order in $\tilde{\Lambda}(\mathbf{r})$, for a consistent expansion of the Hamiltonian to cubic order the highest order expression for $\hat{N}_c$ we require is thus the quadratic expression obtained simply by setting $N_c/\hat{N}_c = 1$;

$$\hat{N}_c = N_c + \int d\mathbf{r} \left[\left\langle \tilde{\Lambda}^\dagger(\mathbf{r})\tilde{\Lambda}(\mathbf{r}) \right\rangle - \tilde{\Lambda}^\dagger(\mathbf{r})\tilde{\Lambda}(\mathbf{r}) \right]. \tag{6.16}$$

A consistent, third-order expansion of the Hamiltonian is then obtained by: (a) discarding $\hat{H}_4$; (b) substituting $\hat{N}_c = N_c$ in $\hat{H}_3$ and $\hat{H}_2$; (c) substituting Eq. (6.16) in $\hat{H}_1$ and $\hat{H}_0$; (d) discarding terms which are of quartic order in the fluctuation

operators, or of equivalent magnitude. This yields

$$
\begin{aligned}
\hat{H}^{(3)} =\ & N_c \int d\mathbf{r}\, \phi_c^*(\mathbf{r}) \left(H_{\mathrm{sp}}(\mathbf{r}) + \frac{\tilde{U}}{2}|\phi_c(\mathbf{r})|^2 \right) \phi_c(\mathbf{r}) \\
& + \sqrt{N_c} \int d\mathbf{r}\, \left[\phi_c^*(\mathbf{r}) \left(H_{\mathrm{sp}}(\mathbf{r}) + \tilde{U}|\phi_c(\mathbf{r})|^2 \right) \tilde{\Lambda}(\mathbf{r}) + \mathrm{h.c.} \right] - \frac{\tilde{U}}{2} \int d\mathbf{r}\, |\phi_c(\mathbf{r})|^4 \\
& + \iint d\mathbf{r}\, d\mathbf{r}'\, \phi_c^*(\mathbf{r}) \left(H_{\mathrm{sp}}(\mathbf{r}) + \tilde{U}|\phi_c(\mathbf{r})|^2 \right) \phi_c(\mathbf{r}) \left[\left\langle \tilde{\Lambda}^\dagger(\mathbf{r}')\tilde{\Lambda}(\mathbf{r}') \right\rangle - \tilde{\Lambda}^\dagger(\mathbf{r}')\tilde{\Lambda}(\mathbf{r}') \right] \\
& + \int d\mathbf{r}\, \tilde{\Lambda}^\dagger(\mathbf{r}) \left(H_{\mathrm{sp}}(\mathbf{r}) + 2\tilde{U}|\phi_c(\mathbf{r})|^2 \right) \tilde{\Lambda}(\mathbf{r}) + \frac{\tilde{U}}{2} \int d\mathbf{r}\, \left[\phi_c^*(\mathbf{r})^2 \tilde{\Lambda}(\mathbf{r})^2 + \mathrm{h.c} \right] \\
& - \frac{\tilde{U}}{\sqrt{N_c}} \int d\mathbf{r}\, \left[\phi_c^*(\mathbf{r})|\phi_c(\mathbf{r})|^2 \tilde{\Lambda}(\mathbf{r}) + \mathrm{h.c.} \right] \\
& + \frac{\tilde{U}}{\sqrt{N_c}} \iint d\mathbf{r}\, d\mathbf{r}'\, \left[\phi_c^*(\mathbf{r})|\phi_c(\mathbf{r})|^2 \left\{ \left\langle \tilde{\Lambda}^\dagger(\mathbf{r}')\tilde{\Lambda}(\mathbf{r}') \right\rangle - \tilde{\Lambda}^\dagger(\mathbf{r}')\tilde{\Lambda}(\mathbf{r}') \right\} \tilde{\Lambda}(\mathbf{r}) + \mathrm{h.c.} \right] \\
& + \frac{\tilde{U}}{\sqrt{N_c}} \int d\mathbf{r}\, \left[\tilde{\Lambda}^\dagger(\mathbf{r})\tilde{\Lambda}(\mathbf{r})^2 \phi_c^*(\mathbf{r}) + \mathrm{h.c.} \right] ,
\end{aligned}
\tag{6.17}
$$

where the terms are grouped in descending order of magnitude.

We wish to obtain, to second order in the fluctuation operators, a final equation of motion in closed form. However, terms appearing in the equation of motion, for example the explicit time dependence of $\tilde{\Lambda}(\mathbf{r})$, potentially introduce even higher-order products of fluctuation operators. To prevent this we work within a consistent Gaussian approximation [68]; that is, we require that in our final equations of motion all *quadratic* products of operators take the form of pair averages. This constitutes a Gaussian approximation in the sense that we assume that all higher-order moments of the fluctuation distribution can be described in terms of the variance [or in this case the variances $\left\langle \tilde{\Lambda}^\dagger(\mathbf{r})\tilde{\Lambda}(\mathbf{r}) \right\rangle$ and $\left\langle \tilde{\Lambda}^\dagger(\mathbf{r})\tilde{\Lambda}(\mathbf{r}) \right\rangle$] [295].

In order for this to be the case in the final equations of motion, we must approximate all cubic products of fluctuation operators appearing in $\hat{H}^{(3)}$ into products of single fluctuation operators multiplied by pair averages. This approximation is identical to the Hartree-Fock factorization of the cubic terms in the symmetry-breaking Hamiltonian in Section 5.2.2 [Eq. (5.7)]. Hence in $\hat{H}^{(3)}$ we make the replacement

$$
\tilde{\Lambda}^\dagger(\mathbf{r})\tilde{\Lambda}(\mathbf{r}')\tilde{\Lambda}(\mathbf{r}') \approx 2 \left\langle \tilde{\Lambda}^\dagger(\mathbf{r})\tilde{\Lambda}(\mathbf{r}') \right\rangle \tilde{\Lambda}(\mathbf{r}') + \left\langle \tilde{\Lambda}(\mathbf{r}')\tilde{\Lambda}(\mathbf{r}') \right\rangle \tilde{\Lambda}^\dagger(\mathbf{r}) ,
\tag{6.18}
$$

and so on, to obtain

$$
\begin{aligned}
\tilde{H}^{(3)} =& N_c \int d\mathbf{r}\, \phi_c^*(\mathbf{r}) \left(H_{\mathrm{sp}}(\mathbf{r}) + \frac{\tilde{U}}{2}|\phi_c(\mathbf{r})|^2 \right) \phi_c(\mathbf{r}) \\
&+ \sqrt{N_c} \int d\mathbf{r} \left[\phi_c^*(\mathbf{r}) \left(H_{\mathrm{sp}}(\mathbf{r}) + \tilde{U}|\phi_c(\mathbf{r})|^2 \right) \tilde{\Lambda}(\mathbf{r}) + \text{h.c.} \right] - \frac{\tilde{U}}{2} \int d\mathbf{r}\, |\phi_c(\mathbf{r})|^4 \\
&+ \iint d\mathbf{r}\, d\mathbf{r}'\, \phi_c^*(\mathbf{r}) \left(H_{\mathrm{sp}}(\mathbf{r}) + \tilde{U}|\phi_c(\mathbf{r})|^2 \right) \phi_c(\mathbf{r}) \left[\left\langle \tilde{\Lambda}^\dagger(\mathbf{r}')\tilde{\Lambda}(\mathbf{r}') \right\rangle - \tilde{\Lambda}^\dagger(\mathbf{r}')\tilde{\Lambda}(\mathbf{r}') \right] \\
&+ \int d\mathbf{r}\, \tilde{\Lambda}^\dagger(\mathbf{r}) \left(H_{\mathrm{sp}}(\mathbf{r},t) + 2\tilde{U}|\phi_c(\mathbf{r})|^2 \right) \tilde{\Lambda}(\mathbf{r}) + \frac{\tilde{U}}{2} \int d\mathbf{r} \left[\phi_c^*(\mathbf{r})^2 \tilde{\Lambda}(\mathbf{r})^2 + \text{h.c} \right] \\
&- \frac{\tilde{U}}{\sqrt{N_c}} \int d\mathbf{r} \left[\phi_c^*(\mathbf{r})|\phi_c(\mathbf{r})|^2 \tilde{\Lambda}(\mathbf{r}) + \text{h.c.} \right] \\
&- \frac{\tilde{U}}{\sqrt{N_c}} \iint d\mathbf{r}\, d\mathbf{r}'\, |\phi_c(\mathbf{r})|^2 \left[\phi_c^*(\mathbf{r}) \left\{ \left\langle \tilde{\Lambda}^\dagger(\mathbf{r}')\tilde{\Lambda}(\mathbf{r}) \right\rangle + \left\langle \tilde{\Lambda}(\mathbf{r}')\tilde{\Lambda}(\mathbf{r}) \right\rangle^* \right\} \tilde{\Lambda}(\mathbf{r}') + \text{h.c.} \right] \\
&+ \frac{\tilde{U}}{\sqrt{N_c}} \int d\mathbf{r} \left[\phi_c^*(\mathbf{r}) \left\{ 2 \left\langle \tilde{\Lambda}^\dagger(\mathbf{r})\tilde{\Lambda}(\mathbf{r}) \right\rangle + \left\langle \tilde{\Lambda}(\mathbf{r})^2 \right\rangle^* \right\} \tilde{\Lambda}(\mathbf{r}) + \text{h.c.} \right].
\end{aligned}
\tag{6.19}
$$

As we have already identified, this approximation of cubic terms is equivalent to that used in the Hartree-Fock-Bogoliubov approach. As discussed in detail in Section 5.2.2, this procedure potentially leads to an inconsistent treatment of interactions. However, as was explicitly demonstrated by Morgan in the development of his static number-conserving description, the primary problem with Hartree-Fock factorization of the cubic operator products is that it omits terms of cubic order in the fluctuation operators which are *larger* than quartic terms which are retained by the quartic Hartree-Fock factorization [Eq. (5.8)] of the quartic term [163, 281]. In the description presented here this inconsistency does not arise, since we have consistently neglected *all* quartic terms.

Hence, the Gaussian fluctuation approximation is internally consistent and leads to self-consistent equations of motion to quadratic order in the fluctuation operators. A feature of the resulting self-consistent equations of motion, as we shall see in the next Section (see also Section 5.3.4), is that the non-condensate is described by a MBdGE which does not contain pair averages of the non-condensate operators. This has the effect of making the identification of self-consistent initial conditions impossible at high temperatures. To extend the theory to these temperatures would require both (a) inclusion of quartic-order terms in the Hamiltonian and (b) relaxation of the Gaussian fluctuation approximation on the cubic terms in order to treat such terms consistently.

6.3 Equations of motion

6.3.1 Deduction of explicit time dependences

Coupled equations of motion for condensate and non-condensate to second order in the fluctuation operators can be deduced from the Heisenberg equation of motion for the fluctuation operator

$$i\hbar\frac{d}{dt}\tilde{\Lambda}(\mathbf{r}) = \left[\tilde{\Lambda}(\mathbf{r}), \tilde{H}^{(3)}\right] + i\hbar\frac{\partial}{\partial t}\tilde{\Lambda}(\mathbf{r}). \tag{6.20}$$

The explicit time derivative in Eq. (6.20) can be expanded as

$$i\hbar\frac{\partial}{\partial t}\tilde{\Lambda}(\mathbf{r}) = -i\hbar\frac{\partial N_c}{\partial t}\frac{1}{2N_c}\tilde{\Lambda}(\mathbf{r}) + \frac{1}{\sqrt{N_c}}i\hbar\frac{\partial \hat{a}_c^\dagger}{\partial t}\delta\hat{\Psi}(\mathbf{r}) + \frac{1}{\sqrt{N_c}}\hat{a}_c^\dagger i\hbar\frac{\partial}{\partial t}\delta\hat{\Psi}(\mathbf{r}). \tag{6.21}$$

Using the identities

$$i\hbar\frac{\partial N_c}{\partial t} = 0, \tag{6.22}$$

$$i\hbar\frac{\partial \hat{a}_c^\dagger}{\partial t} = \int d\mathbf{r}\,\hat{\Psi}^\dagger\left[i\hbar\frac{\partial \phi_c(\mathbf{r})}{\partial t}\right], \tag{6.23}$$

$$i\hbar\frac{\partial}{\partial t}\delta\hat{\Psi}(\mathbf{r}) = -\hat{a}_c\int d\mathbf{r}'\,Q(\mathbf{r},\mathbf{r}')\left[i\hbar\frac{\partial \phi_c(\mathbf{r}')}{\partial t}\right] - \phi(\mathbf{r})\int d\mathbf{r}'\left[i\hbar\frac{\partial \phi_c^*(\mathbf{r}')}{\partial t}\right]\delta\hat{\Psi}(\mathbf{r}'), \tag{6.24}$$

proved in Ref. [68], this reduces to

$$\begin{aligned}
i\hbar\frac{\partial}{\partial t}\tilde{\Lambda}(\mathbf{r}) = &-\frac{\hat{N}_c}{\sqrt{N_c}}\int d\mathbf{r}'\,Q(\mathbf{r},\mathbf{r}')\left[i\hbar\frac{\partial \phi_c(\mathbf{r}')}{\partial t}\right] - \phi_c(\mathbf{r})\int d\mathbf{r}'\left[i\hbar\frac{\partial \phi_c^*(\mathbf{r}')}{\partial t}\right]\tilde{\Lambda}(\mathbf{r}') \\
&+ \int d\mathbf{r}'\,\phi_c^*(\mathbf{r}')\left[i\hbar\frac{\partial \phi_c(\mathbf{r}')}{\partial t}\right]\tilde{\Lambda}(\mathbf{r}) \\
&+ \frac{1}{\sqrt{N_c}}\int d\mathbf{r}'\left[i\hbar\frac{\partial \phi_c(\mathbf{r}')}{\partial t}\right]\tilde{\Lambda}^\dagger(\mathbf{r}')\frac{N_c}{\hat{N}_c}\tilde{\Lambda}(\mathbf{r}).
\end{aligned} \tag{6.25}$$

As these terms will appear in the final equation of motion, to remain within the Gaussian fluctuation approximation of Section 6.2.2 it is necessary to remove all beyond-quadratic products of field operators, and consistently replace all quadratic products with their expectation values. Expanding the number-operators in this way

gives

$$
i\hbar\frac{\partial}{\partial t}\tilde{\Lambda}(\mathbf{r}) = -\sqrt{N_c}\int d\mathbf{r}'\left[Q(\mathbf{r},\mathbf{r}') - \frac{\left\langle\tilde{\Lambda}^\dagger(\mathbf{r}')\tilde{\Lambda}(\mathbf{r})\right\rangle}{N_c}\right]\left[i\hbar\frac{\partial\phi_c(\mathbf{r}')}{\partial t}\right]
$$
$$
- \phi_c(\mathbf{r})\int d\mathbf{r}'\left[i\hbar\frac{\partial\phi_c^*(\mathbf{r}')}{\partial t}\right]\tilde{\Lambda}(\mathbf{r}') + \int d\mathbf{r}'\,\phi_c^*(\mathbf{r}')\left[i\hbar\frac{\partial\phi_c(\mathbf{r}')}{\partial t}\right]\tilde{\Lambda}(\mathbf{r})\,.
$$

$$(6.26)$$

The commutator appearing in Eq. (6.20) will require evaluation of the commutator between two fluctuation operators, given exactly by

$$
\left[\tilde{\Lambda}(\mathbf{r}),\tilde{\Lambda}^\dagger(\mathbf{r}')\right] = \frac{\hat{N}_c}{N_c}Q(\mathbf{r},\mathbf{r}') - \frac{1}{N_c}\delta\hat{\Psi}^\dagger(\mathbf{r}')\delta\hat{\Psi}(\mathbf{r})\,. \tag{6.27}
$$

To the quadratic order of approximation we require, this reduces to [using Eq. (6.16)]

$$
\left[\tilde{\Lambda}(\mathbf{r}),\tilde{\Lambda}^\dagger(\mathbf{r}')\right] = Q(\mathbf{r},\mathbf{r}')\left[1 + \int d\mathbf{r}''\frac{\left\langle\tilde{\Lambda}^\dagger(\mathbf{r}'')\tilde{\Lambda}(\mathbf{r}'')\right\rangle - \tilde{\Lambda}^\dagger(\mathbf{r}'')\tilde{\Lambda}(\mathbf{r}'')}{N_c}\right] - \frac{\tilde{\Lambda}^\dagger(\mathbf{r}')\tilde{\Lambda}(\mathbf{r})}{N_c}\,, \tag{6.28}
$$

and enforcing the Gaussian fluctuation approximation reduces this further to

$$
\left[\tilde{\Lambda}(\mathbf{r}),\tilde{\Lambda}^\dagger(\mathbf{r}')\right] = Q(\mathbf{r},\mathbf{r}') - \frac{\left\langle\tilde{\Lambda}^\dagger(\mathbf{r}')\tilde{\Lambda}(\mathbf{r})\right\rangle}{N_c}\,. \tag{6.29}
$$

Equation (6.29) is the highest-order form of the commutator we require in order to deduce quadratic equations of motion. For second- and third-order terms in the cubic Hamiltonian $\tilde{H}^{(3)}$ a lower-order approximation to the commutator is appropriate to avoid higher-order terms appearing; this is given by

$$
\left[\tilde{\Lambda}(\mathbf{r}),\tilde{\Lambda}^\dagger(\mathbf{r}')\right] = Q(\mathbf{r},\mathbf{r}')\,. \tag{6.30}
$$

6.3.2   Deduction of equations of motion

We now expand the formal equation of motion for the fluctuation operator [Eq. (6.20)] using the appropriate approximation to the explicit time derivatve [Eq. (6.26)], and the full commutator with the Hamiltonian $\tilde{H}^{(3)}$, in which terms linear in the fluctuation operators are expanded using the quadratic approximate commutator of Eq. (6.29) and terms quadratic or cubic in the fluctuation operators are expanded

using the zero-order approximate commutator of Eq. (6.30). This produces

$$
\begin{aligned}
i\hbar \frac{d}{dt}\tilde{\Lambda}(\mathbf{r}) = \sqrt{N_c} \int d\mathbf{r}'\, Q(\mathbf{r},\mathbf{r}') &\Bigg(\Bigg\{ H_{\mathrm{sp}}(\mathbf{r}') + \tilde{U}\left[\left(1 - \frac{1}{N_c}\right)|\phi_c(\mathbf{r}')|^2 + 2\frac{\langle \tilde{\Lambda}^\dagger(\mathbf{r}')\tilde{\Lambda}(\mathbf{r}')\rangle}{N_c}\right] \\
&\quad - i\hbar\frac{\partial}{\partial t} \Bigg\} \phi_c(\mathbf{r}') + \tilde{U}\phi_c^*(\mathbf{r})\frac{\langle \tilde{\Lambda}(\mathbf{r}')^2\rangle}{N_c} \Bigg) \\
&- \frac{1}{\sqrt{N_c}} \int d\mathbf{r}' \Bigg\{ \langle \tilde{\Lambda}(\mathbf{r}')\tilde{\Lambda}(\mathbf{r})\rangle\left[H_{\mathrm{sp}}(\mathbf{r}') + 2\tilde{U}|\phi_c(\mathbf{r}')|^2 - i\hbar\frac{\partial}{\partial t}\right]\phi_c(\mathbf{r}') \\
&\quad - \tilde{U}\phi_c^*(\mathbf{r}')\langle \tilde{\Lambda}(\mathbf{r}')\tilde{\Lambda}(\mathbf{r})\rangle|\phi_c(\mathbf{r}')|^2 \Bigg\} \\
&+ \int d\mathbf{r}'\, Q(\mathbf{r},\mathbf{r}')\Big\{ \left[H_{\mathrm{sp}}(\mathbf{r}') + 2\tilde{U}|\phi(\mathbf{r}')|^2\right]\tilde{\Lambda}(\mathbf{r}') + \tilde{U}\tilde{\Lambda}^\dagger(\mathbf{r}')\phi_c(\mathbf{r}')^2 \Big\} \\
&- \phi_c(\mathbf{r}) \int d\mathbf{r}' \left[i\hbar\frac{\partial \phi_c^*(\mathbf{r}')}{\partial t}\right]\tilde{\Lambda}(\mathbf{r}') \\
&- \tilde{\Lambda}(\mathbf{r}) \int d\mathbf{r}'\, \phi_c^*(\mathbf{r}')\left[H_{\mathrm{sp}}(\mathbf{r}') + \tilde{U}|\phi_c(\mathbf{r}')|^2 - i\hbar\frac{\partial}{\partial t}\right]\phi_c(\mathbf{r}').
\end{aligned}
\tag{6.31}
$$

Taking the expectation value of this expression, and performing an iterative re-substitution in which beyond-quadratic terms are consistently eliminated [68] one obtains the number-conserving generalized GPE

$$
\begin{aligned}
i\hbar \frac{\partial \phi_c(\mathbf{r})}{\partial t} = &\left\{ H_{\mathrm{sp}}(\mathbf{r}) + \tilde{U}\left[\left(1 - \frac{1}{N_c}\right)|\phi_c(\mathbf{r})|^2 + 2\frac{\tilde{n}(\mathbf{r},\mathbf{r})}{N_c}\right] - \lambda_2 \right\}\phi_c(\mathbf{r}) \\
&+ \tilde{U}\phi_c^*(\mathbf{r})\frac{\tilde{m}(\mathbf{r},\mathbf{r})}{N_c} \\
&- \tilde{U}\int d\mathbf{r}'\, |\phi_c(\mathbf{r}')|^2 \left(\frac{\tilde{n}(\mathbf{r},\mathbf{r}')}{N_c}\phi_c(\mathbf{r}') + \phi_c^*(\mathbf{r}')\frac{\tilde{m}(\mathbf{r},\mathbf{r}')}{N_c}\right),
\end{aligned}
\tag{6.32}
$$

where we have re-introduced the normal and anomalous average notation introduced in Chapter 5 [Eqs. (5.9) and (5.10)], and the GGPE eigenvalue λ_2 is given by

$$
\begin{aligned}
\lambda_2 = \int d\mathbf{r}\, \phi_c^*(\mathbf{r})&\left\{ H_{\mathrm{sp}}(\mathbf{r}) + \tilde{U}\left[\left(1 - \frac{1}{N_c}\right)|\phi_c(\mathbf{r})|^2 + 2\frac{\tilde{n}(\mathbf{r},\mathbf{r})}{N_c}\right] - i\hbar\frac{\partial}{\partial t} \right\}\phi_c(\mathbf{r}) \\
&+ \tilde{U}\int d\mathbf{r}\, \phi_c^*(\mathbf{r})^2 \frac{\tilde{m}(\mathbf{r},\mathbf{r})}{N_c}.
\end{aligned}
\tag{6.33}
$$

To obtain consistent equations of motion for the non-condensate, to which the GGPE must be coupled, one can substitute Eq. (6.32) into Eq. (6.31) while neglect-

ing higher-order terms[1]. This yields the number-conserving modified Bogoliubov-de Gennes equations

$$i\hbar\frac{\partial}{\partial t}\left(\begin{array}{c} \tilde{\Lambda}(\mathbf{r}) \\ \tilde{\Lambda}^{\dagger}(\mathbf{r}) \end{array}\right) = \int d\mathbf{r}' \left(\begin{array}{cc} \mathcal{L}(\mathbf{r},\mathbf{r}') & \mathcal{M}(\mathbf{r},\mathbf{r}') \\ -\mathcal{M}^{*}(\mathbf{r},\mathbf{r}') & -\mathcal{L}^{*}(\mathbf{r},\mathbf{r}') \end{array}\right)\left(\begin{array}{c} \tilde{\Lambda}(\mathbf{r}') \\ \tilde{\Lambda}^{\dagger}(\mathbf{r}') \end{array}\right),\qquad(6.34)$$

where

$$\mathcal{L}(\mathbf{r},\mathbf{r}') = \delta(\mathbf{r}-\mathbf{r}')\left[H_{\mathrm{sp}}(\mathbf{r}') + \tilde{U}|\phi_{c}(\mathbf{r}')|^{2} - \lambda_{0}\right]$$
$$+ \int d\mathbf{r}''\,Q(\mathbf{r},\mathbf{r}'')\tilde{U}|\phi_{c}(\mathbf{r}'')|^{2}Q(\mathbf{r}'',\mathbf{r}'),\quad(6.35)$$

and

$$M(\mathbf{r},\mathbf{r}') = \int d\mathbf{r}''\,Q(\mathbf{r},\mathbf{r}'')\tilde{U}\phi(\mathbf{r}'')^{2}Q^{*}(\mathbf{r}'',\mathbf{r}')\,.\qquad(6.36)$$

These equations are equivalent to the previously stated number-conserving MBdGE [Eq. (5.59)]; the latter are obtained from Eq. (6.34) and its complex conjugate by an expansion in terms of Bogoliubov quasiparticles.

6.3.3 Discussion

The generalized Gross-Pitaevskii equation [Eq. (6.32)] and the modified Bogoliubov-de Gennes equations [Eq. (6.34)] complete the fully dynamical, second-order, and number-conserving description obtained by S. Gardiner and Morgan [68], and used within a linear response treatment by Morgan [69–71] (see Section 5.3.4). In this thesis, we develop these equations into a form where fully dynamical time evolution can be realized numerically. However, before we begin to outline our method for the simultaneous numerical solution of Eqs. (6.32) and (6.34), a few comments are in order.

Firstly it is important to note that, in contrast to the GPE eigenvalue λ_0 — which can be considered a low-order approximation to the chemical potential — λ_2 is a *complex* eigenvalue. The meaning of the imaginary part of λ_2 can be understood by considering the (implicit) time dependence of N_c, which is given (to quadratic

---

[1]Neglecting higher-order terms is, in fact, equivalent to substituting in the ordinary GPE [68].

order) by

$$
\begin{aligned}
i\hbar \frac{dN_c}{dt} &= i\hbar \frac{d}{dt}\left[N - \int d\mathbf{r}\, \left\langle \tilde{\Lambda}^\dagger(\mathbf{r})\tilde{\Lambda}(\mathbf{r})\right\rangle \right], \\
&= -\int d\mathbf{r}\, \left\{ \left\langle \tilde{\Lambda}^\dagger(\mathbf{r})\left[i\hbar \frac{d}{dt}\tilde{\Lambda}(\mathbf{r})\right]\right\rangle + \left\langle \left[i\hbar \frac{d}{dt}\tilde{\Lambda}^\dagger(\mathbf{r})\right]\tilde{\Lambda}(\mathbf{r})\right\rangle \right\}, \\
&= \tilde{U}\int d\mathbf{r}\, \left[\phi_c^*(\mathbf{r})^2 \tilde{m}(\mathbf{r},\mathbf{r}) - \tilde{m}^*(\mathbf{r},\mathbf{r})\phi_c(\mathbf{r})^2 \right], \\
&= (\lambda_2 - \lambda_2^*)N_c.
\end{aligned}
\tag{6.37}
$$

Thus, the imaginary part of λ_2 acts to keep the condensate mode $\phi_c(\mathbf{r})$ normalized to unity despite the growth or decay of the condensate population. This illustrates the presence of consistent number dynamics in the coupling between the GGPE and MBdGE, which constitutes a very desirable feature of this second-order description. In the first-order description (see Section 5.3.4) one obtains the same MBdGE coupled to the ordinary GPE: this combination manifestly does *not* lead to consistent number dynamics, because the condensate size is fixed while the non-condensate size is not. Indeed, the first-order description can only exhibit consistency when it is viewed as the limit of the second-order description as $N \to \infty$, in which the condensate constitutes an infinite atomic reservoir [68]. The zeroth-order description, consisting of the GPE alone, is trivially number-consistent, as it ignores the growth and decay of the condensate altogether. The number-dynamic consistency of the zero-, first-, and second-order descriptions are illustrated schematically in Fig. 6.1.

Secondly, we note that the terms $\mathcal{L}(\mathbf{r}, \mathbf{r}')$ appearing in the MBdGE consist only of an "ordinary" GPE Hamiltonian and the "ordinary" GPE eigenvalue, and that the terms $\mathcal{M}$ are also in no way altered from the first-order description. As has been previously stated (see Sections 5.2.2, 5.2.3, 5.3.4, and 6.2.2) this certainly appears inconsistent. In particular, for the MBdGE coupled to a solution of the zero-order ordinary GPE, $\phi_c^{(0)}(\mathbf{r})$, the eigenvalue λ_0 is well-defined, and the spinors $[\phi_c^{(0)}(\mathbf{r}), 0]^T$ and $[0, \phi_c^{(0)*}(\mathbf{r})]^T$ are exact, zero-energy solutions of the MBdGE. When coupled to a solution of the *generalized* GPE, $\phi_c^{(2)}(\mathbf{r})$, however, these properties are lost and any attempt to restore them by upgrading the MBdGE alone results in inconsistent number-dynamics.

This problem of the GGPE wavefunction $\phi_c^{(2)}(\mathbf{r})$ appearing in the MBdGE is particularly acute at high temperatures, where it eventually makes it impossible to find self-consistent equilibrium solutions to the second-order description. It can be viewed purely as a consequence of applying the theory outside of its regime of
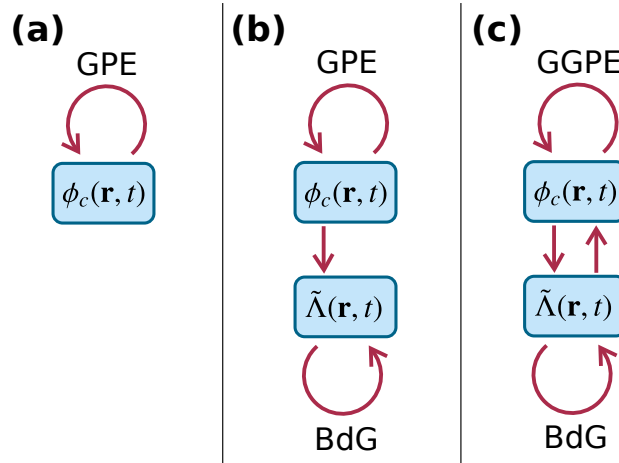
Figure 6.1: Schematic representation of the zeroth-, first-, and second-order number-conserving equations of motion. At zeroth order, (a), the non-condensate is ignored and the condensate mode $\phi_c(\mathbf{r})$ is described by the Gross-Pitaevskii equation (GPE) [Eq. (5.58)]. At first order, (b), the GPE is coupled to modified Bogoliubov-de Gennes equations (MBdGE) [Eq. (6.34)] for the non-condensate fluctuation operator $\tilde{\Lambda}(\mathbf{r})$. At this order, the evolution of $\tilde{\Lambda}(\mathbf{r})$ depends on the evolution of $\phi_c(\mathbf{r})$, but the converse is not true; this order of approximation can be interpreted as treating the condensate as an infinite atomic reservoir. At second order, (c), the non-condensate is again described by the MBdGE. However, the evolution of the condensate is now determined by the generalized Gross-Pitaevskii equation (GGPE) [Eq. (6.32)]; this pairing of equations produces fully self-consistent number dynamics.

validity. This problem was discussed in detail by Morgan [70] in his study of condensate excitations at finite-temperature [69–71]; in this work he demonstrated that the second-order description remains self-consistent at high temperatures provided one restricts oneself to a linear response treatment, in which a self-consistent equilibrium solution is not necessary. As we wish to give a fully dynamical treatment, and thus require a self-consistent equilibrium initial condition, we are thus restricted to low temperatures where such self-consistent solutions can be found.

6.4   Numerical implementation

6.4.1   Elimination of complex eigenvalue

In this Section we develop a pseudospectral split-step method for evolving the combined GGPE and MBdGE system. In order to do so, it is of great convenience to eliminate the imaginary part of the GGPE eigenvalue λ_2 [Eq. (6.33)] by describing the condensate by a mode function normalized to the condensate population N_c. Hence, we define

$$\psi(\mathbf{r}) = \sqrt{N_c}\phi_c(\mathbf{r}), \tag{6.38}$$

in terms of which the GGPE can be written [using Eq. (6.37)] as

$$
\begin{aligned}
i\hbar\frac{\partial\psi(\mathbf{r})}{\partial t} &= \Big[H_{\mathrm{sp}}(\mathbf{r}) + U_0|\psi(\mathbf{r})|^2 - \lambda_2\Big]\psi(\mathbf{r}) + U_0\left[\tilde{n}(\mathbf{r},\mathbf{r}) - \frac{|\psi(\mathbf{r})|^2}{N_c}\right]\psi(\mathbf{r}) \\
&\quad + U_0\tilde{n}(\mathbf{r},\mathbf{r})\psi(\mathbf{r}) - \frac{U_0}{N_c}\int d\mathbf{r}'\,\psi(\mathbf{r}')|\psi(\mathbf{r}')|^2\tilde{n}(\mathbf{r},\mathbf{r}') \\
&\quad + U_0\tilde{m}(\mathbf{r},\mathbf{r})\psi^*(\mathbf{r}) - \frac{U_0}{N_c}\int d\mathbf{r}'\,\psi^*(\mathbf{r}')|\psi(\mathbf{r}')|^2\tilde{m}(\mathbf{r},\mathbf{r}')\,,
\end{aligned}
\tag{6.39}
$$

and the MBdGE as

$$
\begin{aligned}
i\hbar\frac{\partial}{\partial t}\tilde{\Lambda}(\mathbf{r}) &= \Big[H_{\mathrm{sp}}(\mathbf{r}) + U_0|\psi(\mathbf{r})|^2 - \lambda_0\Big]\tilde{\Lambda}(\mathbf{r}) \\
&\quad + U_0|\psi(\mathbf{r})|^2\tilde{\Lambda}(\mathbf{r}) - \frac{U_0}{N_c}\int d\mathbf{r}'\,\psi^*(\mathbf{r}')|\psi(\mathbf{r}')|^2\tilde{\Lambda}(\mathbf{r}')\psi(\mathbf{r}) \\
&\quad + U_0\psi(\mathbf{r})^2\tilde{\Lambda}^{\dagger}(\mathbf{r}) - \frac{U_0}{N_c}\int d\mathbf{r}'\,\psi(\mathbf{r}')|\psi(\mathbf{r}')|^2\tilde{\Lambda}^{\dagger}(\mathbf{r}')\psi(\mathbf{r})\,.
\end{aligned}
\tag{6.40}
$$

Here, we have chosen to write the equations in a form which emphasises the significant structural analogies between the GGPE and the MBdGE. The eigenvalues appearing in these equations are (1) the "GPE eigenvalue" λ_0:

$$\lambda_0 = \frac{1}{N_c}\int d\mathbf{r}\,\psi^*(\mathbf{r})[H_{\mathrm{sp}}(\mathbf{r}) + U_0|\psi(\mathbf{r})|^2]\psi(\mathbf{r})\,, \tag{6.41}$$

and (2) the adjusted "GGPE eigenvalue":

$$
\begin{aligned}
\lambda_2 \equiv \lambda_0 + \lambda' = \lambda_0 &+ \frac{U_0}{N_c}\int d\mathbf{r}\,\psi^*(\mathbf{r})\left[2\tilde{n}(\mathbf{r},\mathbf{r}) - \frac{1}{N_c}|\psi(\mathbf{r})|^2\right]\psi(\mathbf{r}) \\
&+ \frac{U_0}{2N_c}\left[\psi(\mathbf{r})^{*2}\tilde{m}(\mathbf{r},\mathbf{r}) + \psi(\mathbf{r})^2\tilde{m}^*(\mathbf{r},\mathbf{r})\right].
\end{aligned}
\tag{6.42}
$$

Both these eigenvalues are now explicitly real.

6.4.2   Quasiparticle decomposition at $T = 0$

Assuming we start at thermal and dynamical equilibrium, we can use the Bogoliubov quasiparticle decomposition of the non-condensate introduced previously

$$\begin{pmatrix} \tilde{\Lambda}(\mathbf{r}) \\ \tilde{\Lambda}^{\dagger}(\mathbf{r}) \end{pmatrix} = \sum_k \tilde{b}_k \begin{pmatrix} u_k(\mathbf{r}) \\ v_k(\mathbf{r}) \end{pmatrix} + \sum_k \tilde{b}_k^{\dagger} \begin{pmatrix} v_k^*(\mathbf{r}) \\ u_k^*(\mathbf{r}) \end{pmatrix}. \tag{6.43}$$

Assuming all time-dependence to reside in the mode functions $u_k(\mathbf{r})$ and $v_k(\mathbf{r})$, with the quasiparticle creation and annihilation operators $\tilde{b}_k^{\dagger}$ and $\tilde{b}_k$ time-independent, the MBdGE take the form

$$\begin{aligned} i\hbar \frac{\partial}{\partial t} u_k(\mathbf{r}) = &\left[H_{\mathrm{sp}}(\mathbf{r}) + U_0 |\psi(\mathbf{r})|^2 - \lambda_0 \right] u_k(\mathbf{r}) \\ &+ U_0 |\psi(\mathbf{r})|^2 u_k(\mathbf{r}) - \frac{U_0}{N_c} \int d\mathbf{r}' \, \psi^*(\mathbf{r}') |\psi(\mathbf{r}')|^2 u_k(\mathbf{r}') \psi(\mathbf{r}) \\ &+ U_0 \psi(\mathbf{r})^2 v_k(\mathbf{r}) - \frac{U_0}{N_c} \int d\mathbf{r}' \, \psi(\mathbf{r}') |\psi(\mathbf{r}')|^2 v_k(\mathbf{r}') \psi(\mathbf{r}), \end{aligned} \tag{6.44}$$

and

$$\begin{aligned} i\hbar \frac{\partial}{\partial t} v_k^*(\mathbf{r}) = &\left[H_{\mathrm{sp}}(\mathbf{r}) + U_0 |\psi(\mathbf{r})|^2 - \lambda_0 \right] v_k^*(\mathbf{r}) \\ &+ U_0 |\psi(\mathbf{r})|^2 v_k^*(\mathbf{r}) - \frac{U_0}{N_c} \int d\mathbf{r}' \, \psi^*(\mathbf{r}') |\psi(\mathbf{r}')|^2 v_k^*(\mathbf{r}') \psi(\mathbf{r}) \\ &+ U_0 \psi(\mathbf{r})^2 u_k^*(\mathbf{r}) - \frac{U_0}{N_c} \int d\mathbf{r}' \, \psi(\mathbf{r}') |\psi(\mathbf{r}')|^2 u_k^*(\mathbf{r}') \psi(\mathbf{r}). \end{aligned} \tag{6.45}$$

Assuming the following pair averages for the quasiparticle creation and annihilation operators [see Eq. (5.16)];

$$\left\langle \hat{b}_k^{\dagger} \hat{b}_l \right\rangle = \delta_{kl} N_k = \delta_{kl} \left(e^{(\epsilon_k - \mu)/k_{\mathrm{B}}T} - 1 \right)^{-1}, \tag{6.46}$$

$$\left\langle \hat{b}_k \hat{b}_l \right\rangle = \left\langle \hat{b}_k^{\dagger} \hat{b}_l^{\dagger} \right\rangle = 0, \tag{6.47}$$

we obtain quasiparticle expressions for the non-condensate density matrix and anomalous average [see Eqs. (5.18) and (5.19)]

$$\tilde{n}(\mathbf{r}, \mathbf{r}') = \sum_k N_k u_k(\mathbf{r}) u_k^*(\mathbf{r}') + \sum_k (N_k + 1) v_k^*(\mathbf{r}) v_k(\mathbf{r}'), \tag{6.48}$$

$$\tilde{m}(\mathbf{r}, \mathbf{r}') = \sum_k N_k u_k(\mathbf{r}) v_k^*(\mathbf{r}') + \sum_k (N_k + 1) v_k^*(\mathbf{r}) u_k(\mathbf{r}'). \tag{6.49}$$

In the above we have implicitly assumed the quasiparticles to have bosonic com-

mutation relations; in reality this is only approximately true due to the definition of $\tilde{\Lambda}(\mathbf{r})$ (see Section 5.3.2). While it is hard to comment on the general validity of this assumption [79] we note that Morgan's work at finite temperature [69–71] does not seem to be affected by this assumption, and that to the (quadratic) order of approximation we have considered, using the alternative fluctuation operator $\hat{\Lambda}_c(\mathbf{r})$ (Section 5.3.2), which does produce bosonic quasiparticles, ultimately yields the same results [68]. Therefore, certainly for the zero-temperature initial conditions we study, the issue of exact quasiparticle commutation relations can be neglected.

Starting at $T = 0$ Eqs. (6.48) and (6.49) become

$$\tilde{n}(\mathbf{r}, \mathbf{r}') = \sum_k v_k^*(\mathbf{r}, t) v_k(\mathbf{r}', t), \tag{6.50}$$

$$\tilde{m}(\mathbf{r}, \mathbf{r}') = \sum_k v_k^*(\mathbf{r}, t) u_k(\mathbf{r}', t), \tag{6.51}$$

$$\tag{6.52}$$

yielding for the diagonal terms in particular

$$\tilde{n}(\mathbf{r}, \mathbf{r}) = \sum_k |v_k(\mathbf{r}, t)|^2, \tag{6.53}$$

$$\tilde{m}(\mathbf{r}, \mathbf{r}) = \sum_k u_k(\mathbf{r}, t) v_k^*(\mathbf{r}, t). \tag{6.54}$$

$$\tag{6.55}$$

Using these relations we proceed, in the next Section, to re-cast the GGPE in terms of the quasiparticle mode functions, and re-cast the combined GGPE and MBdGE in the final form which we will use to conduct a simultaneous numerical solution.

6.4.3 Re-casting of equations

The primary difficultly in working with the coupled GGPE-MBdGE system is the problem of orthogonalization: *both* equations contain terms which function to maintain orthogonality between the condensate and non-condensate. This is in contrast to the case of the first-order GPE-MBdGE system, where the GPE evolves in isolation from the MBdGE; in this first-order system the evolution of the MBdGE can be computed by *ignoring* the projector terms throughout the evolution and simply applying them at the end (see Section 5.3.4 and Ref. [309]). If one were to similarly ignore the projectors during the evolution of the second-order GGPE-MBdGE system one would then have to re-orthogonalize both the condensate and quasiparticle

modes with respect to an *unknown* basis at the end of the evolution. Consequently, the projection terms must be explicitly included in any evolution scheme. In this Section we develop such a scheme, by re-casting the GGPE and MBdGE in a form which exploits their apparent symmetries, and allows us to include the projection terms within a split-step method that can be implemented numerically.

After substituting the $T = 0$ expressions for the non-condensate density and anomalous average [Eqs. (6.50) and (6.51)] into the GGPE [Eq. (6.39)], the GGPE and MBdGE can be recast in the form

$$i\hbar\frac{\partial\psi(\mathbf{r})}{\partial t} = [H_{\text{GP}}(\mathbf{r}) + B(\mathbf{r})]\,\psi(\mathbf{r}) + \sum_k A_k(\mathbf{r})v_k^*(\mathbf{r})\,, \tag{6.56}$$

$$i\hbar\frac{\partial u_k(\mathbf{r})}{\partial t} = H_{\text{GP}}(\mathbf{r})u_k(\mathbf{r}) + A_k(\mathbf{r})\psi(\mathbf{r})\,, \tag{6.57}$$

$$i\hbar\frac{\partial v_k^*(\mathbf{r})}{\partial t} = H_{\text{GP}}(\mathbf{r})v_k^*(\mathbf{r}) + A_k^*(\mathbf{r})\psi(\mathbf{r})\,, \tag{6.58}$$

where

$$H_{\text{GP}}(\mathbf{r}) = H_{\text{sp}}(\mathbf{r}) + U_0|\psi(\mathbf{r})|^2 - \lambda_0\,, \tag{6.59}$$

$$B(\mathbf{r}) = U_0\left[\sum_k |v_k(\mathbf{r})|^2 - \frac{|\psi(\mathbf{r})|^2}{N_c}\right] - \lambda'\,, \tag{6.60}$$

$$A_k(\mathbf{r}) = U_0\left[v_k(\mathbf{r})\psi(\mathbf{r}) + u_k(\mathbf{r})\psi^*(\mathbf{r}) - I_k\right]\,, \tag{6.61}$$

$$I_k = \frac{1}{N_c}\int d\mathbf{r}\,\left[v_k(\mathbf{r})\psi(\mathbf{r}) + u_k(\mathbf{r})\psi^*(\mathbf{r})\right]|\psi(\mathbf{r})|^2\,. \tag{6.62}$$

This reformulation of the problem allows one to write the coupled evolution of the condensate wavefunction and the first M quasiparticle modes as a nonlinear matrix equation in a $2M + 1$-dimensional spinor space:

$$i\hbar\frac{\partial}{\partial t}\zeta(\mathbf{r}) = \Gamma(\mathbf{r})\zeta(\mathbf{r})\,. \tag{6.63}$$

Here the vector $\zeta(\mathbf{r})$ is defined by

$$\zeta(\mathbf{r}) = \left[\psi(\mathbf{r}), v_1^*(\mathbf{r}), v_2^*(\mathbf{r}), \ldots, v_M^*(\mathbf{r}), u_1(\mathbf{r}), u_2(\mathbf{r}), \ldots, u_M(\mathbf{r})\right]^T\,, \tag{6.64}$$

and the operator $\Gamma(\mathbf{r})$ is defined by

$$
\Gamma(\mathbf{r}) = \begin{pmatrix}
H_{\mathrm{GP}} + B & A_1 & A_2 & \ldots & A_M & 0 & 0 & \cdots & 0 \\
A_1^* & H_{\mathrm{GP}} & 0 & \cdots & 0 & 0 & 0 & \cdots & 0 \\
A_2^* & 0 & H_{\mathrm{GP}} & \cdots & 0 & 0 & 0 & \cdots & 0 \\
\vdots & \vdots & \vdots & \ddots & \vdots & 0 & 0 & \cdots & 0 \\
A_M^* & 0 & 0 & \cdots & H_{\mathrm{GP}} & 0 & 0 & \cdots & 0 \\
A_1 & 0 & 0 & \cdots & 0 & H_{\mathrm{GP}} & 0 & \cdots & 0 \\
A_2 & 0 & 0 & \cdots & 0 & 0 & H_{\mathrm{GP}} & \cdots & 0 \\
\vdots & \vdots & \vdots & \vdots & \vdots & \vdots & \vdots & \ddots & \vdots \\
A_M & 0 & 0 & \cdots & 0 & 0 & 0 & \cdots & H_{\mathrm{GP}}
\end{pmatrix}, \quad (6.65)
$$

where we have omitted the position argument $(\mathbf{r})$ of all terms for clarity. In any actual calculation, this spinor space is rendered finite-dimensional by the need for a finite quasiparticle momentum cut-off M. Consequently, all subsequent summations over quasiparticle index k appearing in this Chapter should be taken to run from 1 to M.

As we have already accounted for all creation and annihilation operators through the quasiparticle decomposition, each entry in the matrix defining Γ can be thought of as an operator in the first-quantized sense[2]. From an analytic perspective, this notation seems to achieve little more than 'tidying' — abstracting away much of the detail. Importantly, however, all the operators which are off-diagonal in the spinor space [the operators $A_k(\mathbf{r})$] are diagonal in the position representation (they multiply by a spatially-varying function). In contrast, all the operators which have off-diagonal components in the position representation [that is, the kinetic energy operator implicitly contained in $H_{\mathrm{sp}}(\mathbf{r})$ and hence in $H_{\mathrm{GP}}(\mathbf{r})$] appear only on the diagonal in the spinor space.

From a numerical perspective this property is extremely useful, as it makes the evolution amenable to a split-step approximation (see Appendix B). This is achieved by splitting $\Gamma(\mathbf{r})$ into the sum of a term due to linear parts of the evolution, $\Gamma_{\mathrm{L}}(\mathbf{r})$, and a term representing nonlinear parts of the evolution, $\Gamma_{\mathrm{N}}(\mathbf{r})$. These are defined

---

[2]That is, an operator which could appear on the right side of a single-particle Schrödinger equation.

by

$$\Gamma_{\rm L} = \begin{pmatrix} H_{\rm L} & 0 & \cdots & 0 \\ 0 & H_{\rm L} & \cdots & \vdots \\ \vdots & \vdots & \ddots & 0 \\ 0 & \cdots & 0 & H_{\rm L} \end{pmatrix}, \tag{6.66}$$

and

$$\Gamma_{\rm N} = \begin{pmatrix} H_{\rm N}+B & A_1 & A_2 & \ldots & A_M & 0 & 0 & \cdots & 0 \\ A_1^* & H_{\rm N} & 0 & \cdots & 0 & 0 & 0 & \cdots & 0 \\ A_2^* & 0 & H_{\rm N} & \cdots & 0 & 0 & 0 & \cdots & 0 \\ \vdots & \vdots & \vdots & \ddots & \vdots & 0 & 0 & \cdots & 0 \\ A_M^* & 0 & 0 & \cdots & H_{\rm N} & 0 & 0 & \cdots & 0 \\ A_1 & 0 & 0 & \cdots & 0 & H_{\rm N} & 0 & \cdots & 0 \\ A_2 & 0 & 0 & \cdots & 0 & 0 & H_{\rm N} & \cdots & 0 \\ \vdots & \vdots & \vdots & \vdots & \vdots & \vdots & \vdots & \ddots & \vdots \\ A_M & 0 & 0 & \cdots & 0 & 0 & 0 & \cdots & H_{\rm N} \end{pmatrix}, \tag{6.67}$$

where we have also defined

$$H_{\rm L}(\mathbf{r}) = H_{\rm sp}(\mathbf{r}) - \lambda_0, \tag{6.68}$$

and

$$H_{\rm N}(\mathbf{r}) = H_{\rm GP}(\mathbf{r}) - H_{\rm L}(\mathbf{r}) = U_0|\psi(\mathbf{r})|^2. \tag{6.69}$$

We re-iterate at this point that all terms appearing in Γ_L and Γ_N are implicitly position-dependent, but this is omitted for clarity in all matrix-form expressions.

Written in this form, Γ_L contains all kinetic energy terms; while these terms are not diagonal in the position representation, they do all lie on the diagonal in the spinor space. Consequently, the evolution due to the kinetic energy terms can be computed for each mode function separately. In contrast, while Γ_N does contain off-diagonal elements in the spinor space, each element of Γ_N is diagonal in the position representation. Consequently, the evolution due to these terms can be computed straightforwardly over a discrete spatial grid.

6.4.4   Split-step evolution

In the spinor space, the split-step approximation for the evolution of the system over short times δt is given by

$$\zeta(\mathbf{r}, t + \delta t) = e^{-i\Gamma(\mathbf{r})\delta t/\hbar}\zeta(\mathbf{r}, t) \approx e^{-i\Gamma_{\mathrm{N}}(\mathbf{r})\delta t/2\hbar}e^{-i\Gamma_{\mathrm{L}}(\mathbf{r})\delta t/\hbar}e^{-i\Gamma_{\mathrm{N}}(\mathbf{r})\delta t/\hbar}\zeta(\mathbf{r}, t), \qquad (6.70)$$

where each of the three evolution operators on the right is assumed to act instantaneously, and the symmetrization reduces the error to the order of δt^3 (see Appendix B). Since Γ_{L} is diagonal in the spinor space, we have

$$e^{-i\Gamma_{\mathrm{L}}\delta t/\hbar} = \begin{pmatrix} e^{-iH_{\mathrm{L}}\delta t/\hbar} & 0 & \cdots & 0 \\ 0 & e^{-iH_{\mathrm{L}}\delta t/\hbar} & \cdots & \vdots \\ \vdots & \vdots & \ddots & 0 \\ 0 & \cdots & 0 & e^{-iH_{\mathrm{L}}\delta t/\hbar} \end{pmatrix}. \qquad (6.71)$$

Numerically, this can easily be implemented using a pseudospectral method, in which one works with a discrete representation of each of the mode functions [$\psi(\mathbf{r})$, $u_k(\mathbf{r})$, etc.] on a suitable pseudospectral grid determined by the eigenfunctions of $H_{\mathrm{L}}(\mathbf{r})$. With respect to this discrete representation a matrix operator for $e^{-iH_{\mathrm{L}}\delta t/\hbar}$ can be constructed, and applied to each mode function individually (see Appendix B).

The operator Γ_{N} is more problematic because it is not diagonal in the spinor space, and because of the orthogonalization terms it contains. However, each of its entries *is* diagonal in the position representation, meaning we only need exponentiate Γ_{N} in the spinor space in order to obtain an operator we can evaluate and use for short-time propagation: such an operator — in distinct contrast to $e^{-i\Gamma_{\mathrm{L}}\delta t/\hbar}$ which consists of an application of $e^{-iH_{\mathrm{L}}\delta t/\hbar}$ to each mode *individually* — *couples* the mode functions by acting on *all modes at once*. The advantage of such an operator is that it almost entirely[3] overcomes the orthogonalization problem inherent in any uncoupled treatment of the modes.

The evolution due to the term $e^{-i\Gamma_{\mathrm{N}}\delta t/\hbar}$ can be obtained by considering the matrices $\tilde{\Gamma}_{\mathrm{N}}^{(M)}$, which we define to be $2M + 1$-dimensional matrices of complex numbers which share the structure of Γ_{N}; that is, they are defined by an expression equivalent

---

[3]A correction for numerical round-off error is still required in order to preserve orthogonality over long times, which can be achieved by explicitly orthogonalizing the quasiparticle modes with respect to the condensate. Our experience of this correction is that applying it after every timestep does not cause decay of the total atom number, indicating that it does indeed operate only at the level of machine precision (see Chapter 7).

to Eq. (6.67) but with the diagonal matrices A_k, A_k^* etc. replaced with complex coefficients representing the actual values of the functions $A_k(\mathbf{r})$, $A_k^*(\mathbf{r})$ etc. at a *specific* value of $\mathbf{r}$. Within a numerical calculation, these matrices inhabit the $2M + 1$-dimensional spinor space *only*, with one such matrix for every spatial grid point in $\mathbf{r}$. At each individual grid point, the evolution due to $e^{-i\Gamma_\mathrm{N}\delta t/\hbar}$ is thus produced by the action of $e^{-i\tilde{\Gamma}_\mathrm{N}^{(M)}\delta t/\hbar}$ within the spinor space.

One could proceed by numerically diagonalizing, and thence exponentiating, $\tilde{\Gamma}_\mathrm{N}^{(M)}$ for each spatial grid point in turn. However, because the *structure* of $\tilde{\Gamma}_\mathrm{N}^{(M)}$ is independent of $\mathbf{r}$, one can avoid the high computational cost of numerical diagonalization by finding an analytic form for $e^{-i\tilde{\Gamma}_\mathrm{N}^{(M)}\delta t/\hbar}$. In principle, this only needs to be done for the specific number of quasiparticle modes M one wishes to propagate. The actual analytic calculation of $e^{-i\tilde{\Gamma}_\mathrm{N}^{(M)}\delta t/\hbar}$ for specific M is best left to a computer algebra system (e.g., Wolfram Mathematica [337]). However, for all $M > 2$ we have observed that the results can be written in the general form

$$e^{-i\Gamma_\mathrm{N}\delta t/\hbar} =$$

$$\begin{pmatrix}
T_{\cos} - BT_{\sin}/2 & -A_1 T_{\sin} & -A_2 T_{\sin} & \ldots & -A_M T_{\sin} & 0 & \cdots & 0 \\
-A_1^* T_{\sin} & A_1 A_1^* T_{\mathrm{mix}} & A_2 A_1^* T_{\mathrm{mix}} & \cdots & A_M A_1^* T_{\mathrm{mix}} & 0 & \cdots & 0 \\
-A_2^* T_{\sin} & A_1 A_2^* T_{\mathrm{mix}} & A_2 A_2^* T_{\mathrm{mix}} & \cdots & A_M A_2^* T_{\mathrm{mix}} & 0 & \cdots & 0 \\
\vdots & \vdots & \vdots & \ddots & \vdots & 0 & \cdots & 0 \\
-A_M^* T_{\sin} & A_1 A_M^* T_{\mathrm{mix}} & A_2 A_M^* T_{\mathrm{mix}} & \cdots & A_M A_M^* T_{\mathrm{mix}} & 0 & \cdots & 0 \\
-A_1 T_{\sin} & A_1 A_1 T_{\mathrm{mix}} & A_2 A_1 T_{\mathrm{mix}} & \cdots & A_M A_1 T_{\mathrm{mix}} & 0 & \cdots & 0 \\
-A_2 T_{\sin} & A_1 A_2 T_{\mathrm{mix}} & A_2 A_2 T_{\mathrm{mix}} & \cdots & A_M A_2 T_{\mathrm{mix}} & 0 & \cdots & 0 \\
\vdots & \vdots & \vdots & \vdots & \vdots & \vdots & \ddots & \vdots \\
-A_M T_{\sin} & A_1 A_M T_{\mathrm{mix}} & A_2 A_M T_{\mathrm{mix}} & \cdots & A_M A_M T_{\mathrm{mix}} & 0 & \cdots & 0
\end{pmatrix}$$

$$+ \begin{pmatrix}
0 & 0 & \cdots & 0 \\
0 & T_{\exp} & \cdots & 0 \\
\vdots & \vdots & \ddots & \vdots \\
0 & 0 & \cdots & T_{\exp}
\end{pmatrix}, \quad (6.72)$$

where

$$T_{\exp} = e^{-iH_N \delta t/\hbar} \,, \tag{6.73}$$

$$T_{\cos} = e^{-i(H_N+B/2)\delta t/\hbar} \cos\left(\frac{\sqrt{B^2 + 4\sum_k |A_k|^2}\,\delta t}{2\hbar} \right), \tag{6.74}$$

$$T_{\sin} = \frac{2ie^{-i(H_N+B/2)\delta t/\hbar}}{\sqrt{B^2 + 4\sum_k |A_k|^2}} \sin\left(\frac{\sqrt{B^2 + 4\sum_k |A_k|^2}\,\delta t}{2\hbar} \right), \tag{6.75}$$

$$T_{\min} = \frac{T_{\cos} + T_{\sin}B/2 - T_{\exp}}{\sum_k |A_k|^2} \,. \tag{6.76}$$

At any specific point $\mathbf{r}$ on the computational grid, the expression Eq. (6.72) allows one to compute the time evolution due to Γ_N immediately after evaluating the functions $A_k(\mathbf{r})$ etc. at that specific point. Note, however, that these functions themselves can only be computed at an individual grid point once the necessary non-local integrals have been numerically evaluated over the entire grid. The resulting time evolution can be succinctly expressed as $2M + 1$ coupled equations:

$$\psi(t + \delta t) = \left(T_{\cos} - \frac{BT_{\sin}}{2} \right)\psi(t) - T_{\sin}\sum_k A_k v_k^*(t), \tag{6.77}$$

$$v_k^*(t + \delta t) = -A_k^* T_{\sin}\psi(t) + T_{\exp}v_k^*(t) + T_{\min}\sum_j A_k^* A_j v_j^*(t), \tag{6.78}$$

$$u_k(t + \delta t) = -A_k T_{\sin}\psi(t) + T_{\exp}u_k(t) + T_{\min}\sum_j A_k A_j v_j^*(t). \tag{6.79}$$

Applying these coupled equations separately at each value of $\mathbf{r}$ on the appropriate computational grid then reproduces exactly the action of $e^{-i\Gamma_N \delta t/\hbar}$, as desired. In the next Chapter we consider, in detail, a specific application of this method to a test system: a quasi-1D, periodic, δ-kicked atomic BEC, which constitutes a BEC analogue of the well-known quantum kicked-rotor.

Chapter 7: Coherence and instability in a driven Bose-Einstein condensate

7.1   Introduction

In this Chapter we apply the split step numerical method for evolving the second-order, number-conserving equations of motion, developed in Chapter 6 and consisting of coupled GGPE and MBdGE, to a test system: the δ-kicked-rotor-BEC. This system consists of a quasi-1D, toroidally trapped atomic BEC driven by periodic δ-kicks from a spatially-varying potential of sinusoidal form. In contrast to first-order descriptions, which predict rapid, unbounded growth of the non-condensate in resonant parameter regimes, the consistent treatment of condensate depletion in our fully-time-dependent, second-order description acts to damp this growth, leading to oscillations in the (non-)condensate population and the coherence of the system. Although our description leads to different dynamics around resonant parameter regimes, these regimes occur where the GPE predicts them. Furthermore, our description retains some, but not all, of the features of the dynamics predicted by the GPE.

We begin by introducing the δ-kicked-rotor-BEC (Section 7.2), which constitutes a generalization to the interacting case of the atom-optical kicked rotor. We discuss previous work on the system, using both the GPE and the first-order number-conserving description of GPE plus MBdGE. In Section 7.3 we outline our second-order description of the δ-kicked-rotor-BEC (Section 7.3.1), including the introduction of appropriate dimensionless units which we then use to express the second-order number-conserving equations of motion of the system (Section 7.3.2). We then give the specific details of the numerical solution method for this system (Section 7.3.3). In Section 7.4 we give a thorough discussion of our results, which illustrate the advantages of our self-consistent, second-order description.

7.2   The δ-kicked-rotor-BEC

Our chosen test-system is a quasi-1D, toroidally-trapped, repulsively-interacting atomic BEC driven by δ-kicks from a spatial cosine potential [Fig. 7.1], which we term the δ-kicked-rotor-BEC. This system is a BEC analogue of the quantum δ-
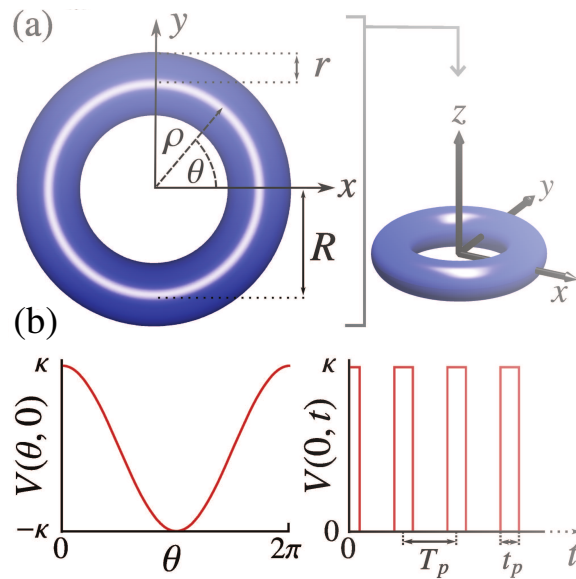
Figure 7.1: The δ-kicked-rotor-BEC system considered in this chapter: An atomic Bose-Einstein condensate is held in a quasi-1D, toroidally-shaped trap (a), and driven by δ-kicks from a sinusoidal perturbing potential (b).

kicked rotor [338–342], a paradigm quantum-chaotic system in which periodic driving leads to complex behaviour, including dynamical localization [338, 339, 342] and quantum resonances (associated with ballistic increase in the kinetic energy) [338–341]. Atom-optical realizations of such systems [341–344] comprise an exciting area of research into quantum-chaotic phenomena. Extension of such systems into the regime of BECs has also become an active area of research, in which several new phenomena have been predicted [48, 56–60, 308, 345–347]. In the mean-field approximation, the nonlinearity of the GPE introduces the potential for true wave chaos to enter the system, and this can strongly influence δ-kicked-rotor-BEC dynamics [58, 345, 346]; in particular, the structure of *nonlinear* quantum resonances in the δ-kicked rotor-BEC was recently elucidated [60], revealing previously unobserved resonance profiles with a sharp asymmetric cut-off.

However, as we have noted in previous Chapters, even at $T = 0$ in a system of finite size there is always a finite non-condensate fraction. The influence of the non-condensate on the dynamics can be accounted for using a variety of theoretical descriptions, as we have discussed in detail in Chapter 5. Highly important in a driven system such as this, however, is the tendency of the far-from-equilibrium dynamics resulting from the driving to cause significant particle transfer from the condensate to the non-condensate fraction. This tendency for dynamical depletion has been observed under quite general circumstances [48, 49, 56, 57, 59, 181, 308]

and, when rapid, such dynamical depletion has commonly been supposed to presage destruction of the BEC as a coherent entity.

As discussed in Chapters 5 and 6, the study of dynamical depletion due to driving at low temperatures is an ideal target for number-conserving descriptions. The first-order, number-conserving description of Castin and Dum [181] (the GPE and MBdGE system — see Section 5.3.4) has been the approach of choice in the study of such systems, and in particular of δ-kicked BEC systems such as we consider here [48, 56, 57, 59, 308]. This work has revealed a general tendency towards rapid growth in the number of non-condensate atoms N_t, and has commonly been interpreted as demonstrating that driving rapidly destroys the condensate in such systems. It is appropriate to consider what is occurring in a little more detail, however.

The growth of the non-condensate is at its most rapid in parameter regimes associated with (nonlinear) quantum resonances, and as such this growth can be seen to result directly from linear dynamical instabilities in the GPE; that is, sensitivity to initial conditions in the linearized regime. These dynamical instabilities are a direct manifestation of the true wave chaos which enters into the GPE due to its nonlinearity [49]. We note that the presence of such instabilities is a generic feature of most nonlinear systems, and is in no way unique to the δ-kicked rotor. However, a treatment of a system posessing such linear instabilities using the first-order number-conserving description is hampered by this description's lack of self-consistency with regard to the total atom number [48, 56, 57, 59, 308]. In particular growth in the non-condensate number N_t should, in reality, be exactly matched by depletion in the condensate number N_c; hence, as atoms transfer from N_c to N_t, qualitatively one expects mean-field interactions and hence further transfer to "switch off" at some stage. Within a first-order description such a "switch-off" is prevented by the lack of a consistent back-action of the non-condensate growth on the condensate dynamics: as shown in Fig. 6.1 the linearized, first-order description treats the condensate as an effectively undepletable "particle bath" which feels no effect from the non-condensate.

Consequently, whether or not a successful "switch-off" of non-condensate growth can, or ever does, occur before the destruction of the condensate has remained an open question. By applying the second-order number-conserving description of S. Gardiner and Morgan to this problem in the fully dynamical form outlined in Chapter 6, we are able to demonstrate that such a "switch-off" can, and in many
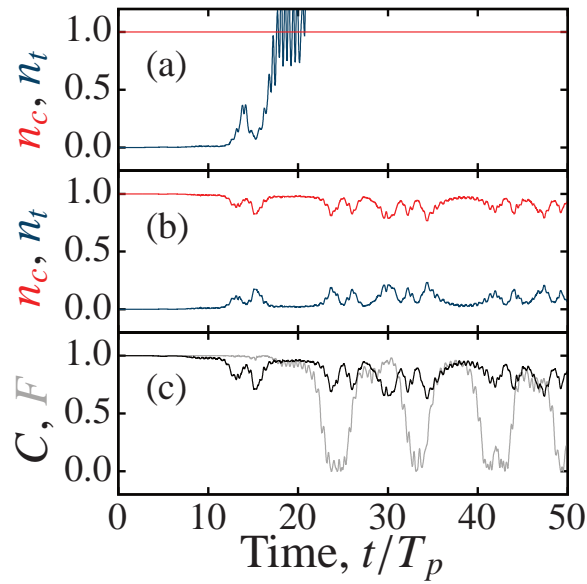
Figure 7.2: Evolution of condensate and non-condensate fractions $n_c = N_c/N$ and $n_t = N_t/N$ in (a) first- and (b) second-order number-conserving descriptions ($N = 10^4$, $g_T = 2.5 \times 10^{-4}$, $T_p = 9.255$, $\kappa = 0.5$). In (c) we show the coherence measure C [Eq. (7.27)] in the second-order description, and the fidelity, F [Eq. (7.28)], of the condensate mode between descriptions.

parameter regimes does, occur in the δ-kicked-rotor-BEC. We do this by numerically exploring resonant parameter regimes which, in the first-order description, lead to rapid, unbounded growth of the non-condensate. Our principal finding is the damping of this growth in the second-order description [Fig. 7.2(a,b)]. We also compute the coherence of the system and the departure of the second-order description from the GPE [Fig. 7.2(c)] for varying total atom number N. We show that, despite considerable differences in dynamics between the descriptions around resonant parameter regimes, the GPE accurately predicts the location of these resonant parameter regimes. The sharp, asymmetric cut-offs identified in [60] are qualitatively preserved, however we show that the accompanying exponential oscillations are strongly modified for experimentally realistic atom numbers.

7.3 Second-order, number-conserving description

7.3.1 Physical system

We consider N bosonic atoms of mass m, held in a toroidal potential $V_T(\rho, z) = m\omega^2[(\rho - R)^2 + z^2]/2$ [Fig. 7.1(a)], interacting with repulsive s-wave contact inter-

actions, and subject to a temporally and spatially periodic driving potential $V(\theta, t)$ [Fig. 7.1(b)]. We have already noted in Chapter 1 that toroidal potentials similar to V_T can be created and precisely controlled using all-optical methods [47, 143]. As in Chapter 2, we assume sufficiently strong radial and axial confinement, and that the harmonic length $r \equiv \sqrt{\hbar/m\omega}$ is much less than the external radius R of the toroidal potential [45], in order to reduce the system Hamiltonian to a dimensionless (length unit R, time unit $mR^2/\hbar$), one-dimensional form [60]:

$$\hat{H} = \int d\theta \, \hat{\Psi}^\dagger(\theta) \left[-\frac{1}{2} \frac{\partial^2}{\partial \theta^2} + V(\theta, t) + \frac{g_T}{2} \hat{\Psi}^\dagger(\theta) \hat{\Psi}(\theta) \right] \hat{\Psi}(\theta) . \tag{7.1}$$

Here, the (dimensionless) interaction strength $g_T = 2a_s R/r^2$. The approximation that the system is quasi-one-dimensional requires that the total energy remain small compared to $\hbar\omega$; in a driven system, such as we consider, this places a time-limit on its validity. However, when beginning with a large, zero-momentum condensate satisfying this condition, the approximation can be expected to hold reasonably well as long as a majority of the atoms remain in the zero-momentum mode.

As in previous studies of the δ-kicked-rotor-BEC [56, 57, 59, 60], we model the driving potential as a train of δ-kicks

$$V(\theta, t) = \kappa \cos(\theta) \sum_{n=0}^{\infty} \delta(t - nT_p) , \tag{7.2}$$

with (dimensionless) kicking period T_p. Such a kicking potential may be approximated in experiment using short pulses of off-resonant laser light [340–342]. For example, a qualitatively similar driving potential, $V_2(\theta, t) = V(2\theta, t)$, could be generated using counter-propagating Laguerre-Gaussian laser modes [348], in which case $\kappa = \Omega^2 t_p/8\Delta$ (for laser detuning Δ, Rabi frequency Ω, and pulse duration t_p). Alternatively, the exact $V(\theta, t)$ we use here could be generated by applying a linear potential $\kappa x/t_p R$ throughout the trap [347] using, for example, magnetic field gradients as in Chapter 3.

7.3.2 Dimensionless equations of motion

As described in detail in Chapters 5 and 6 we define the condensate mode $\psi(\theta)$ (with corresponding creation operator $\hat{a}_c^\dagger$) as the eigenfunction of the single-body density matrix $\langle \hat{\Psi}^\dagger(\theta') \hat{\Psi}(\theta) \rangle$ with the largest eigenvalue N_c (the number of condensate atoms), to which it is normalized; that is, $\int d\theta \, |\psi(\theta)|^2 = N_c \equiv \langle \hat{a}_c^\dagger \hat{a}_c \rangle$. Following the procedure of Chapter 6 we expand the field operator according to the number-

conserving partition

$$\hat{\Psi}(\theta) = \hat{a}_c \psi(\theta)/\sqrt{N_c} + \delta\hat{\Psi}(\theta), \tag{7.3}$$

where

$$\delta\hat{\Psi}(\theta) \equiv \int d\theta' \, Q(\theta, \theta')\hat{\Psi}(\theta'), \tag{7.4}$$

and the projector $Q(\theta, \theta')$ takes the form

$$Q(\theta, \theta') = \delta(\theta - \theta') - \psi(\theta)\psi^*(\theta')/N_c. \tag{7.5}$$

After introducing the number-conserving fluctuation operator

$$\tilde{\Lambda}(\theta) \equiv \hat{a}_c^\dagger \delta\hat{\Psi}(\theta)/\sqrt{N_c}, \tag{7.6}$$

the non-condensate normal and anomalous averages

$$\tilde{n}(\theta, \theta') \equiv \langle\tilde{\Lambda}^\dagger(\theta')\tilde{\Lambda}(\theta)\rangle, \tag{7.7}$$

$$\tilde{m}(\theta, \theta') \equiv \langle\tilde{\Lambda}(\theta')\tilde{\Lambda}(\theta)\rangle, \tag{7.8}$$

and

$$\tilde{f}(\theta) \equiv \frac{1}{N_c} \int d\theta' \, |\psi(\theta')|^2 \left[\tilde{n}(\theta, \theta')\psi(\theta') + \psi^*(\theta')\tilde{m}(\theta', \theta)\right], \tag{7.9}$$

the ultimate result of this expansion is identical to that in Chapter 6, but now in one-dimensional and dimensionless form, and consists of the GGPE

$$\frac{\partial\psi(\theta)}{\partial t} = \left\{H_{\mathrm{GP}}(\theta) - \lambda_2 + g_T\left[2\tilde{n}(\theta, \theta) - \frac{|\psi(\theta)|^2}{N_c}\right]\right\}\psi(\theta) + g_T\tilde{m}(\theta, \theta)\psi^*(\theta) - g_T\tilde{f}(\theta), \tag{7.10}$$

where

$$H_{\mathrm{GP}}(\theta) \equiv -\frac{1}{2}\frac{\partial^2}{\partial\theta^2} + V(\theta, t) + g_T|\psi(\theta)|^2, \tag{7.11}$$

and

$$\lambda_2 = \lambda_0 + \frac{U_0}{N_c} \int d\mathbf{r} \left\{\psi^*(\theta)\left[2\tilde{n}(\theta, \theta) - \frac{1}{N_c}|\psi(\theta)|^2\right]\psi(\theta)\right.$$
$$\left. + \frac{U_0}{2N_c}\left[\psi(\theta)^{*2}\tilde{m}(\theta, \theta) + \psi(\theta)^2\tilde{m}^*(\theta, \theta)\right]\right\}, \tag{7.12}$$

and

$$\lambda_0 = (1/N_c) \int d\theta \, \psi^*(\theta)H_{\mathrm{GP}}(\theta)\psi(\theta), \tag{7.13}$$

and the MBdGE for the quasiparticle mode functions;

$$
i\frac{\partial}{\partial t}\left(\begin{array}{c} u_k(\theta) \\ v_k(\theta) \end{array}\right) = \int d\theta' \left(\begin{array}{cc} L(\theta,\theta') & M(\theta,\theta') \\ -M^*(\theta,\theta') & -L^*(\theta,\theta') \end{array}\right)\left(\begin{array}{c} u_k(\theta') \\ v_k(\theta') \end{array}\right), \qquad (7.14)
$$

where the quasiparticle mode functions $\{u_k(\theta), v_k(\theta)\}$ are normalized by $\int d\theta\,[|u_k(\theta)|^2 - |v_k(\theta)|^2] = 1$, and

$$
L(\theta,\theta') = \delta(\theta - \theta')[H_{\text{GP}}(\theta') - \lambda_0] + g_T \int d\theta''\, Q(\theta,\theta'')|\psi(\theta'')|^2 Q(\theta'',\theta'), \quad (7.15)
$$

$$
M(\theta,\theta') = g_T \int d\theta''\, Q(\theta,\theta'')\psi(\theta'')^2 Q^*(\theta'',\theta')\,. \qquad (7.16)
$$

In order to use the numerical method developed in the previous Chapter, and for consistency with previous studies [56, 57, 59, 60], we begin at zero temperature, and thus express the normal and anomalous averages as

$$
\tilde{n}(\theta,\theta') = \sum_{k=1}^{\infty}\left[v_k(\theta')v_k^*(\theta) + v_{-k}(\theta')v_{-k}^*(\theta)\right], \qquad (7.17)
$$

$$
\tilde{m}(\theta,\theta') = \sum_{k=1}^{\infty}\left[u_k(\theta')v_k^*(\theta) + u_{-k}(\theta')v_{-k}^*(\theta)\right]. \qquad (7.18)
$$

Here, the k index quantifies the momentum associated with the equilibrium quasiparticle eigenmodes, prior to application of the driving potential $V(\theta,t)$[1]. There is no need to renormalize ultraviolet divergences due to the anomalous average $\tilde{m}$ as described in Chapter 5; such infinities formally do not arise in one dimension, making this procedure unnecessary here.

For comparison, in the δ-kicked-rotor-BEC system the first-order description of S. Gardiner and Castin and Dum [66, 181, 304, 305], used previously in time-dependent studies of non-condensate dynamics in δ-kicked BECs [48, 56, 57, 59, 308], consists of the ordinary GPE

$$
i\frac{\partial\psi(\theta)}{\partial t} = [H_{\text{GP}}(\theta) - \lambda_0]\psi(\theta)\,, \qquad (7.19)
$$

coupled to the MBdGE [Eq. (7.14)]. The GPE alone constitutes a zeroth-order description, although it may be possible to infer higher-order processes from a pure

---

[1]Note that, unlike the k index in previous Chapters which has implicitly been restricted to $k \geq 0$, k here has been chosen to run over all (positive and negative) integer values except 0, as this makes counting more convenient

GPE treatment [60] (see also Section 5.4). Unlike the first-order description consisting of GPE plus MBdGE, the GPE alone at least constitutes an internally consistent theoretical description in terms of number-dynamics.

7.3.3 Numerical simulation

We take the $T = 0$ equilibrium state, in the absence of driving, as our initial condition. The initial condensate mode is therefore spatially homogeneous: $\psi(\theta) = \sqrt{N_c/2\pi}$. This sets $\lambda_0 = g_T N_c/2\pi$, and the initial stationary quasiparticle modes to be

$$
\begin{pmatrix} u_k(\theta) \\ v_k(\theta) \end{pmatrix} = \frac{1}{2} \begin{pmatrix} A_k + A_k^{-1} \\ A_k - A_k^{-1} \end{pmatrix} \frac{e^{ik\theta}}{\sqrt{2\pi}},
\tag{7.20}
$$

where

$$
A_k = A_{-k} = \left(\frac{k^2}{k^2 + 4\lambda_0} \right)^{1/4}.
\tag{7.21}
$$

These mode functions display the correct behaviour in both the limit of no interparticle interactions — since $v_k(\theta) = 0$ if $g_T = 0$, and we recover the momentum eigenstates for free particles on a ring — and in the limit of high kinetic energy — since $v_k(\theta) \to 0$ as $|k| \to \infty$, regardless of the (finite) value of g_T, and we recover the free-particle momentum eigenstates. Hence, the number of non-condensate particles is

$$
N_t \equiv N - N_c = \int d\theta\, \tilde{n}(\theta, \theta) = \frac{1}{2} \sum_{k=1}^{\infty} \left(A_k - A_k^{-1} \right)^2,
\tag{7.22}
$$

and we set

$$
\lambda_2 = \frac{g_T}{2\pi} \left(N - 1 + \sum_{k=1}^{\infty} \left[A_k^2 - 1 \right] \right).
\tag{7.23}
$$

To numerically determine a self-consistent $T = 0$ solution to Eqs. (7.10) and (7.14), for given values of N and g_T, we set $N_c = N$, and then; (a) calculate A_k up to a cut-off momentum $|k| = m$; (b) determine N_t from the A_k; (c) make the replacement $N_c = N - N_t$. We repeat steps (a)–(c) until convergence. To determine the driven dynamics, we evolve Eqs. (7.10) and (7.14) using the pseudospectral split-step method outlined in Chapter 6 on a Fourier grid (see Appendix B for details of the Fourier pseudospectral implementation). The δ-kicks from the external potential can be incorporated into the dynamics quasi-analytically by implementing the mappings

$$
\psi(\theta) \to e^{-i\kappa \cos\theta} \psi(\theta),
\tag{7.24}
$$

$$
u_k(\theta) \to e^{-i\kappa \cos\theta} u_k(\theta),
\tag{7.25}
$$

$$
v_k(\theta) \to e^{i\kappa \cos\theta} v_k(\theta),
\tag{7.26}
$$

numerically, for every mode and at the instant of every kick.

As explained in detail in Chapter 6, evolving the GGPE-MBdGE system involves diagonalizing Eqs. (7.10) and (7.14), expressed as a nonlinear integro-differential equation in a $2M + 1$-dimensional spinor space, analytically for small timesteps, and reorthogonalizing $\{u_k, v_k\}$ with respect to ψ after each timestep to prevent build-up of rounding errors. All simulations have been checked for convergence in timestep, grid size, and quasiparticle cut-off momentum M. Figure 7.3 illustrates the convergence of the method in M; interestingly, while quantities such as the anomalous average are known to converge rather slowly in M when one calculates them for equilibrium situations [70, 71], the overall time-evolution given by the split-step method converges much more rapidly; $M = 4$ is numerically indistinguishable from $M = 64$ (our typical choice in this Chapter) over the evolved time. This can be understood as a feature of the δ-kicked-rotor-BEC, in which the driving couples the condensate particularly strongly to only a few quasiparticle modes [59, 60].

7.4 Numerical results and discussion

7.4.1 Results

In Fig. 7.2 we plot the condensate and non-condensate fractions ($n_c = N_c/N$ and $n_t = N_t/N$) for parameters which, in the first-order description, lead to rapid growth of the non-condensate (becoming unphysical after ~ 20 kicks) [Fig. 7.2(a)]. In the second-order description [Fig. 7.2(b)] the self-consistent "back-action" of the non-condensate rapidly damps out this growth, leading instead to complementary oscillations in n_t and n_c. We also track the overall coherence of the system through the spatially-averaged coherence measure

$$C = \iint d\theta \, d\theta' \, g_1(\theta, \theta') g_1(\theta', \theta), \tag{7.27}$$

where $g_1(\theta, \theta') = \left\langle \hat{\Psi}^\dagger(\theta') \hat{\Psi}(\theta) \right\rangle / N$ is the first-order correlation function, and compare the evolution of ψ in the GGPE with the GPE prediction (ψ_{GPE}) through the fidelity

$$F = \frac{\left| \int d\theta \, \psi_{\text{GPE}}^*(\theta) \psi(\theta) \right|^2}{N N_c}. \tag{7.28}$$

The spatially-averaged coherence measure C is equal to unity only in the limit of a pure condensate, where the non-condensate fraction is exactly zero (i.e., the single-body density matrix is exactly factorizable). The GGPE then reduces to the
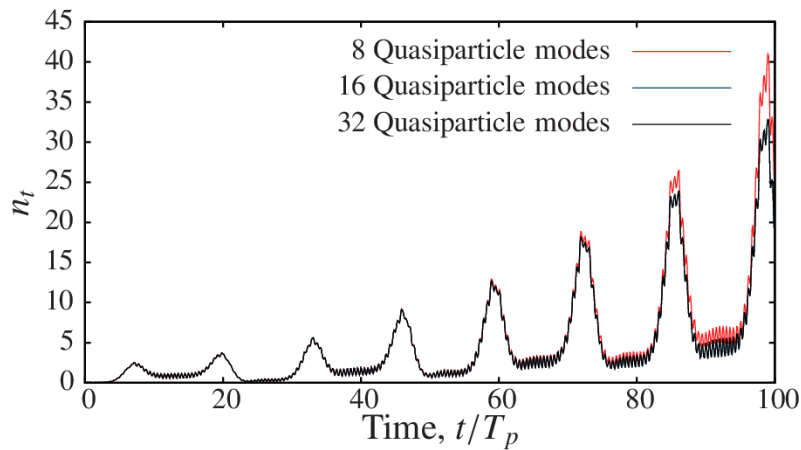
Figure 7.3: Convergence of second-order number-conserving dynamics in the number of quasiparticle modes propagated. The evolution of the number of non-condensate atoms in the δ-kicked-rotor-BEC when $N = 10^5$, $g_T = 10^{-5}$, $T = 10$, and $\kappa = 0.2$, is shown for different numbers of propagated quasiparticle modes (this number being equal to twice the quasiparticle cut-off momentum M) . In each case the number of spatial grid points around the ring is 64, and the numerical timestep is chosen from this using the Courant-Freidrichs-Lewy condition (see Appendix B). Reducing the timestep further at the same grid size does not change the result, nor does using a larger number of points. One sees that, whilst quantities such as the anomalous average may converge rather slowly in M when one calculates them statically [70, 71], the evolution conducted using the split-step method converges much more rapidly.

GPE, and $F = 1$. Otherwise both C and F take values between zero and unity. In Fig. 7.2(c) we show the time evolution of C and F. The evolution of C is linked to the purity of the state, and hence shows oscillations which closely mirror those in n_t. The evolution of F shows a strong initial decrease as the non-condensate begins to influence the dynamics. This is followed by a series of larger-amplitude oscillations with strong revivals; these revivals indicate re-phasing effects, occurring due to the small number of well-occupied momentum modes, as evidenced by the rapid convergence in M shown in Fig. 7.3.

Similar behaviour persists across the T_p–g_T parameter space covered by Fig. 7.4, which we note is accessible to recent experiments (e.g., effective g_T in excess of 10^{-3} and atom numbers up to 3×10^5 are reached in [47]). In Fig. 7.4(a) we show the time averaged response to weak driving ($\kappa = 0.5$), by plotting the occupation of modes with non-zero momentum, $1 - n_0$, averaged over the first 100 kicks. Here,
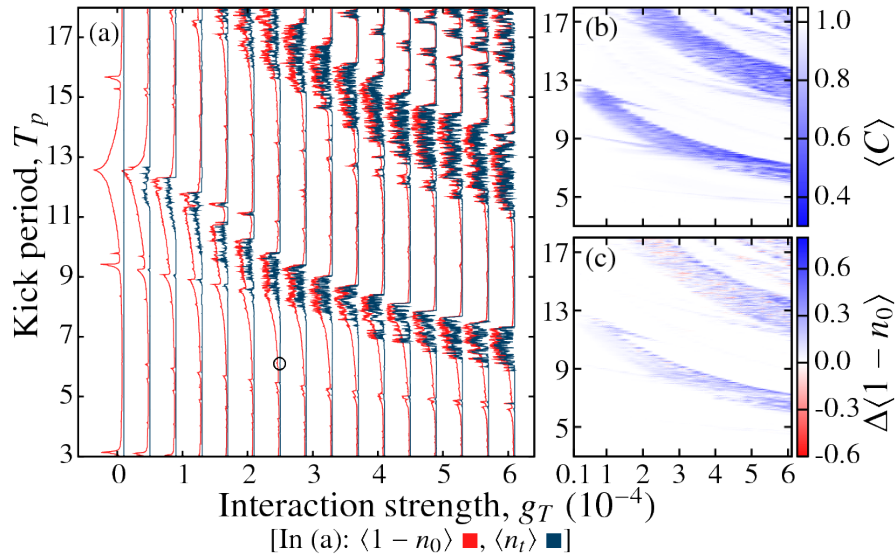
Figure 7.4: BEC response in the second-order description ($N = 10^4$, $\kappa = 0.5$): (a) relative population of $k \neq 0$ momentum modes among all atoms, $\langle 1 - n_0 \rangle$, and non-condensate fraction, $\langle n_t \rangle$; (b) coherence measure $\langle C \rangle$ [Eq. (7.27)]; and (c) $\langle 1 - n_0 \rangle$ as predicted by the GPE, minus its value in the second-order description. Averages are taken over the first 100 kicks. The black circle in (a) indicates the parameters used in figures 3 and 4.

we have defined the momentum mode occupation

$$n_k = \frac{\langle \hat{a}_k^\dagger \hat{a}_k \rangle}{N} , \qquad (7.29)$$

where $\hat{a}_k^\dagger$ creates an atom with momentum k. This notation for momentum mode occupation should not be confused with our notation for the condensate fraction (n_c) and non-condensate fraction (n_t). The occupations n_k are easily obtained as the diagonal elements of the momentum-representation single-particle density matrix: $n_k = \rho(k, k)$. The latter can be obtained numerically as the Fourier transform of the position-representation single-particle density matrix; within our second-order treatment this is given by

$$\rho(\theta, \theta') = \psi^*(\theta')\psi(\theta) + \sum_{k=1}^{\infty} \left[v_k(\theta')v_k^*(\theta) + v_{-k}(\theta')v_{-k}^*(\theta) \right] . \qquad (7.30)$$

We note that this gives the occupation of momentum mode k among *all* atoms, not solely the condensate or non-condensate. However, the same occupations among only the condensate or non-condensate atoms can also be easily computed, by selecting only the relevant part of the single-particle density matrix in Eq. (7.30). The
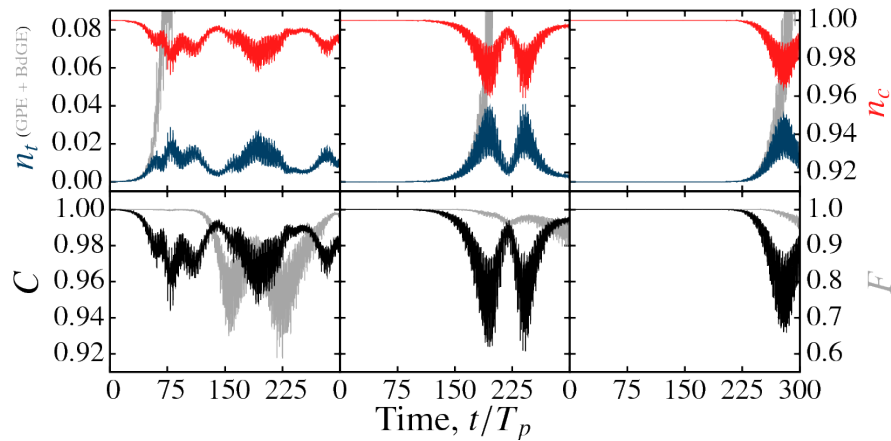
Figure 7.5: Comparison of first- and second-order descriptions close to a nonlinear resonance explored in [60] [parameters $g_T N = 2.5$, $T_p = 6.12$, $\kappa = 0.5$, corresponding to the black circle in Fig. 7.4(a)]. Condensate and non-condensate fractions n_c and n_t, coherence measure C [Eq. (7.27)], and the fidelity of the condensate mode between descriptions, F [Eq. (7.28)], are shown. Columns correspond (left to right) to $N = 10^4$, 10^8, and 10^{12}; agreement of the initial growth in n_t between the second-order (dependent on g_T and N) and first-order (dependent on $g_T N$) descriptions over such a range is a useful test of the second-order numerics.

structure of this response over the range of Fig. 7.4(a), modelled with the GPE alone, was recently elucidated by Monteiro *et al.* in Ref. [60]: the response is dominated by linear resonances corresponding to the first two primary quantum resonances of the δ-kicked rotor as $g_T \to 0$ [340]. Higher-order linear resonances are generally seen to decay with increasing g_T, while nonlinear resonances appear, having no analogue in the linear regime [60]. In the first-order description (GPE plus MBdGE) all these resonant areas of parameter space are associated with rapid growth of the non-condensate fraction n_t due to linear instabilities in the GPE dynamics [56, 57, 59]. In contrast, we find that in the second-order description (GGPE plus MBdGE) this growth is damped out: throughout Fig. 7.4(a) the 100-kick average of n_t remains below 0.6. Nonetheless, we find that the resonances are located in the same regions of parameter space in both descriptions, and that the asymmetric profiles and sharp cut-offs seen in Ref. [60] remain.

7.4.2 Discussion

The detailed response of the system in the second-order description, accompanying the general damping of non-condensate growth, falls into three regimes with respect
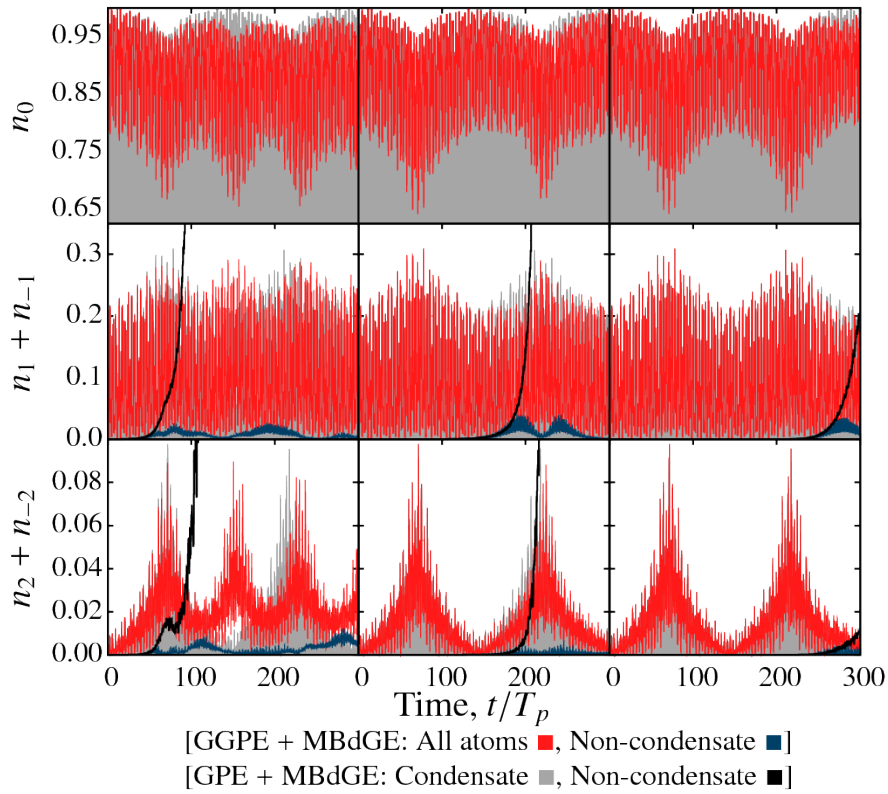
Figure 7.6: Relative populations, n_k, of low momentum modes in the first- and second-order descriptions (parameters as in Fig. 7.5). In the second-order description n_k is shown among all atoms and among the non-condensate atoms; in the first-order description n_k is shown among condensate atoms (as a bar chart) and among the non-condensate atoms (with a three-period moving average). Columns correspond (left to right) to $N = 10^4, 10^8,$ and 10^{12}.

to the first-order description. The first regime occurs far from the main resonances [i.e., in regions of low $\langle 1 - n_0 \rangle$ in Fig. 7.4(a)]. Here the non-condensate growth is insignificant over the 100-kick timescale in both the first- and second-order descriptions. Hence, the first-order description agrees well with the second-order description in this regime. The second regime occurs close to the main resonances [large $\langle 1 - n_0 \rangle$ in Fig. 7.4(a)]. Here the second-order description results in significantly different dynamics, as shown by the behaviour of $\langle C \rangle$ [Fig. 7.4(b)] and the difference in response between descriptions, as measured by the difference in $\langle 1 - n_0 \rangle$ and shown in [Fig. 7.4(c)]. Most importantly, the unbounded non-condensate growth seen in the first-order description is damped out in the second-order description. The average non-condensate fraction $\langle n_t \rangle$ does, however, remain enhanced in the second-order description in this regime [Fig. 7.4(a)]. In cases of significant en-

hancement the small parameter of the theory, n_t/n_c, approaches or exceeds 0.5, indicating that a higher-order or potentially non-perturbative description would be necessary to quantitatively follow the dynamics up to and beyond 100 kicks.

The third, and most interesting, regime occurs towards the edges of the main resonances and at subsidiary, nonlinear resonances [Figs. 7.5 and 7.6]: here n_t/n_c remains within the range of validity of the second-order description, but the dynamics differ significantly from the zero- and first-order descriptions. In Figs. 7.5 and 7.6 we illustrate this regime by comparing the first- and second-order descriptions, for varying N but fixed $g_T N$, close to a nonlinear resonance studied in Ref. [60] [black circle in Fig. 7.4(a)]. Figure 7.5 shows that the dynamics in the second-order description match the GPE for times which increase with N. This increase is slow, however; for realistic N ($\ll 10^8$) the loss of coherence, unaccounted for in the GPE and measured by decay in C, quickly becomes significant. Furthermore, in Fig. 7.6 we see that, on the same timescales associated with significant decay in C, the dynamics of the relative populations n_k, as studied in Ref. [60] using the GPE, noticeably differ in our second-order description. Compared to the first-order description, rapid growth of the non-condensate begins at the same time in our second-order description. However, transfer of population to the non-condensate is driven by, and sensitive to, atom-atom interactions. Hence, decreasing population of the condensate, consistently accounted for in the second-order description, reduces the mean-field interactions, and hence the rate of population transfer.

We observe population oscillations between condensate and non-condensate fractions, accompanied by oscillations in the coherence C and fidelity F [Fig. 7.5]. In Fig. 7.6 we also observe the exponential oscillations in the population, $n_2 + n_{-2}$, of the second momentum mode reported in Ref. [60]; however, for realistic atom numbers the frequency of these oscillations is quickly increased by the presence of a significant non-condensate fraction. The significant differences between the second- and first-order descriptions in this regime, where n_t/n_c remains small for long times, suggest that the *self-consistency* of the second-order description, rather than its higher-order treatment of fluctuations, is the fundamental cause of its improved description of coupled condensate and non-condensate dynamics.

Conclusions

In this thesis we have investigated the static properties and non-equilibrium dynamics of bright solitary matter waves in zero-temperature atomic BECs, and explored the non-equilibrium dynamics of a driven atomic BEC at finite temperature using a second-order, number-conserving description.

Working within the zero-temperature, mean-field (Gross-Pitaevskii) description, we analysed the non-equilibrium dynamics of bright solitary matter-waves in three-dimensional situations. Inspired by the analogy between bright solitary matter waves and the bright soliton solutions of the nonlinear Schrödinger equation, we proposed a feasible experimental scheme for generating pairs of bright solitary waves with well-controlled velocities and relative phases. This scheme has two important potential applications: Firstly, it could potentially be used as the first stage of a bright solitary wave interferometer. Secondly, we have explicitly demonstrated that the stability of repeatedly re-collided bright solitary waves created using this scheme provides a potential experimental test of the accuracy of the mean-field description of these waves.

We have also assessed, in detailed quantitative terms, the relationship between static bright solitary waves in the Gross-Pitaevskii description and the static bright soliton solutions of the nonlinear Schrödinger equation. Although our analysis is restricted to zero temperature, it is sufficient to show that the regime in which bright solitary waves are highly soliton-like will be a challenging one to reach in experiment. This has important implications for experiments attempting to realize many of the currently-proposed manifestations of beyond-mean-field effects in bright solitary matter waves — for example the formation of macroscopic quantum superpositions — as these current proposals implicitly assume the quasi-1D, nonlinear Schrödinger limit to be reached.

With a view to describing the operation of a real bright solitary wave interferometer, we have considered in detail several theoretical descriptions of finite-temperature dynamics. Among these, we have identified the second-order, number-conserving description of S. Gardiner and Morgan as the best candidate for a description of coupled condensate and non-condensate non-equilibrium dynamics at low temperatures, as appropriate for a bright solitary wave interferometry experiment. We

have reviewed in detail the theoretical foundations of this description, and cast the integro-differential equations of motion in a form which can be solved numerically in a fully dynamical way.

Finally, we have implemented such a numerical solution for a quasi-one-dimensional, periodic, driven test-system — the δ-kicked-rotor-BEC. We have shown that the rapid depletion of an initially zero-temperature equilibrium state due to the driving, a central prediction of the first-order number-conserving description, can in fact be damped by the self-consistent "back-action", of the non-condensate on the condensate included in the second-order description.

Possible future work

A primary direction for future work would be to extend the fully-dynamical number-conserving description we have implemented, for the δ-kicked rotor BEC, in Part II of this thesis, and apply it to the study of the same bright solitary wave dynamics considered in Part I. An advantage of studying these systems with a number-conserving approach is that it would allow one to follow the dynamics of the system — in particular keeping track of the depletion and overall coherence of the system as we have done for the δ-kicked rotor BEC — for relatively long times at low temperatures; this is in contrast to previous treatments using the truncated Wigner PGPE [43], which are restricted to short times [171].

In addition to bright solitary matter wave dynamics in the low-temperature regime, it would be interesting to consider equilibrium initial conditions closer to T_c (or after dynamical depletion to the extent that $N_t \gtrsim N_c$). However, while such situations have been treated using the second-order number-conserving description within a linear response treatment by Morgan [69–71], it seems that an extension of the second-order dynamical description will be required to correctly describe such regimes in a fully dynamical way. Such an extension poses a considerably challenging goal for future research. Alternatively, the application of a c-field description of the dynamics through the SPGPE [171], which may in fact be more appropriate in this regime, also remains largely unexplored. With parallel progress on number-conserving and c-field methods in this area, it may even be possible to find an "overlap regime" of temperatures at which the two descriptions agree: if this were the case then the two descriptions, when taken together, would give a tractable beyond-mean-field description of non-equilibrium dynamics, valid for long times, in atomic BECs from $T = 0$ up to $T \gtrsim T_c$. This would represent a considerable

theoretical achievement.

Another interesting direction of research is into the links between non-equilibrium dynamics and the process of thermalization in kicked systems. The thermalization of closed quantum systems, and its links to integrability and quantum chaos [63, 64], is a topic at the forefront of fundamental experimental [349, 350] and theoretical [65, 351–355] research. Kicked systems such as the kicked-rotor-BEC, which offer the possibility to adjust the degree of integrability by changing the external potential, interaction strength and atom number, present an attractive target for application of these ideas. In particular, the emergence of thermodynamic behaviour [351] in such systems as the atom number increases is a fundamental question that remains to be addressed fully. The second-order number-conserving description we have implemented numerically for the δ-kicked-rotor-BEC in this thesis, and perhaps higher-order modifications of it, could provide an important transitional link between the mean-field description and the full many-body dynamics of the system; in particular as they capture considerably more information about the system than the former, but remain more computationally tractable than the latter.

Appendix A: Solutions to integrals and equations arising in variational methods

A.1 Overview

This Appendix lists several integral identities, and the general solution of a specific form of quartic equation, which arise when determining ansatz approximations to the solution of the 3D GPE in Chapter 4. These identities and the quartic solution were originally obtained by S. A. Gardiner and S. A. Wrathmall, in a different notation to that used in Chapter 4. Here, we present them within the notation of Chapter 4 for convenience.

A.2 Useful integrals

Considering a Gaussian ansatz to be proportional to $e^{-k^2 x^2}$, for completeness we reprise the following sequence of well-known integral identities, all of which are necessary to determine the corresponding variational energy functional:

$$\int_{-\infty}^{\infty} dx\, e^{-2k^2 x^2} = \frac{\sqrt{\pi/2}}{k} \Rightarrow \int_{-\infty}^{\infty} dx\, e^{-4k^2 x^2} = \frac{\sqrt{\pi}}{2k}, \qquad (A.1)$$

$$\int_{-\infty}^{\infty} dx\, x^2 e^{-2k^2 x^2} = -\frac{1}{4k}\frac{\partial}{\partial k}\int_{-\infty}^{\infty} dx\, e^{-2k^2 x^2} = \frac{\sqrt{\pi/2}}{4k^3}, \qquad (A.2)$$

$$\int_{-\infty}^{\infty} dx\, \left(\frac{\partial}{\partial x}e^{-k^2 x^2}\right)^2 = 4k^4 \int_{-\infty}^{\infty} dx\, x^2 e^{-k^2 x^2} = k\sqrt{\pi/2}. \qquad (A.3)$$

Comparable integral identities exist when considering an ansatz proportional to $\operatorname{sech}(kx)$. Thus:

$$\int_{-\infty}^{\infty} dx\, \operatorname{sech}^2(kx) = \left[\frac{\tanh(kx)}{k}\right]_{-\infty}^{\infty} = \frac{2}{k}, \qquad (A.4)$$

$$\int_{-\infty}^{\infty} dx\, \operatorname{sech}^4(kx) = \left[\frac{\{\operatorname{sech}^2(kx) + 2\}\tanh(kx)}{3k}\right]_{-\infty}^{\infty} = \frac{4}{3k}, \qquad (A.5)$$

$$\int_{-\infty}^{\infty} dx\, \left[\frac{\partial}{\partial x}\operatorname{sech}(kx)\right]^2 = k^2 \int_{-\infty}^{\infty} dx\, \tanh^2(kx)\operatorname{sech}^2(x)$$

$$= \frac{k}{3}\left[\tanh(kx)\right]_{-\infty}^{\infty} = \frac{2k}{3}, \qquad (A.6)$$

all of which are necessary to determine the energy of a standard bright soliton solution to the nonlinear Schrödinger equation. However, we also require a contribution arising from the existence of an external harmonic confining potential. Hence, we determine

$$
\begin{aligned}
\int_{-\infty}^{\infty} dx\, x^2 \mathrm{sech}^2(kx) &= 2\int_{0}^{\infty} dx\, x^2 \mathrm{sech}^2(kx) \\
&= \frac{2}{k^3}\Big[\mathrm{Li}_2\big(-e^{-2kx}\big) + kx\big\{kx\tanh(kx) - kx - 2\ln\big(1 + e^{-2kx}\big)\big\}\Big]_0^{\infty} \\
&= \frac{2}{k^3}\left[\mathrm{Li}_2(0) - \mathrm{Li}_2(-1)\right] \\
&= \frac{2}{k^3}\eta(2) = \frac{\pi^2}{6k^3},
\end{aligned}
$$

(A.7)

where $\mathrm{Li}_y(x) \equiv \sum_{n=1}^{\infty} x^n/n^y$ is a polylogarithm, and $-\mathrm{Li}_y(-1) = \eta(y)$, the Dirichlet η function, with $\eta(2) = \pi^2/12$.

A.3 Solution to the quartic equations

We require a general solution to a quartic in ℓ of the form

$$
\ell^4 + b\ell - c = 0,
$$

(A.8)

where b and c are positive real constants, and ℓ must also take positive real values to be physically meaningful. This can be rephrased as the product of two quadratics in ℓ:

$$
\left[\ell^2 + \alpha\ell + \frac{1}{2}\left(\alpha^2 - \frac{b}{\alpha}\right)\right]\left[\ell^2 - \alpha\ell + \frac{1}{2}\left(\alpha^2 + \frac{b}{\alpha}\right)\right] = 0,
$$

(A.9)

so long as $(b^2/\alpha^2 - \alpha^4)/4 = c$. Hence, α, which remains to be determined, must solve $\alpha^6 + 4c\alpha^2 - b^2$.

Defining $\xi = \alpha^2$, the problem of determining α reduces to finding values of ξ to solve the depressed cubic equation

$$
\xi^3 + 4c\xi - b^2 = 0.
$$

(A.10)

Defining

$$
A = \sqrt[3]{\frac{b^2}{2} + \sqrt{\frac{b^4}{4} + \frac{64c^3}{27}}}, \quad B = \sqrt[3]{\frac{b^2}{2} - \sqrt{\frac{b^4}{4} + \frac{64c^3}{27}}},
$$

(A.11)

the three roots of Eq. (A.10) are given by:

$$\xi_1 = A + B, \tag{A.12}$$

$$\xi_2 = -(A + B)/2 + i\sqrt{3}(A - B)/2, \tag{A.13}$$

$$\xi_3 = -(A + B)/2 - i\sqrt{3}(A - B)/2. \tag{A.14}$$

Any one of these will solve Eq. (A.10), however we choose ξ_1; as b and c are assumed positive real, ξ_1 is also conveniently guaranteed positive real.

Substituting in $\alpha = \sqrt{\xi_1}$, we can apply the quadratic formula to both the factors (enclosed in square brackets) on the left hand side of Eq. (A.9). This reveals the four roots to be

$$\ell_1 = \frac{-\sqrt{\xi_1} + \sqrt{-\xi_1 + 2b/\sqrt{\xi_1}}}{2}, \tag{A.15}$$

$$\ell_2 = \frac{-\sqrt{\xi_1} - \sqrt{-\xi_1 + 2b/\sqrt{\xi_1}}}{2}, \tag{A.16}$$

$$\ell_3 = \frac{\sqrt{\xi_1} + \sqrt{-\xi_1 - 2b/\sqrt{\xi_1}}}{2}, \tag{A.17}$$

$$\ell_4 = \frac{\sqrt{\xi_1} - \sqrt{-\xi_1 - 2b/\sqrt{\xi_1}}}{2}. \tag{A.18}$$

Recalling that b and ξ_1 are positive real, ℓ_3 and ℓ_4 are clearly complex, and therefore not of interest to us. Noting that

$$\xi_1^3 = A^3 + B^3 + 3AB(A + B) = b^2 - 4c\xi_1, \tag{A.19}$$

we can see that $A^3 + B^3 \equiv b^2 > \xi_1^3$, hence $4b^2 > \xi_1^3$ and thus $2b/\sqrt{\xi_1} > \xi_1$. Roots ℓ_1 and ℓ_2 are therefore real, but ℓ_2 is guaranteed negative. However, from Eq. (A.19) it also follows that

$$b > \xi_1\sqrt{\xi_1} \Rightarrow 2b/\sqrt{\xi_1} > 2\xi_1 \Rightarrow 2b/\sqrt{\xi_1} - \xi_1 > \xi_1$$
$$\Rightarrow \sqrt{-\xi_1 + 2b/\sqrt{\xi_1}} > \sqrt{\xi_1}. \tag{A.20}$$

Hence ℓ_1 is guaranteed positive real, and is the only solution of interest.

Thus, the single positive real root of Eq. (A.8) is

$$\ell = \frac{\chi^{1/2}b^{1/3}}{2^{7/6}}\left\{\left[\left(\frac{2}{\chi}\right)^{3/2}-1\right]^{1/2}-1\right\},\tag{A.21}$$

with

$$\chi = \left\{1+\left[1+\frac{(c/3)^3}{(b/4)^4}\right]^{1/2}\right\}^{1/3}+\left\{1-\left[1+\frac{(c/3)^3}{(b/4)^4}\right]^{1/2}\right\}^{1/3},\tag{A.22}$$

and where values of all fractional powers are taken to be real, and positive when a positive root exists.

Appendix B: Pseudospectral methods for PDEs

B.1 Basis expansion

In this thesis we are generally concerned with solving nonlinear partial differential equations (or integro-differential equations) of the time-dependent form

$$i\frac{\partial\psi(\mathbf{r},t)}{\partial t} = \left[-\frac{1}{2}\nabla^2 + V(\mathbf{r}) + \delta V(\mathbf{r},t) + \mathcal{N}(\mathbf{r},t,\psi)\right]\psi(\mathbf{r},t)\,, \tag{B.1}$$

and of the stationary form

$$\left[-\frac{1}{2}\nabla^2 + V(\mathbf{r}) + \mathcal{N}(\mathbf{r},0,\psi)\right]\psi(\mathbf{r},0) = 0\,. \tag{B.2}$$

Here, we have explicitly split the potential into a time-independent term $V(\mathbf{r})$, and a time-dependent perturbation satisfying $\delta V(\mathbf{r},t=0) = 0$. The final term $\mathcal{N}(\mathbf{r},t,\psi)$ is a general nonlinear term, which may contain non-local integral terms[1].

A particularly convenient basis for the solution of Eqs. (B.1) and (B.2) is given by the *scaled* orthonormal eigenstates of the time-independent, linear, Hermitian operator

$$\mathcal{L}(\mathbf{r}) = -\frac{1}{2}\nabla^2 + V(\mathbf{r})\,. \tag{B.3}$$

Specifically, a truncated expansion in this basis is given by

$$\psi(\mathbf{r},t) = \sum_{j=1}^{N} c_j(t)\tilde{\chi}_j(\mathbf{r})\,, \tag{B.4}$$

where

$$\tilde{\chi}_j(\mathbf{r}) = \alpha\chi_j(\tilde{\mathbf{r}})\,. \tag{B.5}$$

Here $c_j(t)$ are time-dependent, complex coefficients and the real functions $\chi_j(\mathbf{r})$ satisfy the eigenvalue equation

$$\mathcal{L}\chi_j(\mathbf{r}) = \varepsilon_j\chi_j(\mathbf{r})\,, \tag{B.6}$$

---

[1]It should not, however, contain inverse powers of ψ.

Depending on the form of $\mathcal{L}(\mathbf{r})$ and the boundary conditions of the problem, the basis functions $\tilde{\chi}_j(\mathbf{r})$ generally take the form of an orthogonal polynomial of order i, potentially multiplied by an exponential factor, or of plane waves in the case $V(\mathbf{r}) = 0$. They thus obey the orthonormalization relation

$$\int d\mathbf{r}\, \chi_j(\mathbf{r})\chi_k^*(\mathbf{r}) = \delta_{jk}\,. \tag{B.7}$$

The rescaled vector $\tilde{\mathbf{r}}$ is defined in m spatial dimensions by

$$\tilde{\mathbf{r}} = [\gamma_{x_1}x_1, \ldots, \gamma_{x_m}x_m]^T\,, \tag{B.8}$$

where γ_{x_j} are independent, real scaling factors. To clarify, in this notation the original vector $\mathbf{r}$ is given by

$$\mathbf{r} = [r_1, \ldots, r_m]^T\,. \tag{B.9}$$

Finally, the factor $\alpha = \sqrt{\prod_{j=1}^m \gamma_{x_j}}$ guarantees the orthonormality of the scaled basis functions,

$$\int d\mathbf{r}\, \tilde{\chi}_j(\mathbf{r})\tilde{\chi}_k^*(\mathbf{r}) = \delta_{jk}\,. \tag{B.10}$$

This choice of basis is advantageous for three primary reasons:

- The basis functions satisfy the boundary conditions associated with $\mathcal{L}(\mathbf{r})$, which should generally also be satisfied by the solutions to Eqs. (B.1) and (B.2)[2]

- Construction of a discrete operator form of $\mathcal{L}(\mathbf{r})$ in this basis is reasonably straightforward. Indeed, if $\gamma_j = 1$ for all j then this is simply the diagonal matrix $\delta_{jk}\varepsilon_j$.

- If the nonlinear term is sufficiently large to alter the length scale of the solution, the scaling factors γ_j allow one to adapt the basis to the new length scale, while still satisfying the appropriate boundary conditions and leaving the construction of a discrete form of $\mathcal{L}(\mathbf{r})$ relatively straightforward.

---

[2]A potential exception is when the nonlinear term $\mathcal{N}(\mathbf{r}, t, \psi)$ contains inverse powers of ψ; hence our choice not to consider this case.

B.2 Quadrature grid

A discrete spatial representation of the wavefunction is given by

$$\psi_l(t) = \psi(\mathbf{r}_l, t) = \sum_{j=1}^{N} c_j(t) \tilde{\chi}_j(\mathbf{r}_l), \tag{B.11}$$

with spatial grid points $\mathbf{r}_l$. In a pseudospectral method, the connection between this discrete spatial representation $\psi_l(t)$ and the spectral coefficients $c_j(t)$ is made by choosing the points $\mathbf{r}_l$ to lie on an appropriate Gaussian quadrature grid; specifically, with the appropriate Gaussian quadrature grid points $\mathbf{r}_l$ and weights w_l, one can express the integral

$$c_k(t) = \int d\mathbf{r} \, \psi^*(\mathbf{r}, t) \tilde{\chi}_k(\mathbf{r}), \tag{B.12}$$

as

$$c_k(t) = \sum_{l=1}^{N} \psi_l^*(t) \tilde{\chi}_k(\mathbf{r}_l) w_l. \tag{B.13}$$

Although the details vary with the form of the basis functions, the quadrature points are typically given by the zeros of the $(N+1)$th basis function $\tilde{\chi}(\mathbf{r})$, and the quadrature rule Eq. (B.13) is generally exact. For example, if the basis functions take the form of orthogonal polynomials multiplied by an exponential weight factor then the appropriate quadrature will be valid for an overall polynomial factor of up to order $2N + 1$ [356].

The quadrature rule allows one to cast transformations between the discrete position representation and the truncated spectral representation, both written in vector form, in terms of the matrix M;

$$\vec{c}(t) = M\vec{\psi}(t), \tag{B.14}$$

$$\vec{\psi}(t) = M^{-1}\vec{c}(t), \tag{B.15}$$

where

$$M_{kl} = \tilde{\chi}_k(\mathbf{r}_l) w_l, \tag{B.16}$$

$$M_{kl}^{-1} = \tilde{\chi}_l(\mathbf{r}_k). \tag{B.17}$$

That $MM^{-1} = M^{-1}M = 1$ is easily verified using the orthonormality of the $\tilde{\chi}_k$;

$$(MM^{-1})_{kl} = \sum_{j=1}^{N} \tilde{\chi}_k(\mathbf{r}_j) w_j \tilde{\chi}_l(\mathbf{r}_j) = \delta_{kl}. \tag{B.18}$$

Once in possession of the appropriate quadrature grid and weights, and hence the matrices M and M^{-1}, one can construct a matrix form of the operator $\mathcal{L}(\mathbf{r})$ which acts on the discrete position representation vector $\vec{\psi}(t)$. This matrix form is given by

$$P = M^{-1}LM \tag{B.19}$$

where the entries of the matrix L are the matrix elements

$$L_{kl} = \int d\mathbf{r}\, \tilde{\chi}_l(\mathbf{r})\mathcal{L}(\mathbf{r})\tilde{\chi}_k(\mathbf{r})\,. \tag{B.20}$$

These matrix elements can be analytically determined for a given set of basis functions. As stated above, in the unscaled case (that is, when $\gamma_{x_j} = 1\ \forall\, j$) one has the simple result $L_{kl} = \delta_{kl}\varepsilon_k$.

B.3   Solution scheme

B.3.1   Static solution

Because $\delta V(\mathbf{r}, t)$ and $\mathcal{N}(\mathbf{r}, t, \psi)$ are diagonal in the discrete position representation, once in possession of the matrix P one can construct a matrix form, $R(t, \vec{\psi})$, of the entire operator $\mathcal{L}(\mathbf{r}) + \delta V(\mathbf{r}, t) + \mathcal{N}(\mathbf{r}, t, \psi)$ at a given time. The elements of $R(t, \vec{\psi})$ are given by

$$R_{kl}(t, \vec{\psi}) = P_{kl} + \delta_{kl}\delta V(\mathbf{r}_l, t) + \delta_{kl}\mathcal{N}(\mathbf{r}_l, t, \psi_l)\,. \tag{B.21}$$

In the static case, dropping the t argument, one has

$$R_{kl}(\vec{\psi}) = P_{kl} + \delta_{kl}\mathcal{N}(\mathbf{r}_l, \psi_l)\,, \tag{B.22}$$

and hence one seeks a solution $\vec{\psi}$ to the system of nonlinear equations

$$R(\vec{\psi})\vec{\psi} = 0\,. \tag{B.23}$$

Solving such a nonlinear system is a well-known numerical problem which can in principle be solved by a simple modified Newton method. However, the venerable `MINPACK` implementation of the Powell hybrid method provides a highly efficient numerical solution [357, 358]. Convergence can be considerably improved by providing this algorithm with the Jacobian matrix,

$$J_{kl} = \frac{\partial}{\partial\psi_l} \sum_l R(\vec{\psi})_{kl}\psi_l\,, \tag{B.24}$$

in analytical form. Helpfully, this is possible for the nonlinear operators $\mathcal{N}(\mathbf{r}, t, \psi)$ we consider in this thesis, although the resulting expressions for the GGPE are extremely lengthy.

In principle, one should also variationally minimise the energy of the resulting solution with respect to the scaling factors γ_{x_j} in order to achieve the best possible numerical solution for a given basis size N. However, it is typically a less complicated numerical process to pick a suitable set of γ_{x_j} — for example, these are chosen based on the ansatz solutions in the computations of Chapter 4 — and simply to increase N until convergence is reached.

B.3.2 Dynamic solution

Matrix multiplication

The pseudospectral method also lends itself directly to a split-step method for computing the time-evolution of the system. This is achieved by writing the approximate formal solution in the discrete position representation

$$\vec{\psi}(t + \delta t) \approx e^{-iR(t,\vec{\psi})\delta t}\vec{\psi}(t)\,. \tag{B.25}$$

Here, within the exponential operator $\vec{\psi}$ is assumed to be constant over the timestep. Defining the nonlinear matrix $Q(t, \vec{\psi} = R(t, \vec{\psi}) - P$, this can be further approximated by

$$\vec{\psi}(t + \delta t) \approx e^{-iQ(t,\vec{\psi})\delta t/2}e^{-iP\delta t}e^{-iQ(t,\vec{\psi})\delta t/2}\vec{\psi}(t)\,, \tag{B.26}$$

where the error is of order δt^3. Again, all terms in the exponential operators are assumed to be constant over a given portion of the time step. The matrix $e^{-iP\delta t}$ can be computed from P once at the beginning of the evolution, and used, unmodified, for all subsequent time steps. In order to exponentiate P it is necessary to find its eigenvalues and eigenvectors, and the largest eigenvalue of P, $p_{\max}$, can be used to calculate an appropriate timestep from the Courant-Friedrichs-Lewy condition [359, 360];

$$p_{\max}\delta t \lesssim 1\,. \tag{B.27}$$

Fast Fourier transforms

In the case $V(\mathbf{r}) = 0$ and with periodic boundary conditions, complex Fourier series are the most appropriate choice of basis functions. These basis functions offer two main advantages: Firstly, the appropriate quadrature grid is uniformly spaced, and

does not require one to find the zeros of high-order polynomials. Secondly, the basis scaling factors γ_{x_j} are extraneous and can be set to unity. Finally, one does not need to conduct a matrix multiplication — which requires $\mathcal{O}(N^2)$ floating point operations — to apply the operator $e^{-iP\delta t}$. Indeed, because all scaling factors can be set to unity the matrix L is necessarily diagonal, with elements $L_{kl} = \delta_{kl}k^2/2$. Consequently one can expand multiplication by $e^{-iP\delta t}$ as

$$e^{-iP\delta t}\vec{\psi} = M^{-1}e^{-iL\delta t}M\vec{\psi}. \tag{B.28}$$

Noting that for a Fourier basis M and M^{-1} are, respectively, forward and inverse discrete Fourier transforms, one can thus achieve the whole operation with $\mathcal{O}(N \log N)$ floating point operations using a suitable fast-Fourier transform library [361]. A similar saving can also be made, albeit in a more complex form and on a non-uniform grid, in the case of hard-wall boundary conditions where Chebyshev polynomials are the most appropriate basis functions [360].

References

[1] F. Dalfovo, S. Giorgini, L. P. Pitaevskii, and S. Stringari, *Theory of Bose-Einstein condensation in trapped gases*, Rev. Mod. Phys. **71**, 463 (1999)

[2] M. H. Anderson, J. R. Ensher, M. R. Matthews, C. E. Wieman, and E. A. Cornell, *Observation of Bose-Einstein Condensation in a Dilute Atomic Vapor*, Science **269**, 198 (1995)

[3] K. B. Davis, M. O. Mewes, M. R. Andrews, N. J. van Druten, D. S. Durfee, D. M. Kurn, and W. Ketterle, *Bose-Einstein Condensation in a Gas of Sodium Atoms*, Phys. Rev. Lett. **75**, 3969 (1995)

[4] M. R. Matthews, B. P. Anderson, P. C. Haljan, D. S. Hall, C. E. Wieman, and E. A. Cornell, *Vortices in a Bose-Einstein Condensate*, Phys. Rev. Lett. **83**, 2498 (1999)

[5] K. W. Madison, F. Chevy, W. Wohlleben, and J. Dalibard, *Vortex Formation in a Stirred Bose-Einstein Condensate*, Phys. Rev. Lett. **84**, 806 (2000)

[6] J. R. Abo-Shaeer, C. Raman, J. M. Vogels, and W. Ketterle, *Observation of Vortex Lattices in Bose-Einstein Condensates*, Science **292**, 476 (2001)

[7] C. Raman, J. R. Abo-Shaeer, J. M. Vogels, K. Xu, and W. Ketterle, *Vortex Nucleation in a Stirred Bose-Einstein Condensate*, Phys. Rev. Lett. **87**, 210402 (2001)

[8] S. Burger, K. Bongs, S. Dettmer, W. Ertmer, K. Sengstock, A. Sanpera, G. V. Shlyap-nikov, and M. Lewenstein, *Dark Solitons in Bose-Einstein Condensates*, Phys. Rev. Lett. **83**, 5198 (1999)

[9] J. Denschlag *et al.*, *Generating Solitons by Phase Engineering of a Bose-Einstein Condensate*, Science **287**, 97 (2000)

[10] K. E. Strecker, G. B. Partridge, A. G. Truscott, and R. G. Hulet, *Formation and propagation of matter-wave soliton trains*, Nature **417**, 150 (2002)

[11] L. Khaykovich, F. Schreck, G. Ferrari, T. Bourdel, J. Cubizolles, L. D. Carr, Y. Castin, and C. Salomon, *Formation of a Matter-Wave Bright Soliton*, Science **296**, 1290 (2002)

[12] S. L. Cornish, S. T. Thompson, and C. E. Wieman, *Formation of Bright Matter-Wave Solitons during the Collapse of Attractive Bose-Einstein Condensates*, Phys. Rev. Lett. **96**, 170401 (2006)

[13] L. D. Fadeev and L. A. Takhtajan, *Hamiltonian Methods in the Theory of Solitons* (Springer-Verlag, Berlin, 1987)

[14] N. Akhmediev, A. Ankiewicz, and M. Taki, *Waves that appear from nowhere and disappear without a trace*, Phys. Lett. A **373**, 675 (2009)

[15] A. Hasegawa and F. Tappert, *Transmission of stationary nonlinear optical pulses in dispersive dielectric fibers. I. Anomalous dispersion*, Appl. Phys. Lett. **23**, 142 (1973)

[16] H. A. Haus and W. S. Wong, *Solitons in optical communications*, Rev. Mod. Phys. **68**, 423 (1996)

[17] V. Zakharov and A. Shabat, *Exact theory of two-dimensional self-focusing and one-dimensional self-modulation of waves in nonlinear media*, Sov. Phys. JETP **34**, 62

(1972), [Zh. Eksp. Teor. Fiz. **61**, 118 (1971)]

[18] J. Satsuma and N. Yajima, *Initial Value Problems of One-Dimensional Self-Modulation of Nonlinear Waves in Dispersive Media*, Prog. Theor. Phys. Suppl. **55**, 284 (1974)

[19] J. P. Gordon, *Interaction forces among solitons in optical fibers*, Opt. Lett. **8**, 596 (1983)

[20] A. D. Martin, C. S. Adams, and S. A. Gardiner, *Bright solitary-matter-wave collisions in a harmonic trap: Regimes of solitonlike behavior*, Phys. Rev. A **77**, 013620 (2008)

[21] A. D. Martin, C. S. Adams, and S. A. Gardiner, *Bright Matter-Wave Soliton Collisions in a Harmonic Trap: Regular and Chaotic Dynamics*, Phys. Rev. Lett. **98**, 020402 (2007)

[22] N. G. Parker, A. M. Martin, C. S. Adams, and S. L. Cornish, *Bright solitary waves of trapped atomic Bose-Einstein condensates*, Physica D **238**, 1456 (2009)

[23] N. G. Parker, S. L. Cornish, C. S. Adams, and A. M. Martin, *Bright solitary waves and trapped solutions in Bose-Einstein condensates with attractive interactions*, J. Phys. B **40**, 3127 (2007)

[24] E. A. Donley, N. R. Claussen, S. L. Cornish, J. L. Roberts, E. A. Cornell, and C. E. Wieman, *Dynamics of collapsing and exploding Bose-Einstein condensates*, Nature **412**, 295 (2001)

[25] J. L. Roberts, N. R. Claussen, S. L. Cornish, E. A. Donley, E. A. Cornell, and C. E. Wieman, *Controlled Collapse of a Bose-Einstein Condensate*, Phys. Rev. Lett. **86**, 4211 (2001)

[26] R. J. Dodd, M. Edwards, C. J. Williams, C. W. Clark, M. J. Holland, P. A. Ruprecht, and K. Burnett, *Role of attractive interactions on Bose-Einstein condensation*, Phys. Rev. A **54**, 661 (1996)

[27] N. G. Parker, A. M. Martin, S. L. Cornish, and C. S. Adams, *Collisions of bright solitary matter waves*, J. Phys. B **41**, 045303 (2008)

[28] B. J. Dąbrowska-Wüster, S. Wüster, and M. J. Davis, *Dynamical formation and interaction of bright solitary waves and solitons in the collapse of Bose-Einstein condensates with attractive interactions*, New J. Phys. **11**, 053017 (2009)

[29] A. D. Cronin, J. Schmiedmayer, and D. E. Pritchard, *Optics and interferometry with atoms and molecules*, Rev. Mod. Phys. **81**, 1051 (2009)

[30] T. L. Gustavson, P. Bouyer, and M. A. Kasevich, *Precision Rotation Measurements with an Atom Interferometer Gyroscope*, Phys. Rev. Lett. **78**, 2046 (1997)

[31] A. Peters, K. Y. Chung, and S. Chu, *Measurement of gravitational acceleration by dropping atoms*, Nature **400**, 849 (1999)

[32] M. R. Andrews, C. G. Townsend, H.-J. Miesner, D. S. Durfee, D. M. Kurn, and W. Ketterle, *Observation of Interference Between Two Bose Condensates*, Science **275**, 637 (1997)

[33] Y. Shin, M. Saba, T. A. Pasquini, W. Ketterle, D. E. Pritchard, and A. E. Leanhardt, *Atom Interferometry with Bose-Einstein Condensates in a Double-Well Potential*, Phys. Rev. Lett. **92**, 050405 (2004)

[34] T. Schumm, S. Hofferberth, L. M. Andersson, S. Wildermuth, S. Groth, I. Bar-Joseph, J. Schmiedmayer, and P. Krüger, *Matter-wave interferometry in a double well on an atom chip*, Nature Physics **1**, 57 (2005)

[35] Y.-J. Wang, D. Z. Anderson, V. M. Bright, E. A. Cornell, Q. Diot, T. Kishimoto,

M. Prentiss, R. A. Saravanan, S. R. Segal, and S. Wu, *Atom Michelson Interferometer on a Chip Using a Bose-Einstein Condensate*, Phys. Rev. Lett. **94**, 090405 (2005)

[36] M. Fattori, C. D'Errico, G. Roati, M. Zaccanti, M. Jona-Lasinio, M. Modugno, M. Inguscio, and G. Modugno, *Atom Interferometry with a Weakly Interacting Bose-Einstein Condensate*, Phys. Rev. Lett. **100**, 080405 (2008)

[37] F. Baumgärtner, R. J. Sewell, S. Eriksson, I. Llorente-Garcia, J. Dingjan, J. P. Cotter, and E. A. Hinds, *Measuring Energy Differences by BEC Interferometry on a Chip*, Phys. Rev. Lett. **105**, 243003 (2010)

[38] J. Grond, U. Hohenester, I. Mazets, and J. Schmiedmayer, *Atom interferometry with trapped Bose-Einstein condensates: impact of atom–atom interactions*, New J. Phys. **12**, 065036 (2010)

[39] D. K. Faust and W. P. Reinhardt, *Analysis of a Bose-Einstein Condensate Double-Well Atom Interferometer*, Phys. Rev. Lett. **105**, 240404 (2010)

[40] K. Maussang, G. E. Marti, T. Schneider, P. Treutlein, Y. Li, A. Sinatra, R. Long, J. Estève, and J. Reichel, *Enhanced and Reduced Atom Number Fluctuations in a BEC Splitter*, Phys. Rev. Lett. **105**, 080403 (2010)

[41] C. Weiss and Y. Castin, *Creation and Detection of a Mesoscopic Gas in a Nonlocal Quantum Superposition*, Phys. Rev. Lett. **102**, 010403 (2009)

[42] A. I. Streltsov, O. E. Alon, and L. S. Cederbaum, *Scattering of an attractive Bose-Einstein condensate from a barrier: Formation of quantum superposition states*, Phys. Rev. A **80**, 043616 (2009)

[43] A. D. Martin and J. Ruostekoski, *Quantum dynamics of atomic bright solitons and soliton interferometer* (2011), arXiv:1111.5686

[44] S. L. Cornish, N. G. Parker, A. M. Martin, T. E. Judd, R. G. Scott, T. M. Fromhold, and C. S. Adams, *Quantum reflection of bright matter-wave solitons*, Physica D **238**, 1299 (2009)

[45] P. L. Halkyard, M. P. A. Jones, and S. A. Gardiner, *Rotational response of two-component Bose-Einstein condensates in ring traps*, Phys. Rev. A **81**, 061602 (2010)

[46] C. Ryu, M. F. Andersen, P. Cladé, V. Natarajan, K. Helmerson, and W. D. Phillips, *Observation of Persistent Flow of a Bose-Einstein Condensate in a Toroidal Trap*, Phys. Rev. Lett. **99**, 260401 (2007)

[47] A. Ramanathan, K. C. Wright, S. R. Muniz, M. Zelan, W. T. Hill, C. J. Lobb, K. Helmerson, W. D. Phillips, and G. K. Campbell, *Superflow in a Toroidal Bose-Einstein Condensate: An Atom Circuit with a Tunable Weak Link*, Phys. Rev. Lett. **106**, 130401 (2011)

[48] S. A. Gardiner, D. Jaksch, R. Dum, J. I. Cirac, and P. Zoller, *Nonlinear matter wave dynamics with a chaotic potential*, Phys. Rev. A **62**, 023612 (2000)

[49] S. A. Gardiner, *(Quantum) chaos in Bose-Einstein condensates*, J. Mod. Optics **49**, 1971 (2002)

[50] N. P. Proukakis and B. Jackson, *Finite-temperature models of Bose-Einstein condensation*, J. Phys. B **41**, 203002 (2008)

[51] T. Gasenzer and J. M. Pawlowski, *Towards far-from-equilibrium quantum field dynamics: A functional renormalisation-group approach*, Physics Letters B **670**, 135 (2008)

[52] Z.-Y. Ma, M. B. d'Arcy, and S. A. Gardiner, *Gravity-Sensitive Quantum Dynamics in Cold Atoms*, Phys. Rev. Lett. **93**, 164101 (2004)

[53] S. Schlunk, M. B. d'Arcy, S. A. Gardiner, and G. S. Summy, *Experimental Observa-*

tion of High-Order Quantum Accelerator Modes, Phys. Rev. Lett. **90**, 124102 (2003)

[54] T. P. Billam and S. A. Gardiner, *Quantum resonances in an atom-optical δ -kicked harmonic oscillator*, Phys. Rev. A **80**, 023414 (2009)

[55] S. A. Gardiner, J. I. Cirac, and P. Zoller, *Quantum Chaos in an Ion Trap: The Delta-Kicked Harmonic Oscillator*, Phys. Rev. Lett. **79**, 4790 (1997)

[56] C. Zhang, J. Liu, M. G. Raizen, and Q. Niu, *Transition to Instability in a Kicked Bose-Einstein Condensate*, Phys. Rev. Lett. **92**, 054101 (2004)

[57] J. Liu, C. Zhang, M. G. Raizen, and Q. Niu, *Transition to instability in a periodically kicked Bose-Einstein condensate on a ring*, Phys. Rev. A **73**, 013601 (2006)

[58] D. L. Shepelyansky, *Delocalization of quantum chaos by weak nonlinearity*, Phys. Rev. Lett. **70**, 1787 (1993)

[59] J. Reslen, C. E. Creffield, and T. S. Monteiro, *Dynamical instability in kicked Bose-Einstein condensates*, Phys. Rev. A **77**, 043621 (2008)

[60] T. S. Monteiro, A. Rançon, and J. Ruostekoski, *Nonlinear Resonances in delta-Kicked Bose-Einstein Condensates*, Phys. Rev. Lett. **102**, 014102 (2009)

[61] S. Schlunk, M. B. d'Arcy, S. A. Gardiner, D. Cassettari, R. M. Godun, and G. S. Summy, *Signatures of Quantum Stability in a Classically Chaotic System*, Phys. Rev. Lett. **90**, 054101 (2003)

[62] C. Weiss and N. Teichmann, *Differences between Mean-Field Dynamics and N-Particle Quantum Dynamics as a Signature of Entanglement*, Phys. Rev. Lett. **100**, 140408 (2008)

[63] A. Polkovnikov, K. Sengupta, A. Silva, and M. Vengalattore, *Colloquium: Nonequilibrium dynamics of closed interacting quantum systems*, Rev. Mod. Phys., 863–883(2011)

[64] V. Yukalov, *Equilibration and thermalization in finite quantum systems*, Laser Physics Letters **8**, 485 (2011)

[65] V. A. Yurovsky and M. Olshanii, *Memory of the Initial Conditions in an Incompletely Chaotic Quantum System: Universal Predictions with Application to Cold Atoms*, Phys. Rev. Lett. **106**, 025303 (2011)

[66] C. W. Gardiner, *Particle-number-conserving Bogoliubov method which demonstrates the validity of the time-dependent Gross-Pitaevskii equation for a highly condensed Bose gas*, Phys. Rev. A **56**, 1414 (1997)

[67] Y. Castin and R. Dum, *Low-temperature Bose-Einstein condensates in time-dependent traps: Beyond the U(1) symmetry-breaking approach*, Phys. Rev. A **57**, 3008 (1998)

[68] S. A. Gardiner and S. A. Morgan, *Number-conserving approach to a minimal self-consistent treatment of condensate and noncondensate dynamics in a degenerate Bose gas*, Phys. Rev. A **75**, 043621 (2007)

[69] S. A. Morgan, M. Rusch, D. A. W. Hutchinson, and K. Burnett, *Quantitative Test of Thermal Field Theory for Bose-Einstein Condensates*, Phys. Rev. Lett. **91**, 250403 (2003)

[70] S. A. Morgan, *Response of Bose-Einstein condensates to external perturbations at finite temperature*, Phys. Rev. A **69**, 023609 (2004)

[71] S. A. Morgan, *Quantitative test of thermal field theory for Bose-Einstein condensates. II*, Phys. Rev. A **72**, 043609 (2005)

[72] D. S. Jin, J. R. Ensher, M. R. Matthews, C. E. Wieman, and E. A. Cornell, *Collective*

Excitations of a Bose-Einstein Condensate in a Dilute Gas, Phys. Rev. Lett. **77**, 420 (1996)

[73] D. S. Jin, M. R. Matthews, J. R. Ensher, C. E. Wieman, and E. A. Cornell, *Temperature-Dependent Damping and Frequency Shifts in Collective Excitations of a Dilute Bose-Einstein Condensate*, Phys. Rev. Lett. **78**, 764 (1997)

[74] M.-O. Mewes, M. R. Andrews, N. J. van Druten, D. M. Kurn, D. S. Durfee, C. G. Townsend, and W. Ketterle, *Collective Excitations of a Bose-Einstein Condensate in a Magnetic Trap*, Phys. Rev. Lett. **77**, 988 (1996)

[75] D. M. Stamper-Kurn, H.-J. Miesner, S. Inouye, M. R. Andrews, and W. Ketterle, *Collisionless and Hydrodynamic Excitations of a Bose-Einstein Condensate*, Phys. Rev. Lett. **81**, 500 (1998)

[76] T. P. Billam, S. L. Cornish, and S. A. Gardiner, *Realizing bright-matter-wave-soliton collisions with controlled relative phase*, Phys. Rev. A **83**, 041602(R) (2011)

[77] T. P. Billam, S. A. Wrathmall, and S. A. Gardiner, *Variational determination of approximate bright matter-wave soliton solutions in anisotropic traps*, Phys. Rev. A **85**, 013627 (2012)

[78] T. P. Billam and S. A. Gardiner, *Coherence and instability in a driven Bose-Einstein condensate: a fully dynamical number-conserving approach*, New J. Phys. **14**, 013038 (2012)

[79] S. A. Gardiner and T. P. Billam *Number-conserving approaches for atomic Bose-Einstein condensates: an overview*, In N. P. Proukakis *et al.*, editors, *Quantum Gases: Finite temperature and non-equilibrium dynamics*, World Scientific, Singapore (to appear 2011)

[80] J. L. Helm, T. P. Billam, and S. A. Gardiner, *Bright matter wave soliton collisions at narrow barriers* (2011), arXiv:1203.3080

[81] B. Gertjerenken, T. P. Billam, L. Khaykovich, and C. Weiss, *Scattering of bright quantum matter-wave solitons*, In Preparation(2011)

[82] C. Pethick and H. Smith, *Bose-Einstein condensation in dilute gases* (Cambridge University Press, Cambridge, 2002) ISBN 9780521665803

[83] L. Pitaevskii and S. Stringari, *Bose-Einstein Condensation* (Clarendon Press, Oxford, 2003)

[84] J. A. Dunningham and K. Burnett, *Sub-shot-noise-limited measurements with Bose-Einstein condensates*, Phys. Rev. A **70**, 033601 (2004)

[85] J. J. Cooper, D. W. Hallwood, and J. A. Dunningham, *Entanglement-enhanced atomic gyroscope*, Phys. Rev. A **81**, 043624 (2010)

[86] J. E. Debs, P. A. Altin, T. H. Barter, D. Döring, G. R. Dennis, G. McDonald, R. P. Anderson, J. D. Close, and N. P. Robins, *Cold-atom gravimetry with a Bose-Einstein condensate*, Phys. Rev. A **84**, 033610 (2011)

[87] F. Sorrentino *et al.*, *The Space Atom Interferometer project: status and prospects*, Journal of Physics: Conference Series **327**, 012050 (2011)

[88] W. Pauli, *The Connection Between Spin and Statistics*, Phys. Rev. **58**, 716 (1940)

[89] P. Ehrenfest and J. R. Oppenheimer, *Note on the Statistics of Nuclei*, Phys. Rev. **37**, 333–338 (Feb 1931)

[90] C. J. Foot, *Atomic Physics* (Oxford University Press, Oxford, 2005)

[91] C. C. Bradley, C. A. Sackett, J. J. Tollett, and R. G. Hulet, *Evidence of Bose-Einstein Condensation in an Atomic Gas with Attractive Interactions*, Phys. Rev. Lett. **75**,

1687 (1995)

[92] G. Roati, M. Zaccanti, C. D'Errico, J. Catani, M. Modugno, A. Simoni, M. Inguscio, and G. Modugno, ^{39}K *Bose-Einstein Condensate with Tunable Interactions*, Phys. Rev. Lett. **99**, 010403 (2007)

[93] G. Modugno, G. Ferrari, G. Roati, R. J. Brecha, A. Simoni, and M. Inguscio, *Bose-Einstein Condensation of Potassium Atoms by Sympathetic Cooling*, Science **294**, 1320 (2001)

[94] S. L. Cornish, N. R. Claussen, J. L. Roberts, E. A. Cornell, and C. E. Wieman, *Stable 85Rb Bose-Einstein Condensates with Widely Tunable Interactions*, Phys. Rev. Lett. **85**, 1795 (2000)

[95] T. Weber, J. Herbig, M. Mark, H.-C. Nägerl, and R. Grimm, *Bose-Einstein Condensation of Cesium*, Science **299**, 232 (2003)

[96] A. Griesmaier, J. Werner, S. Hensler, J. Stuhler, and T. Pfau, *Bose-Einstein Condensation of Chromium*, Phys. Rev. Lett. **94**, 160401 (2005)

[97] S. Kraft, F. Vogt, O. Appel, F. Riehle, and U. Sterr, *Bose-Einstein Condensation of Alkaline Earth Atoms:* ^{40}Ca, Phys. Rev. Lett. **103**, 130401 (2009)

[98] S. Stellmer, M. K. Tey, B. Huang, R. Grimm, and F. Schreck, *Bose-Einstein Condensation of Strontium*, Phys. Rev. Lett. **103**, 200401 (2009)

[99] Y. N. M. de Escobar, P. G. Mickelson, M. Yan, B. J. DeSalvo, S. B. Nagel, and T. C. Killian, *Bose-Einstein Condensation of* ^{84}Sr, Phys. Rev. Lett. **103**, 200402 (2009)

[100] S. Stellmer, M. K. Tey, R. Grimm, and F. Schreck, *Bose-Einstein condensation of* ^{86}Sr, Phys. Rev. A **82**, 041602 (2010)

[101] P. G. Mickelson, Y. N. Martinez de Escobar, M. Yan, B. J. DeSalvo, and T. C. Killian, *Bose-Einstein condensation of* ^{88}Sr *through sympathetic cooling with* ^{87}Sr, Phys. Rev. A **81**, 051601 (2010)

[102] Y. Takasu, K. Maki, K. Komori, T. Takano, K. Honda, M. Kumakura, T. Yabuzaki, and Y. Takahashi, *Spin-Singlet Bose-Einstein Condensation of Two-Electron Atoms*, Phys. Rev. Lett. **91**, 040404 (2003)

[103] T. Fukuhara, S. Sugawa, and Y. Takahashi, *Bose-Einstein condensation of an ytterbium isotope*, Phys. Rev. A **76**, 051604 (2007)

[104] T. Fukuhara, S. Sugawa, Y. Takasu, and Y. Takahashi, *All-optical formation of quantum degenerate mixtures*, Phys. Rev. A **79**, 021601 (2009)

[105] S. Sugawa, R. Yamazaki, S. Taie, and Y. Takahashi, *Bose-Einstein condensate in gases of rare atomic species*, Phys. Rev. A **84**, 011610 (2011)

[106] M. Lu, N. Q. Burdick, S. H. Youn, and B. L. Lev, *Strongly Dipolar Bose-Einstein Condensate of Dysprosium*, Phys. Rev. Lett. **107**, 190401 (2011)

[107] D. G. Fried, T. C. Killian, L. Willmann, D. Landhuis, S. C. Moss, D. Kleppner, and T. J. Greytak, *Bose-Einstein Condensation of Atomic Hydrogen*, Phys. Rev. Lett. **81**, 3811 (1998)

[108] A. Robert, O. Sirjean, A. Browaeys, J. Poupard, S. Nowak, D. Boiron, C. I. Westbrook, and A. Aspect, *A Bose-Einstein Condensate of Metastable Atoms*, Science **292**, 461 (2001)

[109] F. Pereira Dos Santos, J. Léonard, J. Wang, C. J. Barrelet, F. Perales, E. Rasel, C. S. Unnikrishnan, M. Leduc, and C. Cohen-Tannoudji, *Bose-Einstein Condensation of Metastable Helium*, Phys. Rev. Lett. **86**, 3459 (2001)

[110] J. Kasprzak *et al.*, *Bose-Einstein condensation of exciton polaritons*, Nature **443**, 409

(2006)

[111] T. Nikuni, M. Oshikawa, A. Oosawa, and H. Tanaka, *Bose-Einstein Condensation of Dilute Magnons in* TlCuCl$_3$, Phys. Rev. Lett. **84**, 5868 (2000)

[112] T. Giamarchi, C. Rüegg, and O. Tchernyshyov, *Bose-Einstein condensation in magnetic insulators*, Nature Phys. **4**, 198 (2008)

[113] J. Klaers, J. Schmitt, F. Vewinger, and M. Weitz, *Bose-Einstein condensation of photons in an optical microcavity*, Nature **468**, 545 (2010)

[114] P. Kapitza, *Viscosity of Liquid Helium below the λ-Point*, Nature **141**, 74 (1938)

[115] J. F. Allen and A. D. Misener, *Flow of Liquid Helium II*, Nature **141**, 75 (1938)

[116] E. J. Yarmchuk, M. J. V. Gordon, and R. E. Packard, *Observation of Stationary Vortex Arrays in Rotating Superfluid Helium*, Phys. Rev. Lett. **43**, 214 (1979)

[117] K. G. Lagoudakis, M. Wouters, M. Richard, A. Baas, I. Carusotto, R. André, L. S. Dang, and B. Deveaud-Plédran, *Quantized vortices in an exciton–polariton condensate*, Nature Phys. **4**, 706 (2008)

[118] A. Amo, J. Lefrère, S. Pigeon, C. Adrados, C. Ciuti, I. Carusotto, R. Houdré, E. Giacobino, and A. Bramati, *Superfluidity of polaritons in semiconductor microcavities*, Nature Phys. **5**, 805 (2009)

[119] J. R. Abo-Shaeer, C. Raman, and W. Ketterle, *Formation and Decay of Vortex Lattices in Bose-Einstein Condensates at Finite Temperatures*, Phys. Rev. Lett. **88**, 070409 (2002)

[120] M. S. Paoletti and D. P. Lathrop, *Quantum Turbulence*, Annual Review of Condensed Matter Physics **2**, 213 (2011)

[121] E. A. L. Henn, J. A. Seman, G. Roati, K. M. F. Magalhães, and V. S. Bagnato, *Emergence of Turbulence in an Oscillating Bose-Einstein Condensate*, Phys. Rev. Lett. **103**, 045301 (2009)

[122] T. W. Neely, E. C. Samson, A. S. Bradley, M. J. Davis, and B. P. Anderson, *Observation of Vortex Dipoles in an Oblate Bose-Einstein Condensate*, Phys. Rev. Lett. **104**, 160401 (2010)

[123] N. G. Berloff and B. V. Svistunov, *Scenario of strongly nonequilibrated Bose-Einstein condensation*, Phys. Rev. A **66**, 013603 (2002)

[124] N. G. Berloff, *Interactions of vortices with rarefaction solitary waves in a Bose-Einstein condensate and their role in the decay of superfluid turbulence*, Phys. Rev. A **69**, 053601 (2004)

[125] N. Berloff and C. Yin, *Turbulence and Coherent Structures in Two-Component Bose Condensates*, J. Low Temp. Phys. **145**, 187 (2006)

[126] N. G. Berloff and A. J. Youd, *Dissipative Dynamics of Superfluid Vortices at Nonzero Temperatures*, Phys. Rev. Lett. **99**, 145301 (2007)

[127] N. G. Parker and C. S. Adams, *Emergence and Decay of Turbulence in Stirred Atomic Bose-Einstein Condensates*, Phys. Rev. Lett. **95**, 145301 (2005)

[128] C. C. Bradley, C. A. Sackett, and R. G. Hulet, *Bose-Einstein Condensation of Lithium: Observation of Limited Condensate Number*, Phys. Rev. Lett. **78**, 985 (1997)

[129] E. Timmermans, P. Tommasini, M. Hussein, and A. Kerman, *Feshbach resonances in atomic Bose-Einstein condensates*, Phys. Rep. **315**, 199 (1999)

[130] C. Chin, R. Grimm, P. Julienne, and E. Tiesinga, *Feshbach resonances in ultracold gases*, Rev. Mod. Phys. **82**, 1225 (2010)

[131] J. M. Gerton, D. Strekalov, I. Prodan, and R. G. Hulet, *Direct observation of growth and collapse of a Bose-Einstein condensate with attractive interactions*, Nature **408**, 692 (2000)

[132] J. A. Dunningham, *Using quantum theory to improve measurement precision*, Contemp. Phys. **47**, 257 (2006)

[133] M.-O. Mewes, M. R. Andrews, D. M. Kurn, D. S. Durfee, C. G. Townsend, and W. Ketterle, *Output Coupler for Bose-Einstein Condensed Atoms*, Phys. Rev. Lett. **78**, 582 (1997)

[134] S. Inouye, T. Pfau, S. Gupta, A. Chikkatur, A. Görlitz, D. Pritchard, and W. Ketterle, *Observation of phase-coherent amplification of atomic matter waves*, Nature **402**, 641 (1999)

[135] I. Bloch, T. W. Hänsch, and T. Esslinger, *Atom Laser with a cw Output Coupler*, Phys. Rev. Lett. **82**, 3008 (1999)

[136] M. Lewenstein, A. Sanpera, V. Ahufinger, B. Damski, A. Sen(De), and U. Sen, *Ultracold atomic gases in optical lattices: mimicking condensed matter physics and beyond*, Advances in Physics **56**, 243 (2007)

[137] I. Bloch, J. Dalibard, and W. Zwerger, *Many-body physics with ultracold gases*, Rev. Mod. Phys. **80**, 885 (2008)

[138] O. Morsch and M. Oberthaler, *Dynamics of Bose-Einstein condensates in optical lattices*, Rev. Mod. Phys. **78**, 179 (2006)

[139] V. I. Yukalov, Laser Physics **19**, 1 (2008)

[140] J. Fortágh and C. Zimmermann, *Magnetic microtraps for ultracold atoms*, Rev. Mod. Phys. **79**, 235 (2007)

[141] I. Lesanovsky, T. Schumm, S. Hofferberth, L. M. Andersson, P. Krüger, and J. Schmiedmayer, *Adiabatic radio-frequency potentials for the coherent manipulation of matter waves*, Phys. Rev. A **73**, 033619 (2006)

[142] A. S. Arnold, C. S. Garvie, and E. Riis, *Large magnetic storage ring for Bose-Einstein condensates*, Phys. Rev. A **73**, 041606 (2006)

[143] S. Franke-Arnold, J. Leach, M. J. Padgett, V. E. Lembessis, D. Ellinas, A. J. Wright, J. M. Girkin, P. Öhberg, and A. S. Arnold, *Optical ferris wheel for ultracold atoms*, Opt. Express **15**, 8619 (2007)

[144] S. K. Schnelle, E. D. van Ooijen, M. J. Davis, N. R. Heckenberg, and H. Rubinsztein-Dunlop, *Versatile two-dimensional potentials for ultra-cold atoms*, Opt. Express **16**, 1405 (2008)

[145] N. Houston, E. Riis, and A. S. Arnold, *Reproducible dynamic dark ring lattices for ultracold atoms*, J. Phys. B **41**, 211001 (2008)

[146] K. Henderson, C. Ryu, C. MacCormick, and M. G. Boshier, *Experimental demonstration of painting arbitrary and dynamic potentials for Bose-Einstein condensates*, New J. Phys. **11**, 043030 (2009)

[147] N. R. Cooper and Z. Hadzibabic, *Measuring the Superfluid Fraction of an Ultracold Atomic Gas*, Phys. Rev. Lett. **104**, 030401 (2010)

[148] M. Greiner, C. A. Regal, and D. S. Jin, *Emergence of a molecular Bose-Einstein condensate from a Fermi gas*, Nature **426**, 537 (2003)

[149] M. W. Zwierlein, C. A. Stan, C. H. Schunck, S. M. F. Raupach, S. Gupta, Z. Hadzibabic, and W. Ketterle, *Observation of Bose-Einstein Condensation of Molecules*, Phys. Rev. Lett. **91**, 250401 (2003)

[150] S. Giorgini, L. P. Pitaevskii, and S. Stringari, *Theory of ultracold atomic Fermi gases*, Rev. Mod. Phys. **80**, 1215 (2008)

[151] C. J. Myatt, E. A. Burt, R. W. Ghrist, E. A. Cornell, and C. E. Wieman, *Production of Two Overlapping Bose-Einstein Condensates by Sympathetic Cooling*, Phys. Rev. Lett. **78**, 586 (1997)

[152] J. Stenger, S. Inouye, D. M. Stamper-Kurn, H.-J. Miesner, A. P. Chikkatur, and W. Ketterle, *Spin domains in ground-state Bose-Einstein condensates*, Nature **396**, 345 (1998)

[153] B. Damski, L. Santos, E. Tiemann, M. Lewenstein, S. Kotochigova, P. Julienne, and P. Zoller, *Creation of a Dipolar Superfluid in Optical Lattices*, Phys. Rev. Lett. **90**, 110401 (2003)

[154] N. Henkel, R. Nath, and T. Pohl, *Three-Dimensional Roton Excitations and Supersolid Formation in Rydberg-Excited Bose-Einstein Condensates*, Phys. Rev. Lett. **104**, 195302 (2010)

[155] F. Maucher, N. Henkel, M. Saffman, W. Królikowski, S. Skupin, and T. Pohl, *Rydberg-Induced Solitons: Three-Dimensional Self-Trapping of Matter Waves*, Phys. Rev. Lett. **106**, 170401 (2011)

[156] N. N. Bogoliubov, J. Phys. USSR **11**, 23 (1947)

[157] A. Griffin, *A brief history of our understanding of BEC: from Bose to Beliaev* (1999), arXiv:cond-mat/9901123v1

[158] A. J. Leggett, *Bose-Einstein condensation in the alkali gases: Some fundamental concepts*, Rev. Mod. Phys. **73**, 307 (2001)

[159] J. F. Annett, *Superconductivity, Superfluids, and Condensates* (OUP, Oxford, 2004)

[160] A. Griffin, T. Nikuni, and E. Zaremba, *Bose-Condensed Gases at Finite Temperatures* (Cambridge University Press, Cambridge, 2009)

[161] A. Fetter and J. Walecka, *Quantum theory of many-particle systems* (Dover, New York, 1971) ISBN 9780486428277

[162] J. Negele and H. Orland, *Quantum many-particle systems* (Perseus Books, New York, 1998) ISBN 9780738200521

[163] S. A. Morgan, *A gapless theory of Bose-Einstein condensation in dilute gases at finite temperature*, J. Phys. B **33**, 3847 (2000)

[164] R. P. Feynman, *Statistical Mechanics: A set of lectures* (Addison-Wesley, New York, 1972)

[165] F. Gerbier, J. H. Thywissen, S. Richard, M. Hugbart, P. Bouyer, and A. Aspect, *Critical Temperature of a Trapped, Weakly Interacting Bose Gas*, Phys. Rev. Lett. **92**, 030405 (2004)

[166] W. Mullin, *Bose-Einstein condensation in a harmonic potential*, Journal of Low Temperature Physics **106**, 615 (1997)

[167] S. Giorgini, L. P. Pitaevskii, and S. Stringari, *Condensate fraction and critical temperature of a trapped interacting Bose gas*, Phys. Rev. A **54**, R4633 (1996)

[168] R. P. Smith, R. L. D. Campbell, N. Tammuz, and Z. Hadzibabic, *Effects of Interactions on the Critical Temperature of a Trapped Bose Gas*, Phys. Rev. Lett. **106**, 250403 (2011)

[169] N. Tammuz, R. P. Smith, R. L. D. Campbell, S. Beattie, S. Moulder, J. Dalibard, and Z. Hadzibabic, *Can a Bose Gas Be Saturated?*, Phys. Rev. Lett. **106**, 230401 (2011)

[170] M. J. Davis and P. B. Blakie, *Critical Temperature of a Trapped Bose Gas: Compar-*

ison of Theory and Experiment, Phys. Rev. Lett. **96**, 060404 (2006)

[171] P. B. Blakie, A. S. Bradley, M. J. Davis, R. J. Ballagh, and C. W. Gardiner, *Dynamics and statistical mechanics of ultra-cold Bose gases using c-field techniques*, Adv. Phys. **57**, 363 (2008)

[172] R. P. Smith, N. Tammuz, R. L. D. Campbell, M. Holzmann, and Z. Hadzibabic, *Condensed Fraction of an Atomic Bose Gas Induced by Critical Correlations*, Phys. Rev. Lett. **107**, 190403 (2011)

[173] O. Penrose and L. Onsager, *Bose-Einstein Condensation and Liquid Helium*, Phys. Rev. **104**, 576 (1956)

[174] D. S. Petrov, M. Holzmann, and G. V. Shlyapnikov, *Bose-Einstein Condensation in Quasi-2D Trapped Gases*, Phys. Rev. Lett. **84**, 2551 (2000)

[175] E. H. Lieb and W. Liniger, *Exact Analysis of an Interacting Bose Gas. I. The General Solution and the Ground State*, Phys. Rev. **130**, 1605 (1963)

[176] D. I. H. Holdaway, C. Weiss, and S. A. Gardiner, *Quantum theory of bright matter wave solitons in harmonic confinement* (2011), arXiv:1203.6006

[177] M. Peskin and D. Schroeder, *Introduction to quantum field theory* (Addison-Wesley Pub. Co., New York, 1995) ISBN 9780201503975

[178] V. Yukalov, *Bose-Einstein condensation and gauge symmetry breaking*, Laser Physics Letters **4**, 632 (2007)

[179] A. Griffin, *Excitations in a Bose-condensed liquid* (Cambridge University Press, Cambridge, 1993) ISBN 9780521432719

[180] J. O. Andersen, *Theory of the weakly interacting Bose gas*, Rev. Mod. Phys. **76**, 599 (2004)

[181] Y. Castin and R. Dum, *Instability and Depletion of an Excited Bose-Einstein Condensate in a Trap*, Phys. Rev. Lett. **79**, 3553 (1997)

[182] C. W. Gardiner and M. J. Davis, *The stochastic Gross–Pitaevskii equation: II*, J. Phys. B **36**, 4731 (2003)

[183] A. Polkovnikov, *Quantum corrections to the dynamics of interacting bosons: Beyond the truncated Wigner approximation*, Phys. Rev. A **68**, 053604 (2003)

[184] P. B. Blakie and M. J. Davis, *Projected Gross-Pitaevskii equation for harmonically confined Bose gases at finite temperature*, Phys. Rev. A **72**, 063608 (2005)

[185] F. London, *The λ-Phenomenon of Liquid Helium and the Bose-Einstein Degeneracy*, Nature **141**, 643 (1938)

[186] L. Tisza, *Transport Phenomena in Helium II*, Nature **141**, 913 (1938)

[187] L. D. Landau, J. Phys. USSR **5**, 71 (1941)

[188] D. A. W. Hutchinson, E. Zaremba, and A. Griffin, *Finite Temperature Excitations of a Trapped Bose Gas*, Phys. Rev. Lett. **78**, 1842 (1997)

[189] D. M. Ceperley, *Path integrals in the theory of condensed helium*, Rev. Mod. Phys. **67**, 279 (1995)

[190] L. D. Carr and J. Brand, *Multidimensional Solitons: Theory*, in *Emergent Nonlinear Phenomena in Bose-Einstein Condensates*, Springer Series on Atomic, Optical and Plasma Physics, edited by P. G. Kevrekidis, D. J. Frantzeskakis, and R. Carretero-González (Springer, Berlin, 2008) p. 133

[191] F. K. Abdullaev and J. Garnier, *Bright Solitons in Bose-Einstein Condensates: Theory*, in *Emergent Nonlinear Phenomena in Bose-Einstein Condensates*, Springer Series on Atomic, Optical and Plasma Physics, edited by P. G. Kevrekidis, D. J.

Frantzeskakis, and R. Carretero-González (Springer, Berlin, 2008) p. 25

[192] R. Carretero-González, D. J. Frantzeskakis, and P. G. Kevrekidis, *Nonlinear waves in Bose-Einstein condensates: physical relevance and mathematical techniques*, Nonlinearity **21**, R139 (2008)

[193] Y. Kodama and A. Hasegawa, *Effects of initial overlap on the propagation of optical solitons at different wavelengths*, Opt. Lett. **16**, 208 (1991)

[194] V. V. Afanasjev and V. A. Vysloukh, *Interaction of initially overlapping solitons with different frequencies*, J. Opt. Soc. Am. B **11**, 2385 (1994)

[195] T. Dauxois and M. Peyrard, *Physics of Solitons* (Cambridge University Press, 2006)

[196] V. M. Pérez-García, H. Michinel, and H. Herrero, *Bose-Einstein solitons in highly asymmetric traps*, Phys. Rev. A **57**, 3837 (1998)

[197] U. Al Khawaja, H. T. C. Stoof, R. G. Hulet, K. E. Strecker, and G. B. Partridge, *Bright Soliton Trains of Trapped Bose-Einstein Condensates*, Phys. Rev. Lett. **89**, 200404 (2002)

[198] L. D. Carr and J. Brand, *Spontaneous Soliton Formation and Modulational Instability in Bose-Einstein Condensates*, Phys. Rev. Lett. **92**, 040401 (2004)

[199] V. Y. F. Leung, A. G. Truscott, and K. G. H. Baldwin, *Nonlinear atom optics with bright matter-wave soliton trains*, Phys. Rev. A **66**, 061602 (2002)

[200] L. Salasnich, A. Parola, and L. Reatto, *Condensate bright solitons under transverse confinement*, Phys. Rev. A **66**, 043603 (2002)

[201] L. Salasnich, A. Parola, and L. Reatto, *Effective wave equations for the dynamics of cigar-shaped and disk-shaped Bose condensates*, Phys. Rev. A **65**, 043614 (Apr 2002)

[202] A. M. Kamchatnov and V. S. Shchesnovich, *Dynamics of Bose-Einstein condensates in cigar-shaped traps*, Phys. Rev. A **70**, 023604 (2004)

[203] L. Khaykovich and B. A. Malomed, *Deviation from one dimensionality in stationary properties and collisional dynamics of matter-wave solitons*, Phys. Rev. A **74**, 023607 (2006)

[204] L. Salasnich, B. A. Malomed, and F. Toigo, *Matter-wave vortices in cigar-shaped and toroidal waveguides*, Phys. Rev. A **76**, 063614 (2007)

[205] L. Salasnich and B. A. Malomed, *Solitons and solitary vortices in pancake-shaped Bose-Einstein condensates*, Phys. Rev. A **79**, 053620 (2009)

[206] V. E. Zakharov and A. B. Shabat, *A scheme for integrating the nonlinear equations of mathematical physics by the method of the inverse scattering problem. I*, Functional Analysis and Its Applications **8**, 226 (1974)

[207] L. N. Hand and J. D. Finch, *Analytical Mechanics* (Cambridge University Press, Cambridge, 1998)

[208] M. J. Ablowitz and H. Segur, *Solitons and the inverse scattering transform* (SIAM, Philadelphia, 1981)

[209] P. Drazin and R. Johnson, *Solitons: an introduction*, Cambridge texts in applied mathematics (Cambridge University Press, 1989) ISBN 9780521336550

[210] G. Boffetta and A. R. Osborne, *Computation of the direct scattering transform for the nonlinear Schrödinger equation*, J. Comp. Phys. **102**, 252 (1992)

[211] V. I. Karpman, *Soliton Evolution in the Presence of Perturbation*, Physica Scripta **20**, 462 (1979)

[212] Y. S. Kivshar and B. A. Malomed, *Dynamics of solitons in nearly integrable systems*,

Rev. Mod. Phys. **61**, 763 (1989)

[213] B. A. Malomed, *Chapter 2 Variational methods in nonlinear fiber optics and related fields* (Elsevier, 2002) p. 71

[214] N. R. Quintero, F. G. Mertens, and A. R. Bishop, *Generalized traveling-wave method, variational approach, and modified conserved quantities for the perturbed nonlinear Schrödinger equation*, Phys. Rev. E **82**, 016606 (2010)

[215] J. N. Maki and T. Kodama, *Phenomenological Quantization Scheme in a Nonlinear Schrödinger Equation*, Phys. Rev. Lett. **57**, 2097 (1986)

[216] R. Scharf and A. R. Bishop, *Soliton chaos in the nonlinear Schrödinger equation with spatially periodic perturbations*, Phys. Rev. A **46**, R2973 (1992)

[217] R. Scharf and A. R. Bishop, *Length-scale competition for the one-dimensional nonlinear Schrödinger equation with spatially periodic potentials*, Phys. Rev. E **47**, 1375 (1993)

[218] R. Scharf, *Soliton chaos and lengthscale competition in nonlinear dynamics*, Chaos, Solitons & Fractals **5**, 2527 (1995)

[219] S. A. Morgan, R. J. Ballagh, and K. Burnett, *Solitary-wave solutions to nonlinear Schrödinger equations* , Phys. Rev. A **55**, 4338 (1997)

[220] Y. S. Kivshar, T. J. Alexander, and S. K. Turitsyn, *Nonlinear modes of a macroscopic quantum oscillator*, Phys. Lett. A **278**, 225 (2001)

[221] N. G. Parker, N. P. Proukakis, M. Leadbeater, and C. S. Adams, *Soliton-Sound Interactions in Quasi-One-Dimensional Bose-Einstein Condensates*, Phys. Rev. Lett. **90**, 220401 (2003)

[222] P. A. Ruprecht, M. J. Holland, K. Burnett, and M. Edwards, *Time-dependent solution of the nonlinear Schrödinger equation for Bose-condensed trapped neutral atoms*, Phys. Rev. A **51**, 4704 (1995)

[223] L. P. Pitaevskii, *Dynamics of collapse of a confined Bose gas*, Physics Letters A **221**, 14 (1996)

[224] Yu. Kagan, G. V. Shlyapnikov, and J. T. M. Walraven, *Bose-Einstein Condensation in Trapped Atomic Gases*, Phys. Rev. Lett. **76**, 2670 (1996)

[225] Yu. Kagan, A. E. Muryshev, and G. V. Shlyapnikov, *Collapse and Bose-Einstein Condensation in a Trapped Bose Gas with Negative Scattering Length*, Phys. Rev. Lett. **81**, 933 (1998)

[226] S. K. Adhikari, *Mean-field model of interaction between bright vortex solitons in Bose-Einstein condensates*, New J. Phys. **5**, 137 (2003)

[227] C. Huepe, S. Métens, G. Dewel, P. Borckmans, and M. E. Brachet, *Decay Rates in Attractive Bose-Einstein Condensates*, Phys. Rev. Lett. **82**, 1616 (1999)

[228] L. Bergé, T. J. Alexander, and Y. S. Kivshar, *Stability criterion for attractive Bose-Einstein condensates*, Phys. Rev. A **62**, 023607 (2000)

[229] N. Akhmediev, M. P. Das, and A. V. Vagov, *Bose-Einstein condensation of atoms with attractive interaction*, International Journal of Modern Physics B **13**, 625 (1999)

[230] M. Houbiers and H. T. C. Stoof, *Stability of Bose condensed atomic ^{7}Li*, Phys. Rev. A **54**, 5055 (1996)

[231] L. D. Carr and Y. Castin, *Dynamics of a matter-wave bright soliton in an expulsive potential*, Phys. Rev. A **66**, 063602 (2002)

[232] V. M. Pérez-García, H. Michinel, J. I. Cirac, M. Lewenstein, and P. Zoller, *Dynamics of Bose-Einstein condensates: Variational solutions of the Gross-Pitaevskii equa-*

tions, Phys. Rev. A **56**, 1424 (1997)

[233] V. I. Yukalov and E. P. Yukalova, *Optimal trap shape for a Bose gas with attractive interactions*, Phys. Rev. A **72**, 063611 (2005)

[234] A. Gammal, T. Frederico, and L. Tomio, *Critical number of atoms for attractive Bose-Einstein condensates with cylindrically symmetrical traps*, Phys. Rev. A **64**, 055602 (2001)

[235] A. Gammal, L. Tomio, and T. Frederico, *Critical numbers of attractive Bose-Einstein condensed atoms in asymmetric traps*, Phys. Rev. A **66**, 043619 (2002)

[236] C. M. Savage, N. P. Robins, and J. J. Hope, *Bose-Einstein condensate collapse: A comparison between theory and experiment*, Phys. Rev. A **67**, 014304 (2003)

[237] H. Saito and M. Ueda, *Intermittent Implosion and Pattern Formation of Trapped Bose-Einstein Condensates with an Attractive Interaction*, Phys. Rev. Lett. **86**, 1406 (2001)

[238] S. Wüster, J. J. Hope, and C. M. Savage, *Collapsing Bose-Einstein condensates beyond the Gross-Pitaevskii approximation*, Phys. Rev. A **71**, 033604 (2005)

[239] P. A. Altin, G. R. Dennis, G. D. McDonald, D. Döring, J. E. Debs, J. D. Close, C. M. Savage, and N. P. Robins, *Collapse and three-body loss in a ^{85}Rb Bose-Einstein condensate*, Phys. Rev. A **84**, 033632 (2011)

[240] A. Minguzzi, S. Succi, F. Toschi, M. P. Tosi, and P. Vignolo, *Numerical methods for atomic quantum gases with applications to Bose-Einstein condensates and to ultracold fermions*, Physics Reports **395**, 223 (2004)

[241] B. Josephson, *Possible new effects in superconductive tunnelling*, Phys. Lett. **1**, 251 (1962)

[242] M. I. Rodas-Verde, H. Michinel, and V. M. Pérez-García, *Controllable Soliton Emission from a Bose-Einstein Condensate*, Phys. Rev. Lett. **95**, 153903 (2005)

[243] A. V. Carpentier, H. Michinel, M. I. Rodas-Verde, and V. M. Pérez-García, *Analysis of an atom laser based on the spatial control of the scattering length*, Phys. Rev. A **74**, 013619 (2006)

[244] P. Y. P. Chen and B. A. Malomed, *A model of a dual-core matter-wave soliton laser*, J. Phys. B **38**, 4221 (2005)

[245] H. Saito and M. Ueda, *Dynamically Stabilized Bright Solitons in a Two-Dimensional Bose-Einstein Condensate*, Phys. Rev. Lett. **90**, 040403 (2003)

[246] B. Malomed, *Soliton management in periodic systems* (Springer, Berlin, 2006) ISBN 9780387256351

[247] D. Poletti, T. J. Alexander, E. A. Ostrovskaya, B. Li, and Y. S. Kivshar, *Dynamics of Matter-Wave Solitons in a Ratchet Potential*, Phys. Rev. Lett. **101**, 150403 (2008)

[248] D. Poletti, E. A. Ostrovskaya, T. J. Alexander, B. Li, and Y. S. Kivshar, *Ratchet-induced matter–wave transport and soliton collisions in Bose-Einstein condensates*, Physica D **238**, 1338 (2009)

[249] V. Ahufinger, A. Mebrahtu, R. Corbalán, and A. Sanpera, *Quantum switches and quantum memories for matter-wave lattice solitons*, New Journal of Physics **9**, 4 (2007)

[250] P. Pedri and L. Santos, *Two-Dimensional Bright Solitons in Dipolar Bose-Einstein Condensates*, Phys. Rev. Lett. **95**, 200404 (2005)

[251] R. Nath, P. Pedri, and L. Santos, *Stability of Dark Solitons in Three Dimensional Dipolar Bose-Einstein Condensates*, Phys. Rev. Lett. **101**, 210402 (2008)

[252] I. Tikhonenkov, B. A. Malomed, and A. Vardi, *Anisotropic Solitons in Dipolar Bose-Einstein Condensates*, Phys. Rev. Lett. **100**, 090406 (2008)

[253] T. Karpiuk, M. Brewczyk, S. Ospelkaus-Schwarzer, K. Bongs, M. Gajda, and K. Rzążewski, *Soliton Trains in Bose-Fermi Mixtures*, Phys. Rev. Lett. **93**, 100401 (2004)

[254] N. G. Parker and D. A. Smith, *p-wave stabilization of three-dimensional Bose-Fermi solitons*, Phys. Rev. A **85**, 013604 (2012)

[255] K. E. Strecker, G. B. Partridge, A. G. Truscott, and R. G. Hulet, *Bright matter wave solitons in Bose-Einstein condensates*, New J. Phys. **5**, 73 (2003)

[256] S. Wüster, B. J. Dabrowska-Wüster, A. S. Bradley, M. J. Davis, P. B. Blakie, J. J. Hope, and C. M. Savage, *Quantum depletion of collapsing Bose-Einstein condensates*, Phys. Rev. A **75**, 043611 (2007)

[257] A. I. Streltsov, O. E. Alon, and L. S. Cederbaum, *Swift Loss of Coherence of Soliton Trains in Attractive Bose-Einstein Condensates*, Phys. Rev. Lett. **106**, 240401 (2011)

[258] A. I. Streltsov, O. E. Alon, and L. S. Cederbaum, *Role of Excited States in the Splitting of a Trapped Interacting Bose-Einstein Condensate by a Time-Dependent Barrier*, Phys. Rev. Lett. **99**, 030402 (2007)

[259] O. E. Alon, A. I. Streltsov, and L. S. Cederbaum, *Multiconfigurational time-dependent Hartree method for bosons: Many-body dynamics of bosonic systems*, Phys. Rev. A **77**, 033613 (2008)

[260] A. D. Martin, *Theoretical Studies of Bright Solitons in Trapped Atomic Bose-Einstein Condensates*, Ph.D. thesis, University of Durham (2008)

[261] S. Händel, A. L. Marchant, T. P. Wiles, S. A. Hopkins, and S. L. Cornish, *Magnetic transport apparatus for the production of ultracold atomic gases in the vicinity of a dielectric surface*, Rev. Sci. Inst. **83**, 013105 (2012)

[262] N. R. Claussen, S. J. J. M. F. Kokkelmans, S. T. Thompson, E. A. Donley, E. Hodby, and C. E. Wieman, *Very-high-precision bound-state spectroscopy near a ^{85}Rb Feshbach resonance*, Phys. Rev. A **67**, 060701 (2003)

[263] U. Al Khawaja and H. T. C. Stoof, *Formation of matter-wave soliton molecules*, New J. Phys. **13**, 085003 (2011)

[264] T. Ernst and J. Brand, *Resonant trapping in the transport of a matter-wave soliton through a quantum well*, Phys. Rev. A **81**, 033614 (2010)

[265] C. Lee and J. Brand, *Enhanced quantum reflection of matter-wave solitons*, Europhys. Lett. **73**, 321 (2006)

[266] X. D. Cao and B. A. Malomed, *Soliton-defect collisions in the nonlinear Schrödinger equation*, Phys. Lett. A **206**, 177 (1995)

[267] J. Holmer, J. Marzuola, and M. Zworski, *Fast Soliton Scattering by Delta Impurities*, Comm. Math. Phys. **274**, 187 (2007)

[268] D. W. Hallwood, K. Burnett, and J. Dunningham, *Macroscopic superpositions of superfluid flows*, New J. Phys. **8**, 180 (2006)

[269] J. A. Dunningham, J. J. Cooper, and D. W. Hallwood, *Quantum metrology with rotating matter waves in different geometries*, arXiv:1102.0164(2011)

[270] S. Boixo, A. Datta, M. J. Davis, S. T. Flammia, A. Shaji, and C. M. Caves, *Quantum Metrology: Dynamics versus Entanglement*, Phys. Rev. Lett. **101**, 040403 (2008)

[271] A. B. Tacla and C. M. Caves, *Entanglement-based perturbation theory for highly anisotropic Bose-Einstein condensates*, Phys. Rev. A **84**, 053606 (2011)

[272] V. M. Pérez-García, H. Michinel, J. I. Cirac, M. Lewenstein, and P. Zoller, *Low Energy Excitations of a Bose-Einstein Condensate: A Time-Dependent Variational Analysis*, Phys. Rev. Lett. **77**, 5320 (1996)

[273] Y. Lai and H. A. Haus, *Quantum theory of solitons in optical fibers. II. Exact solution*, Phys. Rev. A **40**, 854 (1989)

[274] N. P. Proukakis and K. Burnett, *Generalized Mean Fields for Trapped Atomic Bose-Einstein Condensates*, J. Res. Natl. Inst. Stand. Technol. **101**, 457 (1996), http://nvlpubs.nist.gov/nistpubs/jres/101/4/j4prouka.pdf

[275] N. P. Proukakis, *Self-consistent quantum kinetics of condensate and non-condensate via a coupled equation of motion formalism*, J. Phys. B **34**, 4737 (2001)

[276] A. Griffin, *Conserving and gapless approximations for an inhomogeneous Bose gas at finite temperatures*, Phys. Rev. B **53**, 9341 (1996)

[277] D. A. W. Hutchinson, K. Burnett, R. J. Dodd, S. A. Morgan, M. Rusch, E. Zaremba, N. P. Proukakis, M. Edwards, and C. W. Clark, *Gapless mean-field theory of Bose-Einstein condensates*, J. Phys. B **33**, 3825 (2000)

[278] T. Bergeman, D. L. Feder, N. L. Balazs, and B. I. Schneider, *Bose condensates in a harmonic trap near the critical temperature*, Phys. Rev. A **61**, 063605 (2000)

[279] M. D. Lee, S. A. Morgan, M. J. Davis, and K. Burnett, *Energy-dependent scattering and the Gross-Pitaevskii equation in two-dimensional Bose-Einstein condensates*, Phys. Rev. A **65**, 043617 (2002)

[280] S. A. Morgan, M. D. Lee, and K. Burnett, *Off-shell T matrices in one, two, and three dimensions*, Phys. Rev. A **65**, 022706 (2002)

[281] S. A. Morgan, *A Gapless Theory of Bose-Einstein Condensation in Dilute Gases at Finite Temperature*, Ph.D. thesis, University of Oxford (1999)

[282] M. D. Lee, *Interactions in Low-Dimensional Bose-Einstein Condensates*, Ph.D. thesis, University of Oxford (2002)

[283] N. M. Hugenholtz and D. Pines, *Ground-State Energy and Excitation Spectrum of a System of Interacting Bosons*, Phys. Rev. **116**, 489 (1959)

[284] H. Shi and A. Griffin, *Finite-temperature excitations in a dilute Bose-condensed gas*, Physics Reports **304**, 1 (1998)

[285] R. J. Dodd, M. Edwards, C. W. Clark, and K. Burnett, *Collective excitations of Bose-Einstein-condensed gases at finite temperatures*, Phys. Rev. A **57**, R32 (1998)

[286] V. I. Yukalov and H. Kleinert, *Gapless Hartree-Fock-Bogoliubov approximation for Bose gases*, Phys. Rev. A **73**, 063612 (2006)

[287] N. P. Proukakis, S. A. Morgan, S. Choi, and K. Burnett, *Comparison of gapless mean-field theories for trapped Bose-Einstein condensates*, Phys. Rev. A **58**, 2435 (1998)

[288] D. A. W. Hutchinson, R. J. Dodd, and K. Burnett, *Gapless Finite-T Theory of Collective Modes of a Trapped Gas*, Phys. Rev. Lett. **81**, 2198 (1998)

[289] M. Rusch, S. A. Morgan, D. A. W. Hutchinson, and K. Burnett, *Second Order Theory of Excitations in Trapped Bose Condensates at Finite Temperatures*, Phys. Rev. Lett. **85**, 4844 (2000)

[290] S. Giorgini, *Collisionless dynamics of dilute Bose gases: Role of quantum and thermal fluctuations*, Phys. Rev. A **61**, 063615 (2000)

[291] J. Reidl, A. Csordás, R. Graham, and P. Szépfalusy, *Finite-temperature excitations of Bose gases in anisotropic traps*, Phys. Rev. A **59**, 3816 (1999)

[292] S. Giorgini, *Damping in dilute Bose gases: A mean-field approach*, Phys. Rev. A **57**, 2949 (1998)

[293] R. Walser, J. Williams, J. Cooper, and M. Holland, *Quantum kinetic theory for a condensed bosonic gas*, Phys. Rev. A **59**, 3878 (1999)

[294] R. Walser, J. Cooper, and M. Holland, *Reversible and irreversible evolution of a condensed bosonic gas*, Phys. Rev. A **63**, 013607 (2000)

[295] T. Köhler and K. Burnett, *Microscopic quantum dynamics approach to the dilute condensed Bose gas*, Phys. Rev. A **65**, 033601 (2002)

[296] E. Zaremba, T. Nikuni, and A. Griffin, *Dynamics of Trapped Bose Gases at Finite Temperatures*, J. Low Temp. Phys. **116**, 277 (1999)

[297] B. Jackson and E. Zaremba, *Finite-Temperature Simulations of the Scissors Mode in Bose-Einstein Condensed Gases*, Phys. Rev. Lett. **87**, 100404 (2001)

[298] B. Jackson and E. Zaremba, *Accidental Suppression of Landau Damping of the Transverse Breathing Mode in Elongated Bose-Einstein Condensates*, Phys. Rev. Lett. **89**, 150402 (2002)

[299] J. E. Williams, E. Zaremba, B. Jackson, T. Nikuni, and A. Griffin, *Dynamical Instability of a Condensate Induced by a Rotating Thermal Gas*, Phys. Rev. Lett. **88**, 070401 (2002)

[300] B. Jackson, N. P. Proukakis, C. F. Barenghi, and E. Zaremba, *Finite-temperature vortex dynamics in Bose-Einstein condensates*, Phys. Rev. A **79**, 053615 (2009)

[301] B. Jackson, N. P. Proukakis, and C. F. Barenghi, *Dark-soliton dynamics in Bose-Einstein condensates at finite temperature*, Phys. Rev. A **75**, 051601 (2007)

[302] Yu. Kagan and B. V. Svistunov, *Evolution of Correlation Properties and Appearance of Broken Symmetry in the Process of Bose-Einstein Condensation*, Phys. Rev. Lett. **79**, 3331 (1997)

[303] M. Wilkens and C. Weiss, *Particle number fluctuations in an ideal Bose gas*, J. Mod. Opt. **44**, 1801 (1997)

[304] M. Girardeau and R. Arnowitt, *Theory of Many-Boson Systems: Pair Theory*, Phys. Rev. **113**, 755 (1959)

[305] M. D. Girardeau, *Comment on "Particle-number-conserving Bogoliubov method which demonstrates the validity of the time-dependent Gross-Pitaevskii equation for a highly condensed Bose gas"*, Phys. Rev. A **58**, 775 (1998)

[306] F. Mohling and A. Sirlin, *Low-Lying Excitations in a Bose Gas of Hard Spheres*, Phys. Rev. **118**, 370 (1960)

[307] F. Mohling and M. Morita, *Temperature Dependence of the Low-Momentum Excitations in a Bose Gas of Hard Spheres*, Phys. Rev. **120**, 681 (1960)

[308] L. Rebuzzini, R. Artuso, S. Fishman, and I. Guarneri, *Effects of atomic interactions on quantum accelerator modes*, Phys. Rev. A **76**, 031603 (2007)

[309] S. A. Gardiner, *Quantum Measurement, Quantum Chaos, and Bose-Einstein Condensates*, Ph.D. thesis, Leopold-Franzens-Universität Innsbruck (2000)

[310] B. V. Svistunov, J. Moscow Phys. Soc. **1**, 373 (1991)

[311] Yu. Kagan, B. V. Svistunov, and G. Shlyapnikov, *Kinetics of Bose condensation in an interacting Bose gas*, Sov. Phys. JETP **74**, 279 (1992), [Zh. Eksp. Teor. Fiz. **101**, 528 (1992)], http://www.jetp.ac.ru/cgi-bin/dn/e_074_02_0279.pdf

[312] Yu. Kagan, B. V. Svistunov, and G. Shlyapnikov, *Erratum: Kinetics of Bose-Einstein condensation in an interacting Bose gas [Sov. Phys. JETP. 74, 279 (1992)]*, Sov.

Phys. JETP **75**, 387 (1992)

[313] Yu. Kagan and B. V. Svistunov, *Kinetics of the onset of long-range order during Bose condensation in an interacting gas*, Sov. Phys. JETP **78**, 187 (1994), [Zh. Eksp. Teor. Fiz. **105**, 353 (1994)], http://www.jetp.ac.ru/cgi-bin/dn/e_078_02_0187.pdf

[314] M. J. Davis, S. A. Morgan, and K. Burnett, *Simulations of thermal Bose fields in the classical limit*, Phys. Rev. A **66**, 053618 (2002)

[315] K. Góral, M. Gajda, and K. Rzążewski, *Thermodynamics of an interacting trapped Bose-Einstein gas in the classical field approximation*, Phys. Rev. A **66**, 051602 (2002)

[316] H. H. Rugh, *Dynamical Approach to Temperature*, Phys. Rev. Lett. **78**, 772 (1997)

[317] M. J. Davis and P. B. Blakie, *Calculation of the microcanonical temperature for the classical Bose field*, J. Phys. A **38**, 10259 (2005)

[318] M. J. Davis, S. A. Morgan, and K. Burnett, *Simulations of Bose Fields at Finite Temperature*, Phys. Rev. Lett. **87**, 160402 (2001)

[319] T. P. Simula and P. B. Blakie, *Thermal Activation of Vortex-Antivortex Pairs in Quasi-Two-Dimensional Bose-Einstein Condensates*, Phys. Rev. Lett. **96**, 020404 (2006)

[320] A. Sinatra, Y. Castin, and C. Lobo, *A Monte Carlo formulation of the Bogolubov theory*, J. Mod. Opt. **47**, 2629 (2000)

[321] A. Sinatra, C. Lobo, and Y. Castin, *Classical-Field Method for Time Dependent Bose-Einstein Condensed Gases*, Phys. Rev. Lett. **87**, 210404 (2001)

[322] A. Sinatra, C. Lobo, and Y. Castin, *The truncated Wigner method for Bose-condensed gases: limits of validity and applications*, J. Phys. B **35**, 3599 (2002)

[323] C. Lobo, A. Sinatra, and Y. Castin, *Vortex Lattice Formation in Bose-Einstein Condensates*, Phys. Rev. Lett. **92**, 020403 (2004)

[324] A. A. Norrie, R. J. Ballagh, and C. W. Gardiner, *Quantum turbulence and correlations in Bose-Einstein condensate collisions*, Phys. Rev. A **73**, 043617 (2006)

[325] R. G. Scott, D. A. W. Hutchinson, and C. W. Gardiner, *Disruption of reflecting Bose-Einstein condensates due to interatomic interactions and quantum noise*, Phys. Rev. A **74**, 053605 (2006)

[326] R. G. Scott, T. E. Judd, and T. M. Fromhold, *Exploiting Soliton Decay and Phase Fluctuations in Atom Chip Interferometry of Bose-Einstein Condensates*, Phys. Rev. Lett. **100**, 100402 (2008)

[327] C. W. Gardiner, J. R. Anglin, and T. I. A. Fudge, *The stochastic Gross-Pitaevskii equation*, J. Phys. B **35**, 1555 (2002)

[328] A. S. Bradley, P. B. Blakie, and C. W. Gardiner, *Properties of the stochastic Gross–Pitaevskii equation: finite temperature Ehrenfest relations and the optimal plane wave representation*, J. Phys. B **38**, 4259 (2005)

[329] A. S. Bradley, C. W. Gardiner, and M. J. Davis, *Bose-Einstein condensation from a rotating thermal cloud: Vortex nucleation and lattice formation*, Phys. Rev. A **77**, 033616 (2008)

[330] H. T. C. Stoof, *Initial Stages of Bose-Einstein Condensation*, Phys. Rev. Lett. **78**, 768 (1997)

[331] H. T. C. Stoof, *Coherent Versus Incoherent Dynamics During Bose-Einstein Condensation in Atomic Gases*, J. Low Temp. Phys. **114**, 11 (1999)

[332] S. P. Cockburn and N. P. Proukakis, *The stochastic Gross-Pitaevskii equation and some applications*, Laser Physics **19**, 558 (2009)

[333] S. P. Cockburn, H. E. Nistazakis, T. P. Horikis, P. G. Kevrekidis, N. P. Proukakis, and D. J. Frantzeskakis, *Matter-Wave Dark Solitons: Stochastic versus Analytical Results*, Phys. Rev. Lett. **104**, 174101 (2010)

[334] S. P. Cockburn, A. Negretti, N. P. Proukakis, and C. Henkel, *Comparison between microscopic methods for finite-temperature Bose gases*, Phys. Rev. A **83**, 043619 (2011)

[335] C. N. Weiler, T. W. Neely, D. R. Scherer, A. S. Bradley, M. J. Davis, and B. P. Anderson, *Spontaneous vortices in the formation of Bose-Einstein condensates*, Nature **455**, 948 (2008)

[336] O. Fialko, A. S. Bradley, and J. Brand, *Quantum Tunneling of a Vortex between Two Pinning Potentials*, Phys. Rev. Lett. **108**, 015301 (2012)

[337] Wolfram Research Inc., *Mathematica: Version 8.0* (Wolfram Research Inc., Champaign, Illinois, 2010)

[338] G. Casati, B. V. Chirikov, F. M. Izrailev, and J. Ford, *Stochastic Behavior in Classical and Quantum Hamiltonian Systems* (Springer, Berlin, 1979) p. 334

[339] F. M. Izrailev and D. L. Shepelyanskii, *Quantum resonance for a rotator in a nonlinear periodic field*, Theor. Math. Phys. **43**, 553 (1980)

[340] M. Saunders, P. L. Halkyard, K. J. Challis, and S. A. Gardiner, *Manifestation of quantum resonances and antiresonances in a finite-temperature dilute atomic gas*, Phys. Rev. A **76**, 043415 (2007)

[341] C. Ryu, M. F. Andersen, A. Vaziri, M. B. d'Arcy, J. M. Grossman, K. Helmerson, and W. D. Phillips, *High-Order Quantum Resonances Observed in a Periodically Kicked Bose-Einstein Condensate*, Phys. Rev. Lett. **96**, 160403 (2006)

[342] F. L. Moore, J. C. Robinson, C. F. Bharucha, B. Sundaram, and M. G. Raizen, *Atom Optics Realization of the Quantum δ-Kicked Rotor*, Phys. Rev. Lett. **75**, 4598 (1995)

[343] M. K. Oberthaler, R. M. Godun, M. B. d'Arcy, G. S. Summy, and K. Burnett, *Observation of Quantum Accelerator Modes*, Phys. Rev. Lett. **83**, 4447 (1999)

[344] G. J. Duffy, A. S. Mellish, K. J. Challis, and A. C. Wilson, *Nonlinear atom-optical δ-kicked harmonic oscillator using a Bose-Einstein condensate*, Phys. Rev. A **70**, 041602 (2004)

[345] S. Wimberger, R. Mannella, O. Morsch, and E. Arimondo, *Resonant Nonlinear Quantum Transport for a Periodically Kicked Bose Condensate*, Phys. Rev. Lett. **94**, 130404 (2005)

[346] L. Rebuzzini, S. Wimberger, and R. Artuso, *Delocalized and resonant quantum transport in nonlinear generalizations of the kicked rotor model*, Phys. Rev. E **71**, 036220 (2005)

[347] B. Mieck and R. Graham, *Bose-Einstein condensate of kicked rotators with time-dependent interaction*, J. Phys. A **38**, L139 (2005)

[348] L. Allen, M. W. Beijersbergen, R. J. C. Spreeuw, and J. P. Woerdman, *Orbital angular momentum of light and the transformation of Laguerre-Gaussian laser modes*, Phys. Rev. A **45**, 8185 (1992)

[349] T. Kinoshita, T. Wenger, and D. S. Weiss, *A quantum Newton's cradle*, Nature **440**, 900 (2006)

[350] I. E. Mazets, T. Schumm, and J. Schmiedmayer, *Breakdown of Integrability in a Quasi-1D Ultracold Bosonic Gas*, Phys. Rev. Lett. **100**, 210403 (2008)

[351] P. Reimann, *Foundation of Statistical Mechanics under Experimentally Realistic Conditions*, Phys. Rev. Lett. **101**, 190403 (2008)

[352] M. Rigol, V. Dunjko, and M. Olshanii, *Thermalization and its mechanism for generic isolated quantum systems*, Nature **452**, 854 (2008)

[353] M. Rigol, *Breakdown of Thermalization in Finite One-Dimensional Systems*, Phys. Rev. Lett. **103**, 100403 (2009)

[354] L. F. Santos, A. Polkovnikov, and M. Rigol, *Entropy of Isolated Quantum Systems after a Quench*, Phys. Rev. Lett. **107**, 040601 (2011)

[355] M. C. Bañuls, J. I. Cirac, and M. B. Hastings, *Strong and Weak Thermalization of Infinite Nonintegrable Quantum Systems*, Phys. Rev. Lett. **106**, 050405 (2011)

[356] M. Abramowitz and I. Stegun, *Handbook of Mathematical Functions* (Dover, New York, 1964)

[357] J. J. Moré, B. S. Garbow, and K. E. Hillstrom, *User Guide for MINPACK-1*, Tech. Rep. ANL-80-74 (Argonne National Laboratory, Argonne, Ill., 1980)

[358] J. J. Moré, D. C. Sorensen, K. E. Hillstrom, and B. S. Garbow, *The MINPACK Project*, in *Sources and Development of Mathematical Software*, edited by W. J. Cowell (Prentice-Hall, New York, 1984) p. 88

[359] R. Courant, K. Friedrichs, and H. Lewy, *On the partial difference equations of mathematical physics*, IBM Journal of Research and Development **11**, 215 (1967), [Mathematische Annalen **100**, 32 (1928)], http://www.stanford.edu/class/cme324/classics/courant-friedrichs-lewy.pdf

[360] J. P. Boyd, *Chebyshev and Fourier Spectral Methods*, 2nd ed. (Dover, New York, 2000)

[361] M. Frigo and S. G. Johnson, *The design and implementation of FFTW3*, Proc. IEEE **93**, 216 (2005)